14 January 2011 | $10

Science

AAAS

EDITORIAL

NEWS OF THE WEEK

NEWS FOCUS

LETTERS

BOOKS *ET AL.*

EDUCATION FORUM

PERSPECTIVES

CONTENTS continued >>

page 138

page 148

COVER

Tens of thousands of books appear in this photograph of the interior of the sculpture *Idiom*, by Matej Krén. On page 176, Michel *et al*. describe an even larger collection: a 5.2-million-book corpus containing 4% of all books ever published. Statistical analysis of this corpus makes it possible to study cultural trends quantitatively.

Original sculpture (Municipal Library of Prague): Matej Krén/ Photograph: Zdeněk Urbánek

DEPARTMENTS

pages 155 & 192

page 214

CREDIT (BOTTOM): KRISTI M. MILLER

SCIENCEONLINE

SCIENCEXPRESS
www.sciencexpress.org

Translational Pausing Ensures Membrane Targeting and Cytoplasmic Splicing of *XBP1u* mRNA
K. Yanagitani et al.
A peptide-mediated translational pause facilitates the unconventional splicing of a messenger RNA on the endoplasmic reticulum.
10.1126/science.1197142

Proteome Half-Life Dynamics in Living Human Cells
E. Eden et al.
In times of stress, long-lived proteins increase their durability.
10.1126/science.1199784

Aberrant Overexpression of Satellite Repeats in Pancreatic and Other Epithelial Cancers
D. T. Ting et al.
Noncoding RNAs transcribed from DNA repeats in heterochromatin are expressed at surprisingly high levels in tumors.
10.1126/science.1200801

KOI-126: A Triply Eclipsing Hierarchical Triple with Two Low-Mass Stars
J. A. Carter et al.
The Kepler telescope detected a triple stellar system and reveals details of the structure of low-mass stars.
10.1126/science.1201274

2500 Years of European Climate Variability and Human Susceptibility
U. Büntgen et al.
Variability of central European temperature and precipitation shows correlations with some major historical changes.
10.1126/science.1197175

SCIENCENOW
www.sciencenow.org
Highlights From Our Daily News Coverage

Hubble Confirms Nature of Mysterious Green Blob
'Hanny's Voorwerp' has been an enigma since its discovery in 2007.
http://scim.ag/fa3RAV

Rising Seas Look Inevitable
Effects of global warming will persist, even if we stop emitting greenhouse gases.
http://scim.ag/fw98J3

Measures to Save Ozone Stemmed a Lot More Global Warming
1980s spray-can clampdown prevented even larger temperature increase, modeling shows.
http://scim.ag/hlo11u

SCIENCESIGNALING
www.sciencesignaling.org
The Signal Transduction Knowledge Environment
11 January issue: http://scim.ag/ss011111

RESEARCH ARTICLE: Activation State of the M3 Muscarinic Acetylcholine Receptor Modulates Mammalian Odorant Receptor Signaling
Y. R. Li and H. Matsunami

PERSPECTIVE: Autonomic Modulation of Olfactory Signaling
R. A. Hall
Crosstalk between neurotransmitter signaling and odorant signaling may enhance the sense of smell.

MEETING REPORT: Cilia 2010—The Surprise Organelle of the Decade
E. F. Smith and R. Rohatgi
Scientists discussed advances in cilia biology and the role of cilia in development and disease.

TEACHING RESOURCE: Signaling by Neuronal Swelling
R. D. Fields
Physical changes associated with the electrical activity of neurons mediate intercellular signaling.

SCIENCECAREERS
Free Career Resources for Scientists
www.sciencecareers.org/career_magazine

A Veterinary Scientist's Unique Career Path
S. Webb
D.V.M.-Ph.D. Laura Richman's discovery of a novel elephant herpesvirus led to a career in human translational medicine.
http://scim.ag/fy4p5p

Discovering Unsung African-American Chemists
S. Weininger and L. Gortler
The two Knox brothers had distinguished careers in chemistry at a time when that was very difficult for African Americans.
http://scim.ag/ha7Vtc

SCIENCETRANSLATIONAL MEDICINE
www.sciencetranslationalmedicine.org
Integrating Medicine and Science
12 January issue: http://scim.ag/stm011211

RESEARCH ARTICLE: Identification of an Adenylyl Cyclase Inhibitor for Treating Neuropathic and Inflammatory Pain
H. Wang et al.

PERSPECTIVE: Targeting Pain Where It Resides … In the Brain
R. Sharif-Naeini and A. I. Basbaum
An adenylyl cyclase 1 inhibitor acting on the anterior cingulate cortex alleviates neuropathic pain.

RESEARCH ARTICLE: Carrier Testing for Severe Childhood Recessive Diseases by Next-Generation Sequencing
C. J. Bell et al.
>> News story p. 130

PERSPECTIVE: Molecular Technologies Open New Clinical Genetic Vistas
L. Jackson and R. E. Pyeritz

PODCAST
L. Jackson and O. Smith
New genome-sequencing technologies may enable expansion of carrier and prenatal genetic testing.

SCIENCEPODCAST
www.sciencemag.org/multimedia/podcast
Free Weekly Show

Download the 14 January *Science* Podcast to hear about genetically modifying chickens to curb the spread of influenza, reducing testing anxiety through writing, the science of loneliness, and more.

SCIENCEINSIDER
news.sciencemag.org/scienceinsider
Science Policy News and Analysis

SCIENCEONLINE FEATURE
www.sciencemag.org/sciext/gonzoscientist/

THE GONZO SCIENTIST: The Science Hall of Fame
The frequency with which names appear in books has been used to create a pantheon of the most famous scientists of the past two centuries (with video).
>> News story p. 135; Research Article p. 176

SCIENCE (ISSN 0036-8075) is published weekly on Friday, except the last week in December, by the American Association for the Advancement of Science, 1200 New York Avenue, NW, Washington, DC 20005. Periodicals Mail postage (publication No. 484460) paid at Washington, DC, and additional mailing offices. The title SCIENCE is a registered trademark of the AAAS. Domestic individual membership and subscription (51 issues): $149 ($74 allocated to subscription). Domestic institutional subscription (51 issues): $990; Foreign postage extra: Mexico, Caribbean (surface mail) $55; other countries (air assist delivery) $85. First class, airmail, student, and emeritus rates on request. Canadian rates with GST available upon request, GST #1254 88122. Publications Mail Agreement Number 1069624. **Printed in the U.S.A.**

Change of address: Allow 4 weeks, giving old and new addresses and 8-digit account number. **Postmaster:** Send change of address to AAAS, P.O. Box 96178, Washington, DC 20090–6178. **Single-copy sales:** $10.00 current issue, $15.00 back issue prepaid includes surface postage; bulk rates on request. The identification code for *Science* is 0036-8075. *Science* is indexed in the *Reader's Guide to Periodical Literature* and in several specialized indexes.

AAAS
ADVANCING SCIENCE, SERVING SOCIETY

EDITED BY STELLA HURTLEY

Influenza in Flight >>

Avian influenza is a persistent problem, directly challenging commercial chicken producers, threatening wild bird populations, and providing a reservoir for variants that might emerge as human pathogens. **Lyall *et al.*** (p. 223) have taken the first steps toward producing transgenic domestic chickens that block onward transmission of influenza virus. An RNA "decoy" was made that contained the sequence for the virus's polymerase enzyme that is essential for replication. In infected chickens, the virus was not able to replicate effectively enough to transmit infection, but the chickens still died from influenza, so some refinement will be needed to make a useful disease-resistant flock. Nevertheless, the strategy offers the potential for significant advantages over vaccination, avoiding the risks from strain variation, cryptic circulation, and resistance.

Watching the Restructuring of Working Surfaces

The surfaces of inorganic materials can often restructure if they are heated in an atmosphere of reactive gases—the conditions that industrial catalysts normally encounter during use. Experimental studies of these restructuring processes have been challenging because many surface-sensitive methods work best under high vacuum. Recently, techniques have been developed that allow surface structure to be determined in the presence of gases with partial pressures reaching nearly 1 atmosphere. **Tao and Salmeron** (p. 171) review some of the changes that can occur in nanoparticles, metal surfaces, and catalysts when the vacuum environment is replaced with reactive gases such as nitrous oxide, carbon monoxide, and hydrogen.

Controlling Inflammation

Lipids that mediate the inflammatory response are synthesized from arachidonic acid by the enzyme 5-lipoxygenase (5-LOX). An intrinsic instability of 5-LOX has been proposed to regulate its activity. Structures of related enzymes have shown that the C terminus penetrates the enzyme so that the main chain carboxylate of the C-terminal residue binds the catalytic iron. **Gilbert *et al.*** (p. 217) identified a sequence that probably destabilizes the orientation of the C terminus in 5-LOX and, by substituting this sequence, were able to purify a stable enzyme and determine its crystal structure. The structure is consistent with the proposed mechanism of enzyme inactivation and provides a basis for the design of 5-LOX–specific inhibitors.

Books, Books, and More Books

The printed word has great power to enlighten, but it is impossible for an individual person to read more than a fraction of all books written, let alone to apply quantitative methods to analyze linguistic and cultural changes as they manifest themselves in words appearing in books. **Michel *et al.*** (p. 176, published online 16 December) performed an informatic analysis of approximately 4% of all books printed ranging from the year 1800 to 2000 and present analyses of the evolution of grammar, obsolescence of words, and which kinds of people become famous, when, and for how long. They also dissect the impact of censorship and suppression, notably during the Nazi period, which the authors term "culturomics." The analysis suggests new ways to think, not only about books and text analysis but also about culture, history, and the social sciences.

Computer Scientists Learn from Flies

Designing distributed networks of computers that work together to solve a problem without any single processor receiving all of the inputs or observing all of the outputs represents a difficult problem. **Afek *et al.*** (p. 183) noted the similarity of this problem to the process of patterning of sensory bristles on the fruit fly. By studying the developmental process in the fly and modeling its mechanism, the authors derived an algorithm that works efficiently to solve the computer science problem of identifying what is known as a "maximal independent set" that may prove useful in the design of wireless networks.

Quantum Half-Measures

Superfluid properties of fermionic systems stem from the pairing of the constituent fermions that then undergo Bose-Einstein condensation. Usually, the pairs are made up of spins of opposite orientation. When such superconductors are exposed to a magnetic field, they either expel it entirely or form a lattice of vortices, each encompassing a precisely quantized magnetic flux. However, spin triplet phases observed in the exotic superconductor, Sr_2RuO_4, have been predicted to support vortices with half the flux of regular vortices. **Jang *et al.*** (p. 186) measured the magnetization of pieces of Sr_2RuO_4 with annular geometry and observed the formation of magnetization steps of half the usual height, consistent with the presence of half-quantum vortices, which may help in future quantum computing applications.

Toluene Transformation

In addition to functioning as a solvent, the aromatic hydrocarbon toluene is a raw material for synthesis of a variety of pharmaceuticals, cosmetics, and agrichemicals. However, currently applied oxidation methods are somewhat inefficient and often require corrosive conditions. **Kesavan *et al.*** (p. 195) now show that nanoparticles composed of a gold and palladium mixture can catalyze the oxidation of toluene to a commercially useful ester, benzyl benzoate, with high yield and selectivity. The reaction uses O_2 as oxidant and proceeds in the absence of solvent.

CREDITS (TOP TO BOTTOM): NORRIE RUSSELL/THE ROSLIN INSTITUTE, UNIVERSITY OF EDINBURGH; GILBERT *ET AL.*

Harnessing Janus Behavior

Clusters of atoms or particles will behave in ways intermediate between single atoms or particles and bulk material. **Chen *et al.*** (p. 199) designed colloidal Janus particles with a charged surface on one half and a water-hating surface on the other. This schizoid nature caused the particles to cluster and pack in specific arrangements, which could be controlled through the addition of salt. With the right balance of forces, chiral helices formed with occasional spontaneous switch in handedness when connections between neighboring particles were broken and reformed.

The Strength of Convection

The rate of formation of deep water in the North Atlantic has a major effect on the overturning circulation of the Atlantic Ocean, which in turn affects global climate. A great deal of information about ocean overturning circulation can be had by determining the amount of radiocarbon throughout the water column. **Thornalley *et al.*** (p. 202; see the Perspective by **Sarnthein**) provide radiocarbon records from five deepwater sites in the North Atlantic, spanning the interval from 22 to 10 thousand years ago, to reconstruct the history of North Atlantic deepwater formation. The data suggest connections between the strength of overturning circulation, the origins of different water masses, and patterns of atmospheric circulation, which have a strong influence on land temperatures and global climate.

Rise of the Dinosaurs

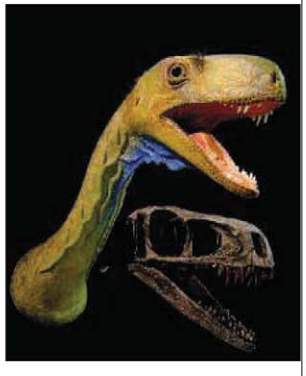

Dinosaurs emerged in the Triassic and became dominant toward its end, some 220 million years ago. One of the best records of the early evolution of dinosaurs is preserved in the Ischigualasto Formation in northwestern Argentina. To understand controls on this early evolution, **Martinez *et al.*** (p. 206) traced the abundance, emergence, and extinctions of dinosaurs and other vertebrate species, and they describe a basal theropod that clarifies some early dinosaur relations. By 230 million years ago, dinosaurs were both the dominant carnivores and small herbivores in this region. Other herbivores gradually became extinct locally, implying that the dinosaurs did not suddenly expand into vacant niches.

Write Your Worries Away

Tests and exams are stressful for many people. Students who "choke" at an exam may perform less well than their knowledge base warrants. Such results can accumulate to generate reduced educational achievements and expectations. Studying young adults performing math tests, **Ramirez and Beilock** (p. 211) found that a brief intervention—writing about their anxiety about the upcoming exam—helped students to do better in the exam. Perhaps by acknowledging their fears, students were able to tame distracting emotions.

Death of the Salmon

Despite large reductions in fisheries harvests, wild salmon stocks in Canada are suffering high levels of mortality before they manage to reproduce—40 to 95% of fish are dying each year en route to their spawning grounds. **Miller *et al.*** (p. 214) have found a consistent association between fish mortality and a specific genomic expression signal. The past 10 years have seen unprecedentedly warm river temperatures, and salmon have died in greatest numbers in "hotspots" along the river system, possibly as a result of poor oxygen availability and disease, with some stocks being more severely affected than others.

The Power of Women's Tears

Emotional tears are thought to be uniquely human and have puzzled biologists and psychologists for many years. Using a double-blind study comparing female emotional tears with control saline, **Gelstein *et al.*** (p. 226, published online 6 January) investigated whether human tears may convey a chemosignal. Even though the tears could not be smelled, tears nevertheless decreased the sexual appeal of women's faces. Female tears also lowered sexual arousal and reduced testosterone levels in men. A subsequent brain-imaging study highlighted differences in functional activation in the brain. Emotional tears thus seem to contain chemosensory signals related to sociosexual behavior.

CREDIT: MIKE HETTNER, PAUL SERENO, AND TODD MARSHALL

INTRODUCING

AAAS **Member**Central

The exclusive new website for the AAAS member community.

AAAS MemberCentral is a new website focused on helping you — the scientists, engineers, educators, students, policymakers, and concerned citizens who make up the AAAS community — connect like never before.

On MemberCentral you can contribute to discussion groups or blogs, participate in a webinar, or share photos of your field research. You can exchange ideas, learn about your fellow members, and gain fresh insights into issues that matter to you the most. MemberCentral is also an easy access point for a wide variety of other AAAS membership benefits, like discounts on cars and books, travel opportunities, and more.

Experience MemberCentral for yourself. Visit MemberCentral.aaas.org today and log in using your *Science* online username and password.

AAAS

MemberCentral.aaas.org

Freeman A. Hrabowski III is president of the University of Maryland, Baltimore County. He chaired the committee that wrote the report *Expanding Underrepresented Minority Participation: America's Science and Technology Talent at the Crossroads*. E-mail: hrabowsk@umbc.edu.

Boosting Minorities in Science

MANY COUNTRIES ARE INCREASING INVESTMENTS IN SCIENCE AND TECHNOLOGY TO IMPROVE THEIR economies and the well-being of their citizens. For the United States, this priority was emphasized in the influential National Academies 2005 report *Rising Above the Gathering Storm*, which called for new funding to bolster education in science, technology, engineering, and mathematics (STEM). But this past September, the Academies reported in *Expanding Underrepresented Minority Participation* that the United States faces a major obstacle in fulfilling this goal.* Because the minority groups underrepresented in science and engineering are the most rapidly growing in the U.S. population, the country must develop strategies to harness this resource to grow a robust science and engineering workforce and remain globally competitive.

The U.S. labor market is projected to grow faster in science and engineering than in any other sector, according to the U.S. Bureau of Labor and Statistics. In 2006, underrepresented minorities, including African Americans, Hispanics, and Native Americans, constituted only 9% of the nation's science and engineering labor force, while accounting for nearly 30% of the population. Non-U.S. students (particularly from China and India) account for almost all of the growth in U.S. STEM doctorates awarded in the past 15 years, but many eventually return to their own countries, taking their talents with them.

At present, only 6% of all 24-year-old Americans hold an undergraduate degree in STEM disciplines; for African Americans, Hispanics, and Native Americans, the percentage hovers at 2 to 3%. To reach a national target of 10% (a target already achieved by several countries), the United States will need to quadruple the number of underrepresented minorities with undergraduate degrees in these disciplines. A good place to start is retaining those minority undergraduate students who begin their studies in pursuit of degrees in STEM fields. At present, only about 20% of minority STEM aspirants complete STEM degrees, compared to 33% of white STEM aspirants. Preventing attrition will raise the number of minority doctoral students and will likely boost interest among younger minority students. Increased retention will require increased financial support; the Academies 2010 report estimates that such support would require $150 million per year to start. An urgent task for colleges and universities is to redesign first-year STEM classes to encourage active learning and collaboration. Engaging students through these types of classes should improve the performance of all students, and it could be particularly helpful in reducing the high rate of attrition for many minorities in STEM subjects.

Just as important for minority students are social support and mentoring. Some are the first in their families to go to college; others simply feel isolated. Fortunately, lessons have been learned from proven, broad-based initiatives such as the U.S. National Science Foundation's Louis Stokes Alliances for Minority Participation and the U.S. National Institutes of Health's Minority Access to Research Careers program. Best practices include precollege summer programs, substantive early research experiences, academic support, social integration, and faculty involvement.

Over the long term, it is imperative that the United States improve the quality of science and math instruction for minorities through the precollege years. Better teacher preparation would particularly benefit minority students, who still have substantial achievement gaps in math and science as compared to white students. It is also necessary for schools to provide advanced science courses and proper academic advising to ensure that more students are prepared to succeed in college science. In the United States, with the new Common Core State Standards Initiative for mathematics, universities and school systems can together strengthen teaching and develop appropriate curricular and assessment materials. Such collaboration will be critical as the nation strives to engage more students in science and engineering. **– Freeman A. Hrabowski III**

10.1126/science.1202388

*www.nap.edu/catalog.php?record_id=12984#toc.

EDITED BY KRISTEN MUELLER AND JAKE YESTON

ANTHROPOLOGY

Island Arrivals

One of the last major human expansions was the Polynesian colonization of the South Pacific Islands, extending from New Zealand to Hawaii in the north and several remote islands thousands of kilometers to the east. This colonization had a huge impact on the flora and fauna of the region. The timing and duration of this migration have been debated, and estimates and radiocarbon dates range over thousands of years. Wilmshurst *et al.* assessed more than 1400 radiocarbon dates from the various islands and grouped them on the basis of which materials were analyzed and how well they represented human occupation (for example, short-lived seeds in archaeological contexts versus marine shells, which carry additional uncertainties). Their grouping of the most reliable materials and ages implies that colonization proceeded in two short episodes, first in the Society Islands from 1025 to 1120 CE, then elsewhere to the east from 1190 to 1290 CE. These ages are later and briefer than many previous assessments for this expansion. — BH

Proc. Natl. Acad. Sci. U.S.A. 10.1073/pnas.1015876108 (2010).

CELL SIGNALING

Deadly Insulin Receptors

A new way of signaling has been detected for one of the most highly studied hormone receptors: the insulin and the related insulin-like growth factor receptors. These receptors, when activated by ligand binding, initiate signaling mechanisms that protect cells from apoptosis and favor cell survival. Thus Boucher *et al*. were surprised to find that in mouse brown adipose tissue cell lines, the loss of both receptors in the same cell actually made cells resistant to stimuli that normally promote apoptosis. Ligand deprivation of receptor-expressing cells, however, did not cause this effect. This suggests that the receptors, in the absence of hormone binding, are not "turned off" but rather appear to be producing a signal that is permissive for cell death. The receptors thus join a family known as "dependence receptors" because in their presence, a cell is addicted to the presence of growth factor in order to prevent the proapoptotic effect of the unliganded receptor. — LBR

Sci. Signal. **3**, ra87 (2010).

NEUROSCIENCE

Less Is More

In the vertebrate central nervous system, intercellular junctions (synapses) that form between neurons control the transmission of information associated with learning, memory, and behavior. Forging this network is a dynamic process, involving proteins at the synaptic cleft that function in the formation, maturation, and remodeling of these connections. Robbins *et al*. genetically engineered mice to overexpress or lack SynCAM1, a cell adhesion molecule that links synaptic neurons. Electron microscopy revealed a decrease in the number of excitatory synapses that formed in the forebrain of postnatal and adult SynCAM1-deficient mice as compared to normal mice. Conversely, an increase in excitatory synapses in the same region was observed in animals overexpressing SynCAM1. The surprise was that activity-dependent decreases in synaptic strength were impaired when SynCAM1 expression was increased, indicating a loss of this plasticity mechanism when there are more neuronal connections. Mice overexpressing SynCAM1 also performed poorly in spatial learning and memory tests. The authors propose that too much SynCAM1 may stabilize synapses to an extent that prevents the elimination of ineffective connections, a pruning process that supports synaptic plasticity. — LC

Neuron **68**, 894 (2010).

GENETICS

Separation in Hybridization

Hybridization between two plant species followed by a chromosomal doubling can lead to new species such as the allopolyploid species *Arabidopsis suecica*. Such hybridization requires genomic silencing and deletion because of functional redundancy among homoeologs (genes that encode proteins that perform similar functions among species). Using microarrays, Chang *et al.* determined the relative contribution of the parental strains to the transcriptome of *A. suecica*. They found that the retention of homoeologous genes that are translated into interacting pairs of proteins tended to belong to one parent or the other and that protein networks arising from genes originating in both of the hybrid parents were underrepresented. On the basis of these results, the authors surmise that the bias against genetically mixed complexes may contribute to a greater phenotypic diversity within the hybrid species and may explain the evolutionary success of polyploid species. — LMZ

Genome Biol. **11**, R125 (2010).

CREDITS (TOP TO BOTTOM): JIM ZUCKERMAN/CORBIS; CAROLINE JOSEFSSON AND LUCA COMAI

MOLECULAR BIOLOGY

Un-ruley Translation

Several inherited neurodegenerative diseases are referred to as "triplet repeat disorders" because they are caused by the aberrant expansion of three consecutive nucleotides near or within specific disease genes. CAG and CTG repeats, for example, are found in certain forms of myotonic dystrophy, spinocerebellar ataxia, and Huntington's disease. Numerous hypotheses have been proposed to explain how these DNA repeats contribute to disease pathogenesis, including toxic or inhibitory interactions of the expanded encoded RNA or protein with the normal protein.

Adding further complexity to the issue is the new discovery that triplet repeat sequences do not always obey canonical rules of protein synthesis. Studying RNA constructs harboring expanded CAG and CTG repeats, Zu *et al*. found that the repeats were translated in all three reading frames, thereby generating aberrant proteins containing polyglutamine, polyalanine, or polyserine. Synthesis of these proteins occurred in the absence of an ATG start codon (normally a prerequisite for translational initiation), possibly because the repeats form hairpin structures that allow initiation to occur at suboptimal sites. These results suggest that such proteins may play a role in the pathogenesis of CAG and CTG expansion disorders and, in a more general sense, they raise the possibility that other repeat sequences in the genome once thought to be silent may in fact be translated into proteins. — PAK

Proc. Natl. Acad. Sci. U.S.A. 10.1073/pnas.1013343108 (2010).

CHEMISTRY

Supports for Mechanisms

The mechanism of the low-temperature oxidation of CO by gold nanoclusters on oxide supports could depend on whether the oxide is a reducible metal, such as iron or titanium, or a nonreducible one, such as zinc. Carley *et al*. studied the oxidation of CO by gold nanoparticles supported on Fe_2O_3 and ZnO. The catalysts were exposed to a transient pulse of reactants (CO and O_2) in an argon carrier at room temperature. When the catalysts were predosed with ^{18}O-labeled water to form labeled surface hydroxyl groups, the initial CO_2 product that formed on the zinc oxide support carried all three possible isotope distributions, but on iron oxide support, the initial CO_2 product was fully ^{18}O-labeled. These results are consistent with the formation of a nondissociative bicarbonate intermediate on the zinc oxide support, contrasting with a CO dissociation mechanism on iron oxide, where the adsorbed carbon reacts with surface hydroxyls. This dissociative mechanism is supported by x-ray photoelectron spectra, which showed the formation of adsorbed carbon after exposure to CO and O_2 (but not CO alone). Density functional theory calculations show that oxidation of the gold atoms at the edge of the adsorbed clusters, along with the formation of surface bonds, can compensate for the high energy input needed to cleave CO and O_2. — PDS

Phys. Chem. Chem. Phys. **13**, 10.1039/c0cp01852j (2011).

MATERIALS SCIENCE

Order of a Sort

In amorphous solids and liquids, there is no long-range translational or rotational ordering of the atoms, whereas in crystalline materials, the positions of all the atoms can be ascertained by symmetry from knowing the positions of only a few of them. In between these extremes are glassy materials, which have short- and medium-range order that spans from nearest neighbors to about 100 nm. The nature of this ordering has been a mystery and is very hard to probe experimentally, because any interference peaks that might be generated from a small volume are smeared out under normal diffraction conditions. Hirata *et al.* studied the structure of a $Zr_{2/3}Ni_{1/3}$ metallic glass using nanobeam electron diffraction combined with ab initio molecular dynamics simulations. The electron beam could be tuned in size down to a minimum diameter approaching 0.3 nm. At a diameter of 0.72 nm, the authors were able to see distinct diffraction spots; these took on a twofold symmetry similar to that of a crystal when probed with a 0.36-nm-diameter beam. Voronoi polyhedra were used to design a local atomic environment from which the authors were able to compare their diffraction data with simulations, including the case of a pair of clusters that shared a common face. The overlapping of these data appears to confirm the recently proposed cluster model for the description of short- and medium-range order in a metallic glass. — MSL

Nat. Mater. **10**, 28 (2011).

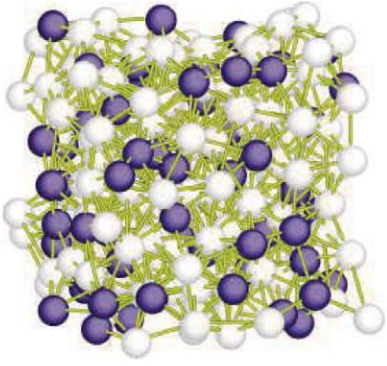

CREDIT: HIRATA *ET AL.*, *NAT. MATER.* **10**, 28 (2011)

www.sciencemag.org

Science

1200 New York Avenue, NW
Washington, DC 20005
Editorial: 202-326-6550, FAX 202-289-7562
News: 202-326-6581, FAX 202-371-9227
Bateman House, 82-88 Hills Road
Cambridge, UK CB2 1LQ
+44 (0) 1223 326500, FAX +44 (0) 1223 326501

Subscription Services For change of address, missing issues, new orders and renewals, and payment questions: 866-434-AAAS (2227) or 202-326-6417, FAX 202-842-1065. Mailing addresses: AAAS, P.O. Box 96178, Washington, DC 20090-6178 or AAAS Member Services, 1200 New York Avenue, NW, Washington, DC 20005

Institutional Site Licenses please call 202-326-6755 for any questions or information

Reprints: Author Inquiries 800-635-7181
Commercial Inquiries 803-359-4578

Permissions 202-326-7074, FAX 202-682-0816

Member Benefits AAAS/Barnes&Noble.com bookstore www.aaas.org/bn; AAAS Online Store www.apisource.com/aaas/ code MKB6; AAAS Travels: Betchart Expeditions 800-252-4910; Apple Store www.apple.com/eppstore/aaas; Bank of America MasterCard 1-800-833-6262 priority code FAA3YU; Cold Spring Harbor Laboratory Press Publications www.cshlpress.com/affiliates/aaas.htm; GEICO Auto Insurance www.geico.com/landingpage/go51.htm?logo=17624; Hertz 800-654-2200 CDP#343457; Office Depot https://bsd.officedepot.com/portalLogin.do; Seabury & Smith Life Insurance 800-424-9883; Subaru VIP Program 202-326-6417; VIP Moving Services www.vipmayflower.com/domestic/index.html; Other Benefits: AAAS Member Services 202-326-6417 or www.aaasmember.org.

science_editors@aaas.org	(for general editorial queries)
science_letters@aaas.org	(for queries about letters)
science_reviews@aaas.org	(for returning manuscript reviews)
science_bookrevs@aaas.org	(for book review queries)

Published by the American Association for the Advancement of Science (AAAS), *Science* serves its readers as a forum for the presentation and discussion of important issues related to the advancement of science, including the presentation of minority or conflicting points of view, rather than by publishing only material on which a consensus has been reached. Accordingly, all articles published in *Science*—including editorials, news and comment, and book reviews—are signed and reflect the individual views of the authors and not official points of view adopted by AAAS or the institutions with which the authors are affiliated.

AAAS was founded in 1848 and incorporated in 1874. Its mission is to advance science, engineering, and innovation throughout the world for the benefit of all people. The goals of the association are to: enhance communication among scientists, engineers, and the public; promote and defend the integrity of science and its use; strengthen support for the science and technology enterprise; provide a voice for science on societal issues; promote the responsible use of science in public policy; strengthen and diversify the science and technology workforce; foster education in science and technology for everyone; increase public engagement with science and technology; and advance international cooperation in science.

Information for Authors
See pages 352 and 353 of the 15 January 2010 issue or access www.sciencemag.org/about/authors

Save the Cucumbers?

When it comes to overfishing, tuna and sharks tend to hog the limelight. But spare a thought for the sea cucumbers. These elongated, leathery echinoderms, used in Asian soups and medicine, are being rapidly depleted, according to the first quantitative global analysis, published online 30 December in *Fish and Fisheries*.

Marine ecologists Heike Lotze and Sean Anderson of Dalhousie University in Halifax, Canada, and colleagues analyzed global catch data and, where available, management reports from regional authorities. They found that 81% of sea cucumber fisheries have declined, many substantially. Meanwhile, the rising demand for the creatures, which can fetch up to $400 per kilogram dry weight, has made fisheries start to decline much sooner than before—typically after 6 years rather than the 34 years it took in 1960.

Sea cucumbers are vulnerable to overfishing because they grow and reproduce slowly and aggregate in particular areas, making them easy to catch. Compounding the problem, more than a third of sea cucumber fisheries have no regulations at all, Lotze says—an argument for setting up marine reserves for these unlikely poster animals.

Science and Magic: Mexicans Choose Both

In Mexico, magical beliefs go hand in hand with strong faith in science, a recent survey of public perception of science and technology shows.

The study, compiled by the country's National Council on Science and Technology and the National Institute of Statistics and Geography, found that a large percentage of Mexicans believe in homeopathy, acupuncture, lucky numbers, and ESP. About 38% agree that "space vehicles from other civilizations" visit Earth. At the same time, most Mexicans surveyed also said the country needs more researchers, and more than eight in 10 agreed that they depend too much on faith over science.

"In developing nations, there is a greater tendency to believe in magic of various kinds," says Jon Miller, director of the International Center for the Advancement of Scientific Literacy at the University of Michigan, Ann Arbor. Miller, who wrote many of the survey questions used, says acceptance of both science and religion is highest in developing countries. "They tend to view them as separate issues," he says.

Mexicans both fear and respect scientists, the survey showed: 57% of people interviewed agreed that "due to their knowledge, scientific researchers have power that makes them dangerous."

Ingenious Engineers

This year, innovations in biotechnology have snatched up two of the three heftiest National Academy of Engineering prizes. The annual Charles Stark Draper Prize goes to Frances H. Arnold, a molecular engineer at the California Institute of Technology, and Willem P. C. Stemmer, founder and CEO of Amunix Inc. in Mountain View, California, for their work on the "directed evolution" method of generating enzymes with novel properties, which is now used in fields from biofuel research to drug development. Leroy Hood, co-founder and president of the nonprofit Institute for Systems Biology in Seattle, Washington, wins the biennial Fritz J. and Dolores H. Russ Prize for inventing the first DNA and protein sequencers and synthesizers, as well as an inkjet printer for DNA arrays. The annual Bernard M. Gordon Prize for Innovation in Engineering and Technology Education goes to Edward Crawley of the Massachusetts Institute of Technology, who created the Conceive, Design, Implement, Operate Initiative, an engineering curriculum that emphasizes hands-on learning. Each prize comes with $500,000 and will be awarded at a ceremony on 22 February.

Clockwise from top left: Arnold, Stemmer, Hood, and Crawley.

SUBATOMIC SHUFFLE

Prefer particle physics to poker? Pick up a deck of the Quark Matter Card Game, and you can have both. Instead of kings and queens, the cards feature quarks (up, down, and strange); muons, electrons, and their neutrinos; and antiparticles for all.

Hungarian high school students Csaba Török and Judit Csörgő invented the deck with Judit's father, Tamás, a physicist at the KFKI Research Institute for Particle and Nuclear Physics in Budapest. The simplest game is "Anti," in which players quickly identify particle and antiparticle combinations, bearing in mind a quantum-mechanical property called "color" indicated by the color of the card. It's an abstract concept, but "even children who cannot read can learn the rules," Tamás says. For adult players, he recommends "Quark Matter," which starts with cards densely piled to represent the quark-gluon plasmas physicists cook up at Brookhaven National Laboratory's Relativistic Heavy Ion Collider (RHIC), where Tamás works on the PHENIX experiment. Players draw cards according to the physics of how the plasma expands and reforms into particles known as hadrons.

The cards and rule book can be ordered or downloaded from the self-publishing site Lulu (http://scim.ag/qm-cards). Now RHIC physicists can play the game while waiting for the beam, Tamás says. In any case, he says, "It's a really nice feeling to walk around with elementary particles in your pocket."

CREDITS (TOP TO BOTTOM): SEAN ANDERSON; INSET: IMAGE QUEST MARINE; NAE (4); QUARK MATTER; INSET: SOURCE: TAMÁS CSÖRGŐ

Transgenic chickens block flu spread
132

Dinosaurs' tangled roots
134

GENETIC TESTING

New High-Tech Screen Takes Carrier Testing to the Next Level

In the fall of 2008, Stephen Kingsmore, a longtime gene hunter, was approached by two biotech entrepreneurs. One of them, Craig Benson, had just learned that his 5-year-old daughter had juvenile Batten disease, a rare, fatal, inherited, neurological disorder. The pair had a question for Kingsmore: Could he develop a cheap, reliable genetic test for Batten and other equally horrible diseases, available to all parents to prevent the conception or birth of affected children? Their goal was simple: Do everything possible to eradicate these diseases, because, knowing now which genes cause them, we can.

At the time this kind of screening, called carrier testing, was relatively uncommon. Both parents need to carry the same mutated gene for their child to develop a disease like Batten, and many of these recessive diseases are vanishingly rare. The number of affected children born each year can be in the single digits. Given that, it hasn't made fiscal sense to offer tests for dozens of diseases to everyone when so few couples will be carriers of any given one. In communities in which certain mutated genes pop up more often, such as Ashkenazi Jews, carrier testing has been common for years and has drastically reduced the number of babies born with diseases like Tay-Sachs.

But DNA sequencing technology was moving fast and costs were dropping. What the two men proposed might now be doable, Kingsmore thought. He took on the project.

Two years later, Kingsmore, bioinformaticist Callum Bell, and their colleagues describe in a paper published online this week by *Science Translational Medicine* (http://stm.sciencemag.org/content/3/65/65ra4.full) what appears to be the broadest application of "next-generation sequencing" to a medical problem. They used technology that, in Kingsmore's words, "sprays the genome with sequences" to look for mutations in the genes behind 448 childhood recessive diseases. The experience has been career-changing for Kingsmore: This week, he moves from the National Center for Genome Resources in Santa Fe, which conducts basic genetics research, to Children's Mercy Hospital in Kansas City, Missouri. There, with support from the hospital and the Beyond Batten Disease Foundation formed by Benson and his wife, Charlotte, he will work to make the test clinically available, he hopes for $500, before the end of the year. The test will be sold by the foundation, which will use some of the proceeds for research into Batten disease and support for families living with it.

This carrier test is different from others now offered, including one for more than 100 diseases sold through physicians around the United States by the California company Counsyl. Those tests all hunt for previously identified genetic mutations for various diseases, working from a list that cobbles together what's been described in the scientific literature. This captures many carriers, but not all of them. "For some diseases, the mutations on these panels may only account for 20% of mutations" that can cause disease, says Wendy Chung, who directs the clinical genetics program at Columbia University. This means that someone could be told they're not a carrier when in fact they are.

Next-generation sequencing changes that. Instead of starting with the mutations we know about, it sequences the same DNA again and again to reduce the likelihood of error, and then researchers look for any mutation in a gene involved in one of these rare diseases. The technology is being applied, still experimentally, across medicine, for instance, to diagnose uncommon diseases and to better understand cancer. But the first broad, real-world application will likely be carrier testing of prospective parents, because the medical challenge is straightforward and the technology is nearly ready.

There are still kinks. Among the trickiest is determining whether gene variants that no one has seen before could, when paired with a mutation on the same gene from the other parent, cause disease. We all harbor gene variants that are harmless. Distinguishing those from the pathological is "going to be quite difficult," says Lawrence Brody, chief of the genome technology branch at the National Human Genome Research Institute in Bethesda, Maryland.

Brody should know: For the past 14 years, he's run a database of mutations in *BRCA1* and *BRCA2*, genes involved in breast and ovarian cancer. About 10% of people tested for *BRCA* genes have a variant of uncertain significance. Brody and many others have been trying to determine which of these actually raise cancer risks.

When it comes to Kingsmore's test, "how

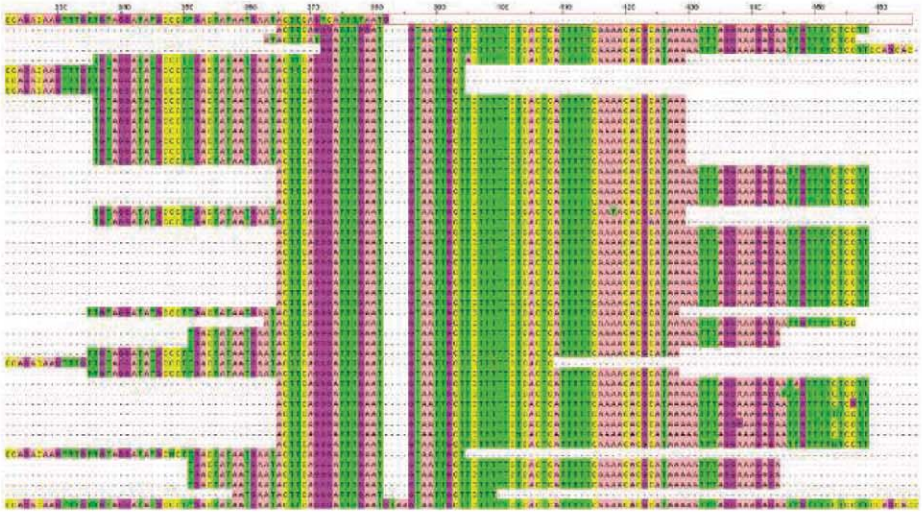

Missing DNA. A new genetic test identifies a four-base deletion that can cause Lesch-Nyhan syndrome, a rare childhood disease, when both parents carry the mutated gene. Here, "next generation sequencing" ran through one person's DNA many times for accuracy. The bottom line is from someone who doesn't carry the mutation.

CREDIT: C. J. BELL *ET AL.*, *SCIENCE TRANSLATIONAL MEDICINE* 3, 65 (12 JANUARY 2011)

Biological impacts of loneliness
138

Did swamps breed cities?
141

many people are going to be confident enough in discovering a new mutation that they'd be willing to terminate a pregnancy?" asks Stephen Quake, who studies biophysics and genomics at Stanford University in Palo Alto, California. Although one goal in all carrier screening is to encourage couples to screen prior to conception, that's currently rare.

In their test, Kingsmore and colleagues screened 104 unrelated individuals; on average people carried mutations for about three of the 448 diseases. The group built computer software to analyze the DNA sequences and, among other things, determine whether they matched mutations already published. They've since expanded the test to cover 570 diseases and are testing it on hundreds more people.

Kingsmore admits to a catch-22 when it comes to assessing whether a new variant is a problem: The best shot at doing so comes from carrier sequencing of many, many people, just as Brody is doing with *BRCA1* and *-2*. But this means that "initially this test will not have perfect knowledge of all diseases." He predicts it will be about a decade before that changes, and he isn't sure what, if anything, physicians and prospective parents should be told about variants of uncertain significance before then.

One benefit of next-generation sequencing is that it's far more accurate than what came before it. When double-checking the mutations that showed up in Kingsmore's small sample against published work, about a fifth of those were wrong. For example, he cites a paper published about 20 years ago on a mutation in a very rare disease, Lesch-Nyhan syndrome, which reported a massive DNA deletion. In fact, the deletion Kingsmore's team found in one person (which was predicted, based on bioinformatics analysis, to have the biological effect described in that older paper) was just four DNA bases long. "They never intended that initial paper to be the definitive paper 20 years ago," says Kingsmore. But as with work in so many rare diseases, studies are sparse and data often hard to come by. He and others hope that sequencing on a much bigger scale will change that, with time. **–JENNIFER COUZIN-FRANKEL**

HIGH-ENERGY PHYSICS

Fermilab to End Its Quest for Higgs Particle This Year

U.S. researchers will soon abandon their search for the most coveted particle in high-energy physics because of a lack of funding.

Researchers working at Fermi National Accelerator Laboratory (Fermilab) in Batavia, Illinois, had wanted to run their 25-year-old atom smasher, the Tevatron, through 2014 in hopes of spotting the so-called Higgs boson before their European counterparts could discover it with their newer, more powerful atom smasher. But officials at the U.S. Department of Energy (DOE), which funds Fermilab, informed lab officials this week that DOE cannot come up with the extra $35 million per year to keep the Tevatron going beyond September.

"Unfortunately, the current budgetary climate is very challenging and additional funding has not been identified. Therefore, … operation of the Tevatron will end in [fiscal year 2011], as originally scheduled," wrote William Brinkman, head of DOE's Office of Science, in a letter to Melvyn Shochet, chair of DOE's High Energy Physics Advisory Panel (HEPAP) and a physicist at the University of Chicago in Illinois. Pier Oddone, director of Fermilab, had stressed that the lab could not forsake future experiments to keep the Tevatron going. "Given the absence of additional funding, it's the right decision," Oddone says.

Brinkman's letter is the final chapter in a long, tense tale for scientists at Fermilab. Last February, officials at the European particle physics lab, CERN, near Geneva, Switzerland, announced that their Large Hadron Collider (LHC) would turn off for all of 2012 for repairs. That opened a window for physicists at Fermilab to spot the Higgs first—although CERN officials are now considering delaying repairs until 2013.

CREDIT: DOE

"[T]he current budgetary climate is very challenging and additional funding has not been identified."

—WILLIAM BRINKMAN, U.S. DEPARTMENT OF ENERGY

In August, Fermilab's scientific advisory panel recommended that lab officials keep running the Tevatron through 2014 even if they didn't get another dime to do so. That advice didn't sit so well with Oddone, who announced a month later that he could squeeze $15 million from the lab's $410 million annual budget but needed DOE to provide $35 million more. In October, a HEPAP subpanel approved Oddone's plan but said the Tevatron should be shuttered if DOE came up empty-handed.

Many physicists believe that the hunt for the Higgs, the theoretical key to explaining how all particles obtain mass, is the most important challenge in the field. They argue that the Tevatron's lower-energy and cleaner collisions could help Fermilab beat CERN in the race to uncover the Higgs if its mass falls in the range indicated indirectly by measurements on other particles—between 121 and 144 times the mass of a proton. Because the Tevatron collides protons into antiprotons, it could also probe how a new particle interacts with, or "couples" to, certain other particles in order to prove whether it's really the Higgs. The LHC cannot probe those connections as easily because it collides protons with protons.

"I think we presented a very good science case for continuing to run, but the fiscal realities just don't allow us to go forward," says Rob Roser, a physicist at Fermilab and co-spokesperson for the 600 researchers working with the CDF particle detector, one of two fed by the Tevatron. But DOE gave scientists a fair hearing, he adds: "They have to make very difficult decisions based on the realities. I can't fault them for that."

–ADRIAN CHO

AVIAN INFLUENZA

Transgenic Chickens Could Thwart Bird Flu, Curb Pandemic Risk

The chicken soup of the future might just be made from transgenic birds that can't get bird flu—if regulators decide they're safe and consumers don't object. U.K. scientists have created transgenic chickens that can't pass on avian influenza, a disease that decimates poultry flocks and that flu scientists fear could spawn an influenza pandemic among humans.

The study, published in this week's issue of *Science* (p. 223), "is extremely interesting as a proof of principle," says Timm Harder, a bird flu researcher at the Friedrich Loeffler Institute in Greifswald, Germany. But whether the chickens and their eggs are safe to eat—and whether the public will buy them—is an open question, Harder notes.

Avian influenza, which comes in many different subtypes, is primarily a disease of wild birds, but it occasionally ends up infecting poultry flocks, in which so-called highly pathogenic strains can spread like wildfire. For the virus, infected poultry flocks are a potential bridge to the human population, and the worry is that avian viruses could trigger a pandemic if they adapt to humans, says Laurence Tiley, a molecular biologist at the University of Cambridge in the United Kingdom and the last author of the new paper. The team also included scientists from the Roslin Institute and the Royal (Dick) School of Veterinary Medicine, both part of the University of Edinburgh, and the Veterinary Laboratories Agency in Weybridge.

Tiley and his colleagues equipped chickens with a so-called RNA-expression cassette, a piece of DNA that makes the birds produce a small, hairpin-shaped piece of RNA that acts as a decoy to polymerase, a key viral enzyme. Instead of binding to the virus's genome, which it helps replicate, polymerase now attaches itself to the hairpin RNA, rendering the enzyme useless. When transgenic chickens were exposed to the deadly H5N1 flu virus, they still succumbed to it. But they didn't pass the virus on to healthy cagemates—neither regular nor transgenic.

That means that only one or a few chickens would become infected if H5N1 entered a flock—in itself a big improvement, says Tiley. But the ultimate goal is to make the chickens completely impervious to the disease by adding several more gene constructs, as well as to introduce resistance against Newcastle disease and Marek's disease, two other viral threats.

Tiley and his colleagues chose their decoy carefully: It matches a short sequence on each of the eight genetic elements of the viral genome to which polymerase binds. To overcome resistance, the virus would have to change not only its polymerase enzyme but also the binding sequence in all eight gene segments, which Tiley says is extremely unlikely. It's "a smart strategy," says Carlos Lois of the University of Massachusetts Medical School in Worcester, but perhaps not foolproof, given that flu is a

RESEARCH FUNDING

Japan Boosts Competitive Grants at Expense of Big Science

TOKYO—Under what Prime Minister Naoto Kan calls "a budget for the reinvigoration of Japan," the country's main research grants program is slated for a whopping 32% increase to $3.2 billion in the coming year. Rank-and-file researchers are sure to be pleased with the better odds of winning support under the fiercely competitive program, says Kazuaki Kawabata, the education ministry's director of research and development policy.

With an emphasis on social welfare spending and "innovative research" to stimulate the economy, the record-breaking $1.1 trillion budget for the fiscal year starting in April is the first drawn up from scratch by Kan's Democratic Party of Japan, which captured the legislature in August 2009. Government-wide science spending has yet to be compiled. But the education ministry, which oversees most research, will see its S&T budget rise 3.3% to $20.2 billion. "Given the nation's fiscal circumstances, I think we have to be very grateful," says Kawabata.

The biggest percentage increase is going to Grants-in-Aid, the main source of support for individuals and small groups. In recent years only 20% of grant applications were successful, leaving a lot of deserving research unfunded, says Kawabata. In addition to giving the program its biggest single-year boost since its establishment in 1965, the administration is planning to relax rules requiring grants to be spent in the year they are awarded. Researchers have long wanted more flexibility in managing money.

In response to other requests from the scientific community, the new budget will expand existing programs and add new ones to foster the career development of younger researchers and ease the return of women to the research workforce after maternity leave, with support growing 5.4% to $414 million.

The Democratic Party's strategy to lean on research to spur economic growth is evident in its support for "innovative" research in life sciences and green technologies, which is rising 9% to $932 million. The portfolio includes stem cells and other aspects of regenerative medicine, next-generation cancer treatments and neuroscience, and creation of a new program under the Japan Science and Technology Agency that will look for "game changing" research in areas such as cost-efficient solar panels, says agency president Koichi Kitazawa.

For rent. A tight budget means the scientific drilling vessel *Chikyu* will spend half the year leased out for oil exploration.

CREDIT: JAMSTEC/IODP

Flu fighters. These transgenic chickens still die from bird flu; the ultimate goal is full resistance.

"master of mutability."

Flu-resistant chickens would have several advantages, says Harder. Bird flu vaccines work against only one subtype, they need to be updated frequently as the virus evolves, and they don't fully protect against infection, giving the virus a chance to spread silently. Flocks with built-in resistance would put an end to all that.

Transgenic chickens could theoretically replace nontransgenic breeds worldwide in a few years, says Michael Greger, director of Public Health and Animal Agriculture at the Humane Society of the United States located in Washington, D.C. That's because the trade in both broiler and egg-laying chickens has become consolidated in a handful of companies, which essentially determine what stocks are used by chicken farmers worldwide.

But Harder points out that these companies don't sell to the vast number of people in the developing world who have a small flock in their backyard or on their rooftop—and that's where avian influenza has been the most difficult to control. The strategy for reaching these small holders, says Tiley, would not be to make them buy their stock from big breeders; instead, he says, it should be possible to provide them with flu-free chickens that they can breed themselves.

–MARTIN ENSERINK

CREDITS (FROM TOP): THE ROSLIN INSTITUTE/UNIVERSITY OF EDINBURGH; PHOTOS BY NORRIE RUSSELL; (SOURCE) MINISTRY OF EDUCATION

For big science, however, the budget offers a mixed bag. Soon after coming to power, the Democratic Party staged a series of hearings that questioned spending on space, earth science, and a next-generation supercomputer (*Science*, 20 November 2009, p. 1046). The new budget, plus money from a supplementary budget adopted last November, provides funding to keep the supercomputer, planned to be the world's fastest, on track for completion in 2012.

JAPAN'S S&T BUDGET UPS AND DOWNS

Basic Grants	▲ UP 32%	to $3.2 billion
Life and Green Sciences*	▲ UP 9%	to $932 million
Young/Women Scientist Aid	▲ UP 5.4%	to $414 million
Major Facilities Construction	▲ UP 2.7%	to $965 million
Space Programs*	▲ UP 0.8%	to $2.2 billion
Earth Sciences	▼ DOWN 2.4%	to $631 million
Atomic Energy	▼ DOWN 3.7%	to $2.5 billion

*These items include support from a supplementary budget.

Winners and losers. The education ministry's science budget will rise 3.3% to $20.2 billion in 2011, with small grants winning the lion's share of the increase.

The space budget will rise a slim 0.8% to $2.2 billion, including $36 million to begin development of a second asteroid-return mission to succeed the Hayabusa sample-return project. Previous administrations had rejected a follow-up to Hayabusa, which was once thought lost in space. But popular interest after the craft returned to Earth this year with asteroid dust apparently warmed political hearts.

Other big science efforts are in for a rough ride. Spending on atomic energy research will drop 3.7% to $2.5 billion. And polar, oceanographic, and earthquake research is being squeezed 2.4%, to $631 million, including a roughly 4% cut for the Japan Agency for Marine-Earth Science and Technology (JAMSTEC), to $433 million. It will be the second annual budget cut in a row for JAMSTEC, which operates the deep-ocean drill ship *Chikyu*. Asahiko Taira, a JAMSTEC executive director, says each of the agency's divisions will have to tighten its belt. And they plan to lease *Chikyu* for commercial oil drilling for half of the year.

The budget will go before the legislature for approval this month. **–DENNIS NORMILE**

ScienceInsider

From the *Science* Policy Blog

The *British Medical Journal* has accused gastroenterologist Andrew Wakefield of committing scientific fraud in the publication of a **1998 paper in *The Lancet* linking vaccines to autism**. The paper had previously been retracted after a government investigation. http://scim.ag/Wakefield_inquiry

Despite a grim employment picture for would-be academic researchers, an outside panel says that the U.S. National Institutes of Health (NIH) should **maintain or even increase the number of graduate students and postdocs** it supports. It's part of the latest review by the National Research Council of NIH's main training program, the National Research Service Award. http://scim.ag/more-NRSA-awards

A new study by the U.K. Academy of Medical Sciences finds that British **biomedical researchers are drowning in paperwork**. The study suggests a new independent agency to coordinate and streamline the system. http://scim.ag/UK_paperwork

New White House Chief of Staff William Daley believes that **optimizing the federal innovation enterprise** might require "reorganization" of agencies. "You can't understand how screwed up it is," he said last month. Daley also defended a private-public joint research program from opponents on Capitol Hill during a stint as commerce secretary in the late 1990s. http://scim.ag/Daley_named http://scim.ag/Daley_ATP

The America COMPETES Act, which President Barack Obama signed last week, seeks to **strengthen education programs at NSF** with changes to graduate training programs, more support for undergraduate research, and a new program to train prospective science teachers. Meanwhile, Energy Department officials were glad that the final version of the act, though stripped down, authorizes small but steady increases for the Office of Science through 2013. http://scim.ag/COMPETES_ED http://scim.ag/COMPETES_DOE

For more science policy news, visit **http://news.sciencemag.org/scienceinsider**.

PALEONTOLOGY

Pint-Sized Predator Rattles The Dinosaur Family Tree

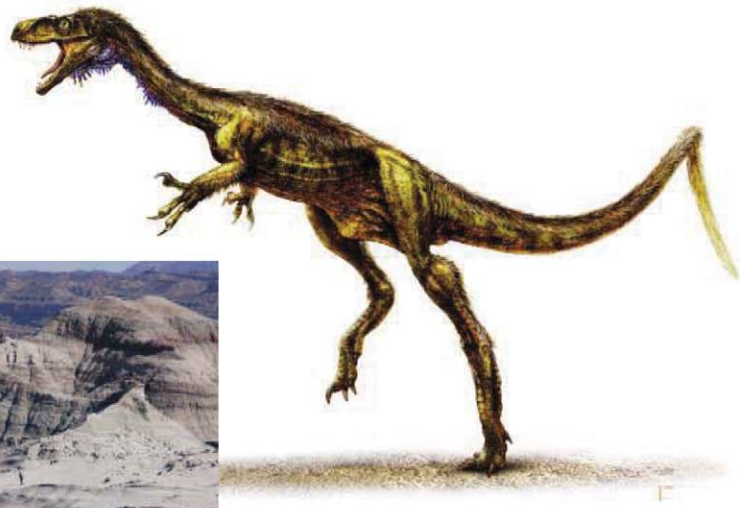

The demise of *Tyrannosaurus rex* and most other dinosaurs some 65 million years ago may grab all the headlines. But paleontologists are equally concerned with puzzling out how these mighty beasts got their start. Who were their ancestors? Did they burst onto the scene, sweeping their older reptilian rivals before them, or take a quieter, more gradual route to world domination?

On page 206, a team working in Argentina reports the discovery of a very early dinosaur—possibly a distant ancestor of *T. rex*—that lived about 230 million years ago, during what paleontologists call the dawn of the dinosaurs. The researchers say the new finds—two specimens that together make up a nearly complete skeleton of a diminutive, 1-meter-long dinosaur—and neighboring fossils show that dinosaurs didn't outcompete other reptiles, but rather gradually replaced them as their predecessors died out for other reasons. More controversially, the team says the fossils show that one of the most well-known early dinosaurs, *Eoraptor*, long considered an ancestor of meat eaters like *T. rex*, was actually an ancestor of gigantic plant-eating dinosaurs like *Apatosaurus*.

"The new specimens are remarkable," says Sterling Nesbitt, a paleontologist at the University of Washington, Seattle. Michael Benton, a paleobiologist at the University of Bristol in the United Kingdom, adds that the fossils—which the discovery team has assigned to a new species called *Eodromaeus murphi*—are "complete enough to add substantially to our knowledge" of early dinosaur evolution.

Tracing the origins of the earliest dinosaurs has been a major challenge for paleontologists because there are no uncontested fossils from their earliest days on Earth. By the time *Eoraptor* and other undisputed early dinosaurs came on the scene about 230 million years ago, most researchers have concluded, dinosaurs had already evolved into three major lineages: ornithischians, which later gave rise to armored beasts like *Stegosaurus* and *Ankylosaurus*; sauropodomorphs, the lineage that led to giant plant eaters like *Apatosaurus* and *Brachiosaurus*; and the meat-eating theropods, such as *T. rex* and *Allosaurus*.

The team that found *Eodromaeus* was led by the same two paleontologists who discovered and described *Eoraptor* in the early

Small daddy? Meter-long *Eodromaeus*, found in northwestern Argentina (*top*), sported serrated teeth and other similarities to later theropods (*bottom*).

1990s: Paul Sereno of the University of Chicago in Illinois, and Ricardo Martinez of the National University of San Juan in Argentina. In 1996, a volunteer from Japan working with Martinez in the Ischigualasto Valley of northwestern Argentina, also known as the Valley of the Moon, unearthed a small vertebra on the side of a hill. When Sereno arrived a couple of months later to help excavate the fossils, he and Martinez at first identified them as *Eoraptor*.

Frustratingly, many of the fossils were embedded in a huge block of rock. "It was an extraordinarily difficult specimen to clean" and prepare for analysis, Sereno says. But once enough of the bones were visible, it became clear "that this was no *Eoraptor*."

Instead, the team concluded, the find was a new species of early theropod. Evidence included its very long, serrated teeth; long finger bones that aided in grasping prey; and pockets in its neck vertebrae for air sacs, which some researchers think helped drive air into the lungs as in today's birds, the descendents of theropod dinosaurs. "I have no doubt that this is a new taxon, a very important one from a critical time … near the beginning of the age of dinosaurs," says Mark Norell, a paleontologist at the American Museum of Natural History in New York City. And Nesbitt says "the authors make a pretty good case that *Eodromaeus* is a theropod."

Sereno and Martinez themselves previously identified *Eoraptor* as the earliest known theropod. But after studying their original specimens more closely and comparing them with *Eodromaeus* and other dinosaurs, they now argue that *Eoraptor* was in fact an early plant-eating sauropodomorph. "No one, even ourselves, predicted this repositioning," Sereno says.

Other researchers are cautious. "Only further research by independent teams can evaluate" this radical shakeup of the early dinosaur tree, says Max Langer, a paleontologist at the University of São Paulo in Brazil. And Langer adds that the uncertainty about where to place *Eoraptor* "emphasizes how similar [early] theropods and sauropodomorphs" were to each other, which, he says, "is expected anyway in the early radiation" of an animal group.

Dinosaur experts are happier with a broader conclusion in the *Science* paper. By 230 million years ago, the authors write, all three dinosaur lineages—ornithischians, theropods, and sauropodomorphs—had already evolved their characteristic dietary behaviors (meat eating versus plant eating) and modes of locomotion (bipedal theropods, four-footed sauropodomorphs). Yet they still made up only about 11% of all vertebrate species at Ischigualasto. Another 30 million years would pass before they became dominant—evidence, the team argues, that dinosaurs did not drive other species to extinction but rather filled ecological niches that other reptiles left empty.

"Dinosaurs had all of their most noted advances prior to their takeover," says Sereno. Benton, who has independently concluded that dinosaurs did not outcompete their rivals, says the new work confirms his own "opportunistic replacement" model for dinosaur ascendancy. "What is new is the greater precision they can bring to bear on its timing," Benton adds. **–MICHAEL BALTER**

CREDITS (TOP TO BOTTOM): ILLUSTRATION BY TODD MARSHALL; PHOTO BY RICARDO MARTINEZ; PHOTO BY MIKE HETTWER

DIGITAL DATA

Google Books, Wikipedia, and the Future of Culturomics

BOSTON—Humanities scholars gathered for an unusual talk here on 8 May at the annual meeting of the American Historical Association. Jean-Baptiste Michel and Erez Lieberman Aiden, mathematicians at nearby Harvard University, focused on issues that are standard material for historians. They discussed, for example, the period of intense censorship in Nazi Germany that began with festive book burnings in 1933 and ended with the Nazi's surrender in 1945. Some of those books were written by Jewish intellectuals, others just contained ideas that were considered "un-German." Some scholars and artists who were highly influential virtually disappeared from public discourse when the Nazi Party came to power, while those favored by Nazi propaganda vaulted to prominence.

What was unusual was the method that Michel and Lieberman Aiden used to study censorship during that period. By tracking the rise and fall of people's names in millions of German and English books, the researchers identified not only people known to have been censored but also many whose suppression was not recorded. The mathematicians did not read those millions of books, of course. Instead, they performed a quantitative analysis of data they obtained from Google Books. "This is fantastic," says Anthony Grafton, a historian from Princeton University who was sitting in the audience. Grafton stresses that the technique is "a new starting point" for historical analysis rather than a replacement. "But it is amazing that you get a coherent picture of censorship in the public sphere."

On page 176 of this issue (and published online 16 December 2010), a team led by Michel and Lieberman Aiden introduce this and many other examples of this data-intensive approach to the humanities, which they call culturomics (*Science*, 17 December 2010, p. 1600). The entire data set that underlies their study—a mapping of the words from 4% of all books ever published—is now online for any researcher to explore. "But even with all those data," cautions Michel, "you'll need to carefully interpret your results." One of the big challenges, for example, is to correctly extract the names of individual people from those 500 billion words. A potentially valuable resource for this type of analysis is Wikipedia, the massive online encyclopedia, which contains entries for nearly 750,000 people born since 1800. But its shortcomings, from the reliability of its information to the organization of its content, become quickly apparent to those who use it. Several efforts are under way to improve Wikipedia as a teaching and research tool, including one by the Association for Psychological Science (APS).

Adrian Veres, one of the co-authors of the Michel *et al*. paper, experienced these problems firsthand. Veres, a chemistry and physics undergraduate at Harvard University, has been using Wikipedia to analyze the fame of scientists whose names appear in books over the centuries. His first task was to identify who among the myriad of people mentioned in books are actually scientists. He started by creating computer algorithms that scour Wikipedia for telltale words such as biologist, chemist, and physicist, as well as keywords that identify people in subfields such as ecology, physiology, and genetics.

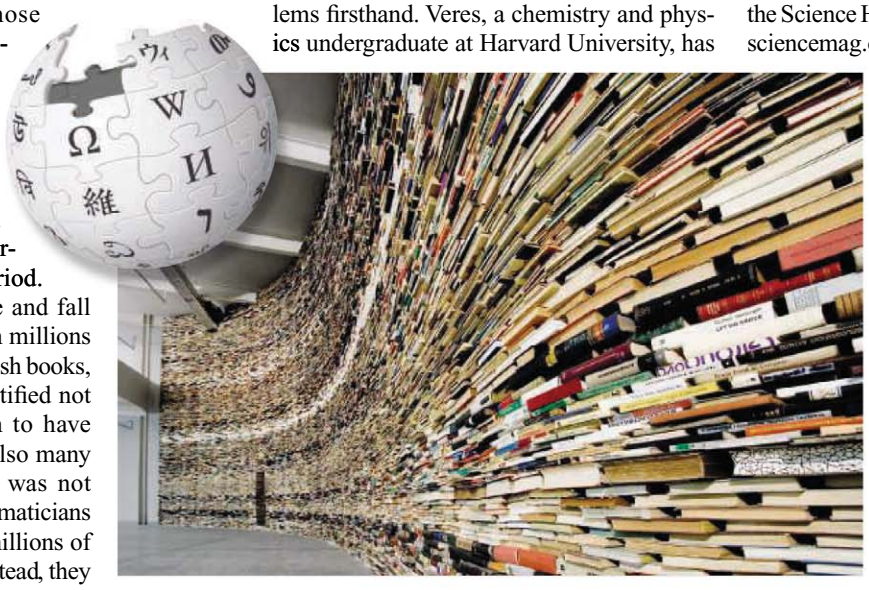

Working relationship. Improvements in Wikipedia will be needed for many research projects using Google's digitized books database.

Wikipedia's content is created through cooperative—and often combative—editing by millions of volunteers. But even if the information is correct, "not all of it is structured data" with clear labels, says Veres. It was a serious challenge for his algorithms to extract biographical information, such as years of birth and death, profession, and nationality, from entries that are a "bag of words." An online community effort called DBpedia has been enforcing structure onto Wikipedia entries, encouraging editors to sort the information into standard fields and then collecting those data for researchers to use. But that effort is only starting.

Veres whittled down about 7000 candidates to a list of 4209 physicists, chemists, biologists, and mathematicians who were alive between the years 1800 and 2000. He then ranked them by "fame"—as measured by the frequency with which those scientists' full names appear in books. He shared the early results of this analysis with *Science*. You may be surprised who tops the list. You can view the Science Hall of Fame online at http://www.sciencemag.org/content/331/6014/143.3.full.

Even so, Veres had to exclude the social sciences from his analysis because the Wikipedia entries were so unreliable. In the field of psychology, for example, Linda Bartoshuk, a psychophysicist and former APS president, was not detected as a scientist because of the paucity of details in her Wikipedia entry. (Bartoshuk was profiled in *Science* on 18 June 2010.)

Psychologists are aware of the problem. "Unfortunately, the quality of information about psychological science in Wikipedia is uneven," says Mahzarin Banaji, current APS president and a psychologist at Harvard. She is calling on psychology researchers, teachers, and students to improve Wikipedia themselves. APS is building a Web portal that will channel the effort with help from Robert Kraut and Rosta Farzan, computer scientists at Carnegie Mellon University in Pittsburgh, Pennsylvania, who specialize in human-computer interaction. The goal is to create "a more complete and accurate representation of our science," says Banaji. The Web portal is slated to debut 1 February at www.psychologicalscience.org.

When they first heard about the "culturomics" approach to the humanities, many scholars reacted "as if this were the coming of the antichrist," says Grafton. "But my reaction is, God look at this new tool!"

–JOHN BOHANNON

CREDITS (LEFT TO RIGHT): WIKIPEDIA; (SEDIMENT) MATEJ KRÉN. (PHOTO) GABRIEL URBÁNEK

ENVIRONMENTAL TECHNOLOGY

Greenhouse–Power Plant Hybrid Set To Make Jordan's Desert Bloom

A novel combination of technologies that has the potential to turn large areas of desert green, producing commercial quantities of food and energy crops, fresh water, and electricity, looks set to have its first large-scale demonstration in Jordan. This week the governments of Jordan and Norway signed an agreement to work with the Sahara Forest Project (SFP), an environmental technology group based in Norway, to build a 20-hectare demonstration center near Aqaba on the Red Sea, which would begin operation in 2015. "It's a holistic approach that could be of major interest to a large number of countries," says Petter Ølberg, Norway's ambassador to Jordan.

The key to SFP is bringing seawater to the desert and evaporating it. A key component is the seawater greenhouse, developed by British inventor Charlie Paton. In Paton's scheme, seawater piped to the greenhouse trickles down over a grid structure that covers the windward side of the greenhouse. As natural breezes blow into the greenhouse through the grid, it evaporates the water, making an interior that is cool and moist—ideal conditions for growing crops. At the other end of the greenhouse, another grid evaporator, fed by seawater heated in black pipes on the greenhouse roof, loads more moisture into the air as it leaves the growing area. Now hot and very humid, the air passes through a maze of vertical polyethylene pipes cooled by cold seawater passing through them. Fresh water condenses on the pipes and trickles down into collectors, to be used for irrigation or drinking.

Since 1992, Paton's Seawater Greenhouse company has built pilot projects in Tenerife, Abu Dhabi, and Oman. Its first commercial contract, a 2000-square-meter greenhouse in Port Augusta, Australia, approved in 2009, harvested its first crop of tomatoes last month. To everyone's surprise, still-moist air blowing out of the pilot greenhouses turns the seemingly arid surrounding soil fertile: Weeds spring up unaided there, but they could just as easily be crops.

Paton teamed up with other experts in engineering, architecture, and environmental technology to form SFP. This group realized that a concentrated solar power plant would make an ideal partner for a seawater greenhouse.

Unlike photovoltaic systems, which convert sunlight directly into electricity, concentrated solar power uses mirrors to focus light onto a heat collector, which then produces steam to drive a turbine generator. Such solar plants work well in sunny desert areas, but they also need water both for cooling at the end of the power cycle and for cleaning the mirrors. A greenhouse could easily share seawater with a power plant; at the same time, the moist greenhouse and nearby vegetation would act as a natural air scrubber, filtering out much of the dust that would otherwise coat the plant's mirrors. In return, the solar plant would power the greenhouse.

Apart from Paton's prototype greenhouses, all of SFP's efforts so far have been theoretical. But a feasibility study drew plaudits at the COP15 climate summit in Copenhagen in 2009. "The Sahara Forest Project appears to be a very interesting example of the more integrated and holistic kind of thinking that we will need a lot more of in the future," said the European Union's energy commissioner at the time, Andris Piebalgs.

In June 2010, the project was presented to King Abdullah II of Jordan while he was visiting Oslo. The king invited an SFP team to visit Jordan in October and meet with five Jordanian ministers. And that led directly to this week's agreement. "The Jordanian authorities were very supportive and open," says Ølberg.

The agreement does not cover the construction cost of the demonstration center. Jordan will provide the 20-hectare site and a corridor to pipe salt water from the Red Sea. Norway will provide $600,000 for three studies: one to survey Jordan's potential for SFP-style facilities; a second to assess the Aqaba site; and a third to probe the possibility of building SFP plants alongside Jordan's planned pipeline to carry water from the Red Sea to the Dead Sea. Construction of the demonstration center will require private money; SFP chief Joakim Hauge says SFP is in discussions with several companies that are keen to invest in it.

The planned demonstration center devotes 4 hectares to greenhouses and 16 hectares to open-air crops, solar reflectors, and support buildings. The solar plant will use linear Fresnel reflectors, long, flat mirror strips that concentrate light onto a pipe carrying a heat-absorbing fluid. Hauge says the center will try out a variety of crops, including algae and halophytes, salt-tolerant plants that can be irrigated with seawater and used as biomass fuel. Salty waste water from an existing desalination plant will also be evaporated to provide more moisture for open-air crops. "The aim is to test as many technologies and combinations of technologies as possible," says Hauge.

SFP aims to start building in 2012 and to begin operations in 2015. If the project is successful, the Aqaba authorities will provide another 200 hectares for expansion.

–DANIEL CLERY

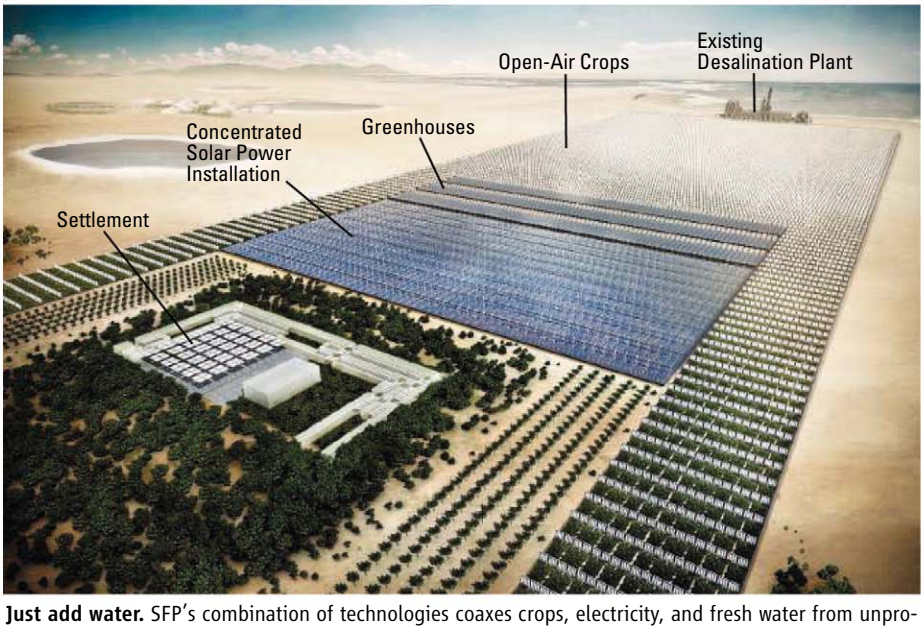

Just add water. SFP's combination of technologies coaxes crops, electricity, and fresh water from unproductive desert.

CREDIT: SAHARA FOREST PROJECT FOUNDATION/SCREENERGY

ScienceNOW

From *Science*'s Online Daily News Site

First Earth-Sized Exoplanet Discovered

Astronomers operating the Kepler telescope orbiting the sun in Earth's wake have discovered an extrasolar planet not much larger than Earth—the smallest exoplanet yet found.

The telescope stared for months on end at the same 150,000 stars in the constellation Cygnus looking for the telltale dimming of a star as a planet passes in front of it. One star, 560 light-years away and designated Kepler-10, dimmed 0.015% every 0.84 days, indicating a planet, dubbed Kepler-10b, orbiting 20 times closer to its star than Mercury orbits the sun. The planet has a diameter 1.42 times Earth's and a density 8.8 times Earth's, and local temperatures are a blazing 1833 K, the team announced this week at the winter meeting of the American Astronomical Society in Seattle, Washington. It's improbable that such a planet could harbor life, but with this milestone behind them, the Kepler team could be announcing the discovery of an Earth-like, habitable exoplanet within a few years. http://scim.ag/earth-size

Mental Retardation Drug Shows Promise

A phase II clinical trial of a drug for treating Fragile X syndrome, the most common inherited form of mental retardation, has delivered encouraging results—but only for patients with a particular genetic mutation.

Sébastien Jacquemont, a medical geneticist at Centre Hospitalier Universitaire Vaudois in Lausanne, Switzerland, and Baltazar Gomez-Mancilla, a neurologist at Novartis Institutes for Biomedical Research in Basel, Switzerland, studied the effects of a drug called AFQ056, developed by the pharmaceutical company Novartis, on 30 young men with Fragile X. They saw no improvement in patients' learning or memory. However, based on questionnaires filled out by the patients' caregivers, seven patients showed reduced repetitive behaviors, hyperactivity, inappropriate speech, and social withdrawal, the team reports online in *Science Translational Medicine*.

These responsive patients all had something in common: an inactive version of *FMR1*, the gene that is mutated in Fragile X. This is a discouraging sign, perhaps, for those without that marker, but a potentially useful tool for identifying the patients most likely to respond to treatment. Next, a larger clinical trial involving 160 people with Fragile X will test the effects of AFQ056 when taken for 3 months. http://scim.ag/FragileX-drug

Bumblebees in a Slump

Several species of bumblebees, which are important pollinators, have declined substantially over the past 2 to 3 decades in the United States, according to a new survey.

A team led by entomologist Sydney Cameron of the University of Illinois, Urbana-Champaign, and colleagues used museum collection databases and field samples to assess historical and current populations of eight of the nearly 50 bumblebee species. Four species thought to be in decline had plummeted by as much as 96%, and their ranges had shrunk by between 23% and 87%, the researchers report online in the *Proceedings of the National Academy of Sciences*. In contrast, four species thought to be stable fluctuated but seemed healthy overall.

The team also found that the rate of infection of *Nosema bombi*, a single-celled parasite that afflicts bees in Europe, was much higher in populations of dwindling species. Cameron and her colleagues are now investigating whether *Nosema* is to blame for the bumblebee decline. In the meantime, Cameron says, it's important to keep breeding facilities disease-free. http://scim.ag/fewer-bees

Lunar Core Finally 'Seen'

Two groups analyzing decades-old data taken by seismometers left on the moon by Apollo astronauts say they have detected lunar seismologists' prime target: a core of iron that is still molten 4.5 billion years after the moon's formation.

A team led by planetary scientist Renee Weber of NASA's Marshall Space Flight Center in Huntsville, Alabama, and a second group led by seismologist Raphaël Garcia of the University of Toulouse in France combed recordings made by the Apollo seismic experiment, which stopped transmitting data back to Earth in the mid-1970s, for signs of moonquake waves that may have reflected off the core. The groups took different approaches, but both came to the conclusion that the moon, like Earth, has a liquid core, they reported at last month's meeting of the American Geophysical Union. The core's radius is about 330 kilometers, Weber and her colleagues report online in *Science*. If the seismic results hold up, researchers say, they would be by far the strongest evidence yet for a liquid core. http://scim.ag/lunar-core

Read the full postings, comments, and more at **http://news.sciencemag.org/sciencenow**.

CREDITS (TOP TO BOTTOM): NASA; JOHANNA JAMES-HEINZ

Why Loneliness Is Hazardous to Your Health

New research suggests that chronic loneliness can cause changes in the cardiovascular, immune, and nervous systems

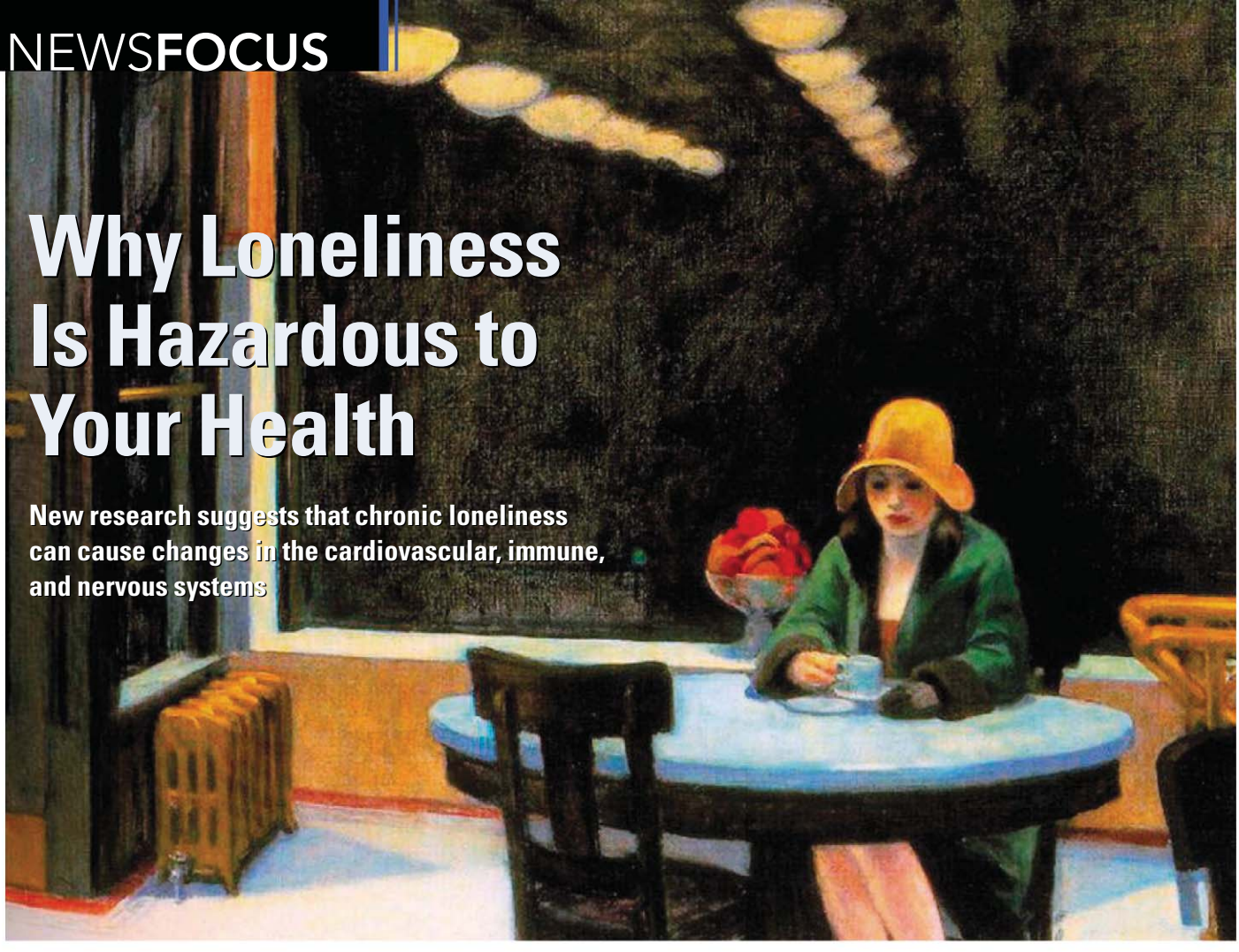

EVERYONE KNOWS WHAT IT'S LIKE TO BE lonely. It often happens during life's transitions: when a student leaves home for college, when an unmarried businessman takes a job in a new city, or when an elderly woman outlives her husband and friends. Bouts of loneliness are a melancholy fact of human existence.

But when loneliness becomes a chronic condition, the impact can be far more serious, says John Cacioppo, a social psychologist at the University of Chicago in Illinois. Cacioppo studies the biological effects of loneliness, and in a steady stream of recent papers, he and collaborators have identified several potentially unhealthy changes in the cardiovascular, immune, and nervous systems of chronically lonely people. Their findings could help explain why epidemiological studies have often found that socially isolated people have shorter life spans and increased risk of a host of health problems, including infections, heart disease, and depression. Their work also adds a new wrinkle, suggesting that it's the subjective experience of loneliness that's harmful, not the actual number of social contacts a person has. "Loneliness isn't at all what people thought it was, and it's a lot more important than people thought it was," Cacioppo says.

Colleagues credit him with building an impressive network of collaborations with researchers in other disciplines to pioneer a new science of loneliness. "He's placed it on the scientific map," says one collaborator, Dorret Boomsma, a behavioral geneticist at Vrije Universiteit Amsterdam in the Netherlands. "He's doing very creative work," says Martha Farah, a cognitive neuroscientist at the University of Pennsylvania. "He's created a new way of thinking about the biology of interpersonal relationships."

A new beginning

Cacioppo hasn't always studied loneliness. In the 1980s and '90s, he made a name for himself with meticulous laboratory studies on various aspects of emotion and cognition, and he's a founder of the field of social neuroscience, which seeks to understand the brain's role in social behavior. (Last month, colleagues elected him president of the newly formed Society for Social Neuroscience.)

Cacioppo says a 1988 *Science* paper suggesting that social isolation increases mortality (29 July 1988, p. 540) prompted him to change the focus of his research. Since then, scores of studies have found that people who lack social support are more prone to a variety of ailments. An analysis of 148 of these studies, published in the July 2010 issue of *PLoS Medicine*, suggests that social isolation increases the risk of death about as much as smoking cigarettes and more than either physical inactivity or obesity.

Compelling as these epidemiological studies are, Cacioppo says, they leave unanswered many questions about the mechanisms involved and about what aspects of social isolation are responsible. In the early 1990s, he set out to tackle these questions. He began by handing out questionnaires to thousands of students at Ohio State University in Columbus, where he was based at the time, and following up with physiological and psychological testing in the lab. For the past 10 years, he has been testing hundreds of Chicago-area residents, working closely with psychologist Louise Hawkley and other University of Chicago colleagues.

This work has convinced Cacioppo that

Online
sciencemag.org
Podcast interview with author Greg Miller.

CREDIT: EDWARD HOPPER/THE BRIDGEMAN ART LIBRARY

loneliness is a health risk on its own, apart from conditions such as depression or stress that are common fellow travelers. More specifically, it seems to be the subjective experience of loneliness that's important for people's well-being rather than any objective measure of social connectivity (the number of close contacts someone has, for example). It's an important distinction that most previous studies had ignored, says Daniel Russell, a psychologist at Iowa State University in Ames. "Some people are socially isolated and they're not lonely," Russell says. "By contrast, some people are lonely even if they have a lot of social contacts."

As a graduate student in the 1970s at the University of California, Los Angeles (UCLA), Russell helped develop the scale Cacioppo now uses in most of his research. The UCLA Loneliness Scale is based on a questionnaire that tries to size up how people perceive their social situation, with questions about how often they feel a lack of companionship, feel they have no one to talk to, or feel out of tune with those around them.

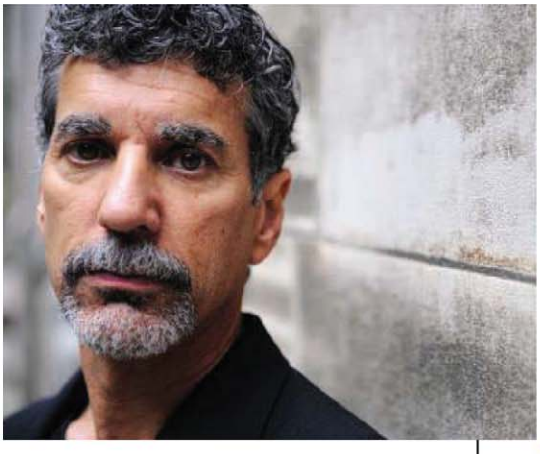

"Loneliness … [is] a lot more important than people thought it was."

—JOHN CACIOPPO, UNIVERSITY OF CHICAGO

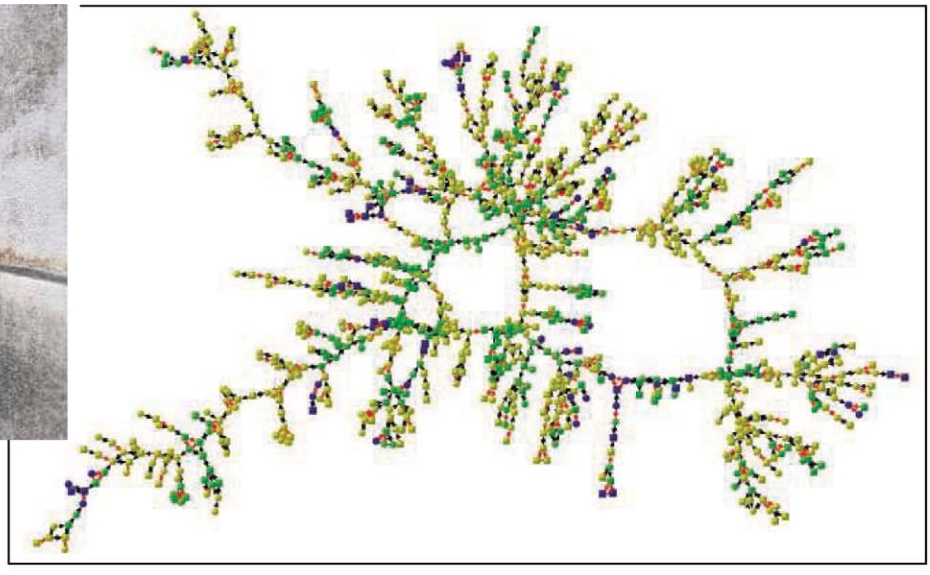

Clusters of loneliness. Loneliness tends to spread among people on the fringes of social networks, according to a 2009 study. Blue dots represent people who reported feeling lonely three or more days a week, green corresponds to two lonely days, and yellow corresponds to less than two lonely days.

Sympathetic feelings

When people score high on the UCLA Loneliness Scale, Cacioppo and colleagues have found, they also tend to exhibit several physiological changes that effectively put the body in a state of alert. In one early study, they found that lonely people exhibit higher vascular resistance, a tightening of the arteries that raises blood pressure. That forces the heart to work harder and can contribute to wear and tear on vessels.

"Those were landmark investigations" that got other researchers interested in potential biological effects of loneliness, says Chris Segrin, a behavioral scientist at the University of Arizona in Tucson.

Lonely people also have elevated molecular markers of stress. Cacioppo's group has found that cortisol and epinephrine are elevated in saliva and urine, respectively. That might help explain why lonely people report feeling more stressed in situations most people experience as only moderately stressful, such as public speaking, Cacioppo says.

Together, these findings point to activation of the sympathetic nervous system, which coordinates the body's fight-or-flight responses. It's as if loneliness prepares the body for some looming threat. Cacioppo thinks that makes evolutionary sense. He argues that being alone, for our distant ancestors, meant abandoning the protection of the group and jeopardizing one's genetic contribution to the next generation. He posits that the physiological changes and anxiety that accompany loneliness are a warning that an individual's social ties have gotten too weak: "It's an aversive signal that motivates us to change our behavior in a way that's good for our genetic survival." In his view, loneliness is a double-edged sword—adaptive in the short term but dangerous when it becomes chronic.

Cacioppo and colleagues have also found evidence that loneliness has a direct impact on the immune system. In a 2007 study in *Genome Biology*, Cacioppo teamed up with UCLA genomics researcher Steve Cole and other colleagues to investigate gene activity across the genome in the white blood cells of 14 participants in a longitudinal study of loneliness among Chicago-area residents. The volunteers selected scored in either the top or the bottom 15% of the study cohort on the UCLA Loneliness Scale.

Two differences between the groups stood out: Lonely people exhibited increased activity for several genes encoding signaling molecules that promote inflammation and decreased activity for genes that normally put the brakes on inflammation. They also showed diminished activity in genes that help mount a defense against viral invaders.

Cole says that jibes with epidemiologic findings that socially isolated people are more susceptible to viruses, from the common cold to HIV, and to cardiovascular disease, which has been linked to excess inflammation. Cole says the team will soon publish a replication of the findings in a group of about 120 participants in the Chicago study. He notes that just feeling a little left out isn't likely to throw the immune system out of whack. "It really takes a person who has taken and consolidated a lonely view of the world to show these changes in gene expression," he says.

Loneliness not only increases wear and tear by keeping the body in alert mode but also may prevent people from recharging their batteries with rest and relaxation. In the March 2010 issue of *Health Psychology*, Cacioppo and colleagues reported that although lonely people sleep a normal number of hours, they report more fatigue

CREDITS (LEFT TO RIGHT): DAN DRY/COURTESY UNIVERSITY OF CHICAGO; J. CACIOPPO *ET AL.*, *JOURNAL OF PERSONALITY AND SOCIAL PSYCHOLOGY*, **97** (DECEMBER 2009) AMERICAN PSYCHOLOGICAL ASSOCIATION

the next day, suggesting that their quality of sleep isn't as good. Segrin says his group has recently replicated this finding and extended it to show that lonely people derive less satisfaction from leisure activities. Their findings are in press at *Health Communications*.

The lonely brain

Studies by Cacioppo and others before him have found that lonely people tend to rate their own social interactions more negatively and form worse impressions of people they meet. Researchers are beginning to show how these biases may be encoded in the brain. In a 2008 study in the *Journal of Cognitive Neuroscience*, Cacioppo and colleagues used functional magnetic resonance imaging to measure metabolic activity in the brains of 23 undergraduate women at the University of Chicago. Those who were lonelier, as rated by the UCLA Loneliness Scale, exhibited less activation in the ventral striatum, a component of the brain's reward circuitry, when they viewed pictures of smiling faces.

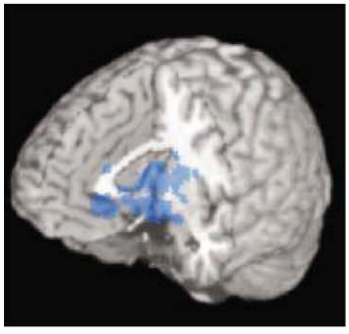

Unrewarding. Lonely people take less enjoyment from social interactions and exhibit less activity (blue) in the ventral striatum.

In another study, Cacioppo and colleagues asked lonely and nonlonely people to perform the Stroop test, a workhorse task in experimental psychology in which people see words presented in colored text one by one on a computer screen, then indicate what color it was. When lonely people saw words that evoked negative social interactions, such as "isolate" or "reject," they took a split second longer to identify the color than they did for negative nonsocial words, such as "vomit." Nonlonely people showed no such delay. To Cacioppo, the findings, as yet unpublished, suggest that lonely people pay extra attention to negative social cues. "It suggests the brain is on the alert for social threats," he says.

A recent study by researchers at Duke University in Durham, North Carolina, meshes with these findings. Neuroscientist Ahmad Hariri and colleagues set out to replicate previous reports that people with anxious tendencies (but not a clinical diagnosis) exhibit more activity in the amygdala, a brain region crucial for threat detection, when they see images of angry or fearful faces. But Hariri's group found that this was true only for the subset of the volunteers who also reported below-average levels of social support. (They did not measure loneliness per se.) To Hariri, the findings, published online 31 August in *Neuropsychologia*, suggest that people's perceptions of social support may calibrate how the amygdala assesses social threats, which in turn could influence their risk for anxiety disorders or other conditions.

Loneliness may also affect the prefrontal cortex, a region important for what cognitive scientists call executive control. In daily life, that often translates to restraint—as in not eating cheeseburgers at every meal or putting the stopper back in the wine bottle after one or two glasses. Epidemiological studies have suggested that people with poor social networks are more likely to eat poorly, consume more alcohol, and exercise less. Several studies have found that lonely people perform poorly on lab tests that require executive control, and at least one study, published in the June 2006 issue of *Social Neuroscience*, found reduced prefrontal cortex activity in socially isolated people.

Contagious … but curable

Evidence that loneliness is partly heritable has emerged from a collaboration between Cacioppo and Boomsma, who oversees a database of Dutch twins and their family members. They've found that genetics accounts for up to half of the individual variation in loneliness. Their most recent study, published in the July 2010 issue of *Behavioral Genetics*, used an abbreviated version of the UCLA Loneliness Scale in a survey sent to 8683 twins and family members. In this group, genetics accounted for 37% of the variability in loneliness, somewhat lower than in some previous studies. Overall, the heritability of loneliness is comparable to that of depression, Boomsma says, but less than that of traits such as high blood pressure and cholesterol levels.

In his 2008 book, *Loneliness: Human Nature and the Need for Social Connection*, Cacioppo hypothesizes that there is a "genetic thermostat" for loneliness that's set differently in different people. That setting determines the degree of distress triggered by social isolation. "You're not inheriting loneliness; you're inheriting how painful it feels to be alone," Cacioppo says.

But environment matters, too, as studies by Russell have shown. College freshmen rank among the loneliest populations he and his colleagues have studied, because they've left behind their family and high school friends and are trying to find their way in a new social ecosystem, Russell says.

According to some measures, society is changing in ways that may make people even lonelier. The U.S. Census Bureau estimates that nearly 29 million people live alone in the United States, a 30% increase from 1980. A widely cited 2006 study in *American Sociological Review* asked a representative sample of the U.S. population how many people they would feel comfortable discussing an important personal issue with. Between 1985 and 2004, the average number dropped from three to two, and the percentage of people who reported having no such confidants rose from 10% to 25%.

And like certain other health risks, loneliness may be contagious. Cacioppo recently teamed up with James Fowler of UC San Diego and Nicholas Christakis of Harvard University to investigate the spread of loneliness through social networks. Scrutinizing data on thousands of people participating in the Framingham Heart Study, Fowler and Christakis have reported that everything from smoking habits to happiness appears to spread from person to person within social networks (*Science*, 23 January 2009, p. 454). So, too, can loneliness, the trio reported in December 2009 in the *Journal of Personality and Social Psychology*.

The news isn't all bad, however. Even for hard cases, Cacioppo believes loneliness can be overcome. He and colleagues recently conducted a meta-analysis of 20 studies on interventions for loneliness. Simply providing social support doesn't seem to work, especially if people know they're being looked after. "If you know people are stopping by to check on you, it makes you feel like more of a loser," Cacioppo says. The most effective interventions were those that borrowed methods from cognitive behavioral therapy to shift people's attention and interpretation of social situations in a more positive direction, the team reported online 17 August 2010 in *Personality and Social Psychology Review*.

As for preventing loneliness, Cacioppo says it helps to know where your own thermostat is set and strive to stay in your comfort zone. In *Loneliness*, he writes: "The degree of social connection that can improve our health and our happiness … is both as simple and as difficult as being open and available to others."

–GREG MILLER

CREDIT: J. CACIOPPO *ET AL.*, *JOURNAL OF COGNITIVE NEUROSCIENCE*, **21** (JANUARY 2009)

ARCHAEOLOGY

Did the First Cities Grow From Marshes?

The world's earliest large settlements may owe their existence as much to the swamps of southern Iraq as to irrigation and agriculture

In his dying moments, Goethe's Faust foresees a happy day when a nearby foul swamp is replaced by green and fertile fields "where men and herds may gain swift comfort from the new-made earth." He might have had a more benign view of marshlands had he pored over the data gathered by a young archaeologist who recently led the first American archaeological research team to Iraq in a quarter-century. She suggests that cities and civilization didn't rise along riverbanks, as most archaeologists have supposed, but out of swamps, which provided rich animal and plant resources to complement irrigation agriculture and animal husbandry. "Almost everywhere we look," says Jennifer Pournelle of the University of South Carolina, Columbia, "the biggest and earliest [human settlements] are in that marsh environment."

Pournelle is on a quest to understand the role of marshes in southern Iraq between 4000 B.C.E. and 3000 B.C.E., when humans first began to live in a network of cities. After a decade of work with satellite and aerial images, she and two colleagues finally got a chance to see the region up close last September, on an expedition with the University of Basra. She presented the team's findings at a meeting in November and hopes to return to Iraq this year.

If she is right, says her former adviser, Guillermo Algaze of the University of California, San Diego, "we may have to rethink how Mesopotamian civilization began." "It's very intriguing," adds archaeologist Jason Ur of Harvard University. "She's proposing a radically different environmental context for the first cities." But additional on-the-ground data will be crucial to convince interested but skeptical colleagues.

Pournelle's view of the importance of marshes goes up against a half-century-old idea that early cities were born along the great rivers of the Near East from advances in farming and irrigation, which created food surpluses that could sustain large settled populations. Archaeologist Robert Adams of the University of Chicago in Illinois, who surveyed southern Iraq in the 1960s and 1970s, found evidence that early settlements were strung along ancient canals or rivers.

As a graduate student with Adams a decade ago, Pournelle led a project to reconstruct the ancient Mesopotamian landscape by combining archaeological site maps with aerial and satellite imagery. During this initial work, Pournelle noticed that the early settlements—from modest villages to sizable cities—showed up on what appeared to be narrow boat paths through dense marsh. Since then, her colleagues have nearly doubled the number of known ancient sites, which have come into view as the modern marshes have been dried up by drought, Turkish dams, and the actions of Saddam Hussein. "The settlements are not pearls on a chain, or cities on rivers, but are located on delta marshlands," concludes Pournelle, who became a remote-sensing expert in her previous career as a military analyst interpreting spy satellite data.

Meanwhile, research on the ancient Persian Gulf environment shows a dramatic rise in sea levels. The waters reached a peak in 4000 B.C.E., flooding the lower reaches of today's southern Iraq and prompting the growth of marsh in the flat, low-lying plain—and coinciding with the growth of the first protocities. Pournelle's remote-sensing studies show that as the waters rose, people built permanent settlements on small ridges, called turtlebacks, that rise only a meter or so above the plain. She believes these ridges offered shelter during flood season and eventually a dry place for storehouses, temples, and administrative centers, some of which have been identified by previous research. These settlements were the core of what became early population centers, such as Eridu, in the 4th millennium B.C.E., and the marshes provided an array of foods and building materials.

Rising tide. Waters flooded ancient Iraq.

Swamp cities? The Iraq marsh may be a last remnant of wetlands that spurred urban evolution.

By about 3500 B.C.E., other urban centers like Uruk—famed as the first true city and birthplace of writing—were developing on small deltas on the northern fringes of the marsh, formed when water coming from upstream broke into multiple channels. Such locations offered year-round water transportation and less flooding while still providing access to birds and fish.

Pournelle argues that the role of irrigation in sustaining large populations has been overstated. "At the very least, marsh resources were an important part of a triad" that included agriculture and cattle grazing, she says. The rise of multiple cities around 3000 B.C.E., therefore, was due in part to their proximity to the rich marshes. She notes that delicate fish and bird bones at sites like Eridu and Uruk have been largely ignored by archaeologists, both because of the focus on sheep and goats and because such bones are not easily preserved. The same is true of reeds, which were important but overlooked materials for constructing houses and ziggurats, she says.

It was the retreat of the Persian Gulf during the 3rd millennium B.C.E. that prompted the first extensive canal systems, Pournelle says. In her view, the canals were a response to this crisis rather than an attempt to expand food surpluses.

Adams praises Pournelle's scientific work but warns that the distinction between marshes, fields, and grazing land may be more blurred than she contends. He and others say that further on-the-ground work is necessary, and Pournelle agrees. She hopes to return with her team in late spring to drill cores to find more clues to the ancient environment—and, perhaps, insight into how civilization was born of the swamps so despised by Faust.

–ANDREW LAWLER

Tectonic Blow Ended Mountain Building, Fired Up Volcanoes

Fifty-five million years ago, Siletzia arrived on North American shores with nary a bump. But the 500-kilometer-wide chunk of drifting oceanic plate had far-reaching geologic effects across the continent's western third, according to a presentation at the meeting. New seismic imaging shows Siletzia throwing a monkey wrench into the gears of the plate tectonics machine and thus reshaping western North America.

Before Siletzia arrived, things tectonic were humming along nicely. The Farallon oceanic plate was creeping northeastward and diving into the mantle beneath North America. But unlike most subducting plates, the Farallon plate wasn't diving very deeply. Instead, it was leveling off and sliding hard against the underside of the North American plate. The drag of the Farallon plate tended to squeeze the overlying plate, crumpling its surface into mountains like a wrinkled rug. The mountain building extended as far as the Black Hills of South Dakota and included the Laramie Mountains of Wyoming. But starting about 50 million years ago, the Farallon plate began diving more steeply into the mantle, ending the era of so-called Laramide mountain building. Geologists wondered why.

The reason subduction steepened, seismologist Eugene Humphreys of the University of Oregon (UO), Eugene, said at the meeting, was the arrival of a thicker patch of the plate called Siletzia. Humphreys and UO colleague Brandon Schmandt reached that conclusion by using seismic waves from earthquakes to image what remains of the Farallon plate in the mantle beneath North America. Using seismic waves the way radiologists use x-rays to form CT images, they drew on the newest records from a dense network of seismometers known as the USArray project (*Science*, 25 September 2009, p. 1620). "We now have a lot more data," says Humphreys. "Now I believe the structures we see."

Most geologists think the thicker Siletzia section of the Farallon plate jammed at the edge of the continent and stopped subduction across the Pacific Northwest. In the OU scenario, however, the Farallon plate didn't just stop; it tore clean through beneath the southern edge of Siletzia. That left the remaining shallowly subducting plate to the south to peel off the base of North America and progressively fall away southward.

As evidence for this scenario, the scientists point to a vertical "curtain" of colder rock they see stretching 600 kilometers down into the mantle beneath Idaho. The curtain, they say, is the dangling remnant of the subducted plate that tore away from the rest of the Farallon plate.

All of this fits with what geologists have inferred happened at the surface, Humphreys said. The ocean crust melting on the hanging slab would have fueled the so-called Challis volcanism through Idaho and into Canada. The broad loss of shallowly subducting plate would have triggered the switch from North American compression and mountain building to the crustal stretching seen today. And the progressive falling away of Farallon plate would have allowed hot mantle rock to rise and drive the flare-up of volcanism seen to the south.

The sharper view of the mantle "ties the tectonic history of the crust with what you can now see in the mantle," says geologist Ray E. Wells of the U.S. Geological Survey in Menlo Park, California. It also helps tie the geology in the north with that in the south, he says: "Now that we can see things under there, they're starting to integrate processes across wide areas."

–R.A.K.

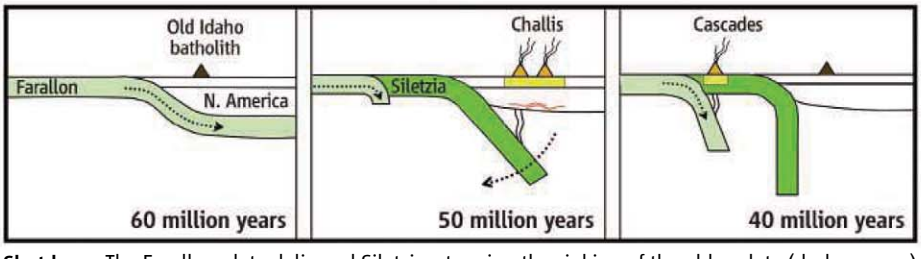

Shutdown. The Farallon plate delivered Siletzia, stopping the sinking of the older plate (darker green).

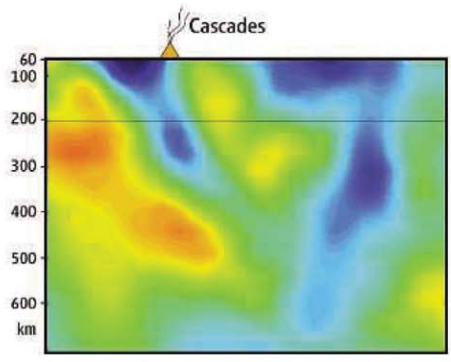

Still hangin'. Seismic imaging reveals a "curtain" of old ocean plate (blue, *right*) left dangling since Siletzia arrived 40 million years ago.

What Heated Up the Eocene?

Talk about your global warming. Fifty-five million years ago, carbon dioxide gushed into the atmosphere over as little as a millennium, acidifying the ocean and scorching the world of the Eocene epoch with a 5°C greenhouse warming. At least two more progressively weaker "hyperthermals" would strike during the next few million years. So where did all that carbon dioxide come from?

The possibilities are expanding, from the sea floor to an ice-free Antarctica. In one presentation, earth systems modeler Andrew Ridgwell of the University of Bristol in the United Kingdom and his colleagues suggested an ocean source. Earth is always wobbling on its axis like a spinning top, and its orbit about the sun is rhythmically stretching into an ellipse and relaxing to more of a circle. By changing how much sunlight falls at different latitudes in different seasons, these orbital variations can make for exceptionally warm summers with extra-cold winters, for example.

Ridgwell and his colleagues included orbital variations in a computer model of early Eocene climate, when the world was slowly warming under a strengthening greenhouse. When the orbital variations in the model combined to make an extreme contrast between summer and winter temperatures, the model's ocean circulation would slow and stagnate. That allowed the deep ocean to warm, warming the sea floor. And that's where natural methane hydrates reside—the "ice that burns." Warm them and they decom-

Snapshots From the Meeting >>

Whoa there! Geodesists have found that the Sierra Nevada mountains of east-central California are rising so fast that they could have achieved their 3-kilometer height in just the past 3 million years, not the past 30 million years, as suggested by some geologists. William Hammond of the Nevada Bureau of Mines and Geology in Reno and his colleagues reported that GPS measurements combined with satellite radar observations of vertical ground motions show the central and southern Sierras are rising at about 1 millimeter per year. "If that number stands, it would be a rip-roaring uplift rate," says geologist Craig Jones of the University of Colorado, Boulder.

Hammond says the high rate across so much of the Sierras argues that they aren't bouncing upward after a heavy piece of the continental plate beneath them peeled off and fell into the mantle. Instead, some aspect of the West Coast's helter-skelter plate tectonics must be responsible.

Blame all around. Remember those millions of airline passengers kept from the skies last spring by the ash of that unpronounceable Icelandic volcano? They can fault any number of geophysical quirks, according to volcanologists gathered at the meeting. There was the persistently ill-directed wind that blew over Eyjafjallajökull volcano toward Europe, of course. But other factors peculiar to Eyjafjallajökull combined to aggravate the problem. Magma melted glacial ice on the summit of the volcano and drove the water to steam that energized the early phase of the eruption, raising a high plume full of particularly fine, far-traveling ash. In addition, the magma carried an unusual amount water of its own. And it was a particularly thick, sticky magma for an Icelandic volcano, which made for an even more explosive eruption. **–R.A.K.**

Showstopper. Several characteristics of Eyjafjallajökull worsened air-traffic disruption.

pose into water and methane. That methane can escape the sea floor, oxidize to carbon dioxide, and warm the world.

In the next talk, paleoceanographer Robert DeConto of the University of Massachusetts, Amherst, and his colleagues claimed that a larger source of carbon dioxide in Eocene times would have been the permanently frozen ground of polar regions. No ice sheets covered polar ground in Eocene times, and the land area of Antarctica was far larger than it is today, DeConto said. That would have made for widespread permafrost, storing organic matter that—if thawed and decomposed—would yield large amounts of carbon dioxide. In their model, extremes of orbital variations caused permafrost to melt in summer and release its carbon dioxide. Enough would have come out fast enough to drive the observed warming, DeConto said.

"I think both Andy and Rob may be right," says paleoceanographer James Zachos of the University of California, Santa Cruz. "I think you're getting contributions from both." Bad news for future warming. **–R.A.K.**

Worry But Don't Panic Over Glacial Losses

With glaciers suddenly galloping to the sea in Greenland and the "weak underbelly" of Antarctic ice beginning to give way, it's hard to keep a cool head, but a couple of glaciologists at the meeting gave it a try. At least in the short term, they said, the situation, while bad, is not always quite as bad as it looks.

Glaciologist Ian Joughin of the University of Washington, Seattle, reported on his and his colleagues' study of the forces acting on the Jakobshavn Glacier of southern Greenland. Jakobshavn accelerated toward the sea early in the decade after warming ocean water destroyed part of its floating ice tongue that had been helping to restrain it.

Jakobshavn is still accelerating and thus increasing the rate of sea level rise—plenty of cause for worry—but Joughin cautioned that Jakobshavn is not totally off its leash. Judging by the glacier's behavior from season to season, restraining forces such as friction with rock at the glacier's sides will likely keep it from accelerating by more than a factor of 3 in this century, not the factor of 10 sometimes bandied about. And even at the slower rate, by 2100 it will have retreated up onto dry land, where friction must slow it greatly.

Still, glaciologist Richard Alley of Pennsylvania State University, University Park, saw cause for some worry as well. Glaciers draining the West Antarctic Ice Sheet are also flowing faster these days. New ocean warmth has melted the floating tongues of some glaciers there, loosening their hold on bumps on the sea floor that had been restraining glacier flow and accelerating ice loss. Flow will slow only when the ice again becomes stuck on a sea-floor bump somewhere farther upstream. Such pulses of ice loss are inevitable and for many glaciers unpredictable, Alley warned, because no one is sure where the bumps are.

If researchers are going to predict such glacial surges, "we'll need to understand what's under the ice," notes glaciologist Robert Bindschadler of NASA's Goddard Space Flight Center in Greenbelt, Maryland.

Faster. Jakobshavn Glacier's acceleration has its limits.

In the meantime, he advises not focusing on just a few glaciers like Jakobshavn. "If we do," he says, "we're likely to get too excited when they accelerate and too relieved when they pause." His advice: Keep your eye on measures of the overall losses from an ice sheet. Those will be steadier, and plenty worrisome. **–RICHARD A. KERR**

LETTERS

edited by Jennifer Sills

Fostering Success at Community Colleges

IN THE EDUCATION FORUM "GROWING ROLES FOR SCIENCE EDUCATION in community colleges" (3 September 2010, p. 1151), G. R. Boggs proposes that community college curriculums be revised to include science projects or research-based experiences.

Most community college students are not prepared to undertake such extracurricular research. In urban colleges, most students must work full or part time, and many of them have involved personal lives. Few would have the time or flexibility to take advantage of the kind of programs Boggs proposes.

Since when has a lack of science research experience been an impediment to community college students expecting to transfer to a 4-year college? For that matter, when has their ultimate goal been to enroll in a 4-year college? The goal of many community college students is to graduate with an associate's degree that might qualify them for professional jobs [often better compensated than those that require a bachelor's degree (*1*)] such as dental and medical assistants, computer specialists, and engineering technicians.

What community college students do need is professional guidance to help them survive academically as they contend with personal and financial predicaments. Such support in community colleges is too often in short supply. According to the National Survey of Counseling Center Directors in 2009, 73% of directors describe their centers as primarily a mental health/psychological center rather than primarily a career development center (*2*). In colleges (including both 4-year and community programs), there are approximately 1500 students per a single counselor (*2*).

Boggs makes but a single reference to improving "student support services," along with tutoring for unprepared students. Additional funding for both, rather than the costly, hardly essential addition of project and research programs, is what community colleges really need.

IGOR V. ZAITSEV

Science Department, Borough of Manhattan Community College, CUNY, New York, NY 10007–1097, USA. E-mail: izaitsev@bmcc.cuny.edu

References

1. J. E. Rosenbaum, J. L. Stephan, J. E. Rosenbaum, *Am. Educ*. **34**, 3 (2010).
2. R. P. Gallagher, "National survey of counseling center directors" (The International Association of Counseling Services, Pittsburgh, PA, 2009); www.iacsinc.org/2009%20National%20Survey.pdf.

Response

ZAITSEV RAISES A VALID ARGUMENT FOR increasing student support services. It is good to see faculty understanding of the obstacles that community college students face. I certainly agree that more resources should be devoted to student guidance, tutoring services, and financial aid, and I strongly advocate for the importance of these programs. However, that does not mean that attention should not also be placed on the quality of the academic program. The Committee of Undergraduate Science Education of the National Research Council states that "[i]nstitutions of higher education should provide diverse opportunities for all undergraduates to study science, mathematics, engineering, and technology as practiced by scientists and engineers, and as early in their academic careers as possible" (*1*). One way to accomplish this is to involve students in science projects or research experiences. There are many examples of undergraduate research projects at community colleges (*2*), including several good examples of student research at Zaitsev's institution (*3*).

Student transfer to upper-division universities is an important goal for many community college students. We need to continue to do what we can to remove the obstacles to their success.

GEORGE R. BOGGS

American Association of Community Colleges, Washington, DC 20036, USA. E-mail: gboggs@aacc.nche.edu

References

1. Committee on Undergraduate Science Education, *Transforming Undergraduate Education in Science, Mathematics, Engineering, and Technology* (National Academy Press, Washington, DC, 1999).
2. B. D. Cejda, N. Hensel, *Undergraduate Research at Community Colleges* (Council on Undergraduate Research, Washington, DC, 2009).
3. Borough of Manhattan Community College, The City University of New York, Annual Student Research Poster Presentations (www.bmcc.cuny.edu/news/news.jsp?id=4903).

Microbe Interactions Undermine Predictions

THE REPORT BY S. TELFER *ET AL*. ("SPECIES interactions in a parasite community drive infection risk in a wildlife population," 8 October 2010, p. 243) demonstrates that the history of infection cannot be summarized by a simplified scenario involving only a host and a microbe. Microorganisms interfere with each other and can modify the transmissibility between humans. For example, in the recent flu pandemics, influenza virus interfered with

rhinoviruses, which modified the transmission and hence the epidemic of H1N1 in France (*1*). Moreover, the severity of the disease is modified by associated bacterial pathogens, as demonstrated in the Spanish flu outbreak, in which bacterial secondary infection played a major role in mortality (*2*). These poorly known and badly controlled elements make prediction models for infectious disease outbreaks ineffective. To base decision-making in public health on such models is dangerous, because of our ignorance in the multiple partners prevailing during an epidemic.

DIDIER RAOULT

URMITE 6236, IRD 198, Faculté de Médecine, 13385 Marseille cedex, France. E-mail: didier.raoult@gmail.com

References

1. J. S. Casalegno *et al.*, *Clin. Microbiol. Infect.* **16**, 326 (2010).
2. D. M. Morens, G. K. Folkers, A. S. Fauci, *J. Infect. Dis.* **200**, 1018 (2009).

Response

WE AGREE WITH RAOULT THAT OUR STUDY emphasizes the need to consider coinfection and interactions between parasites and pathogens in predictive epidemiological models of human diseases. Indeed, one of the objectives of our work is to use wild-rodent model systems to throw light on questions of medical importance. We believe that studies of infections in wild rodents can complement research based on humans and laboratory rodents. Like human populations, wild-rodent populations are genetically variable and are subjected to changing environmental conditions and a range of pathogens, and their close relationship to laboratory rodents facilitates the use of advanced immunological and genomic approaches to understand host-pathogen interactions (*1*). Moreover, because of their short generation time, wild rodents lend themselves to both detailed observational studies and manipulative experiments (*2*, *3*). Our study demonstrates the power of such an approach.

We also agree with Raoult that epidemiological dynamics of a single pathogen within a single host population may be influenced by a range of external factors. However, we believe that even simple models can be effective. For example, epidemiological models that focus on parameters such as the basic reproductive parameter R_0 have been used both to understand differences in disease persistence between populations and to compare alternative control strategies (*4*, *5*). We expect past failures to lead not to abandonment of the approach but to refinement. One important refinement is the investigation, and ultimately the incorporation, of coinfection effects. Indeed, encouragingly, some epidemiological models are already exploring the

Readers' Poll Results

Travel Trade-Offs for Scientists

On 10 December 2010, we asked you to consider the environmental benefits of reduced travel and then choose the option that best reflects your answer to this question: Would you participate in an annual meeting remotely (via video teleconferencing or other technology)?*

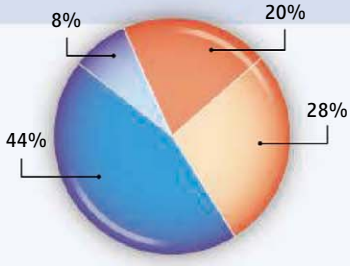

- **Yes:** Participating remotely would be about as valuable as attending in person.
- **Yes:** It would lose some value, but the trade-off would be acceptable given the environmental benefits.
- **No:** It would lose some value, and the trade-off would be unacceptable despite the environmental benefits.
- **No:** Participating remotely would be about as valuable as not attending at all.

Hundreds of you responded, from dozens of countries around the world. Here are your results.

A selection of your thoughts:

"Until we come up with holographic teleconferencing with the ability to eat virtual lunch together in smaller groups, there will always be a need for large gatherings from time to time."
—reader John Burke Burnett

"I think there is at least a chance that once we get into the remote format in a big way and properly, we may wonder how we (as individual participants) ever tolerated all the dead time associated with the old way of doing meetings."
—reader Richard McCulloh

*See the poll, and a link to the related Letter, at www.sciencemag.org/site/extra/polls/20101210-1.xhtml.

Polling results reflect the votes of those who chose to participate; they do not represent a random sample of the population.

NEW
Women in Science Booklet

Science and the L'Oréal Foundation present

Read inspiring profiles of women making a difference in biology.

Free download at ScienceCareers.org/LOrealWIS

impact of coinfection on the dynamics of disease in human populations, and the consequences for disease control (*6*).

SANDRA TELFER,[1,2]* XAVIER LAMBIN,[2] RICHARD BIRTLES,[3] PABLO BELDOMENICO,[4] SARAH BURTHE,[5] STEVE PATERSON,[1] MIKE BEGON[1]

[1]School of Biological Sciences, University of Liverpool, Crown Street, Liverpool L69 7ZB, UK. [2]School of Biological Sciences, University of Aberdeen, Tillydrone Avenue, Aberdeen AB24 2TZ, UK. [3]School of Veterinary Science, University of Liverpool, Leahurst Campus CH64 7TE, UK. [4]Facultad de Ciencias Veterinarias, Universidad Nacional del Litoral, RP Kreder 2805, 3080 Esperanza, Santa Fe, Argentina. [5]Centre for Ecology and Hydrology Edinburgh, Bush Estate, Penicuik, Edinburgh EH26 0QB, UK.

*To whom correspondence should be addressed. E-mail: s.telfer@abdn.ac.uk

References

1. J. A. Jackson *et al.*, *BMC Biol.* **7**, 16 (2009).
2. M. J. Smith *et al.*, *Proc. Natl. Acad. Sci. U.S.A.* **106**, 7905 (2009).
3. A. B. Pedersen, T. J. Grieves, *J. Anim. Ecol.* **77**, 370 (2008).
4. N. C. Grassly *et al.*, *Science* **314**, 1150 (2006).
5. C. Fraser, S. Riley, R. M. Anderson, N. M. Ferguson, *Proc. Natl. Acad. Sci. U.S.A.* **101**, 6146 (2004).
6. L. R. Gibson *et al.*, *BMC Infect. Dis.* **10**, 248 (2010).

Letters to the Editor

Letters (~300 words) discuss material published in *Science* in the past 3 months or matters of general interest. Letters are not acknowledged upon receipt. Whether published in full or in part, Letters are subject to editing for clarity and space. Letters submitted, published, or posted elsewhere, in print or online, will be disqualified. To submit a Letter, go to www.submit2science.org.

An Integrated Approach to Genome Studies

IN THEIR PERSPECTIVE "ENVIRONMENT AND disease risks" (22 October 2010, p. 460), S. M. Rappaport and M. T. Smith make a strong case for applying chemical assays to the "exposome" in epidemiology. Here I emphasize the need to collect and analyze samples at several points in a subject's life span, shifting away from an "end-point" paradigm, as found in most genome-wide association studies, to a more balanced, "kinetics" approach.

To highlight important epidemiological effects, Rappaport and Smith may have overlooked vital points. In addition to environment, methylation, oxidation, and other epigenetic markers of the genome change over the lifetime of an individual. Even somatic mutations can contribute to disease (*1*). Human response to some exposures is invariant, but others exist to which responses vary, and variation can depend upon variations in the genome (*2*, *3*) and epigenome (*4*). Furthermore, whereas some disorders could be chronic exposure conditions, there are also likely to be diseases that represent a latent response—that is, environmental exposure produces no immediate disorder but instead changes factors such as the epigenome to "prime" a person for late pathogenesis (*5*). Pathogenicity could also be suppressed (but not irreversibly) by different changes in the epigenome (*5*).

I believe that exposome assays would be most useful if performed with genome-wide association studies, epigenome-wide association surveys (which currently concentrate on DNA methylation), and studies of the "oxidome" (oxidative damage of genomic and mitochondrial DNA). I would also hope that they would be performed at multiple time points and that combined assays be analyzed to consider effect interactions. This integrated approach would enhance our understanding of complex etiology of chronic and sporadic disorders, and it could suggest preventive and therapeutic strategies.

DEBOMOY K. LAHIRI

Laboratory of Molecular Neurogenetics, Institute of Psychiatric Research, Departments of Psychiatry and of Medical and Molecular Genetics, Indiana University School of Medicine, Indianapolis, IN 46202, USA. E-mail: dlahiri@iupui.edu

References and Notes

1. R. P. Erickson, *Mutat. Res.* **705**, 96 (2010).
2. E. Efrat *et al.*, *Eur. J. Clin. Pharmacol.* **65**, 257 (2009).
3. R. G. York, J. M. Manson, *Toxicol. Appl. Pharmacol.* **72**, 417 (1984).
4. X. Ren *et al.*, *Environ. Health Perspect.*, published online 2 August 2010.
5. D. K. Lahiri, B. Maloney, N. H. Zawia, *Mol. Psychiat.* **14**, 992 (2009).
6. I thank B. Maloney and research grants R01AG18379 and R01AG18884 from the National Institute on Aging, National Institutes of Health, and the Zenith Fellows Award from Alzheimer's Association.

CORRECTIONS AND CLARIFICATIONS

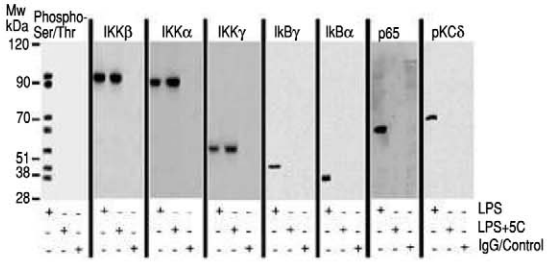

Reports: "SphK1 regulates proinflammatory responses associated with endotoxin and polymicrobial sepsis" by P. Puneet *et al.* (4 June 2010, p. 1290). Figure 2A and fig. S5B in the Supporting Online Material were not the original blots. The original Western blots for Fig. 2A are reproduced here, and fig. S5B has been replaced with the original Western blots in a revised SOM pdf. The results and conclusions of the paper remain unchanged.

ATMOSPHERE

Weathering Defeats

W. Patrick McCray

In December 1966, the *Bulletin of the Atomic Scientists* published an essay by physicist Alvin Weinberg that would become a classic. The then-director of Oak Ridge National Laboratory explored the extent to which social problems might be "circumvented by reducing them to technological problems" (*1*). Although they appeared to be "crisp and beautiful" solutions, Weinberg realized that what he labeled "Technological Fixes" were likely to become "incomplete and metastable" answers whose existence created yet more problems.

James Rodger Fleming's authoritative *Fixing the Sky* explores the history of problem solving via technology as manifested in proposals and programs for controlling the weather. From ancient mythology to the "rain kings" of the 19th century and then concluding with contemporary debates about geoengineering, Fleming (a historian of science at Colby College) shows how scientists' desire to deliberately modify the weather is part of a longer tradition of seeking control over nature.

Mark Twain once quipped that "everyone talks about the weather but no one does anything about it," a claim that the renowned scientists, corporate and military leaders, and charlatans who populate Fleming's book all endeavored to refute.

Rife with hubris and ineptitude, the controversial history of climate control is best understood, Fleming argues, as a tragicomedy of ideas that reflect opportunism and an overdeveloped sense of technological capabilities. While he does not shrink from pointing out the unrealistic expectations of weather fixers (and they often make for an easy target), Fleming takes care not to deride his protagonists. Rather, he places them firmly within the scientific and cultural context of their time. For example, he tells the story of James Pollard Espy, the first meteorologist employed by the U.S. government. Besides establishing a national network of well-equipped weather observers in the 19th century, Espy believed that burning massive tracts of forest would create huge columns of heated air, which would trigger precipitation. Espy pressed his case in Washington, D.C., receiving the moniker "storm king" if not actual success in rain making.

A century later, researchers (including Nobelist Irving Langmuir) at General Electric's research laboratory in Schenectady, New York, undertook a multiyear program, funded in part by the Department of Defense, to explore the possibilities of widespread climate control. Placed in the context of the Cold War, with American generals expressing both a fervid desire for the next superweapon and an abiding faith in technology conditioned by World War II scientific successes, Langmuir's vision to control the global climate for strategic purposes appears understandable. Spurred in part by wildly speculative articles in 1950s popular magazines, hopes for weather control also helped fuel a rapid expansion of the meteorological sciences in general.

Full-blown weather warfare finally appeared in the 1960s in the skies over Vietnam, Laos, and Cambodia. Starting in 1967, American pilots flew more than 2600 sorties (at a cost of more than $18 million) to seed clouds in the hopes of generating rain. The goal of programs such as Project Popeye and Operation Motorpool was, as one advocate put it, "to make mud, not war" and reduce the traffic capacity of major transport routes used by the North Vietnamese Army. Funded by both the Johnson and Nixon administrations, these efforts continued until the "Watergate of weather warfare" thundered onto the front pages of U.S. newspapers in 1971. These programs, of course, were part of the broader war against nature that the U.S. military deployed in Southeast Asia. Claims of these programs' successes proved scientifically unverifiable, and unexpected outcomes of this technological fix were embarrassing congressional hearings and a Soviet propaganda victory.

Fixing the Sky
The Checkered History of Weather and Climate Control
by James Rodger Fleming
Columbia University Press, New York, 2010. 341 pp. $27.95, £19.95. ISBN 9780231144124.

While fascinating for historians of science, Fleming's narrative is especially relevant for contemporary policy-makers and scientists considering ways to mitigate climate change. Since 1992, a growing number of studies—Fleming provides an excellent recounting of how these emerged after the debacle of the 1970s—in both the United States and abroad have advocated some form of climate control as a possible palliative for global warming. The schemes are no less grandiose than those proposed 150 years ago by James Espy: arrays of orbiting mirrors to divert solar radiation, for example, or fleets of 747s dispersing millions of tons of specially engineered nanoparticles into the atmosphere to reflect the Sun's rays. Some plans involve government largesse. Other, more alarming, schemes imagine such planetary experiments conducted under the aegis of private sponsors. Almost all proposals borrow on martial metaphors and imagery, suggesting continued intertwining of climate modification research and military applications.

In highlighting the "foolishness of quick fixes," Fleming makes the persuasive case that history is directly relevant for under-

"Weather made to order?" Cover art from the 20 May 1954 issue of *Collier's*, accompanying an article on "progress in weather control" by U.S. Navy Captain H. T. Orville ("Ike's adviser").

CREDIT: THE ESTATE OF FREDERICK SIEBEL

The reviewer is at the Department of History, University of California, Santa Barbara, Humanities and Social Sciences Building, Santa Barbara, CA 93109, USA. E-mail: pmccray@history.ucsb.edu

standing current plans for weather modification and geoengineering. Today's planetary engineers, he argues, imagine themselves as technological pioneers and are unaware of decades, if not centuries, of similar speculations. More critically, technological solutions for global warming have the potential to distract policy-makers and citizens from strategies based on changing regulatory regimes and people's behavior.

When it comes to addressing climate change, technological fixes remain attractive to many conservative and libertarian politicians and economists. Fleming proposes instead a middle path that seeks neither dominion over weather nor a diminishment of dangers that environmental problems pose for the 21st century. Acknowledging previous attempts at climate control can offer researchers and policy-makers some valuable historical lessons. *Fixing the Sky* provides an essential foundation for understanding the long and dubious scientific tradition from which plans for climate control hail.

References

1. A. M. Weinberg, *Bull. At. Sci.* **22** (10), 4 (1966).

10.1126/science.1201627

HISTORY AND PHILOSOPHY OF SCIENCE

Computing the Climate and More

Richard C. J. Somerville

As a thought experiment, imagine an alternative history of our planet, one in which the digital electronic computer had never been invented. Then ask yourself how our ability to understand 21st-century climate change would have been affected. Because fossil fuels were already dominant in the precomputer era before World War II, it seems likely that even in this alternative history they would power our global energy system. So human-caused climate change would presumably now be well under way, much as it is today. Burning coal, oil, and natural gas would still produce a significant increase in the amount of carbon dioxide in the atmosphere, which would drive an altered greenhouse effect and shift climates around the globe. In this hypothetical world without computers, however, climate science would surely have achieved only a relatively primitive level of understanding. Researchers would have neither the observational evidence to adequately document climate change nor the scientific tools to understand and predict it. In our actual world, that plentiful evidence and those powerful tools both rely heavily on computer models.

A Vast Machine
Computer Models, Climate Data, and the Politics of Global Warming
by Paul N. Edwards
MIT Press, Cambridge, MA, 2010. 546 pp. $32.95, £24.95. ISBN 9780262013925.

Science in the Age of Computer Simulation
by Eric B. Winsberg
University of Chicago Press, Chicago, 2010. 164 pp. $66. ISBN 9780226902029. Paper, $24. ISBN 9780226902043.

A Vast Machine explores the ramifications of this key insight. Paul N. Edwards (a historian of science and technology at the University of Michigan) has written a book that is both a history of modern climate science and an analysis of the relation between that science and today's concerns about global warming. Climate contrarians often assert that computer simulations of climate are unreliable and that climate science should instead deal with observations of the actual climate. Although their primary motivation may be opposition to possible policies, their stated concern is usually a distrust of mainstream climate science. The contrarians insist that this science ought not to depend on an analysis of virtual climates produced by models, which are, after all, mere computer programs. Edwards, however, makes the reader understand that models play a central role in producing nearly all the climate observations that scientists use. For example, converting satellite measurements of atmospheric radiances into "observations" of temperature is a complex task involving models. In six short words, the central message of this book is "without models, there are no data."

Edwards traces the development of modern models of the climate system, research that branched off from numerical weather prediction in the 1950s. Such weather prediction relies on computer simulations that start with observations of present meteoro-

The reviewer is at Scripps Institution of Oceanography, University of California, San Diego, CA 92093–0224, USA. E-mail: rsomerville@ucsd.edu

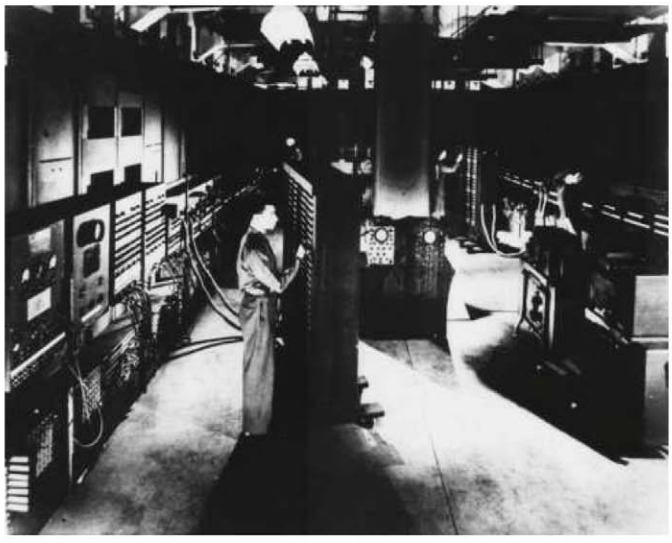

Computing power for early modeling. ENIAC filled a large room, consumed 140 kilowatts, and contained some 18,000 fragile vacuum tubes.

CREDIT: U.S. ARMY

logical conditions and calculate the detailed evolution of the state of the atmosphere (temperature, pressure, winds, and humidity) for up to about two weeks. This model-centered process is the basis of the daily weather forecasts that appear on television, radio, and the Internet and in newspapers. Present-day climate models are usually more comprehensive physically. Typically, such models simulate a complex, interactive system comprising not only the atmosphere but also oceans, snow and ice, land surfaces, and biogeochemical processes. Compared with weather forecast models, climate models also simulate far longer time periods, from months to millennia.

A Vast Machine does an especially good job at recounting details of the historical evolution of these models, without drowning the reader in jargon and, amazingly, without using any mathematics at all. Edwards has interviewed many of the pioneers in the field and has clearly explored the research literature extensively. His account will be readily accessible to that legendary target, the general reader, a broadly educated person interested in science and technology, among other things. Such a reader will, I expect, be particularly interested in Edwards's penetrating analysis of the role of climate science and models in the current political and policy discussion of how best to meet the imposing challenges of confronting man-made climate change.

The book will also fascinate members of the climate modeling research community. Although I have worked in this field for more than 40 years, I encountered many surprising and fascinating nuggets—including the disclosure that one celebrated early climate modeler never learned to program computers. Edwards's coverage does have a few limitations. He primarily emphasizes contributions from scientists in the United States, as he acknowledges, and he focuses much more strongly on the atmosphere than on other important components of the climate system. Within these limitations, the author's impressive scholarship and command of his material have produced a truly magisterial account.

Science in the Age of Computer Simulation is a very different book, and it may primarily intrigue a very different audience. In it, Eric Winsberg (a philosopher of science at the University of South Florida) considers the rise in the importance of computer simulations, not only in climate research but throughout science in general. His concern "is as much about what philosophers of science should learn in the age of simulation as it is about what philosophy can contribute to our understanding of how the digital computer is transforming science." He is interested in issues such as the relationship between experiment and computer simulation. He asks, for example, under what conditions should we expect a computer simulation to be reliable?

Such questions, while of broad importance to science in general, are also highly relevant to climate modeling, and here it may be helpful to establish some historical context. Computer simulations in science began after World War II and were at first confined to meteorology and nuclear weapons research. John von Neumann, a towering figure in 20th-century mathematics and mathematical physics, understood immediately that these two seemingly disparate fields are scientifically closely connected: both being centrally concerned with highly nonlinear fluid dynamics. And in both, carrying out controlled experiments and making measurements present great difficulties. The ENIAC (Electronic Numerical Integrator and Computer), the most important American computer during this period, was completed in late 1945 and initially used for hydrogen bomb calculations. Primitive by modern standards, it had a tiny memory and could carry out fewer than 400 typical multiplications per second. One early numerical weather prediction actually calculated not the meteorological conditions at Earth's surface but atmospheric circulation at an altitude of about 5500 meters. In 1950, such a prediction on the ENIAC required some 24 hours of computing time to produce a 24-hour forecast.

The crude but promising early computer simulations astonished meteorologists and led rapidly to operational numerical weather forecasts in the mid-1950s, first in Sweden and the United States. Some scientists also foresaw a new role for modeling. Von Neumann himself explicitly stated that computer simulations might "replace certain experimental procedures in some selected parts of mathematical physics." Indeed, when carrying out simulations routinely in many fields of science, researchers today often speak of "numerical experiments."

Winsberg comes at this issue from the perspective of a philosopher. He reminds us that philosophy of science has historically always drawn its motivations and directions from the science of the day. He notes that computer simulation now occupies a centrally important place in many fields of science. However, as he points out, such simulations typically are carried out within the constraints of existing fundamental theory, rather than changing or revolutionizing theory. Winsberg suggests that philosophy of science, in these contemporary scientific circumstances, ought now to concern itself with the subject of simulating complex phenomena within existing theory, as opposed to its traditional focus on the creation of novel scientific theories.

In *Science in the Age of Computer Simulation*, Winsberg explores this new direction in depth, with extensive references to both philosophical and scientific developments. He concludes,

> [W]hat we might call the ontological relationship between simulations and experiments is quite complicated. Is it true that simulations are, after all, a particular species of experiment? I have tried to argue against this claim, while at the same time insisting that the differences between simulation and experiment are more subtle than some of the critics of the claim have suggested. Most important, I have tried to argue that we should disconnect questions about the identity of simulations and experiments from questions of the epistemic power of simulations.

Such provocative findings, and Winsberg's exceptionally readable account of the reasoning that led him to them, will interest many general readers as well as scientists and philosophers of science.

10.1126/science.1200208

ATCGATCG

TruSeq™

The most accurate next-gen sequencing technology available.

Every Illumina sequencer is powered by TruSeq—the technology that delivers the most accurate human genome at any coverage. TruSeq produces the highest yield of error-free reads. The most bases over Q30. The greatest number of peer-reviewed publications—more than 1,000 in the past three years.

That's Tru data quality.

Get the proof. Go to
www.illumina.com/TruSeq

HiSeq™ 2000 HiSeq™ 1000 HiScan™ SQ Genome Analyzer$_{IIx}$

illumina®

SCIENCE EDUCATION

Changing the Culture of Science Education at Research Universities

Universities must better recognize, reward, and support the efforts of researchers who are also excellent and dedicated teachers.

W. A. Anderson,[1] U. Banerjee,[2] C. L. Drennan,[3] S. C. R. Elgin,[4] I. R. Epstein[5], J. Handelsman,[6] G. F. Hatfull,[7] R. Losick,[8*] D. K. O'Dowd,[9*] B. M. Olivera,[10] S. A. Strobel,[6] G. C. Walker,[3] I. M. Warner[11]

Professors have two primary charges: generate new knowledge and educate students. The reward systems at research universities heavily weight efforts of many professors toward research at the expense of teaching, particularly in disciplines supported extensively by extramural funding (*1*). Although education and lifelong learning skills are of utmost importance in our rapidly changing, technologically dependent world (*2*), teaching responsibilities in many STEM (science, technology, engineering, and math) disciplines have long had the derogatory label "teaching load" (*3*, *4*). Some institutions even award professors "teaching release" as an acknowledgment of their research accomplishments and success at raising outside research funds.

Some studies suggest little or no correlation between effective teaching, judged by student evaluations, and research, as measured by productivity and citations (*5*). But we contend that excellence in research and teaching need not be mutually exclusive but are instead intertwined and can interact synergistically to increase the effectiveness of both. The distinction between research and teaching is somewhat artificial; professors teach students how to learn from known sources in the classroom, but also how to create new knowledge in their research laboratories.

We are Howard Hughes Medical Institute (HHMI) professors, biomedical research scientists who receive support from HHMI for creating new programs that more effectively engage students in learning science. We represent a diversity of institutions, from well-endowed private universities to large and underfunded state universities. In our opinion, science education should not only provide broad content knowledge but also develop analytical thinking skills, offer understanding of the scientific research process, inspire curiosity, and be accessible to a diverse range of students. We should be preparing students for a lifetime of learning about science with

an understanding of its power and limitations. Evidence shows that approaches that accomplish these goals include active, engaging techniques; inquiry-based approaches; and research courses (*6*).

All of us have experienced the challenges of balancing teaching and research. Our ability to invest time and effort into improving undergraduate science education has been facilitated by extramural support and outside recognition provided by HHMI. How do we now help transform our research universities so that the teaching of science and scientific research are seen more broadly as equally valuable and mutually reinforcing?

Departmental and university cultures often do not adequately value, support, and reward effective pedagogy. Outstanding contributions to research are evaluated by standard measures (e.g., publications and grant support); are recognized globally as well as locally; and are rewarded within the university (e.g., with promotions or salary increases). Teaching, in contrast, is rarely judged and appreciated from the outside and often only minimally from within (*7*, *8*). To establish an academic culture that encourages science faculty to be equally committed to their teaching and research missions, universities must more broadly and effectively recognize, reward, and support the efforts of researchers who are also excellent and dedicated teachers.

Toward this end, we advocate seven initiatives (reflecting our views and not necessarily those of HHMI). Although many of these ideas are not new, the context in higher education has changed because of widespread concern about educating enough scientists and scientifically literate citizens (*9*) and because resources that enable change have improved markedly in recent years (*10*–*12*).

1. *Educate faculty about research on learning.* No scientist would engage in research without exploring previous work in the field, yet few university educators read education research. Universities can demonstrate that they value teaching by treating it as a scholarly activity, such as through faculty training in teaching that is predicated on evidence-based (*10*, *13*) approaches. Training should address education theory, tested practices, and methods to assess learning. Teachers should have time to experiment with new methods, identify strategies that they can implement effectively in specific settings, and take advantage of resources that enable translation of learning principles to teaching practice. These practices must include strategies to engage students in introductory courses, arguably the highest-impact change that could be made (*10*, *13*–*15*).

2. *Create awards and named professorships that provide research support for outstanding teachers*. Many universities recognize outstanding teachers with a special title or a modest monetary award. Campus-wide recognition should also include unrestricted funds, as is typical for named professorships, which make it feasible to sustain research activities while continuing to contribute to teaching excellence. Incorporating talks by these individuals into distinguished science lecture series is an opportunity to introduce innovative pedagogy. This may also attract a new donor population interested in sponsoring named professorships for faculty who have demonstrated excellence in the training of future scientists. In addition to campus-wide recognition, annual department-level awards for excellence in teaching could provide funds, allocated by the dean, to support

[1]Howard University, Washington, DC 20059, USA. [2]University of California, Los Angeles, Los Angeles, CA 90095, USA. [3]Massachusetts Institute of Technology, Cambridge, MA 02139, USA. [4]Washington University, St. Louis, MO 63130, USA. [5]Brandeis University, Waltham, MA 02453, USA. [6]Yale University, New Haven, CT 06520, USA. [7]University of Pittsburgh, Pittsburgh, PA 15260, USA. [8]Harvard University, Cambridge, MA 02138,USA. [9]University of California, Irvine, Irvine, CA 92697, USA. [10]University of Utah, Salt Lake City, UT 84112, USA. [11]Lousiana State University, Baton Rouge, LA 70803, USA.

*To whom correspondence should be addressed. E-mail: losick@mcb.harvard.edu or dkodowd@uci.edu

the scholarly activities of the recipient. This would not only help more faculty who have devoted significant effort to teaching maintain their research programs but also demonstrate to their colleagues that the effort required to achieve teaching excellence is valued. Named lecture series could bring professors from other universities who are distinguished as both research scientists and teachers to deliver a campus-wide lecture on pedagogy and a discipline-specific lecture on their research.

3. Require excellence in teaching for promotion. Formal criteria for tenure and promotion typically indicate that teaching and scholarship carry equal weight. The reality, however, is that most research-oriented universities promote faculty primarily on the basis of research achievements and ability to raise money from sources outside the university. Promotion that requires excellence in teaching would go a long way toward improving education. We need to reach agreement on broad goals of college science education and establish a rubric for evaluating the extent to which teachers are meeting these goals. We must identify the full range of teaching skills and strategies that might be used, describe best practices in the evaluation of teaching effectiveness (*16*, *17*) (particularly approaches that encourage rather than stifle diversity), and define how these might be used and prioritized during the promotion process.

4. *Create teaching discussion groups*. Teaching is often conducted out of sight of departmental colleagues. Even in large introductory classes that are taught by teams of instructors, members of the team are often absent from each other's presentations. To address this, both junior and senior faculty members should be brought together in small, peer teaching groups. Group members would attend each other's lectures and provide confidential critiques that highlight the most effective or innovative teaching strategies used and identify steps to increase effectiveness. Such peer support demonstrates that the department values, and shares responsibility for, good teaching. Group members are exposed to a variety of teaching strategies, some of which may positively affect their own practices. Annual meetings of the faculty at large, hosted by the dean, should routinely include discussion of innovative teaching strategies.

5. *Create cross-disciplinary programs in college-level learning*. Researchers are often left to fend for themselves in attempting to learn and implement best teaching practices and in evaluating how well students learn. Yet many research universities have unexploited resources that could be drawn upon to improve college-level learning. For example, many universities have Departments or Schools of Education, but only a few of those [e.g., (*18*, *19*)] include in their mission undergraduate-level learning or robust connections to, and collaborations with, faculty members in STEM departments. Such collaborations could spawn innovative programs for experimentation and evaluation of teaching practices in the sciences. Psychology Departments often have experts in cognitive science who would be valuable participants in such programs. Though extensive discussion of best teaching practices is beyond the scope of this piece, we refer readers, e.g., to (*10*, *13*, *20*–*23*), as well as the Supporting Online Material.

6. Provide ongoing support for effective science teaching. The National Academies Summer Institute has helped faculty from almost 100 research universities implement principles of scientific teaching (*24*). University-based teaching centers provide professional support to faculty for assessment across disciplines, as well as training teaching assistants. Some STEM programs explicitly include in their mission the support and improvement of STEM education [e.g., (*25*, *26*)]. There is no better way to teach science than to engage students in doing science (*27*–*29*). To provide such opportunities for large numbers of students demands ingenuity, a willingness to seek out and support mentors, and provision of lab and field facilities. Projects that can draw on student peer-mentoring deserve special attention as benefiting both mentor and mentee.

7. *Engage chairs, deans, and presidents*. The critical ingredient in creating a culture that values and promotes both teaching and science is leadership. Chairs of STEM departments, deans of schools, and presidents of universities must elevate the status of the teacher-scientist, communicate the importance they attach to effective teaching, and create and support programs that promote innovation in science education [e.g., (*30*)].

The issues we raise go beyond the sciences. Increasingly, it seems that parents, funders of higher education, and others are questioning the value of the education that research universities provide. The continued vitality of research universities requires that we foster a culture in which teaching and research are no longer seen as being in competition, but as mutually beneficial activities that support two equally important enterprises: generation of new knowledge and education of our students.

References and Notes

1. V. Savkar, J. Lokere, *Time to Decide: The Ambivalence of the World of Science Toward Education* (Nature Education, Cambridge, MA, 2010); http://bit.ly/blWaPr.
2. J. B. Labov, A. H. Reid, K. R. Yamamoto, *CBE Life Sci. Educ.* **9**, 10 (2010).
3. A. L. Johnson, *J. Chem. Educ.* **8**, 115 (1931).
4. L. V. Koos, *The Adjustment of Teaching Load in a University* (Government Printing Office, Washington, DC, 1919); www.archive.org/details/adjustmentofteac00koosuoft.
5. H. W. Marsh, J. Hattie, *J. Higher Educ.* **73**, 603 (2002).
6. R. A. Duschl, H. A. Schweingruber, A. W. Shouse, Eds., *Taking Science to School: Learning and Teaching Science in Grades K–8* (National Academies Press, Washington, DC, 2007).
7. R. Wilson, *Chron. High. Educ.* **57**(3), A1 (2010); http://chronicle.com/article/Why-Teaching-Is-Not-Priority/124301/.
8. M. C. Taylor, *Chron. High. Educ.* **56**(42), A22 (2010); http://chronicle.com/article/An-Academy-to-Support/123779/.
9. Committee on Prospering in the Global Economy of the 21st Century *et al., Rising Above the Gathering Storm: Energizing and Employing America for a Brighter Economic Future* (National Academies Press, Washington, DC, 2007).
10. J. Handelsman, S. Miller, C. Pfund, *Scientific Teaching* (Freeman, New York, 2007).
11. Education Resources Information Center, www.eric.ed.gov/.
12. Multimedia Educational Resource for Learning Online, www.merlot.org/merlot/index.htm.
13. W. B. Wood, *Annu. Rev. Cell Dev. Biol.* **25**, 93 (2009).
14. J. Fairweather, *Linking Evidence and Promising Practices in Science, Technology, Engineering, and Mathematics (STEM) Undergraduate Education: A Status Report for The National Academies National Research Council Board of Science Education* (BOSE) (BOSE, Washington, DC, 2010); www7.nationalacademies.org/bose/Fairweather_Commissioned-Paper.pdf.
15. N. Lasry, E. Mazur, J. Watkins, *Am. J. Phys.* **76**, 1066 (2008).
16. R. B. Barr, J. Tagg, *Change* **27**, 13 (1995); http://ilte.ius.edu/pdf/BarrTagg.pdf.
17. M. W. Klymkowsky, K. Garvin-Doxas, M. Zeilik, *Cell Biol. Educ.* **2**, 155 (2003).
18. University of Maryland Physics Education Research Group, www.physics.umd.edu/perg/.
19. Physics Education Research at Colorado University—Boulder, www.colorado.edu/physics/EducationIssues/.
20. D. Bok, *Our Underachieving Colleges: A Candid Look at How Much Students Learn and Why They Should Be Learning More* (Princeton Univ. Press, Princeton, NJ, 2005).
21. R. R. Hake, *Latin Am. J. Phys. Edu.* **1**, 24 (2007).
22. M. A. McDaniel, A. A. Callender, in *Learning and Memory: A Comprehensive Reference*, J. Byrne *et al*., Eds. (Elsevier, Oxford, 2008).
23. H. Pashler *et al*., *Organizing Instruction and Study to Improve Student Learning* (NCER 2007-2004, National Center for Education Research, U.S. Department of Education, Washington, DC, 2007).
24. C. Pfund *et al.*, *Science* **324**, 470 (2009).
25. STEM at North Carolina State University, http://stem.ncsu.edu/.
26. College of Engineering, https://engineering.purdue.edu/Engr/Academics/Schools.
27. R. Taraban, R. L. Blanton, Eds., *Creating Effective Undergraduate Research Programs in Science* (Teachers College Press, New York, 2008).
28. E. Seymour, A.-B. Hunter, S. L. Laursen, T. DeAntoni, *Sci. Educ.* **88**, 493 (2004).
29. D. Lopatto, *Cell Biol. Educ.* **3**, 270 (2004).
30. C. Wieman, K. Perkins, S. Gilbert, *Change* (March-April 2010).

Supporting Online Material

www.sciencemag.org/cgi/content/full/331/I6014/152/DC1

10.1126/science.1198280

GEOCHEMISTRY

When Continents Formed

Island arc rocks provide a better constraint on when the continental crust was generated.

Bruno Dhuime,[1,2] Chris Hawkesworth,[1] Peter Cawood[1]

When and how the continental crust was generated remains a fundamental question in Earth sciences. It has been widely believed that the trace element–enriched continental crust and the depleted upper mantle are complementary reservoirs, and that the continental crust has grown from the depleted upper mantle (*1*, *2*). Model ages for neodymium (Nd) and hafnium (Hf) isotopes reflect when new continental crust was generated (*2*), and traditionally they have been calculated for crust derived from the depleted mantle (see the figure, left panel). The implication is that the isotope composition of the depleted mantle is similar to that of new continental crustal material as it is extracted from the mantle. However, the isotope composition of island arc rocks, and hence of new continental crust, is different from that of the depleted mantle (*3*, *4*). We argue that model ages should be calculated using the composition of new continental crust, which is generally more enriched isotopically than the depleted mantle.

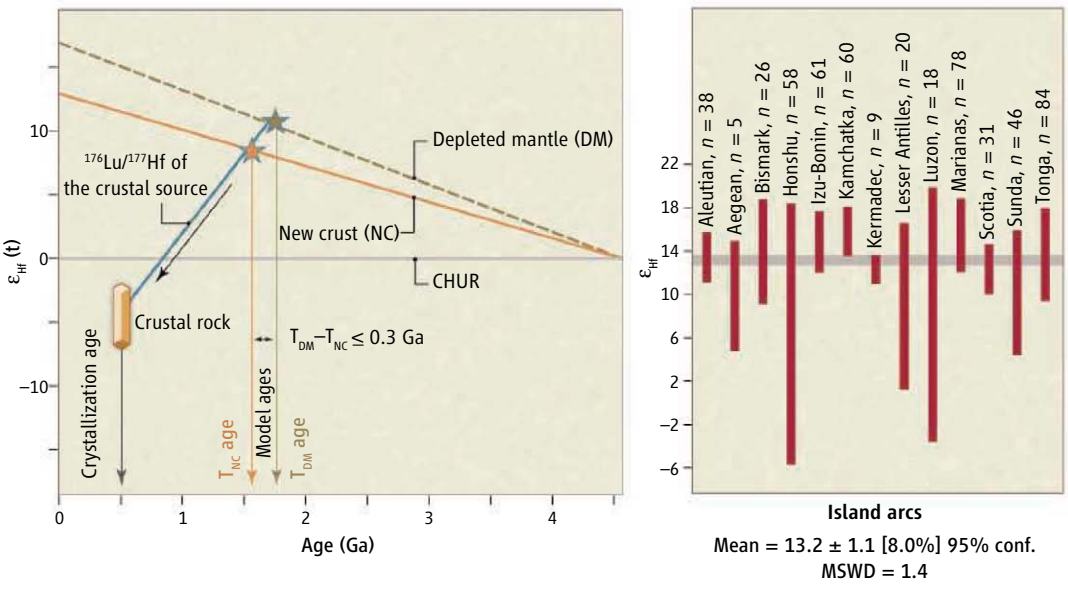

Setting a date. (**Left**) Graphical representation of the Hf isotope evolution of the depleted mantle (DM) and of new continental crust (NC). The DM and NC evolution curves are those for linear evolution from a chondritic uniform reservoir (CHUR) value at Earth's formation [i.e., 0 at 4.56 billion years ago (Ga)] to $\varepsilon_{Hf} = 17$ at the present for the depleted mantle (*6*, *7*), and $\varepsilon_{Hf} = 13.2$ for the new crust (see right panel). Hafnium "model ages" represent when new continental crust was generated, and they are typically calculated using an average $^{176}Lu/^{177}Hf$ ratio for the crustal source of the magma analyzed. Hafnium model ages are younger when calculated from the evolution curve for new continental crust (T_{NC} ages) than for the depleted mantle (T_{DM} ages). (**Right**) A worldwide compilation of Hf isotopes in volcanic rocks from 13 modern island arcs (whole-rock analyses, $n = 534$; GEOROC online database compilation, http://georoc.mpch-mainz.gwdg.de/georoc/Entry.html). Red vertical bars represent the average value (at 2-SD precision) for each island arc. The weighted average of the means of 13 arcs ($\varepsilon_{Hf} = 13.2$) is taken as a proxy for the composition of the present-day new continental crust.

Mass balance calculations indicate that at least 80% the continental crust was generated along destructive plate margins (*5*). This implies that magmas generated along destructive plate margins should be used to constrain the isotope composition of new crust at the time of its formation. The Hf isotope records from modern island arcs worldwide are thought to be more representative of the isotope ratios of new crust being generated from the mantle than are magmas generated along active continental margins, which are more prone to shallow-level processes of crustal contamination. The Hf (and Nd) isotope ratios in island arcs are on average lower than the present-day value for the depleted mantle (see the figure, right panel) (*3*, *4*, *6*, *7*), primarily because of contributions from subducted sediment (*3*, *4*, *8*).

Zircons are the only widely used record available for the first 500 million years of Earth history, and the development of in situ analyses of integrated U-Pb and Hf isotopes in zircon has had a major impact in studies of the evolution of the continental crust (*1*). Hf isotope ratios are expressed as ε_{Hf}, which denotes the deviation of the $^{176}Hf = {}^{177}Hf$ ratio of the sample from the contemporaneous ratio of the chondritic uniform reservoir (CHUR), multiplied by 10^4. Thousands of analyses are now available, and zircons present in sediments and sedimentary rocks provide more representative records than the zircons in igneous rocks (*1*). Analyzing the Hf isotope composition and crystallization age of thousands of zircons worldwide shows that very few zircons plot close to the depleted mantle (*1*) and hence have model ages similar to their crystallization ages. For instance, there is widespread agreement that appreciable volumes of new crust were generated in the late Archean around 2.7 billion years ago (*9*), but late Archean samples all plot appreciably below the depleted mantle curve (*1*). These observations reaffirm that the model ages of continental crust formation should not be calculated from the depleted mantle composition, but rather should be calculated relative to the isotope composition of material that represents new continental crust at the time of its extraction from the mantle (see the figure, left panel).

The best estimate for the present-day composition of the average new crust is $\varepsilon_{Hf} = 13.2 \pm 1.1$, the weighted average of the means of 13 modern island arcs worldwide (see the figure, right panel). The secular evolution of the new continental crust is represented by the red curve in the left panel. Its

[1]Department of Earth Sciences, University of St. Andrews, North Street, St. Andrews, Fife KY16 9AL, UK. [2]Department of Earth Sciences, University of Bristol, Wills Memorial Building, Queen's Road, Bristol BS8 1RJ, UK. E-mail: b.dhuime@bristol.ac.uk

linear evolution is consistent with models for continental growth in which new continental crust is continuously generated along destructive plate margins (*1*, *10*). Relatively few zircons (<2%) plot between the depleted mantle and the new crust curves (*1*), which suggests that incorporation of preexisting crustal material into the mantle source of the pristine continental crust has been a long-standing feature, at least since the onset of plate tectonics and the development of supercontinents around 3.0 billion years ago (*11*).

Model ages calculated from the composition of the new crust are up to 300 million years younger than model ages traditionally calculated from the depleted mantle. As a result, new crust ages are generally more consistent with the geological record, which opens new perspectives in crustal evolution studies based on radiogenic isotopes.

References

1. C. J. Hawkesworth *et al.*, *J. Geol. Soc. London* **167**, 229 (2010).
2. D. J. DePaolo, *Nature* **291**, 193 (1981).
3. W. M. White, P. J. Patchett, *Earth Planet. Sci. Lett.* **67**, 167 (1984).
4. C. Chauvel, E. Lewin, M. Carpentier, N. T. Arndt, J.-C. Marini, *Nat. Geosci.* **1**, 64 (2008).
5. R. L. Rudnick, *Nature* **378**, 573 (1995).
6. V. J. M. Salters, A. Stracke, *Geochem. Geophys. Geosyst.* **5**, Q05B07 (2004).
7. R. K. Workman, S. R. Hart, *Earth Planet. Sci. Lett.* **231**, 53 (2005).
8. T. Plank, *J. Petrol.* **46**, 921 (2005).
9. K. C. Condie, *Geophys. Res. Lett.* **22**, 2215 (1995).
10. S. R. Taylor, S. M. McLennan, *The Continental Crust: Its Composition and Evolution* (Blackwell, Oxford, 1985).
11. P. A. Cawood, A. Kröner, S. Pisarevsky, *Geol. Soc. Am. Today* **16**, 4 (2006).

10.1126/science.1201245

PHYSICS

A New Twist for Electron Beams

Rodney Arthur Herring

Passing an electron beam through carefully prepared holograms creates electron vortex beams that improve resolution and allow samples to be manipulated.

The transmission electron microscope (TEM) has primarily been used by physical and life scientists for imaging structures and compositions ranging in size from atoms to cells. New applications are likely to emerge from recent demonstrations that it is possible to change the nature of the primary electron source used to create images. Normally, an electron is emitted from its source in a TEM as a plane wave. However, as shown on page 192 of this issue by McMorran *et al*. (*1*) as well in recent studies by Verbeeck *et al*. (*2*), passing the electron plane wave through a hologram that contains a dislocation causes it to undergo diffraction and split into an electron vortex beam. This type of electron beam can be used to create higher-resolution images and to manipulate the structure and properties of the sample.

When an electron beam diffracts from these holograms, it has a singularity in the quantum mechanical phase along the center of the beam; the phase is not well defined. Interference effects cause the central beam intensity to vanish, creating instead a vortex of twisted beams spiraling around this node that passes through the microscope (see the figure, panel A). The absence of intensity at the beam center can be used to improve the resolution of the scanning mode of electron imaging, because resolution is determined by the beam's spot size, and the central beam is the most difficult to focus.

Another useful property of these vortex electron beams is that they have an associated orbital angular momentum (OAM). Like an ice dancer doing a spin, the spiraling wavefront of the electron vortex beam carries OAM. However, the electron beams are charged, so the OAM can couple with electrons, electrostatic charges, and magnetic potentials in the sample. Electron vortex beams could be used to induce currents in superconductors, apply magnetic fields at the nanoscale, and make or break electronic bonds. New types of electron beam lithography may enable the building of three-dimensional nanostructures in which atoms are picked up, moved, and set in place rapidly and accurately.

The singularity at the center of the electron vortex also has a topological charge of m that is a measure of the number of the twists per electron wavelength. Here, m increases with the higher-order diffracted beams and enables greater coupling with the atomic structures. The holograms are nanofabricated gratings with a dislocation where one or more lines are added to half of the grating. A dislocation core that adds one line (one grating line forks into two) produces $m = 1$ for the first diffracted beam, $m = 2$ for the second diffracted beam, and so forth. McMorran *et al*. created a hologram with 25 lines added at the dislocation that has $m = 25$ for the first diffracted beam, $m = 50$ for the second diffracted beam, and up to $m = 100$ for the fourth diffracted beam. However, this higher topological charge comes at a price—the intensity of the diffracted beam is lower, and may be too low for adequate coupling with some types of structures.

These limitations aside, an immediate application of electron vortex beams is to produce new types of communication and

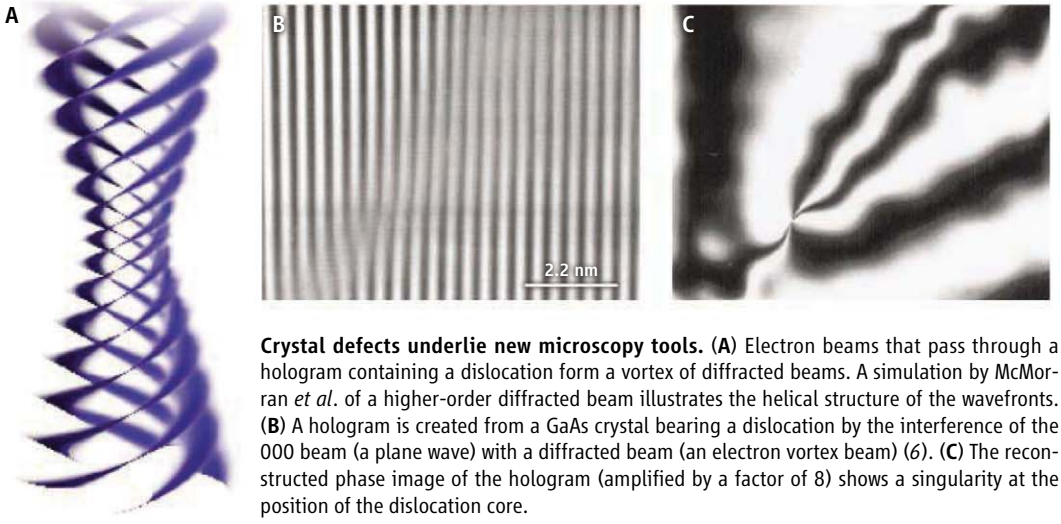

Crystal defects underlie new microscopy tools. (**A**) Electron beams that pass through a hologram containing a dislocation form a vortex of diffracted beams. A simulation by McMorran *et al*. of a higher-order diffracted beam illustrates the helical structure of the wavefronts. (**B**) A hologram is created from a GaAs crystal bearing a dislocation by the interference of the 000 beam (a plane wave) with a diffracted beam (an electron vortex beam) (*6*). (**C**) The reconstructed phase image of the hologram (amplified by a factor of 8) shows a singularity at the position of the dislocation core.

Mechanical Engineering, University of Victoria, Victoria, British Columbia V8W 3P6, Canada. E-mail: rherring@uvic.ca

memory devices at the nanoscale (for example, altering spin states for memory applications). For imaging, the spiral phase of their wavefront will enhance phase contrast microscopy of the edges of samples with low absorption contrast, such as unstained biological specimens, macromolecules, carbon nanotubes, and polymers. For analytical microscopy, electron vortex beams will provide new capabilities for electron energy loss spectroscopy, which can provide information about atomic composition. For structural microscopy, they will provide new crystallographic information of the specimen in the electron diffraction mode. For measurements of the specimen properties, they will provide new optical, electronic, and magnetic information.

The development of these electron vortex beams builds on a number of previous observations. First, it was realized that linearly polarized light beams carry OAM (*3*). Soon thereafter, the trapping and rotation of particles in the vortex produced by diffraction from a hologram containing a dislocation was demonstrated (*4*). The rotation could be reversed by changing the sign of the OAM, either by turning over the hologram or by using the opposite of diffracted beams from the hologram that rotate in the opposite direction. The same method was proposed for electrons in which the hologram consisted of a very thin crystal with a dislocation (*5*). The thin grating provided by a crystal's atomic planes separate the electron vortex beams because the wavelength of high-energy electrons is small, only a few picometers.

A few years ago, Uchida proposed an experiment to my group in which a strained gallium arsenide (GaAs) crystal containing dislocations would be used to create holograms. This kind of experiment had previously been shown possible by diffracted beam holography (see the figure, panels B and C) (*6*). We performed the experiment with Koh Saitoh and his group at Nagoya University but failed in recording the images. However, Uchida and Tonomura (*7*) proved the concept using a stacked, thin film of graphite flakes that produced a semi-helical electron vortex beam.

Using helical-phase plates poses several challenges. They are difficult to fabricate with nanometer precision, they create unwanted internal Bragg and diffuse scattering of the electron beam, and surface contamination distorts their shape. Verbeeck *et al*. (*3*) and McMorran *et al.* came closer to Uchida's proposed crystal hologram by exploiting fabrication of defect holograms with focused ion beam (FIB) methods. A drawback of FIB-made holograms is their coarse grating relative to that of atomic planes, which results in shallower angles of diffraction of the electron vortex beams. However, an advantage that is not available with the crystal hologram is the production of dislocation cores having multiple half gratings. These structures induce large topological charges, as shown by McMorran *et al*.

Researchers should rapidly exploit the new capabilities of electron vortex beams. They are simple to implement, requiring merely the insertion of a dislocated hologram into the condenser aperture of the electron microscope. This capability should enable researchers to image in new ways, make new types of measurements, and manipulate the electrons and atoms in material in a manner never before possible.

References

1. B. J. McMorran *et al*., *Science* **331**, 192 (2011).
2. J. Verbeeck, H. Tian, P. Schattschneider, *Nature* **467**, 301 (2010).
3. L. Allen, M. W. Beijersbergen, R. J. C. Spreeuw, J. P. Woerdman, *Phys. Rev. A* **45**, 8185 (1992).
4. H. He, M. E. J. Friese, N. R. Heckenberg, H. Rubinsztein-Dunlop, *Phys. Rev. Lett.* **75**, 826 (1995).
5. K. Y. Bliokh, Y. P. Bliokh, S. Savel'ev, F. Nori, *Phys. Rev. Lett.* **99**, 190404 (2007).
6. R. A. Herring, G. Pozzi, in *Introduction to Electron Holography*, E. Volkl, L. F. Allard, D. C. Joy, Eds. (Kluwer Academic/Plenum, New York, 1999), pp. 295–310.
7. M. Uchida, A. Tonomura, *Nature* **464**, 737 (2010).

10.1126/science.1200643

PALEOCLIMATE

Northern Meltwater Pulses, CO_2, and Changes in Atlantic Convection

Detailed evidence of how the North Atlantic Meridional Overturning Circulation behaved after the last ice age.

Michael Sarnthein

Global climatic and oceanic conditions underwent fundamental transformations after the last ice age ended about 19,000 years ago. In the North Atlantic, for example, the deglaciation was marked by major changes in the Meridional Overturning Circulation (MOC), which carries warm and highly saline surface water north to cooler regions, where it sinks and creates "deep water" that eventually cycles back to the surface. This process plays a substantial role in regulating climate and levels of atmospheric carbon dioxide (CO_2), and understanding how it operated in the past is important to understanding how it may influence climate in the future. On page 202 of this issue, Thornalley *et al*. (*1*) provide impressive and detailed evidence of how the North Atlantic MOC behaved after the Last Glacial Maximum (LGM), between 19,000 and 10,000 years ago. In particular, they show that the MOC experienced a series of abrupt changes that lasted from decades to centuries, and that some of the water masses involved were far older—and may have stored and released more carbon—than once believed.

Thornalley *et al*.'s findings are based primarily on measurements of the ratio of carbon-14 to carbon-12 ($^{14}C/^{12}C$) in the shells of small marine organisms, called foraminifera, obtained from four marine sediment cores collected south of Iceland in waters between 1200 and 2300 m deep. These isotopic measurements, together with data from Greenland ice cores (*2*) that helped calibrate the ages of the cores, enabled the authors to reconstruct the apparent "ventilation age" of the water masses in which the foraminifera once lived, or roughly how long it had been since the water was near the surface and in equilibrium with the atmosphere. In addition, the authors used another isotopic signature, the ratio of carbon-13 to carbon-12 ($\delta^{13}C$) in benthic (bottom-dwelling) foraminifera, to help reveal the different histories of masses of deep and intermediate water.

Today, intensive convection in the North Atlantic quickly transfers surface waters to depth, and newly formed deep water typi-

Institute for Geosciences, University of Kiel, D24098 Kiel, Germany. E-mail: ms@gpi.uni-kiel.de

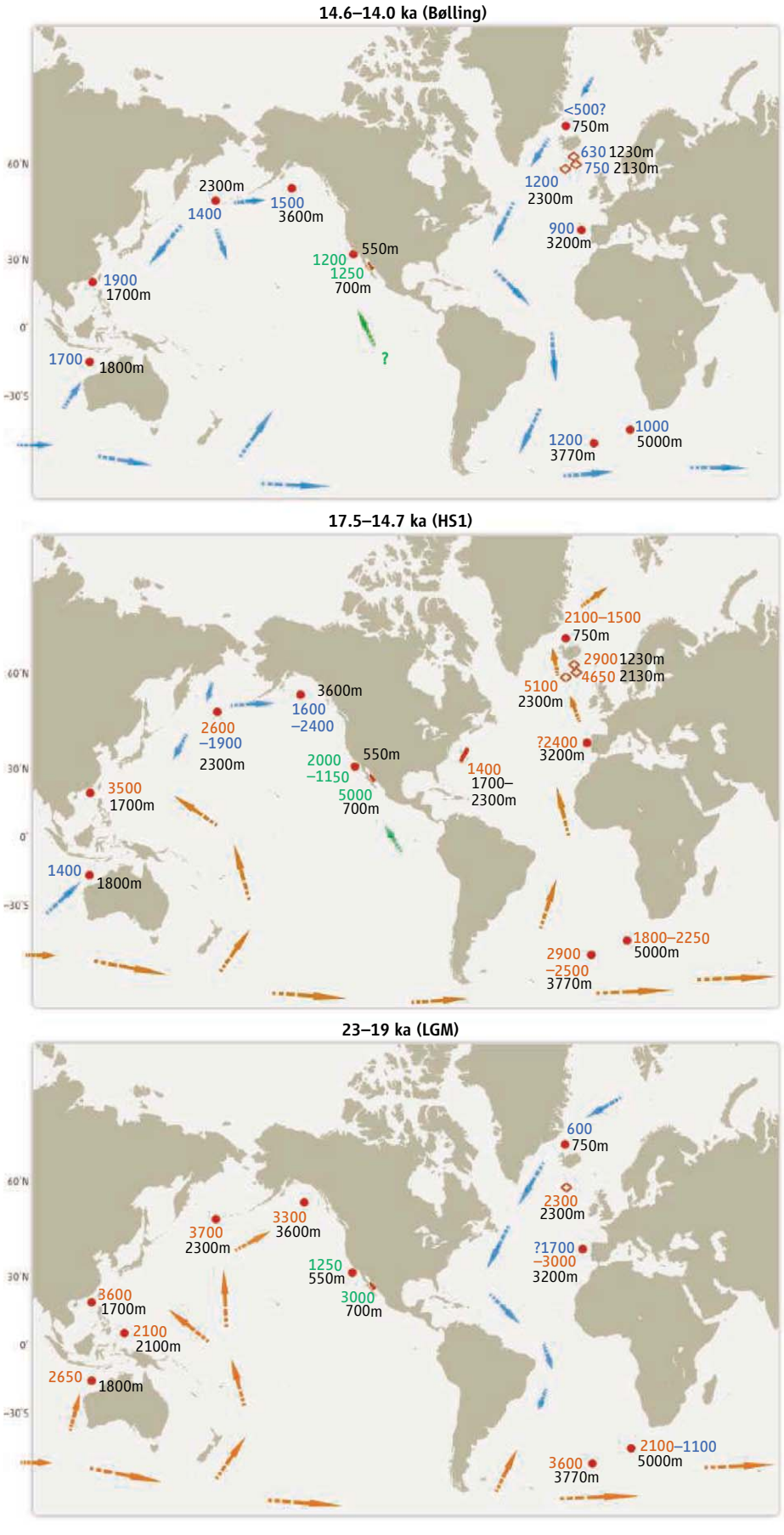

Changing circulation. Average apparent ^{14}C ventilation ages and possible short-term circulation changes of ocean deep and intermediate waters during the Bølling interstadial, Heinrich stadial 1 (HS1), and the Last Glacial Maximum (LGM). Ages in blue are as low as or lower than current ages, indicating good ocean ventilation. Ages in orange are higher than current ages, and represent CO_2-enriched waters. Numbers in green are ^{14}C ages of topmost intermediate waters outside the Nordic Sea, and numbers in black are water depths (rounded). Benthic ventilation ages are ignored, when deduced from planktonic reservoir ages of 400 years, which are assumed constant. Arrows suggest circulation patterns of ventilated (blue) and less ventilated (orange) waters, inferred from the gradual aging of deep waters per analogy to today. {Data are from (*1*) (red diamonds), (*3*), (*6*–*8*), (*17*, *18*), [(*19*); modified] (red dots), and (*9*), U/Th-based coral ages (red bar)}.

cally has a ventilation age of ~500 years. In contrast, Thornalley *et al*. report that during the Heinrich stadial 1 (HS1), a cold interval that occurred between about 17,500 and 14,700 years ago, a mass of extremely old water, up to 5200 years old, reached the Atlantic Ocean's northern "dead end." They suggest this was intermediate water that originated in the Southern Ocean near Antarctica, and its age would once have been considered unreasonable. In addition, they found that the ventilation ages of past surface waters could vary by as much as 2100 years, which agrees with results of other methods (*3*) and challenges a common, but little-substantiated dogma: that past surface waters had ventilation ages of ~400 years, similar to a current age average. The data also reveal a centennial-scale event of deep-water convection in the northeastern Atlantic near the end of HS1, which appears to be related to a prominent meltwater pulse from the Barents Shelf (*4*).

These results document major short-term and regional changes in the MOC that were controlled by differences in the melting of ice in the Northern Hemisphere. And, when melded with findings from other regions obtained with different techniques (*3*, *5*–*9*), they provide a fuller picture of the MOC's history (see the figure). Together, the data support the concept that extremely old deep and intermediate waters existed during the LGM and HS1.

These authors highlight the value of taking a long-term, historical approach to understanding the global ocean's thermohaline circulation system, or "salinity conveyor belt" (*10*, *11*), which is not revealed by short-term physical oceanographic records from the modern era (*12*). For example, inferring apparent ventilation ages from the ^{14}C age of CO_2, which is dissolved in seawater (*13*) and

fixed in carbonate shells, can help researchers estimate where and how fast the conveyor has moved. Today, it appears that a deepwater parcel that forms in the North Atlantic will reach the southernmost Atlantic after about 1400 "^{14}C years," and reach the northeastern Pacific after more than 2200 ^{14}C years; this is equivalent to a deepwater ^{14}C loss of ~250 per mil (‰).

Such old ages and long cycling times are important because they suggest the ocean absorbed, stored, and released vast quantities of carbon in the past. Below 2000-m depth, the gradual aging of modern ocean waters is closely linked to a gradual rise in dissolved CO_2. Today, a 50‰ decrease in global deepwater ^{14}C corresponds approximately to a 7-µmol/kg rise in (natural) dissolved CO_2 in deep water (*14*). Researchers can use this relationship to deduce, from about a dozen existing reconstructions of paleoventilation ages, MOC and CO_2 storage patterns during the LGM and HS1 (see the figure). These "time slices" suggest that deep waters at those times were, on average, ~1000 to ~2000 years older than they are today. Such ages suggest that the ocean absorbed and stored a massive amount of atmospheric CO_2 during the LGM and early HS-1, when atmospheric CO_2 concentrations dropped (*15*). It now appears that deepwater CO_2 concentrations in about half of the ocean's volume then increased to levels that were 14 to 28 µmol/kg higher than today's concentrations. An urgent challenge for paleoceanographers is to improve these estimates by developing a global network of additional paleoventilation ages.

In this context, Thornalley *et al.*'s findings represent real progress. For instance, their extremely old ventilation ages for intermediate and deep waters—together with other high ages—may help explain what happened during the "mystery interval" (*16*), a period of rapid decrease in atmospheric ^{14}C that occurred 17,500 to 14,500 years ago. Overall, the increasing number of apparent ventilation ages of deep and intermediate waters form a highly promising first step to achieving a crucial paleoceanographic objective: linking changes in basin-wide MOC to global climate and the ocean's capacity for storing atmospheric CO_2.

References and Notes

1. D. J. R. Thornalley, S. Barker, W. S. Broecker, H. Elderfield, I. N. McCave, *Science* **331**, 202 (2011).
2. S. O. Rasmussen *et al.*, *J. Geophys. Res.* **111**, D06102 (2006).
3. M. Sarnthein, P. Grootes, J. P. Kennett, M. J. Nadeau, *Geophys. Monogr. Ser.* **173**, 175 (2007).
4. M. Sarnthein *et al.*, in *The Northern North Atlantic: A Changing Environment*, P. R. Schäfer, W. Schlüter, J. Thiede, Eds. (Springer, Berlin, 2000), pp. 365–410.
5. J. F. Adkins, E. A. Boyle, *Paleoceanography* **12**, 337 (1997).
6. T. M. Marchitto, S. J. Lehman, J. D. Ortiz, J. Flückiger, A. van Geen, *Science* **316**, 1456 (2007).
7. S. Barker, G. Knorr, M. J. Vautravers, P. Diz, L. C. Skinner, *Nat. Geosci.* (2010).
8. L. C. Skinner, S. Fallon, C. Waelbroeck, E. Michel, S. Barker, *Science* **328**, 1147 (2010).
9. L. F. Robinson *et al.*, *Science* **310**, 1469 (2005).
10. H. Stommel, *Tellus* **13**, 224 (1961).
11. W. S. Broecker, *Oceanography (Wash. D.C.)* **4**, 79 (1991).
12. C. Wunsch, *Quat. Sci. Rev.* **29**, 1960 (2010).
13. K. Matsumoto, *J. Geophys. Res.* **112** (C9), C09004 (2007).
14. R. M. Key *et al.*, *Global Biochem. Cycles* **18**, GB4031 (2004).
15. J. Yu *et al.*, *Science* **330**, 1084 (2010).
16. W. S. Broecker, S. Barker, *Earth Planet. Sci. Lett.* **256**, 90 (2007).
17. H. Gebhardt *et al.*, *Paleoceanography* **23**, PA4212 (2008).
18. M. Sarnthein, P. M. Grootes, A. Holbourn, W. Kuhnt, H. Kühn, *Earth Planet. Sci. Lett.* (2011).
19. W. S. Broecker *et al.*, *Science* **306**, 1169 (2004).

20. The kind support of B. Schneider with evaluating oceanic CO_2 data and of P. Grootes in discussing this article is gratefully acknowledged.

10.1126/science.1201144

CLIMATE CHANGE

Lessons from Earth's Past

What can be learned from Earth's past to guide our understanding of life in a warming world?

Jeffrey Kiehl

Climate models are invaluable tools for understanding Earth's climate system. But examination of the real world also provides insights into the role of greenhouse gases (carbon dioxide) in determining Earth's climate. Not only can much be learned by looking at the observational evidence from Earth's past, but such knowledge can provide context for future climate change.

The atmospheric CO_2 concentration currently is 390 parts per million by volume (ppmv), and continuing on a business-as-usual path of energy use based on fossil fuels will raise it to ~900 to 1100 ppmv by the end of this century (see the first figure) (*1*). When was the last time the atmosphere contained ~1000 ppmv of CO_2? Recent reconstructions (*2*–*4*) of atmospheric CO_2 concentrations through history indicate that it has been ~30 to 100 million years since this concentration existed in the atmosphere (the range in time is due to uncertainty in proxy values of CO_2). The data also reveal that the reduction of CO_2 from this high level to the lower levels of the recent past took tens of millions of years. Through the burning of fossil fuels, the atmosphere will return to this concentration in a matter of a century. Thus, the rate of increase in atmospheric CO_2 is unprecedented in Earth's history.

What was Earth's climate like at the time of past elevated CO_2? Consider one example when CO_2 was ~1000 ppmv at ~35 million years ago (Ma) (*2*). Temperature data (*5*, *6*) for this time period indicate that tropical to subtropical sea surface temperatures were in the range of 35° to 40°C (versus present-day temperatures of ~30°C) and that sea surface temperatures at polar latitudes in the South Pacific were 20° to 25°C (versus modern temperatures of ~5°C). The paleogeography of this time was not radically different from present-day geography, so it is difficult to argue that this difference could explain these large differences in temperature. Also, solar physics findings show that the Sun was less luminous by ~0.4% at that time (*7*). Thus, an increase of CO_2 from ~300 ppmv to 1000 ppmv warmed the tropics by 5° to 10°C and the polar regions by even more (i.e., 15° to 20°C).

What can we learn from Earth's past concerning the climate's sensitivity to greenhouse gas increases? Accounting for the increase in CO_2 and the reduction in solar irradiance, the net radiative forcing—the change in the difference between the incoming and outgoing radiation energy–of the climate system at 30 to 40 Ma was 6.5 to 10 W m^{-2} with an average of ~8 W m^{-2} (see the second figure). A similar magnitude of forcing existed for other past warm climate periods, such as the warm mid-Cretaceous of 100 Ma (*8*). Using the proxy temperature data and assuming, to first order,

National Center for Atmospheric Research, Boulder, CO 80305, USA. E-mail: jtkon@ucar.edu

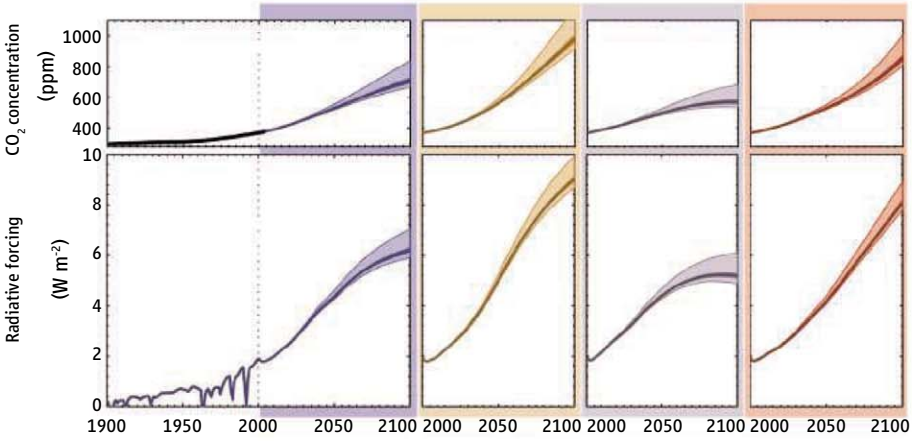

Current and future emissions. Time series for CO_2 concentration and radiative forcing are shown for four scenarios of CO_2 emission into the atmosphere based on energy-economic models described by the IPCC in (*1*). These scenarios are described in the Special Report on Emissions Scenarios by the IPCC. [The graphs are reprinted from (*1*) with permission from Cambridge University Press]

that latitudinal temperature can be fit with a cosine function in latitude (*9*), the global annual mean temperature at this time can be estimated to be ~31°C, versus 15°C during pre-industrial times (around 1750) (*10*). Thus, Earth was ~16°C warmer at 30 to 40 Ma. The ratio of change in surface temperature to radiative forcing is called the climate feedback factor (*11*). The data for 30 to 40 Ma indicate that Earth's climate feedback factor was ~2°C W^{-1} m^{-2}. Estimates (*1*, *11*) of the climate feedback factor from climate model simulations for a doubling of CO_2 from the present-day climate state are ~0.5 to 1°C W^{-1} m^{-2}. The conclusion from this analysis—resting on data for CO_2 levels, paleotemperatures, and radiative transfer knowledge—is that Earth's sensitivity to CO_2 radiative forcing may be much greater than that obtained from climate models (*12*–*14*).

What is the explanation for this discrepancy in estimating climate feedback strength? On long time scales (centuries to millennia), changes in continental ice formation play a role in Earth's climate system (*12*, *14*). Processes related to vegetation and carbon cycle changes may also be important feedbacks in Earth's climate system (*15*). In the modeling approach, the climate feedback factor in simulations that double CO_2 do not include these slower feedback processes. Although these processes operate on slower time scales than may be of immediate interest to societies, these processes are still important to longer-term adaptation issues. Recent modeling studies on the lifetime of atmospheric CO_2 indicate that if the CO_2 concentration reaches ~1000 ppmv, then the time for natural processes to return it to around 300 ppmv is many tens of thousands of years (*16*, *17*). Thus, if atmospheric CO_2 reaches 1000 ppmv, then human civilization will face another world, one that the human species has never experienced in its history (~2 million years). Also, given this long lifetime for elevated CO_2, slower feedback processes will have time to enter into Earth's future climate change. This magnitude and rate of climate change will be even more challenging for the biosphere to adapt to, including the human species (*18*).

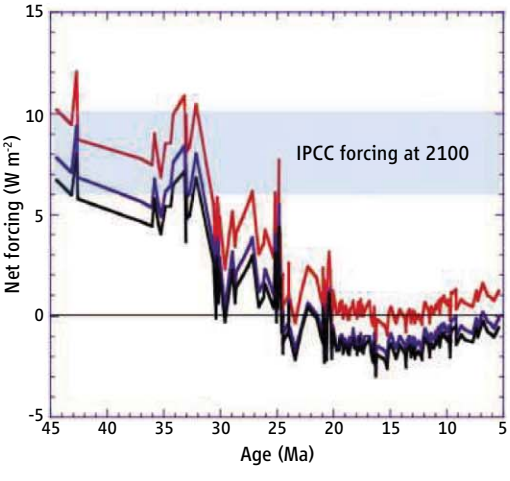

Changes in a warming world. The net radiative forcing due to changes in atmospheric CO_2 concentration and total solar irradiance over the past 45 million years. The three curves represent the range in CO_2 concentration that was reported in (*2*). The shaded region denotes the range in radiative forcing projected to occur by 2100 according to the Intergovernmental Panel on Climate Change (IPCC) Fourth Assessment Report (*1*).

The above arguments weave together a number of threads in the discussion of climate that have appeared over the past few years. They rest on observations and geochemical modeling studies. Of course, uncertainties still exist in deduced CO_2 and surface temperatures, but some basic conclusions can be drawn. Earth's CO_2 concentration is rapidly rising to a level not seen in ~30 to 100 million years, and Earth's climate was extremely warm at these levels of CO_2. If the world reaches such concentrations of atmospheric CO_2, positive feedback processes can amplify global warming beyond current modeling estimates. The human species and global ecosystems will be placed in a climate state never before experienced in their evolutionary history and at an unprecedented rate. Note that these conclusions arise from observations from Earth's past and not specifically from climate models. Will we, as a species, listen to these messages from the past in order to avoid repeating history?

References and Notes

1. *Climate Change 2007: The Physical Science Basis. Contribution of Working Group I to the Fourth Assessment Report of the Intergovernmental Panel on Climate Change*, S. Solomon *et al.*, Eds. (Cambridge Univ. Press, Cambridge, UK, 2007).
2. M. Pagani, J. C. Zachos, K. H. Freeman, B. Tipple, S. Bohaty *Science* **309**, 600 (2005); 10.1126/science.1110063.
3. B. J. Fletcher, S. J. Brentnall, C. W. Anderson, R. A. Berner, D. J. Beerling, *Nat. Geosci.* **1**, 43 (2008).
4. D. O. Breecker, Z. D. Sharp, L. D. McFaddenn, *Proc. Natl. Acad. Sci. U.S.A.* **107**, 576 (2010).
5. P. K. Bijl S. Schouten, A. Sluijs, G. J. Reichart, J. C. Zachos, H. Brinkhuis, *Nature* **461**, 776 (2009).
6. P. N. Pearson *et al.*, *Geology* **35**, 211 (2007).
7. D. O. Gough, *Sol. Phys.* **74**, 21 (1981).
8. D. L. Royer, *Geochim. Cosmochim. Acta* **70**, 5665 (2006).
9. G. R. North, *J. Atmos. Sci.* **32**, 2033 (1975).
10. The cosine temperature expression can be integrated analytically to obtain the global annual mean temperature. Paleotemperatures from (*5*) for a subtropical location and a high southern latitude location were used to determine the two coefficients in the analytical expression for global mean temperature.
11. S. E. Schwartz, *Clim. Change*; 10.1007/s10584-010-9903-9 (2010).
12. J. Hansen *et al.*, *Open Atmos. Sci.* **2**, 217 (2008).
13. P. K. Bijl, A. J. Houben, S. Schouten, S. M. Bohaty, A. Sluijs, G. J. Reichart, J. S. Sinninghe Damsté, H. Brinkhuis, *Science* **330**, 819 (2010).
14. D. J. Lunt *et al.*, *Nat. Geosci.* **3**, 60 (2010).
15. U. Salzmann, A. M. Haywood, D. J. Lunt, *Philos. Trans. R. Soc. Ser. A* **367**, 189 (2009). 10.1098/rsta.2008.0200
16. G. Shaffer, S. M. Olsen, O. P. Pedersen, *Nat. Geosci.* **2**, 105 (2009).
17. D. Archer *et al.*, *Annu. Rev. Earth Sci.* **37**, 117 (2009).
18. S. C. Sherwood, M. Huber, *Proc. Natl. Acad. Sci. U.S.A.* **107**, 9552 (2010).

19. The National Center for Atmospheric Research is sponsored by the National Science Foundation.

10.1126/science.1199380

RETROSPECTIVE

John Bennett Fenn (1917–2010)

David C. Muddiman

The hallmark of a southern gentleman's serpentine path to the Nobel Prize was his admiration for truth and the stimulation of a curious, prepared, and creative mind.

John Fenn was first and foremost genuine and earnest and willing to discuss science and life passionately with anyone. He was a true visionary who understood education, human nature, science, love, and compassion. He died on 10 December at the age of 93. Those who had the privilege of knowing John Fenn are, without question, better for it. The Nobel Prize in Chemistry did not define John Fenn, nor did it change him; he was the same man before and after, always showing a strong sense of humility. He was a one-of-a-kind individual, whose qualities as a person and impact on science are irreplaceable. He had all of this, plus a marvelous sense of humor and a love and great respect for the written word.

John Bennett Fenn was born before the Great Depression in New York City to college-educated parents who instilled in their son the critical importance of education. As a result of the Depression, his family lost their home to foreclosure and his father joined the faculty of Berea College in 1928. At the age of 11, John moved from Hackensack, New Jersey, to Kentucky, matriculated in Berea High School in the early 1930s and continued his education at Berea College, where he received his baccalaureate degree just before the age of 17. John always spoke of Berea College with great fondness, because it was from there that he took away several guiding principles that he lived by the rest of his life, including the importance of a strong work ethic, being open-minded in life and in science, understanding and accepting other people's struggles, and being an inspirational educator.

John decided to continue his education in chemistry and joined the graduate program at Yale University in 1937, working under the auspices of Professor Gösta Åkerlöf. His graduate research project was not stimulating to the young Fenn, so in 1940, he decided to pursue a career in industry. He and his new bride moved to Alabama, where he accepted a position at Monsanto Chemical Company. It was there that John met James W. Mullen II, who later founded Experiment Incorporated in Richmond, Virginia, and became a lifelong friend. In 1942, John moved to Sharpless Chemicals in Michigan. Just over a year later

he moved his career to Richmond, Virginia, to work at Experiment Incorporated on Project Bumblebee, a research effort on the use of ramjets for aircraft propulsion. In 1949 at the age of 32, he published his first paper. Satisfied to be finally in a situation where he was doing highly stimulating research, he began producing numerous papers and patents. In 1952, Fenn joined the faculty at Princeton University to become the Director of Project Squid (funded be the U.S. Office of Naval Research), which focused on propulsion and proved to be a very positive experience.

His seminal research at Princeton made him an internationally recognized expert in free jets and molecular beams. These technologies made possible the reactive scattering experiments that contributed to understanding the dynamics of elementary chemical processes that led to the Nobel Prize in Chemistry in 1986 (which was awarded to Dudley R. Herschbach, Yuan T. Lee, and John C. Polanyi). In 1970, John moved his research program back to Yale University. He used his lifelong scientific experiences coupled with serendipitous encounters with colleagues to carry out the seminal research that led to the electrospray ionization (ESI) revolution. John's development of ESI breathed life into mass spectrometry and has resulted in countless scientific advances across multiple disciplines. It has facilitated revolutionary instrumentation and economic development, and created countless career opportunities for young researchers to whom he was so firmly committed. The true potential of ESI as an analytical and engineering technique has yet to be reached. After mandatory retirement, John moved his research group to Virginia Commonwealth University (VCU) in Richmond, Virginia, where he continued to study and advance ESI as an analytical technique. It was while on the faculty–the city where he began his scientific career—that John was awarded the 2002 Nobel Prize in Chemistry. Clearly, John's path to the prize was serpentine and never could have been predicted by anyone, including him. He did not calculate his path to an extraordinary scientific career, but genuinely pursued ideas that were stimulating and of substantial practical value.

John was a generous and caring man with a strong sense of humility, who frequently went out of his way to make people feel comfortable. I was his colleague at VCU and remember that he would frequently say, "I learn more from my students than they will ever learn from me," a true statement from a modest man of outstanding character and vision. He always felt honored to be asked to participate in any endeavor. He loved attending group meetings, taught as a guest lecturer well into his 80s, and was unbelievably talented at making complex subjects (like thermodynamics) understandable—a skill that can be attributed to his ability to tell great stories. He was passionate about dialogue in the classroom and bemoaned the current state of chemical education with >1000-page text books. He would often say, "The problem with education today is that the material goes from the notebook of the Professor to the notebook of the student without going through the minds of either one of them." John's perspective on education was largely shaped by two key role models in his life, his father and his freshman chemistry teacher Julian Capp. Both were very inspirational to him and the latter excited John about a subject that he most likely would have never studied otherwise.

It is hard to capture the breadth and depth of such a unique individual, who not only walked this planet for nearly a century, but also contributed to this world at nearly every turn. John's spirit of innovation, insistence on simplicity both in life and in research, his impact on science, and his genuine friendship will be sorely missed.

10.1126/science.1201766

Department of Chemistry, North Carolina State University, Raleigh, NC 27695, USA. E-mail: dcmuddim@ncsu.edu

CREDIT: AMERICAN SOCIETY FOR MASS SPECTROMETRY

Join Us in Washington, DC

Attend sessions on the implications of finding other worlds, the next steps in brain-computer interfaces, frontiers in chemistry, the next big solar storm, and more. Talk to leaders in science, technology, engineering, education, and policy-making. Mingle with colleagues at receptions and social events.

It's all available at the world's largest interdisciplinary science gathering. Among 157 scientific sessions, 84 have international participation. Speakers alone represent more than half of the world's top 200 universities and colleges. World-renowned research institutes will be there, too. Attendees will come from nearly 50 countries and almost all of the 50 states and territories of the United States.

Follow us in cyberspace at: http://www.facebook.com/AAAS.Science**. Get regular updates at Twitter.com, #AAASmtg**

Reporters: The EurekAlert! Web site hosts the AAAS Meeting Newsroom. Reporters can obtain details and register at:

www.eurekalert.org/aaasnewsroom

AAAS
ADVANCING SCIENCE, SERVING SOCIETY

AAAS, publisher of *Science*, presents the

2011 Annual Meeting

Science Without Borders

17—21 February • Washington, DC

Alice S. Huang, Ph.D.
AAAS President and
2011 Program Chair

Dear Colleagues,

On behalf of the AAAS Board of Directors, it is my distinct honor to invite you to the 177th Meeting of the American Association for the Advancement of Science (AAAS).

The Annual Meeting is one of the most widely recognized pan-science events, with hundreds of networking opportunities and broad global media coverage. An exceptional array of speakers and attendees will gather at the Walter E. Washington Convention Center in Washington, DC. **You will have the opportunity to interact with an exceptional array of scientists, engineers, educators, and policy-makers who will present the latest thinking and developments in the areas of science, technology, engineering, education, and policy-making.**

The meeting's theme — ***Science Without Borders*** — integrates interdisciplinary science, both across research and teaching, that utilizes diverse approaches as well as the diversity of its practitioners. The program will highlight science and teaching that cross conventional borders or break out from silos, especially in ground-breaking areas of research that highlight new and exciting developments in support of science, technology, and education. Sessions will feature strong scientific content to illustrate the interface of different disciplines or will exemplify a multidisciplinary approach to problem solving.

Everyone is welcome at the AAAS Annual Meeting. Those who join us will choose among a broad range of activities, including plenary and topical lectures by some of the world's leading scientists and engineers, multidisciplinary symposia, cutting-edge seminars, career development workshops, an international exhibition, and a host of networking opportunities.

The Annual Meeting reflects contributions from the AAAS sections, which I gratefully acknowledge. I also extend a personal thanks to the Scientific Program Committee for assembling this outstanding meeting and to our local co-chairs, **Freeman A. Hrabowski III**, president, University of Maryland, Baltimore County; **Ray O. Johnson**, vice president and chief technology officer, Lockheed Martin; and **Robert Tjian**, president, Howard Hughes Medical Institute.

I look forward to seeing you in Washington, DC,

Alice S. Huang
AAAS President and
Senior Faculty Associate in Biology
California Institute of Technology

President's Address

Thursday, 17 February

Alice S. Huang

AAAS President and Senior Faculty Associate in Biology, California Institute of Technology

Dr. Huang is a distinguished virologist and proponent for women in science. She was previously a professor of microbiology and molecular genetics at Harvard Medical School and subsequently dean for science at New York University. She is particularly interested in interdisciplinary research, the organization of higher educational institutions, and in policy issues related to education, science, and technology. She was the first to purify and characterize defective interfering viral particles. Her suggestion that these particles play a major role in viral pathogenesis stimulated work on many viral systems including plant viruses, and has led to the possibility of using these particles for disease prevention.

Friday, 18 February

John P. Holdren

Assistant to the President for Science and Technology, Director of the White House Office of Science and Technology, and Co-Chair of the President's Council of Advisors on Science and Technology

A former AAAS president, Dr. Holdren is highly regarded for his work on energy technology and policy, global climate change, and nuclear arms control and nonproliferation. Prior to joining the Obama administration, Dr. Holdren was Teresa and John Heinz Professor of Environmental Policy and Director of the Program on Science, Technology, and Public Policy at Harvard University's Kennedy School of Government as well as professor in Harvard's Department of Earth and Planetary Sciences and Director of the independent, nonprofit Woods Hole Research Center.

Saturday, 19 February

Frances H. Arnold

Dick and Barbara Dickinson Professor of Chemical Engineering and Biochemistry, California Institute of Technology

Frances Arnold is a pioneer in the use of methods of laboratory evolution to generate novel and useful enzymes and organisms for applications in medicine and in alternative energy. Her multidisciplinary approach reveals insight into the way natural evolution might have occurred. She holds more than 20 patents and patent applications, has co-authored 220 scientific publications, and edited several books on protein engineering and laboratory protein evolution. Dr. Arnold is a member of the National Academy of Sciences, the National Academy of Engineering, and the Institute of Medicine.

Sunday, 20 February

Plenary Panel on Biosecurity

Rita R. Colwell

Distinguished University Professor, University of Maryland, College Park, and Johns Hopkins University Bloomberg School of Public Health

Dr. Colwell recently chaired a study committee of the U.S. National Research Council that wrote, *Responsible Research with Biological Select Agents and Toxins*. A former AAAS president, she has held many advisory positions in the U.S. government, nonprofit science policy organizations, and private foundations as well as in the international scientific research community.

Anthony S. Fauci

Director, National Institute of Allergy and Infectious Diseases, National Institutes of Health

Dr. Fauci oversees an extensive research portfolio of basic and applied research to prevent, diagnose, and treat infectious diseases such as HIV/AIDS and other sexually transmitted infections, influenza, tuberculosis, malaria and illness from potential agents of bioterrorism. He is also a member of the National Science Advisory Board for Biosecurity, which deals with such questions as how to prevent published research in biotechnology from aiding terrorism without slowing scientific progress.

Claire M. Fraser-Liggett

Director of the Institute for Genome Sciences and Professor of Medicine, University of Maryland School of Medicine, Baltimore

Dr. Fraser-Liggett was previously the president and director of The Institute for Genomic Research, and has played a role in the sequencing and analysis of human, animal, plant, and microbial genomes to better understand the role that genes play in development, evolution, physiology, and disease. She has served on a number of National Research Council's committees on counterbioterrorism, domestic animal genomics, polar biology, and metagenomics.

The Honorable Rush Holt

U.S. Congressman
Invited

Prior to his election in 1998 to represent New Jersey's 12th District, Dr. Holt, a physicist, worked as an educator, scientist, and arms control expert. At the U.S. State Department, he monitored the nuclear programs of countries such as Iraq, Iran, North Korea, and the former Soviet Union. He serves on the House Permanent Select Committee on Intelligence, its only scientist.

Moderator: Jeanne Guillemin

Senior Advisor, MIT Security Studies Program, Research Professor, Boston College, Chestnut Hill, MA

Dr. Guillemin has long been involved in issues regarding medicine, infectious diseases, and biological weapons. She documented the U.S.-Russian inquiry into the contested cause of the 1979 Sverdlovsk anthrax outbreak. She also investigated the "yellow rain" controversy of the 1980s. Her latest book is *Biological Weapons: From the Invention of State-Sponsored Programs to Contemporary Bioterrorism*.

Monday, 21 February

Graham Walker

American Cancer Society Research Professor, HHMI Professor, Massachusetts Institute of Technology

Dr. Walker is an American biologist, notable for his work explicating the structure and function of proteins involved in DNA repair and mutagenesis. He also coordinates a program at MIT to develop curricular materials in biology. In 2010, the Howard Hughes Medical Institute (HHMI) announced three grants to MIT that recognize and promote excellence in science education at the Institute. These resources will help faculty pursue some of their most creative ideas by developing new ways to teach and inspire students about science and research.

Topical Lecture Series

G. Wayne Clough

Secretary, Smithsonian Institution

Scientific Literacy – Where Are Our Forçados When We Need Them?

Regina E. Dugan

Director, Defense Advanced Research Projects Agency

Topic To Be Announced

Robert M. Hazen

Senior Staff Scientist, Geophysical Laboratory, Carnegie Institution for Science, and Clarence Robinson Professor of Earth Science, George Mason University

The Deep Carbon Observatory

Samantha B. Joye

Professor of Marine Sciences, University of Georgia, Athens

Offshore Ocean Aspects of the Gulf Oil Well Blowout

Gerard Karsenty

Paul A. Marks Professor and Chair, Department of Genetics and Development, Columbia University Medical Center

Biology Without Walls: The Novel Endocrinology of Bone

Patrick Cunningham

Chief Scientific Adviser to the Government of Ireland

Growing the Knowledge Economy: An Irish Perspective

Colin Phillips

Professor of Linguistics, Neuroscience, and Cognitive Science, University of Maryland, College Park

Linguistic Illusions: Where You See Them, Where You Don't

Lisa Randall

Frank B. Baird, Jr. Professor of Science, Harvard University

String Theory and New Physics

Sean C. Solomon

Director, Department of Terrestrial Magnetism, Carnegie Institution for Science

Exploring the Planet Mercury: The MESSENGER Mission

Subra Suresh

Director, National Science Foundation

Topic To Be Announced

George M. Whitesides

Woodford L. and Ann A. Flowers University Professor, Harvard University

Changing the Paradigms of Science

George Sarton Memorial Lecture in the History and Philosophy of Science

Lawrence M. Principe

Drew Professor of the Humanities, Johns Hopkins University

Revealing the Secrets of Alchemy

John P. McGovern Lecture in the Behavioral Sciences

Linda M. Bartoshuk

Bushnell Professor of Community Dentistry and Behavioral Science, University of Florida, Gainesville

We Live in Different Taste Worlds: How Do We Know and What Does It Mean?

Seminars

Body and Machine

Friday, 18 February

No border is more fundamental than the one between humans and the external world. The limits of our body are defined by our brain—how we grasp an object or move around in a room is determined by how the brain perceives where the body is in space and time.

Linking Mechanics, Robotics, and Neuroscience: Novel Insights from Novel Systems

Organized by Mitra J.Z. Hartmann, Northwestern University, Evanston, IL

SPEAKERS

Jérôme Casas, University of Tours, France; B. Bathellier, Institute for Molecular Pathology
Air-Flow Sensing Hairs in Crickets and Biomimetic Micro-Electro-Mechanical Systems (MEMS) Sensors

Peter M. Narins, University of California, Los Angeles
Mostly Malleus: Ground Sound Detection by the Golden Mole

Mitra J.Z. Hartmann, Northwestern University, Evanston, IL
Characterizing the Complete Mechanosensory Input to the Rat Vibrissal Array

Danica Kragic, Center for Autonomous Systems, Stockholm
Attention, Segmentation, and Learning for Object Manipulation

Francisco J. Valero-Cuevas, University of Southern California, Los Angeles
A Systems-Based Engineering Approach to Sensorimotor Control of the Human Hand

Mind and Machine: The Next Step in Neuroprosthetics and Brain-Computer Interfaces

Organized by Michael D. Mitchell, Ecole Polytechnique Fédérale de Lausanne (EPFL), Switzerland; Christian Simm, Swissnex San Francisco, CA

SPEAKERS

Daniel Moran, Washington University, St. Louis, MO
Electrocorticographic Brain-Computer Interfaces

José del R. Millan, EPFL, Lausanne, Switzerland
Multitasking with Non-Invasive Neuroprosthetics

Christa Neuper, Graz University of Technology, Austria
Future Directions in Hybrid Brain-Computer Interfaces

Andrew Schwartz, University of Pittsburgh, PA
Useful Signals from the Motor Cortex

Dennis McFarland, New York State Department of Health and State University of New York
Brain-Computer Interfaces: Traditional Assumptions Meet Emerging Realities

Other Worlds

Saturday, 19 February

Speakers will represent multidisciplinary and multinational initiatives that are closely coordinated at national and international levels.

Kepler: Looking for Other Earths

Organized by Alan P. Boss, Carnegie Institution for Science, Washington, DC; William J. Borucki, NASA Ames Research Center, Moffet Field, CA

SPEAKERS

William J. Borucki, NASA Ames Research Center, Moffet Field, CA
Kepler Mission Overview and Planet Discoveries

Matthew J. Holman, Harvard–Smithsonian Center for Astrophysics, Cambridge, MA
Searching for Planets by Transit Timing Variations

Sara Seager, Massachusetts Institute of Technology, Cambridge
Planet Discoveries in a Physical Context

William Chaplin, University of Birmingham, United Kingdom
Results for Solar-Like Oscillators Observed by Kepler

Conny Aerts, Instituut voor Sterrenkunde, Leuven, Belgium

Asteroseismology Across the Hertzsprung–Russell Diagram
Martin D. Still, NASA Ames Research Center, Moffet Field, CA
The Kepler Guest Observer Program

Seeking Signs of (ET) Life: The Search Steps Up on Mars and Beyond

Organized by Linda Billings, George Washington University, Washington, DC

SPEAKERS
Mary A. Voytek, NASA, Washington, DC
Greatest Hits and Grand Challenges in Astrobiology
Cassie Conley, NASA, Washington, DC
Preserving the Planets— Ours and Others: Planetary Protection in Space Exploration
Andrew Steele, Carnegie Institution for Science
The Search for Life on Mars: Mars Science Laboratory and Mars Sample Return

The Universe Revealed by High-Resolution, High-Precision Astronomy

Organized by Mark T. Adams, National Radio Astronomy Observatory (NRAO), Charlottesville, VA

SPEAKERS
Geoffrey C. Bower, University of California, Berkeley
Seeking New Planets at Radio Wavelengths
Mark J. Reid, Harvard–Smithsonian Center for Astrophysics, Cambridge, MA
Mapping Our Galaxy in 3D
James A. Braatz, NRAO, Charlottesville, VA
Supermassive Black Holes and Precision Cosmology with Megamasers

Frontiers in Chemistry

Sunday, 20 February

AAAS is celebrating the International Year of Chemistry to acknowledge the achievements of chemistry, its contributions to the well-being of humankind, and what the future may hold.

Frontiers in Organic Materials for Information Processing, Energy, and Sensors

Organized by Seth R. Marder and Jean-Luc Bredas, Georgia Institute of Technology, Atlanta; Tobin J. Marks, Northwestern University, Evanston, IL

SPEAKERS
Alan Heeger, University of California, Santa Barbara
Plastic Solar Cells and Photodetectors: Self-Assembly by Spontaneous Phase Separation
Richard Friend, University of Cambridge, United Kingdom
Current and Future Scientific and Commercial Opportunities for Organic Electronics
Zhenan Bao, Stanford University, CA
Organic Materials Based Flexible Electronic Sensors
Larry Dalton, University of Washington, Seattle
Electro-Optic Technology: Implications for Telecommunications, Computing, and Sensing
Joseph W. Perry, Georgia Institute of Technology, Atlanta
Organic Photonic Materials for All-Optical Signal Processing
Mark E. Thompson, University of Southern California, Los Angeles
New Molecular Materials for Energy-Based Optoelectronics: Solar Energy and Lighting

Molecular Self-Assembly and Artificial Molecular Machines

Organized by Miguel A. Garcia-Garibay, University of California, Los Angeles; Bruce E. Maryanoff, The Scripps Research Institute, La Jolla, CA

SPEAKERS
J. Fraser Stoddart, Northwestern University, Evanston, IL
Fashioning Functional Materials with Integrated Mechanostereochemical Systems
Josef Michl, University of Colorado, Boulder
Artificial Surface-Mounted Molecular Rotors
Nadrian C. Seeman, New York University, New York City
DNA: Not Merely the Secret of Life
M. Reza Ghadiri, The Scripps Research Institute, La Jolla, CA
Toward Single-Molecule DNA Sequencing with Engineered Nanopores
Stacey F. Bent, Stanford University, CA
Nanostructuring for Efficient Energy Conversion
Miguel A. Garcia-Garibay, University of California, Los Angeles
Amphidynamic Crystals and Antificial Molecular Machines

Special Session

AAAS Sustainability Forum

Thursday, 17 February

Organized by Vaughan Turekian, AAAS Center for Science Diplomacy
Pre-registration required

Since its inauguration in 2007, the Forum roundtable has provided ample opportunity to key university actors from around the world to discuss collaborative approaches in building the emerging field of Sustainability Science. This year the focus will be on Sustainability Science and the next global summit on sustainability, the United Nations Conference on Sustainable Development (Rio+20) to be held in Rio de Janeiro in 2012. It will call the world's attention to and direct action toward addressing difficult challenges the planet is facing, including reducing poverty, conserving natural resources, and overcoming financial and economic crisis. This AAAS roundtable is an opportunity to bring together academic experts, business leaders, and policy-makers to help define and shape ideas to feed into the international policy process that is being formulated in advance of the summit. Previous summits have produced global treaties and led to important partnerships to promote sustainability issues. The AAAS Sustainability Forum will help embed the latest policy considerations and science research into the planning process and help identify a potential road map forward in addressing issues of global sustainability. Participation is by invitation only; pre-registration is required. For more information, contact Linda Stroud, lstroud@aaas.org.

Symposium Tracks

Brain and Behavior

Chronic Illness Management and Cognitive Science: Translation Beyond Genes?

Organized by Howard Leventhal, Rutgers University, New Brunswick, NJ

Crossing Borders in Language Science: What Bilinguals Tell Us About Mind and Brain

Organized by Judith F. Kroll, Pennsylvania State University, University Park

Cultural Evolutionary Dynamics of Cooperation

Organized by David M. Carballo, Boston University, MA

From Artificial Limbs to Virtual Reality: How the Brain Represents the Body

Organized by Michael D. Mitchell, Ecole Polytechnique Fédérale de Lausanne, Switzerland; Christian Simm, swissnex San Francisco, CA

From Freud to fMRI: Untangling the Mystery of Stuttering

Organized by Nan Ratner, University of Maryland, College Park

Hunter-Gatherers and Language Change

Organized by Claire Bowern, Yale University, New Haven, CT

Molecules to Mind: Challenges for the 21st Century

Organized by Bruce Altevogt, Institute of Medicine, Washington, DC

Nature, Nurture, and Antisocial Behavior: Biological and Biosocial Research on Crime

Organized by William Alex Pridemore, Indiana University, Bloomington

Neurodegenerative Diseases: A Need for Multidisciplinary and Global Approaches

Organized by Elmar Nimmesgern, European Commission, Brussels, Belgium; Philippe Amouyel, Institut Pasteur de Lille, France

Science Behind Improved Foreign Language Expertise: Meeting the Global Challenge

Organized by Amy S. Weinberg, University of Maryland, College Park

Scientific and Ethical Issues for the Surgical Treatment of Psychiatric Disorders
Organized by Mahlon DeLong, Emory University School of Medicine, Atlanta, GA

The Science of Eating: Perception and Preference in Human Taste
Organized by Albert H. Teich and Rieko Yajima, AAAS Science and Policy Programs, Washington, DC; Jill Pace, American College of Real Estate Lawyers, Rockville, MD

Thinking About Thinking: How Do We Know What We Know?
Organized by Eva Hoogland and Chloe Kembery, European Science Foundation, Strasbourg, France

Transatlantic Synergies To Promote Effective Traumatic Brain Injury Research
Organized by Ramona Hicks, National Institute of Neurological Disorders and Stroke, Bethesda, MD; Patrizia Tosetti, European Commission, Direcorate General-Research/ Health, Brussels, Belgium

Climate Change

Adapting to a Clear and Present Danger: Climate Change and Ocean Ecosystems
Organized by Chad English, Communication Partnership for Science and the Sea, Silver Spring, MD; Mary Ruckelshaus, National Oceanic and Atmospheric Administration (NOAA) Northwest Fisheries Science Center, Seattle, WA ; Scott Doney, Woods Hole Oceanographic Institution, MA

Can Reef Fisheries Take the Heat? Ecological and Economic Impacts of Climate Change
Organized by Joshua E. Cinner, Australian Research Center, Townsville

Changing Climate, Changing Approaches: Conservation in the Face of Climate Change
Organized by Michelle M. McClure, NOAA Northwest Fisheries Science Center, Seattle, WA

Climate Change: Altering the Physics, Ecology, and Socioeconomics of Fisheries
Organized by Rashid Sumaila, University of British Columbia, Vancouver, Canada; William W.L Cheung, University of East Anglia, Norwich, United Kingdom

Comparing National Responses to Climate Change: Networks of Debate and Contention
Organized by Jeffrey P. Broadbent, University of Minnesota, Minneapolis

How Climate Change Affects the Safety of the World's Food Supply
Organized by Ewen C. Todd, Michigan State University, East Lansing

In Hot Water: Rising Public Health Concerns from Changing Ocean Conditions
Organized by Carolyn Sotka, NOAA Oceans and Human Health Initiative, Charleston, SC; Paul Sandifer, NOAA, Washington, DC

Limiting Climate Change: Reducing Black Carbon and Tropospheric Ozone Precursors
Organized by Frank Raes, European Commission, Joint Research Council (JRC) Institute for Environment and Sustainability, Ispra, Italy; Geraldine Barry, European Commission, JRC, Brussels, Belgium

Research Infrastructures: The Emergence of Key Players for Environmental Research
Organized by Janine Delahaut and Elena Righi-Steele, European Commission, Brussels, Belgium

Rethinking Adaptation to a Changing Global Environment
Organized by Gregory P. Dietl, Paleontological Research Institution, Ithaca, NY

Where Ocean Meets Land: Dynamic Shorelines in a Warming World
Organized by Gregory S. Mountain, Rutgers University, Piscataway, NJ; Charna Meth, Consortium for Ocean Leadership, Washington, DC

Education

Aiming for Scientific Literacy by Teaching the Process, Nature, and Limits of Science
Organized by Jay B. Labov, National Academy of Sciences, Washington, DC; Judy Scotchmoor, University of California Museum of Paleontology, Berkeley

Celebrating Marie Curie's 100th Anniversary of Her Nobel Prize in Chemistry
Organized by Penny J. Gilmer, Florida State University, Tallahassee; Alan Rocke, Case Western Reserve University, Cleveland, OH

Engaging Students in Undergraduate STEM Education with a Focus on Global Stewardship
Organized by Jay B. Labov, National Academy of Sciences, Washington, DC; Melvin D. George, University of Missouri, Columbia; Catherine Middlecamp, University of Wisconsin, Madison

Implementing the Vision and Change Report on Undergraduate Biology Education
Organized by Michael M. Cox, University of Wisconsin, Madison; Barbara Illman, U.S. Forest Service, Madison, WI

Invisible Men? Addressing the Participation of Minority Males in Science and Engineering
Organized by Catherine Didion, National Academy of Engineering, Washington, DC

Just-in-Time Support for Science Teaching: Web-Based Approaches
Organized by Nancy P. Moreno and Deanne B. Erdmann, Baylor College of Medicine, Houston, TX

Learning Research and Educational Practice: How Can We Make Better Connections?
Organized by Janice Earle and Soo-Siang Lim, National Science Foundation (NSF), Arlington, VA

Science Without Borders: Learning from TIMSS Advanced 2008
Organized by Patsy Wang-Iverson, Gabriella and Paul Rosenbaum Foundation, Stockton, NJ

Teaching and Learning in the Digital Age: Reliable Resources Across the Disciplines
Organized by Linda N. Fanis, Chemical Education Digital Library, Madison, WI

The Challenge of Teaching Evolution in the Islamic World
Organized by Eugenie C. Scott, National Center for Science Education, Oakland, CA

The University of the Future
Organized by Robert M. Nerem, Georgia Institute of Technology, Atlanta; James J. Duderstadt, University of Michigan, Ann Arbor

Transcending Gender and Ethnic Barriers to Full STEM Participation
Organized by Nicole M. Else-Quest, Villanova University, PA

Emerging Science and Technology

Aeroecology: Transcending Boundaries Among Ecology, Meteorology, and Physics
Organized by Winifred F. Frick, University of California, Santa Cruz; Phillip B. Chilson, University of Oklahoma, Norman

Biological Role and Consequences of Intrinsic Protein Disorder

Organized by H. Jane Dyson and Peter E. Wright, The Scripps Research Institute, La Jolla, CA

Bioprinting: A Future of Regenerative Medicine
Organized by Vladimir Mironov, Medical University of South Carolina, Charleston

Chemically Speaking: How Organisms Talk to Each Other
Organized by Barbara Illman, U.S. Forest Service, Madison, WI; Jerrold Meinwald, Cornell University, Ithaca, NY

Explaining Phase Transitions
Organized by David Lightfoot, Georgetown University, Washington, DC

First Physics from the Large Hadron Collider
Organized by James Gillies, European Organization for Nuclear Research (CERN), Geneva, Switzerland; Katie Yurkewicz, Fermi National Accelerator Laboratory, Batavia, IL

Growth and Form in Mathematics, Physics, and Biology
Organized by L. Mahadevan, Harvard University, Cambridge, MA; Edward Aboufadel, Grand Valley State University, Allendale, MI

Inspiring Researchers: Building on the Legacy of Marie Curie
Organized by Louise Byrne, Research Executive Agency, Brussels, Belgium

Mathematics and Collective Behavior
Organized by Warren Page, City University of New York (Retired), Larchmont, NY

Matter Wave Magic and Technology
Organized by Charles W. Clark, National Institute of Standards and Technology, Gaithersburg, MD

Nanoworld, Megaproblems? The Impact of Nanotechnology on the Environment and Society
Organized by Alberto Pimpinelli, Science and Technology Office of the French Embassy in the United States, Houston, TX

Sharper Images in Astronomy, Microscopy, and Vision Science Using Adaptive Optics
Organized by Christopher Dainty, National University of Ireland, Galway

Superconductivity: From 1911 to 2021
Organized by David Pines, University of California, Davis

Through the Looking Glass: Recent Adventures in Antimatter
Organized by Charles W. Clark, National Institute of Standards and Technology, Gaithersburg, MD

Use of Lasers in Surgery, Regenerative Medicine, and Medical Device Fabrication
Organized by Roger Narayan, University of North Carolina, Chapel Hill

Energy

Biorefinery: Toward an Industrial Metabolism
Organized by Daniel Thomas, University of Technology of Compiegne, France; Adele Martial, Consulate General of France, Chicago, IL

Deepwater Drilling: A Risk Worth Taking?
Organized by Richard D'Souza, Granherne Global Operations, Houston, TX

Energy Efficiency in Europe and the United States: Success Stories and Future Potentials
Organized by Katja Stempfle-Eberl, Baden-Württemberg International, Stuttgart, Germany

Fractures Developing: The Science, Policy, and Perception of Shale Gas Development
Organized by John P. Martin, New York State Energy Research and Development Authority, Albany; Michele L. Aldrich, California Academy of Sciences, San Francisco

If Termites Can Do It, Why Can't Humans?
Organized by Lakshmi N. Reddi and Eduardo Divo, University of Central Florida, Orlando

Mathematics and Our Energy Future
Organized by Mary Lou Zeeman, Bowdoin College, Brunswick, ME; Russel E. Caflisch, Institute for Pure and Applied Mathematics, Los Angeles, CA

Pillars, Polymers, and Computers: Creative Approaches to Electrical Energy Storage
Organized by Ashley Predith, University of Maryland, College Park

Portraits of the California Energy System in 2050: Cutting Emissions by 80 Percent
Organized by Jane C.S. Long, Lawrence Livermore National Laboratory, CA; Susan Hackwood and Miriam John, California Council on Science and Technology, Riverside

Powering the Planet: Generation of Clean Fuels from Sunlight and Water
Organized by Harry B. Gray, Bruce B. Brunschwig, and Jay R. Winkler, California Institute of Technology, Pasadena

The Energy and Water Nexus: Turning a Double Problem into a Solution
Organized by Estathios Peteves, European Commission, JRC Institute for Energy, Petten, Netherlands; Geraldine Barry, European Commission, JRC, Brussels, Belgium

Waste Not, Want Not: Waste As the World's Most Abundant Renewable Resource
Organized by Michael Webber, University of Texas, Austin

Global Collaboration

Bridging Nations and Fields: East Asian Approaches to Science and Technology Policy
Organized by Asuka Hoshikoshi, National Institute of Science and Technology Policy, Tokyo, Japan

Bringing Innovation to International Development: New Actors, New Mechanisms
Organized by Alex Dehgan and Ticora V. Jones, U.S. Agency for International Development, Washington, DC; Mark Doyle, NSF, Arlington, VA

Can Global Science Solve Global Challenges?
Organized by Tracey Elliott, The Royal Society, London, United Kingdom

Cross-Border Responses to Global Challenges: Can Everybody Win?
Organized by David Wilkinson and Geraldine Barry, European Commission, JRC, Brussels, Belgium

Crossing Boundaries and Opening Borders: The European Research Council as Innovation
Organized by Samantha Christey, European Research Council, Brussels, Belgium

Education, Science, and Innovation as Tools for New Engagement with the Islamic World
Organized by Ben Koppelman, The Royal Society, London, United Kingdom

Europe, Africa, and Asia: Rising on the Same Tide
Organized by Geraldine Barry, European Commission, JRC, Brussels, Belgium

Foreign Participation in National Technology Development Programs
Organized by Christopher Hill, George Mason University, Arlington, VA; George R. Heaton, Technology Policy International, Newton Center, MA; David Cheney, SRI International, Arlington, VA

International Territory: Science at Sea, Science in Space, and Science at the Poles
Organized by Susan Humphris, Woods Hole Oceanographic Institution, MA; Charna Meth, Consortium for Ocean Leadership, Washington, DC

Joining Global Efforts in Post-Disaster Recovery and Reconstruction
Organized by Delilah Al Khudhairy, European Commission, JRC Institute for the Protection and Security of the Citizen, Ispra, Italy; Geraldine Barry, European Commission, JRC, Brussels, Belgium

Networks, Collaboration, and Research in a Non-Western Context: The Role of Technology
Organized by B. Paige Miller, University of Wisconsin, River Falls; Ricardo B. Duque, University of Vienna, Austria

Research Integrity in the Global Perspective
Organized by Melissa S. Anderson, University of Minnesota, Minneapolis

Role of U.S. Federal Agencies in Building Scientific Capacity in Developing Countries
Organized by Pallavi Phartiyal, AAAS Science and Policy Programs, Washington, DC

The Crowd and the Cloud: The Future of Online Collaboration
Organized by Michael R. Nelson, Georgetown University, Washington, DC

The Practice of Science Diplomacy in the Earth Sciences
Organized by Thomas J. Casadevall, U.S. Geological Survey, Denver, CO; Ester Sztein, The National Academies, Washington, DC; Melody Brown Burkins, University of Vermont, Burlington

Human Biology and Health

Anthropology and Global Health: Genes, Biology, and Culture
Organized by Cynthia M. Beall, Case Western Reserve University, Cleveland, OH

Diseases Without Borders: TB and AIDS
Organized by Anne E. Goldfeld, Harvard Medical School, Boston, MA

Epigenetic Processes in Development: Gene-Environment Interplay
Organized by Jeanne Brooks-Gunn, Columbia University, New York City; Stephen J. Suomi, National Institutes of Health, Bethesda, MD

Evolutionary Personalized Medicine
Organized by Turkan K. Gardenier, Pragmatica Corp., Vienna, VA

Global Health Care: Advances and Challenges
Organized by Metin Akay, University of Houston, TX

Humans Without Borders: Evolutionary Processes at Work in Humans and Their Relatives
Organized by James J. Smith, Michigan State University, East Lansing; Robin Smith, National Evolutionary Synthesis Center, Durham, NC

Interfering with Gene Expression and Interfering with Disease
Organized by Judy Lieberman, Harvard Medical School, Boston, MA

Medicine Safety in a World of Science Without Borders
Organized by William T. Beck, University of Illinois, Chicago; Guill Wientjes, Ohio State University, Columbus

One Health: From Ideas to Implementation, Rhetoric to Reality
Organized by Barbara Hyde, American Society for Microbiology, Washington, DC
Oral Clefts: Equal Opportunity Disorders

Oral Sex Is Sex and Can Lead to Cancer
Organized by Margarita Zeichner-David, University of Southern California, Los Angeles

Personalized Medicine: Moving Forward or Backward?
Organized by Jennie C. Hunter-Cevera, RTI International, Research Triangle Park, SC; Anice Anderson, Private Consultant, Terre Haute, IN

Reducing the Cost of Health Care Through Science and Engineering
Organized by Raphael C. Lee, University of Chicago, IL; Anice Anderson, Private Consultant, Terre Haute, IN

The Human Body as Supra-Organism, Microbial Observatory, and Ecosystem at Risk
Organized by David A. Relman, Stanford University, Palo Alto, CA; Jeffrey I. Gordon, Washington University School of Medicine, St. Louis

The Surprising Influenza H1N1 Pandemic, Waves I and II: The Race to Vaccinate
Organized by M. Elizabeth Halloran, University of Washington, Seattle

Land and Oceans

2050: Will There Be Fish in the Ocean?
Organized by Villy Christensen, University of British Columbia, Vancouver, Canada

A New Vision for Research: Goals for the National Institute of Food and Agriculture
Organized by Brian A. Larkins, University of Arizona, Tucson; Roger Beachy, U.S. Department of Agriculture, Washington, DC

Beyond Lines on Maps: Marine Spatial Planning for a Dynamic World
Organized by Donald F. Boesch, University of Maryland Center for Environmental Science, Cambridge, MD; Karen L. McLeod, Oregon State University, Corvallis

Borlaug's Impact on World Agriculture: Will There Be a Second Green Revolution?
Organized by Ronald L. Phillips, University of Minnesota, St. Paul; Edward Runge, Texas A&M University, College Station

Fishing for Solutions: Community Institutions for Effective Resource Management
Organized by Astrid J. Scholz, Ecotrust, Portland, OR

From Practice to Theory and Back: Ecosystem Services and Marine Spatial Planning
Organized by Anne Guerry, Stanford University, CA; Mary Ruckelshaus, NOAA Northwest Fisheries Science Center, Seattle, WA ; Paul Sandifer, NOAA, Washington, DC

Global Agricultural History: Mapping the Past for Modeling the Future
Organized by William E. Doolittle, University of Texas, Austin; Mats Widgren, Stockholm University, Sweden

Global and Local Responses to the Nitrogen Challenge: Science, Practice, and Policy
Organized by Todd S. Rosenstock and Thomas P. Tomich, University of California, Davis

GM Crop Regulations: Safety Net or Insurmountable Obstacle?"
Organized by Wayne Parrott, University of Georgia, Athens; Alan McHughen, University of California, Riverside; Donald P. Weeks, University of Nebraska, Lincoln

Invasive Species: What Harm Do They Do?
Organized by Peter Alpert, Invasive Species Advisory Committee, Amherst, MA

Lost at Sea: Where Are the Humans in Marine Ecosystem Management?

Organized by Rebecca Gruby, Larry Crowder, and Morgan Gopnik, Duke University Marine Laboratory, Beaufort, NC

Marine Spatial Planning: A Science-Based Tool for Conservation and the Economy
Organized by Elliott A. Norse, Marine Conservation Biology Institute, Bellevue, WA

Plant Breeding Today: Genomics and Computing Advances Bring Speed and Precision
Organized by Ian Graham and Elspeth Bartlet, University of York, United Kingdom

Science and Society

Astronomical Pioneering: The Implications of Finding Other Worlds
Organized by Jennifer Wiseman and Peyton West, AAAS Science and Policy Programs, Washington, DC

Communicating Diversity in Science: Implications for Climate Change Denial
Organized by Prajwal Kulkarni, U.S. Environmental Protection Agency, Washington, DC

Communication Outside the Box
Organized by Michel Claessens, European Commission, Brussels, Belgium; David Bennett, Delft University of Technology, Netherlands; Richard Jennings, University of Cambridge, United Kingdom

Crossing Boundaries with Citizen Science
Organized by Janis L. Dickinson, The Cornell Lab of Ornithology, Ithaca, NY; Bart Selman, Cornell University, Ithaca, NY

Doing Good with Good OR: Applying Operations Research for Societal Impact
Organized by Karen Smilowitz, Northwestern University, Evanston, IL; Ozlem Ergun, Georgia Institute of Technology, Atlanta

Earth Science and Evolution
Organized by Jere H. Lipps, University of California, Berkeley

Earthwatch and the HSBC Climate Partnership: A Unique Citizen Science Model
Organized by Kristen Kusek, Earthwatch Institute, Boston, MA

Evangelicals, Science, and Policy: Toward a Constructive Engagement
Organized by Peyton West and Jennifer Wiseman, AAAS Science and Policy Programs, Washington, DC

Innovative Strategies for Ensuring Access to the Benefits of Scientific Progress
Organized by Jessica M. Wyndham, AAAS Science and Human Rights Program, Washington, DC; Joseph G. Perpich, JG Perpich, Bethesda, MD

Reaching Out to People in East Asia on Green Issues: Policies and Practices
Organized by Sook-Kyoung Cho, Korea Foundation for the Advancement of Science and Creativity, Seoul; Masataka Watanabe, Japan Science and Technology Agency, Tokyo; Sun Mengxin, China Association for Science and Technology, Beijing

Science Without Borders and Media Unbounded: What Comes Next?
Organized by Bud Ward, *Yale Forum on Climate Change and the Media*, White Stone, VA

Surprise...It's Science! Reaching New Audiences in Unconventional Ways with Festivals
Organized by Jan Riise, European Science Events Association, Onsala, Sweden; Ben Wiehe, MIT Museum, Cambridge, MA

Techno-Optimism or Pessimism? Media Coverage of Quick Fixes for Global Climate Change
Organized by Cristine Russell, Harvard Kennedy School, Cambridge, MA

TV Meteorologists Communicating Climate Change
Organized by Katherine E. Rowan, George Mason University, Fairfax, VA

When Pollution Gets Personal: Ethics of Reporting on Human Exposures
Organized by Julia G. Brody, Silent Spring Institute, Newton, MA

The Science Endeavor

As Borders Dissolve, Which Standards and Mechanisms Prevail?
Organized by Mary Kavanagh, European Commission, Directorate-General for Research, Brussels, Belgium

Crisis Averted? How a Critical Shortage in Helium-3 Was Good and Bad for Science
Organized by Benn Tannenbaum, AAAS Center for Science, Technology, and Security Policy, Washington, DC

Design Thinking To Mobilize Science, Technology, and Innovation for Social Challenges
Organized by Yoko Nitta, Tateo Arimoto, and Suguru Ishiguro, Japan Science and Technology Agency, Tokyo

It Is Unethical Not To Do Research with Animals
Organized by Stuart Zola, Emory University, Atlanta, GA

Measurements as a Cornerstone of Global Trade and Quality of Life
Organized by David Anderson, European Commission, JRC Institute for Reference Materials and Measurements, Geel, Belgium; Geraldine Barry, European Commission, JRC, Brussels, Belgium

Modeling Across Millennia: Interdisciplinary Paths to Ancient Socionatural Systems
Organized by Timothy A. Kohler and Stefani A. Crabtree, Washington State University, Pullman

Networks and Culture of Scientific and Technological Communities in Global Policy
Organized by Denis F. Simon and Darryl Farber, Pennsylvania State University, University Park

Perspectives on Research and Development in the President's FY 2012 Budget Request
Organized by Patrick J. Clemins, AAAS Science and Policy Programs, Washington, DC

Publication Without Borders: Spanning Countries, Disciplines, Audiences, and Roles
Organized by Barbara Gastel, Texas A&M University, College Station

Reaching a Global Standard in Research Integrity
Organized by Chloe Kembery and Vanessa Campo-Ruiz, European Science Foundation, Strasbourg, France

Solving the Weight of Evidence Problem: A Way Forward?
Organized by Heather E. Douglas, University of Tennessee, Knoxville

The Digitization of Science: Reproducibility and Interdisciplinary Knowledge Transfer
Organized by Victoria C. Stodden, Columbia University, New York City

Security

Atomic Detectives: Science Behind International Efforts To Combat Nuclear Terrorism
Organized by Klaus Mayer, European Commission, JRC Institute for Transuranium Elements, Karlsruhe, Germany; Geraldine Barry, European Commission, JRC, Brussels, Belgium

International Neighborhood Watch: Citizen Scientists and International Security

Organized by Gerald L. Epstein, AAAS Center for Science, Technology, and Security Policy, Washington, DC

New START and Nuclear Winter: Climatic Consequences of the Nuclear Weapons Agreement

Organized by Alan Robock, Rutgers University, New Brunswick, NJ; Richard Turco, University of California, Los Angeles

Promoting Security and Sustaining Privacy: How Do We Find the Right Balance?

Organized by Christopher Hankin, Imperial College London, United Kingdom; Benn Tannenbaum, AAAS Center for Science, Technology, and Security Policy, Washington, DC

Reconciling National Security Requirements with Research and Education

Organized by Kavita M. Berger, AAAS Center for Science, Technology, and Security Policy, Washington, DC; Tobin L. Smith, Association of American Universities, Washington, DC

Science and Policy for Environmental Security in the Asia-Pacific Region

Organized by James Scott Hauger and Virginia Watson, Asia-Pacific Center for Security Studies, Honolulu, HI

Space Weather: The Next Big Solar Storm Could Be a Global Katrina

Organized by Thomas J. Bogdan and Terrance Onsager, NOAA, Boulder, CO; Stephan Lechner, European Commission, JRC Institute for Protection and Security of the Citizen, Ispra, Italy

Using Quantitative Content Analysis To Assess the Likelihood of Terrorist Violence

Organized by Allison G. Smith, U.S. Department of Homeland Security, Washington, DC

White-Blue Arctic: Promoting Cooperation and Preventing Conflict in the Arctic Ocean

Organized by Paul Arthur Berkman, University of Cambridge, United Kingdom; Oran Young, University of California, Santa Barbara

Sustainability

Data Cocktails for Biodiversity: Protected Area Management Without the Hangover

Organized by Alan Belward, European Commission, JRC Institute for Environment and Sustainability, Ispra, Italy; Geraldine Barry, European Commission, JRC, Brussels, Belgium

Estimating Earth's Human Carrying Capacity

Organized by Kenneth G. Cassman, University of Nebraska, Lincoln; Ruth Cooper, The Royal Society, London, United Kingdom; David Tilman, University of Minnesota, St. Paul

How Can the World Feed 9 Billion People by 2050 Sustainably and Equitably?

Organized by Kate Von Holle, British Embassy, Washington, DC; Jon Parke, Foresight Program, U.K. Government Office of Science, London

If a Culture of Growth Is Unsustainable, What Should Change?

Organized by Paul H. Reitan, University at Buffalo, NY; Ward Chesworth, University of Guelph, Canada

Mapping and Disentangling Human Decisions in Complex Human-Nature Systems

Organized by Li An, San Diego State University, CA; Stuart Aitken, San Diego State University, CA; Janet Silbernagel, University of Wisconsin, Madison

Research Frontiers in Sustainability Science: Bridging Disciplines and Practices

Organized by William C. Clark, Harvard Kennedy School of Government, Cambridge, MA; Simon A. Levin, Princeton University, NJ

Resource Use and Ecological Resilience in a Tropical Socio-Ecological System

Organized by Oskar Burger and Jose M.V. Fragoso, Stanford University, CA

Social Networks and Sustainability

Organized by Thomas Dietz, Michigan State University, East Lansing; Adam D. Henry, West Virginia University, Morgantown

Telecoupling of Human and Natural Systems

Organized by Jianguo (Jack) Liu and William McConnell, Michigan State University, East Lansing; Thomas J. Baerwald, NSF, Arlington, VA

The Challenge of Measuring Sustainability

Organized by Eugene A. Rosa, Washington State University, Pullman; Thomas Dietz, Michigan State University, East Lansing

Act Now ... Registration Rates Go Up 27 January

Registration

Discounted advance registration rates are available until Thursday, 27 January 2011.

Take advantage of unlimited access to all symposia, seminars, topical lectures, plenary events, career workshops, the International Exhibition, and a variety of networking opportunities.

Professional
$295 Members/$375 New Members/
$399 Non-Members

Postdoc
$235 Members/$315 New Members/
$335 Non-Members

K-12 Teacher
$235 Members/$315 New Members/
$335 Non-Members

Emeritus
$235 Members/$315 New Members/
$335 Non-Members

Student
$60 Members/$70 New Members/
$90 Non-Members

After 27 January 2011, on-site rates apply. For more information visit http://www.aaas.org/meetings.

Housing

Special room rates and benefits are available to Annual Meeting registrants.

Renaissance Downtown
(Headquarters Hotel)
Rate: $232 Single/$252 Double

Embassy Suites Convention Center
Rate: $234 Single/$259 Double

Grand Hyatt Washington
Rate: $239 Single/$264 Double

Hampton Inn Convention Center
Rate: $209 Single/Double

Rooms are available on a first-come, first-served basis until 16 January 2011 for the Grand Hyatt and 23 January for the Renaissance, Embassy Suites, and Hampton Inn.

More Ways To Save

Discount Travel to Washington, DC

For details about discounts on airfare and rail, visit www.aaas.org/meetings and click on "Hotel and Travel" then "Travel Discounts."

To browse the updated program, register, and reserve hotel rooms, visit **www.aaas.org/meetings.**

Science Without Borders

Washington, D.C.

AAAS, publisher of *Science*,
thanks the sponsors and supporters of
the *2011 Annual Meeting*

Presenting sponsor

SUBARU

Canada

HELMHOLTZ ASSOCIATION

EUROPEAN COMMISSION
European Research Area

ESOF2010 EUROSCIENCE OPEN FORUM
PaSsion For ScienCe

THE KAVLI FOUNDATION

FOR WOMEN IN SCIENCE
L'ORÉAL FONDATION D'ENTREPRISE

U.S. DEPARTMENT OF ENERGY | Office of Science

NSF

Johnson & Johnson
PHARMACEUTICAL RESEARCH & DEVELOPMENT, L.L.C.

ACS Chemistry for Life
AMERICAN CHEMICAL SOCIETY

MERCK
Be well

nature climate change

GEICO

Science
AAAS

To learn more about how to become a sponsor of the Annual Meeting, contact:

Jill C. Perla
Manager of Marketing,
Exhibits, and Sponsors
E-mail: jperla@aaas.org
Phone: 202-326-6736

Web site:
http://www.aaas.org/meetings

AAAS
ADVANCING SCIENCE, SERVING SOCIETY

In Situ Studies of Chemistry and Structure of Materials in Reactive Environments

Franklin (Feng) Tao[1]* and Miquel Salmeron[2]*

Most materials and devices typically operate under specific environmental conditions, many of them highly reactive. Heterogeneous catalysts, for example, work under high pressure of reactants or in acidic solutions. The relationship between surface structure and composition of materials during operation and their chemical properties needs to be established in order to understand the mechanisms at work and to enable the design of new and better materials. Although studies of the structure, composition, chemical state, and phase transformation under working conditions are challenging, progress has been made in recent years in the development of new techniques that operate under a variety of realistic environments. With them, new chemistry and new structures of materials that are only present under reaction conditions have been uncovered.

In reactive and corrosive environments (humid air, reactive gases or liquids, acidic solutions, etc.), the surfaces of most materials are likely to restructure, adapting their geometrical and electronic structure to the environments. Such processes have profound effects on the properties of materials and their applications (*1*, *2*). In many cases, the structure and composition of surfaces in vacuum differ markedly from those in the reactive or corrosive environment where they operate. This difference has been illustrated dramatically by using recently developed in situ microscopy and spectroscopy techniques (*3*–*15*).

Until recently the study of surfaces of materials in such environments could only be performed with techniques based on photons, such as Raman and infrared spectroscopy (*11*, *16*), sum frequency generation (*17*), and extended x-ray absorption fine structure (*18*). Resonance techniques, such as Mossbauer spectroscopy (*19*), nuclear magnetic resonance (*20*), and a few others (*2*), have also contributed substantially. However, some of them are sensitive to bulk materials as well as surfaces. Their use in surface studies is limited to special cases, such as grazing incidence geometries. The most notable techniques recently developed for in situ studies include high-pressure scanning tunneling microscopy, environmental scanning/transmission electron microscopy (SEM/TEM), ambient-pressure photoelectron spectroscopy, and in situ scanning transmission x-ray microscopy. The principle of operation of these techniques, along with detailed descriptions of the instruments, can be found in recent literature (*3*, *7*, *21*–*25*). Here, we focus on recently uncovered new phenomena that illustrate in a dramatic way how the chemistry and structure of materials change in reactive environments.

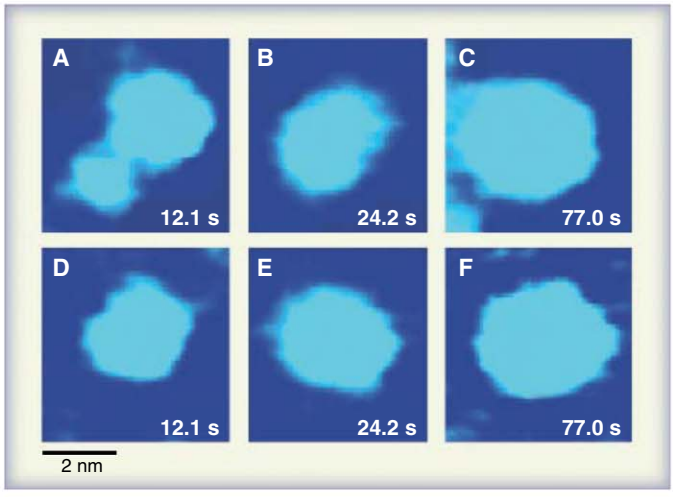

Fig. 1. Video frames captured at 12.1 s (**A**), 24.2 s (**B**), and 77.0 s (**C**) in a liquid cell inside the pole pieces of a TEM. They show a particle growing by coalescence of two smaller particles at 12.1 s (A) and the subsequent relaxation. Video frames (**D**) to (**F**) show a particle growing through steady accretion of atoms [from (*28*)].

Growth of Nanomaterials

The development of improved methods to synthesize semiconductor, metallic, and dielectric nanoparticles depends on a thorough understanding of the growth mechanisms that occur at solid-liquid or solid-gas interfaces. A kinetic model for the growth of particles through colloid chemistry was developed by LaMer, Dinegar, and Reiss in the 1950s (*26*, *27*). In this model, an initial period of rapid self-growth from monomeric species leads to a distribution of particle sizes. Size homogenization is reached progressively through a mechanism called size distribution focusing, where small particles grow at a higher rate than large ones, so that their size catches up with that of the larger ones.

A recent study of the microkinetics of Pt nanoparticle growth in solution was performed in a TEM equipped with a thin liquid cell for in situ growth of nanoparticles (*8*, *28*). This liquid cell consists of a pair of 100-μm-thick silicon wafers, which is coated with 25 nm of silicon nitride on each wafer and sealed with a cover. The center area of the two silicon wafers is then etched to create two electron-transparent windows in the space between a pair of reservoirs containing the Pt reagents and surfactants (*22*). The spatial resolution achievable using this cell is in the range of nanometers, limited by the thickness of view windows and the liquid in between.

In addition to self-growth, which creates a single nanocrystal, a punctuated growth mode takes place through particle attachment. The sequence of TEM images shows how two or more small particles coalesce into a large one (Fig. 1, A to C). In this event, the coalesced particle is polycrystalline. A relaxation period follows, during which no size increase is observed and the shape changes only slightly (*8*), while a transition from polycrystalline to single crystalline takes place. The study revealed that the relaxation time increases with particle size and follows a power law. This relaxation contributes to the size focusing because growth of the smaller particles through addition of monomers can continue during the relaxation time and catch up with the large size of the coalesced particles.

Another example of in situ studies using TEM is the growth of carbon nanofibers. These materials are grown by dissociation of methane in hydrogen at pressures in the torr range on a nickel catalyst supported on $MgAl_2O_4$ at a temperature of 430° and 500° to 540°C (*29*). Monoatomic steps form on the Ni catalyst surface, with the growth of graphene sheets terminating at each of these steps (Fig. 2). The growth of carbon nanofibers is driven by formation and restructuring of the monoatomic step edges of Ni (Fig. 2, B to D), because migration of Ni atoms from bulk to the Ni-graphene interface continuously creates new active sites for the growth of graphene. Density functional theory (DFT) calculations explained these observations by showing that carbon binds more strongly to undercoordinated sites of the step edge compared with sites on the close-packed facets of the Ni catalyst (*29*).

[1]Department of Chemistry and Biochemistry, University of Notre Dame, Notre Dame, IN 46556, USA. [2]Materials Science Division, Lawrence Berkeley National Laboratory, Berkeley, CA 94720, USA.

*To whom correspondence should be addressed. E-mail: ftao@nd.edu (F.T.); mbsalmeron@lbl.gov (M.S.)

Thus, the diffusion of Ni atoms from deep layers to surface and the strong binding of carbon atoms to the Ni interface results in the formation of graphite and the reshaping of the catalyst. The visualization of the growth processes at solid-gas interface at the atomic scale revealed in a clear way the continuous generation of catalytic sites during the reaction in a process that is different from the traditional assumption of a fixed number of stationary active sites in heterogeneous catalysis.

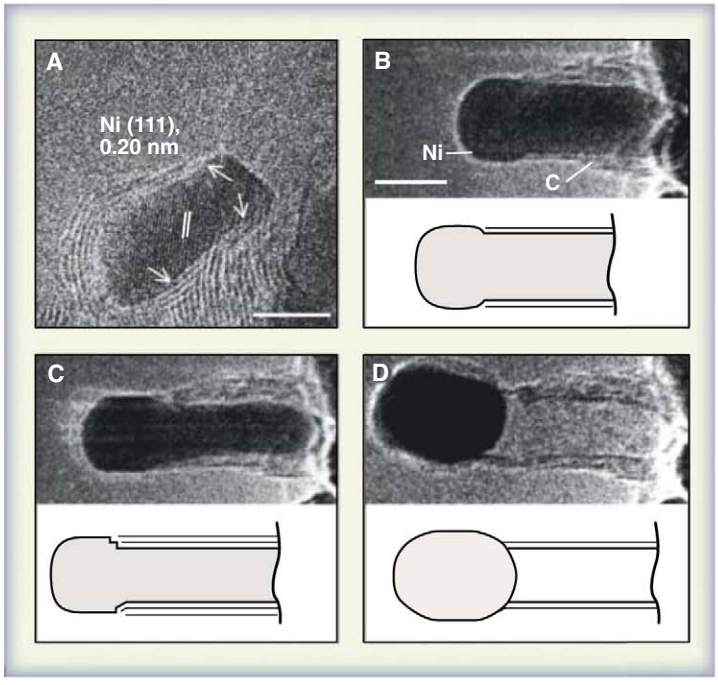

Fig. 2. (**A**) In situ TEM image showing a whisker-type carbon nanofiber. The lattice fringes in the nanofiber correspond to the (002) planes of graphite. Scale bar indicates 5 nm. (**B** to **D**) Image sequence of a growing carbon nanofiber extracted from a video sequence. Scale bar in (B) is 5 nm; (C) and (D) have the same size as (B). (B) to (D) show the elongation/contraction process. Schematic drawings below (B) to (D) are included to help locate the positions of monoatomic Ni step edges at the Ni-graphene interface. These images were acquired in situ with CH_4:H_2 1:1 at a total pressure of 1.6 torr with the sample heated to 500° to 540°C (A) or 536°C [(B) to (D)] [from (*29*)].

Metal Catalysts in Oxidizing and Reducing Environments

Many heterogeneous catalysts perform oxidation reactions, and the interaction of oxygen with most transition metal surfaces can vary with temperature and pressure. At lower temperatures and pressures, oxygen chemisorbs, forming a bond to a surface metal atom. Further reaction at higher temperatures or pressures can incorporate oxygen into the subsurface region and create a surface layer of metal oxide. The build-up of oxygen through the formation of a subsurface oxide on several noble metal catalysts was suggested to be crucial for the catalytic oxidation of hydrocarbons and carbon monoxide (*1*, *2*, *29*, *30*).

Oxygen incorporation into the subsurface region of metal catalysts was investigated by quenching single crystal surfaces such as Ru (0001) and Rh(110) after high exposures at low pressure and long dosing time, followed by ex situ examination in ultrahigh vacuum (UHV) (*31*, *32*). However, it is very likely that the catalyst may have reverted partially or totally to its low-pressure phase after removal from the reactor. Thus, the ex situ studies might not provide access to the phases formed at high pressure.

A recent study using ambient pressure–x-ray photoelectron spectroscopy (AP-XPS) illustrates this point by showing how the phase diagram of the palladium-oxygen system exhibits new phases under pressures in the torr range that are not found in ex situ studies (*10*). In situ x-ray photoelectron spectra of the Pd3d and O1s core levels, which are sensitive to chemical oxidation state, show that three different phases were observed during exposure of Pd(111) to oxygen at a pressure larger than 10^{-6} torr. These results show that certain phases, such as subsurface oxide and bulk oxide, cannot be formed at a pressure and temperature lower than certain threshold conditions. A phase diagram containing four different oxide structures that were observed as a function of pressure and temperature is shown in Fig. 3A. First, a chemisorbed O (2 × 2) structure is formed at low pressure that is kinetically stable at temperatures below a few hundred degrees Celsius under UHV conditions. Then, the topmost surface layer is oxidized, and a two-dimensional oxide with a $\sqrt{6} \times \sqrt{6}$ reconstruction is generated when the pressure is larger than 10^{-6} torr and temperature is below 500° to 630°C. A subsurface oxide is formed at oxygen pressures between 10^{-4} and 0.3 torr and temperatures below 380° to 480°C. Upon further increasing the pressure of oxygen to the Torr range, PdO bulk oxide is formed. The phases formed under oxidizing conditions can be complicated with numerous kinetically stabilized structures that are thermodynamically metastable but still can play a crucial role during catalytic oxidation and reduction reactions.

One method for improving metal catalysts with regard to activity and selectivity is to add other metals and form alloys. The ratio of constituent elements in the surface region of an alloy can vary from its bulk

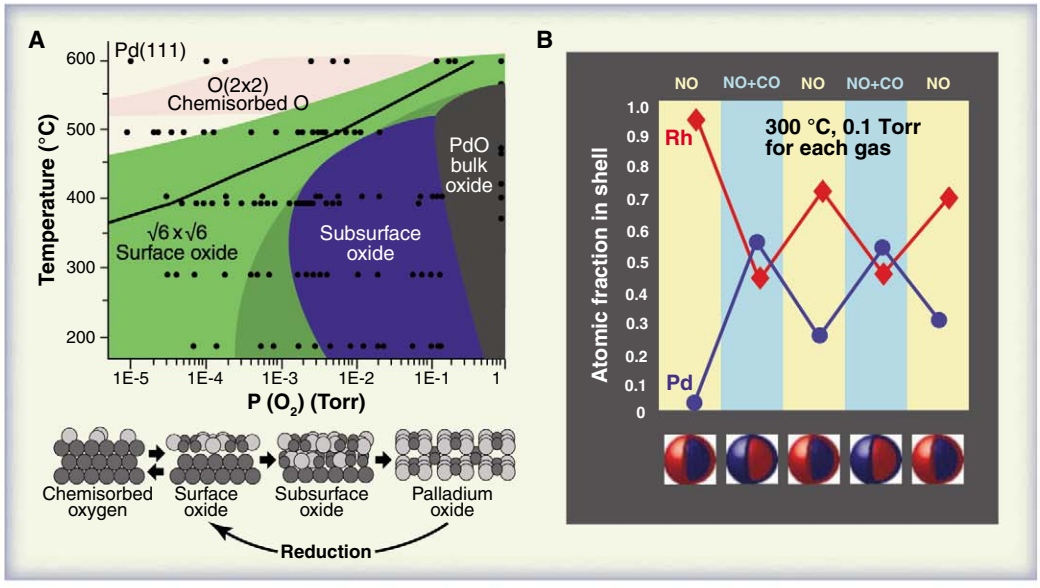

Fig. 3. (**A**) Phase diagram showing the experimentally measured stability regions of the different palladium oxide structures as a function of oxygen partial pressure, *p*, and temperature. These include a O(two-by-two) chemisorbed phase, a $\sqrt{6} \times \sqrt{6}$-monolayer-thick surface oxide, a subsurface oxide, and a bulk PdO. The bottom image is a diagram illustrating the structure of the observed phases. (**B**) Restructuring of the shell region (three to four atomic layers) of bimetallic nanoparticles of $Rh_{0.5}Pd_{0.5}$ (~15 nm in diameter) at 300°C in the presence of gases in the torr range [from (*5*, *10*)].

composition substantially, even under high vacuum conditions. In situ studies using AP-XPS have revealed that the surfaces of Rh_xPd_{1-x} alloy catalysts supported on a silicon wafer exhibit different compositions after changes in the composition of the reactive environment (Fig. 3B) (*5*). In oxidizing environments (pure NO), the surface region is enriched in Rh, whereas the atomic fraction of Pd is increased under reducing conditions. At 300°C, the changes occur rapidly, on the time scale of the experiment, and affect the entire nanoparticle, which becomes equilibrated with the environment by virtue of its small size (~15 nm). The restructuring is driven by the preferential segregation of the constituent metal with lowest surface free energy in reducing environments. Under oxidizing conditions, the formation of Rh-rich shell is driven by the preferential formation of the metallic oxide with higher formation energy.

In situ visualization of Cu nanoparticle catalysts with TEM has also shown that the adsorption energy of reactant molecules on different surfaces can give rise to substantial restructuring (*9*). Cu nanocrystals supported on oxides are widely used as catalysts in several important industrial reactions, including water-gas shift and the formation of alcohols from CO and H_2 (*1*, *2*). At 220°C and in 1.1 torr of pure H_2, Cu nanoparticles supported on ZnO have a morphology rich in (111) and (100) surface orientations (Fig. 4A). When the pure H_2 environment (Fig. 4A) was switched to a mixture of H_2O (0.27 torr) and H_2 (0.83 torr) (Fig. 4B), the particles changed shape, exhibiting a higher fraction of (110) facets (*9*). This process was driven by the high adsorption energy of H_2O on the (110) compared with (111) surface, which results in the preferred formation of nanocrystals with a morphology that minimizes the surface free energy. After purging the H_2O and restoration of a pure H_2 environment, the nanocrystals reverted to their original shape (Fig. 4C) observed at 220°C in 1.1 rorr of H_2, with a lower fraction of (110) facets. Clearly, surface faceting is reaction condition–dependent and reversible. It shows that the active surface structure formed under reaction condition could not be observed after a reaction, further suggesting the necessity of studying surface structure and chemistry of materials under reaction conditions.

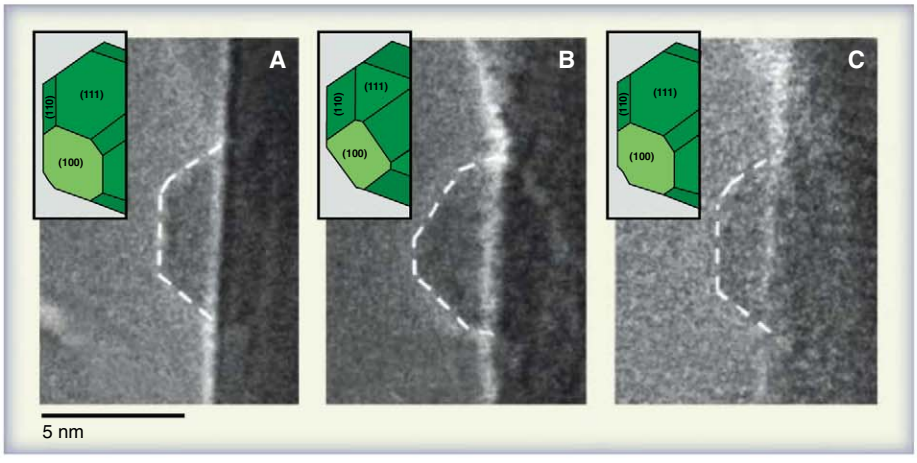

Fig. 4. In situ TEM images showing the reversible shape change of a Cu nanocrystal catalyst collected under different reactants at 220°C. (**A**) Pure H_2 at 1.1 torr, (**B**) H_2:H_2O (3:1) at a total pressure of 1.1 torr, and (**C**) pure H_2 at 1.1 torr. The corresponding Wulff diagrams of the Cu nanocrystals that illustrate the surface planes were inserted [from (*9*)].

Surface Structure of Catalysts Under High Pressures and Temperatures and in Liquids

From the standpoint of thermodynamics, it is necessary to consider the entropic component in the Gibbs free energy of the system, which consists of the catalyst surface and the gas phase of reactants in a reaction system. The entropic contribution is important at high pressure as shown by the roughly 0.4-eV (~40 kJ/mol) difference between the free energy in UHV ($<10^{-10}$ torr) and 760 torr at room temperature. This entropic fraction of the free energy is responsible for the formation of very high coverages at temperatures higher than would be needed at lower pressure. The high coverage structures of reactant molecules obtained by cooling the material to cryogenic temperatures may be metastable, and the thermodynamically stable structure may not be accessed because of kinetic barriers that are insurmountable at low temperature.

Scanning tunneling microscopy (STM) studies under high pressure have been recently performed on Pt(111), Ni(111), and Pt(110) single crystal catalysts (*13*, *33*, *34*). There is no large-scale change in the surface structure of flat and compact Pt(111) and Ni(111) surfaces from low to high pressure (*33*, *34*). On Pt(111), an increase in the CO pressure from 10^{-9} to 1 torr caused the coverage to increase from 0.5 to 0.65 and to finally saturate to a value of 0.68 at 100 torr (Fig. 5A).

Industrial catalysts can contain particles with sizes ranging from 1 nm to a few hundred nanometers (*1*, *35*, *36*). Such small particles have a large fraction of atoms at step edges and corners, which are thought to be the active sites. To model such systems, surfaces with steps and kinks of controlled structure and density can be prepared by cutting a crystal at small angles relative to a low Miller index direction (Fig. 5C) (*37*). Recent studies have shown that the coverage of CO on Pt(557), which consists of 1.2-nm-wide (111)-oriented terraces separated by monoatomic steps, can be as high as 1.0 (Fig. 5B) (*4*). Most importantly, the high coverage of molecules produced when the pressure is higher than 0.1 torr at room temperature results in a substantial restructuring of the catalyst surface, where the terraces break up into triangular-shaped clusters with lateral dimensions of ~2 nm (Fig. 5D). This restructuring significantly increases the density of Pt atoms with low coordination by the increase of density of step edges (*4*). The formation of this new equilibrium structure is favored by the large molecular repulsion resulting from the high density of CO and the facile displacement of step atoms compared with atoms in the flat surface with no steps. The energy cost of this rearrangement is compensated by the decrease in surface free energy through the tilting of CO molecules bound to the low-coordinated edge sites of the nanoclusters, which decreases their repulsion (*4*).

There is an increased interest in the search of bimetallic catalysts for energy conversion and environmental remediation technologies such as control of exhaust emission of vehicles and fuel cell technologies. In these applications, the catalysts operate either under harsh conditions of high temperature and pressure or in acidic solutions. It has been shown that under these conditions some bimetallic catalyst nanoparticles experience evaporation or dissolution and that in many cases one of the constitutive metals is leached away preferentially. An example of this behavior is the evaporation of Ni of Au-Ni catalysts through the formation of nickel carbonyl under reaction condition (*12*). In situ studies using STM show that adsorption of carbon monoxide could induce changes in surface morphology. Figure 5E shows a STM image of the surface of a Au-Ni alloy catalyst before exposure to CO. Under 10 torr of CO, significant changes in the surface structure occurred in minutes (Fig. 5F), where one-atom-high nanoclusters of Au are formed because of the loss of nickel by formation of carbonyls (*12*). Fast imaging of the surface morphology revealed that the rate of Ni removal is linearly dependent on the pressure of CO. Theoretical calculations suggest that this phase separation is a thermodynamic process, in which the increased energy spent to compress CO to a high coverage and to form nickel carbonyl outweighs the decreased energy resulting from the formation of Au-Ni alloy.

The leaching of atoms of one constituent element in bimetallic catalysts occurs at solid-liquid interfaces as well. For example, Cu atoms at the surface of Au-rich Cu-Au alloys are leached away under suitable electrochemical conditions

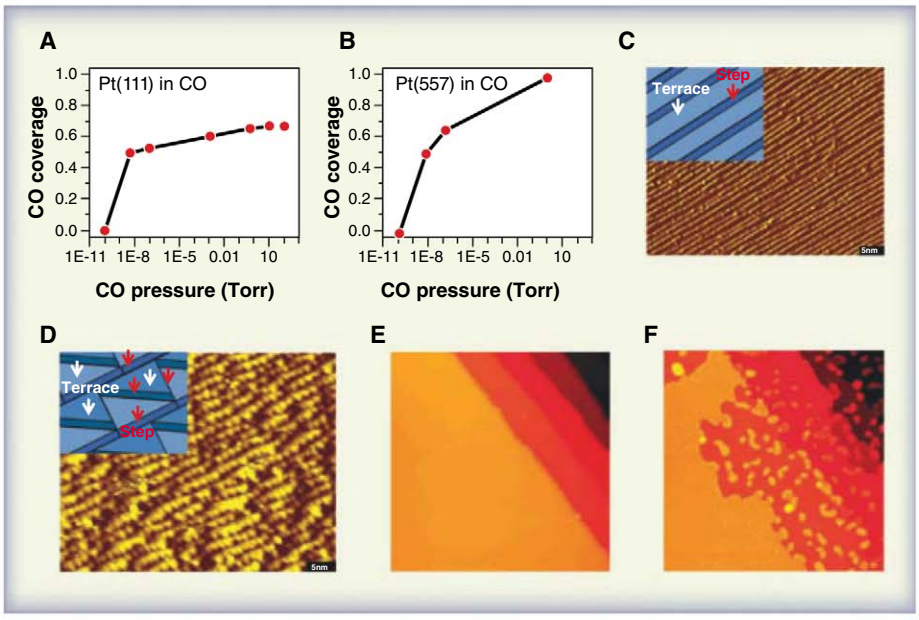

Fig. 5. (**A**) Represented coverage of CO on Pt(111) in the presence of CO at various pressures [from (*33*)]. (**B**) Coverage of CO on Pt(557) in the presence of CO at various pressures [from (*4*)]. (**C**) STM image (40 nm by 50 nm) of Pt(557) with a homogeneous distribution of terraces with a width of 1.2 nm separated by monoatomic steps in UHV; the inset is the structural schematic [from (*4*)]. (**D**) STM image (40 nm by 50 nm) of the restructured surface consisting of triangular nanoclusters with a size of ~2 nm; the inset is the structural schematic [from (*4*)]. (**E** and **F**) STM images (100 nm by 100 nm) of the surface of a Au-Ni alloy catalyst in 10 torr of CO at 0 min and 75 min [from (*12*)].

(*38*). Similarly, atoms of 3d elements in Pt-M (where M is a 3d metal) bimetallic catalysts dissolve in acidic solutions under the working conditions of low-temperature fuel cells (*39*).

Many reactions occur on metal catalysts dispersed on oxide surfaces. The presence of reactant gases can not only change the structure and composition of the metal particles but also induce the formation of an active surface phase of a catalyst. One example is the formation of an active phase in Fischer-Tropsch reactions on Fe_2O_3 catalysts dispersed on support (*14*, *36*). Upon activation of the catalysts in hydrogen at 750 torr and 350°C, α-Fe, Fe_2SiO_4, and Fe_3O_4 are formed. After CO is added to the H_2 gas at 250°C, Fe_xC_y species are formed. These species are suggested to be the active phase. This active phase is identified by using scanning transmission x-ray microscopy (STXM).

Future Challenges and Opportunities

The most active components in various catalysts and sensors are particles with sizes ranging from 1 nm to 1 μm. Many of their unique chemical and physical properties arise from the interactions of their surfaces with the reactive environments. In heterogeneous catalysis, the complexity of the solid-gas and solid-liquid interfaces and their structural and chemical evolution under reaction conditions make understanding catalytic mechanisms extremely challenging. Such understanding requires obtaining in situ information of catalyst systems, particularly their surface structure and chemistry under reaction conditions. In the past, the repertoire of techniques available for this purpose was limited to photon-based techniques and a few others. This has changed recently because new surface-sensitive techniques involving electrons capable of operating under ambient or near-ambient conditions, like those presented in this article, have been developed. However, there are many important issues in the area of heterogeneous catalysis that are still open.

Most processes in energy conversion, such as photo-driven water splitting, involve reactions occurring at solid-liquid or solid-gas interfaces. In situ studies of such processes are far behind compared with the spectacular advances in materials synthesis of the last decades. To bridge this gap, development of additional techniques and methods with the ability to provide information with high spatial and temporal resolution under reaction conditions is highly desirable. Because many chemical processes occur on nanoscale particles, there should be plenty of new chemistry for nanomaterials under reactive environments. Because catalysis on nanoscale materials at solid-gas or solid-liquid interface is important in most of the processes of energy conversion, in situ studies relevant to energy conversion technologies would be crucial for understanding catalytic mechanisms and designing new and efficient catalytic materials for a wide range of energy conversion processes.

References and Notes

1. G. Ertl, H. Knözinger, F. Schüth, J. Weitkamp, *Handbook of Heterogeneous Catalysis* (VCH-Wiley, Weinheim, Germany, 2008).
2. G. A. Somorjai, Y. Li, *Introduction to Surface Chemistry and Catalysis* (VCH-Wiley, Weinheim, Germany, 2010).
3. M. Salmeron, R. Schlogl, *Surf. Sci. Rep.* **63**, 169 (2008).
4. F. Tao *et al.*, *Science* **327**, 850 (2010).
5. F. Tao *et al.*, *Science* **322**, 932 (2008); 10.1126/science.1164170.
6. F. Tao, D. Tang, M. Salmeron, G. A. Somorjai, *Rev. Sci. Instrum.* **79**, 084101 (2008).
7. M. S. Altman, *Science* **327**, 789 (2010).
8. H. Zheng *et al.*, *Science* **324**, 1309 (2009).
9. P. L. Hansen *et al.*, *Science* **295**, 2053 (2002).
10. G. Ketteler *et al.*, *J. Am. Chem. Soc.* **127**, 18269 (2005).
11. I. E. Wachs, C. A. Roberts, *Chem. Soc. Rev.* **39**, 5002 (2010).
12. E. K. Vestergaard *et al.*, *Phys. Rev. Lett.* **95**, 126101 (2005).
13. P. Thostrup *et al.*, *Phys. Rev. Lett.* **87**, 126102 (2001).
14. E. de Smit *et al.*, *Nature* **456**, 222 (2008).
15. J. A. Rodriguez *et al.*, *Science* **318**, 1757 (2007).
16. P. C. Stair, *Curr. Opin. Solid State Mater. Sci.* **5**, 365 (2001).
17. M. Yang, G. A. Somorjai, *J. Am. Chem. Soc.* **126**, 7698 (2004).
18. A. E. Russell, A. Rose, *Chem. Rev.* **104**, 4613 (2004).
19. K. Liu *et al.*, *J. Phys. Chem. C* **114**, 8533 (2010).
20. W. Wang, M. Hunger, *Acc. Chem. Res.* **41**, 895 (2008).
21. J. Frenken, B. Hendriksen, *MRS Bull.* **32**, 1015 (2007).
22. M. J. Williamson, R. M. Tromp, P. M. Vereecken, R. Hull, F. M. Ross, *Nat. Mater.* **2**, 532 (2003).
23. P. L. Gai, *Microsc. Microanal.* **8**, 21 (2002).
24. C. J. Zhang *et al.*, *Nat. Mat.* **9**, 944 (2010).
25. P. A. Grozier, R. G. Wang, R. Sharma, *Ultramicroscopy* **108**, 1432 (2008).
26. V. K. LaMer, R. H. Dinegar, *J. Am. Chem. Soc.* **72**, 4847 (1950).
27. H. Reiss, *J. Chem. Phys.* **19**, 482 (1951).
28. C. B. Murray, *Science* **324**, 1276 (2009).
29. S. Helveg *et al.*, *Nature* **427**, 426 (2004).
30. C. T. Campbell, C. H. F. Peden, *Science* **309**, 713 (2005).
31. R. Blume *et al.*, *J. Phys. Chem. B* **109**, 14052 (2005).
32. P. Dudin *et al.*, *J. Phys. Chem. B* **109**, 13649 (2005).
33. S. R. Longwitz *et al.*, *J. Phys. Chem. B* **108**, 14497 (2004).
34. C. Quiros *et al.*, *Surf. Sci.* **522**, 161 (2003).
35. C. J. Liu, U. Burghaus, F. Besenbacher, Z. L. Wang, *ACS Nano* **4**, 5517 (2010).
36. G. B. Yu *et al.*, *J. Am. Chem. Soc.* **132**, 935 (2010).
37. H. C. Jeong, E. D. Williams, *Surf. Sci. Rep.* **34**, 171 (1999).
38. S. J. Chen *et al.*, *Surf. Sci.* **292**, 289 (1993).
39. J. Zhang, K. Sasaki, E. Sutter, R. R. Adzic, *Science* **315**, 220 (2007).

40. This work was supported by the director, Office of Basic Energy Sciences, Materials Sciences Division of the U.S. Department of Energy under contract no. DE-AC02-05CH11231, and Department of Chemistry and Biochemistry, College of Science, Sustainable Energy Initiative, Radiation Lab, and Office of Research at University of Notre Dame. F.T. would like to acknowledge K. Davis of the University of Notre Dame for assistance with the animation movie.

Supporting Online Material

www.sciencemag.org/cgi/content/full/331/6014/171/DC1
Movie S1

10.1126/science.1197461

Complex Diel Cycles of Gene Expression in Coral-Algal Symbiosis

O. Levy,[1,2]* P. Kaniewska,[2]* S. Alon,[3] E. Eisenberg,[4] S. Karako-Lampert,[1] L. K. Bay,[5] R. Reef,[2,6] M. Rodriguez-Lanetty,[2,7] D. J. Miller,[5]† O. Hoegh-Guldberg[2,5]†

Reef-building corals exhibit complex rhythmic biological behaviors (*1*). Understanding circadian regulation in these organisms is complicated by their photosynthetic endosymbionts (*Symbiodinium* spp.). Photosynthesis by the symbionts results in coral tissue being hyperoxic by day but near hypoxic by night when respiration dominates (*2*). To better understand how corals tune their circadian machinery to respond to external and internal cues, we performed microarray analysis of coral genes (*3*) with *Acropora millepora*. Three coral colonies were sampled at 4-hour intervals over 2 days under ambient light-dark (LD) cycles and under constant darkness (DD) (fig. S1). K-means clustering of the microarray data after Fourier analysis identified several co-regulated (synexpression) clusters consisting of functionally related genes with common temporal expression patterns (figs. S1 to S3 and table S1) (*4*).

A synexpression group of genes that are strictly light-coupled and include coral cryptochromes had an expression peak at midday (zeitgeber time zt6), which corresponds to the period of highest illumination (Fig. 1A) (*1*). The α-type *carbonic anhydrase* (α-CA) in this synexpression cluster potentially underlies the phenomenon of light-enhanced coral calcification (*5*). Other genes in this cluster have known or possible antioxidant functions, including *ferritin*-H, the heme-binding protein 2 (HeBP2), and catalase (fig. S4) (*6*–*8*). These data for corals suggest that the link between the cellular redox state and the circadian clock may be an ancestral trait.

A second group of *A. millepora* genes peaked in expression at midnight (zt18) under normal LD cycles (Fig. 1B) but did not cycle under DD. These genes encode several glycolytic enzymes and other enzymes required for biosynthetic pathways (*4*).

Glycolytic enzymes are regulated by the hypoxia-inducible factor (HIF) 1α transcription factor (*9*), an ortholog of which is present in *A. millepora*. In the coral, HIF expression has a peak at zt14 in LD (fig. S5). The tight temporal clustering of the glycolytic gene group implies regulation by symbiont physiology, which is linked to external light levels.

Molecular chaperones formed another synexpression group that cycles not only under LD (peaking at zt10; 16:00) but also (with the sole exception of *hsp40*) in constant darkness (Fig. 1, C and D). Although chaperones have been linked to the circadian clock (*10*), there are no precedents for extensive coordinated chaperone expression, which probably reflects the diel pattern of stress experienced by symbiotic corals.

Our data may indicate that the HIF system in corals mediates diel cycles in central metabolism, whereas many genes involved in stress responses and protection are coupled to the circadian clock. Our data highlight the physiological complexity of regulatory mechanisms in the coral-algal symbiosis; diel cycles appear to be governed by the circadian clock, with the HIF system most likely operating in parallel.

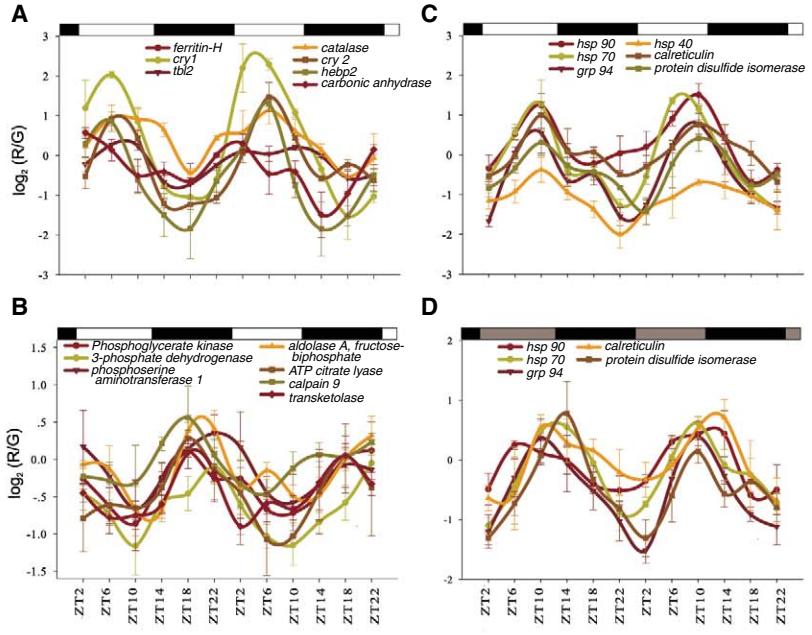

Fig. 1. Temporal gene expression data. RNA samples collected from the symbiotic coral *A. millepora* (*N* = 3) and hybridized to microarray during LD cycles or DD are shown as log ratios of test sample (R)/reference (G) and are plotted according to zeitgeber time; zt2 to zt22 is equivalent to 08:00 to 04:00. Error bars represent the standard error of the mean. (**A**) α–carbonic anhydrase and several antioxidant genes show classical light-dependent circadian regulation, peaking in expression with cryptochromes during the period of highest illumination (zt6 = 12:00). (**B**) Metabolic genes (including three glycolytic enzymes) that peak in expression in the dark (zt18 to zt22 equals 24:00 to 04:00) and may be induced by symbiont-driven hypoxia. (**C** and **D**) A large cluster of chaperones peak in expression at zt10 = 16:00 under both normal (C) LD and (D) DD cycles.

References and Notes

1. O. Levy *et al.*, *Science* **318**, 467 (2007).
2. M. Kühl, Y. Cohen, T. Dalsgaard, B. B. Jorgensen, N. P. Revsbech, *Mar. Ecol. Prog. Ser.* **117**, 159 (1995).
3. L. K. Bay *et al.*, *Mol. Ecol.* **18**, 3062 (2009).
4. Materials and methods are available as supporting material on *Science* Online.
5. B. E. Chalker, D. L. Taylor, *Proc. R. Soc. Lond. B Biol. Sci.* **190**, 323 (1975).
6. K. Orino *et al.*, *Biochem. J.* **357**, 241 (2001).
7. G. Noctor, C. H. Foyer, *Annu. Rev. Plant Physiol. Plant Mol. Biol.* **49**, 249 (1998).
8. J. Hirayama, S. Cho, P. Sassone-Corsi, *Proc. Natl. Acad. Sci. U.S.A.* **104**, 15747 (2007).
9. U. Lendahl, K. L. Lee, H. Yang, L. Poellinger, *Nat. Rev. Genet.* **10**, 821 (2009).
10. G. E. Duffield, *J. Neuroendocrinol.* **15**, 991 (2003).
11. We thank Y. Gothilf for critical discussions and N. Simon-Blecher for assistance in collecting coral samples. This work was supported by the Australian Research Council (O.H.-G. and D.J.M.) and Israel Science Foundation grant no. 699/06. Microarray data are Minimum Information About a Microarray Experiment (MIAME)–compliant and deposited under accession number GSE21658 (National Center for Biotechnology Information GEO). HIF ortholog present in *A. millepora* (GenBank identification EZ037157).

Supporting Online Material

www.sciencemag.org/cgi/content/full/331/6014/175/DC1
Materials and Methods
SOM Text
Figs. S1 to S5
Table S1
References

12 August 2010; accepted 8 December 2010
10.1126/science.1196419

[1]Mina and Everard Goodman Faculty of Life Sciences, Bar-Ilan University, Ramat-Gan 52900, Israel. [2]Global Change Institute, University of Queensland, St. Lucia, QLD 4072, Australia. [3]Department of Neurobiology, Faculty of Life Sciences, Tel Aviv University, Tel Aviv 69978, Israel. [4]Raymond and Beverly Sackler School of Physics and Astronomy, Tel Aviv University, Tel Aviv 69978, Israel. [5]Australian Research Council Centre of Excellence for Coral Reef Studies, James Cook University, Townsville, QLD 4811, Australia. [6]School of Biological Sciences, University of Queensland, St. Lucia, QLD 4072, Australia. [7]Department of Biology, University of Louisiana at Lafayette, Lafayette, LA 70504, USA.

*These authors contributed equally to this work.
†To whom correspondence should be sent. E-mail: David.Miller@jcu.edu.au (D.J.M.); oveh@uq.edu.au (O.H.-G.)

Quantitative Analysis of Culture Using Millions of Digitized Books

Jean-Baptiste Michel,[1,2,3,4,5]*† Yuan Kui Shen,[2,6,7] Aviva Presser Aiden,[2,6,8] Adrian Veres,[2,6,9] Matthew K. Gray,[10] The Google Books Team,[10] Joseph P. Pickett,[11] Dale Hoiberg,[12] Dan Clancy,[10] Peter Norvig,[10] Jon Orwant,[10] Steven Pinker,[5] Martin A. Nowak,[1,13,14] Erez Lieberman Aiden[1,2,6,14,15,16,17]*†

We constructed a corpus of digitized texts containing about 4% of all books ever printed. Analysis of this corpus enables us to investigate cultural trends quantitatively. We survey the vast terrain of 'culturomics,' focusing on linguistic and cultural phenomena that were reflected in the English language between 1800 and 2000. We show how this approach can provide insights about fields as diverse as lexicography, the evolution of grammar, collective memory, the adoption of technology, the pursuit of fame, censorship, and historical epidemiology. Culturomics extends the boundaries of rigorous quantitative inquiry to a wide array of new phenomena spanning the social sciences and the humanities.

Reading small collections of carefully chosen works enables scholars to make powerful inferences about trends in human thought. However, this approach rarely enables precise measurement of the underlying phenomena. Attempts to introduce quantitative methods into the study of culture (*1*–*6*) have been hampered by the lack of suitable data.

We report the creation of a corpus of 5,195,769 digitized books containing ~4% of all books ever published. Computational analysis of this corpus enables us to observe cultural trends and subject them to quantitative investigation. 'Culturomics' extends the boundaries of scientific inquiry to a wide array of new phenomena.

The corpus has emerged from Google's effort to digitize books. Most books were drawn from over 40 university libraries around the world. Each page was scanned with custom equipment (*7*), and the text was digitized by means of optical character recognition (OCR). Additional volumes, both physical and digital, were contributed by publishers. Metadata describing the date and place of publication were provided by the libraries and publishers and supplemented with bibliographic databases. Over 15 million books have been digitized [~12% of all books ever published (*7*)]. We selected a subset of over 5 million books for analysis on the basis of the quality of their OCR and metadata (Fig. 1A and fig. S1) (*7*). Periodicals were excluded.

The resulting corpus contains over 500 billion words, in English (361 billion), French (45 billion), Spanish (45 billion), German (37 billion), Chinese (13 billion), Russian (35 billion), and Hebrew (2 billion). The oldest works were published in the 1500s. The early decades are represented by only a few books per year, comprising several hundred thousand words. By 1800, the corpus grows to 98 million words per year; by 1900, 1.8 billion; and by 2000, 11 billion (fig. S2).

The corpus cannot be read by a human. If you tried to read only English-language entries from the year 2000 alone, at the reasonable pace of 200 words/min, without interruptions for food or sleep, it would take 80 years. The sequence of letters is 1000 times longer than the human genome: If you wrote it out in a straight line, it would reach to the Moon and back 10 times over (*8*).

To make release of the data possible in light of copyright constraints, we restricted this initial study to the question of how often a given 1-gram or *n*-gram was used over time. A 1-gram is a string of characters uninterrupted by a space; this includes words ("banana", "SCUBA") but also numbers ("3.14159") and typos ("excesss"). An *n*-gram is a sequence of 1-grams, such as the phrases "stock market" (a 2-gram) and "the United States of America" (a 5-gram). We restricted *n* to 5 and limited our study to *n*-grams occurring at least 40 times in the corpus.

Usage frequency is computed by dividing the number of instances of the *n*-gram in a given year by the total number of words in the corpus in that year. For instance, in 1861, the 1-gram "slavery" appeared in the corpus 21,460 times, on 11,687 pages of 1208 books. The corpus contains 386,434,758 words from 1861; thus, the frequency is 5.5×10^{-5}. The use of "slavery" peaked during the Civil War (early 1860s) and then again during the civil rights movement (1955–1968) (Fig. 1B)

In contrast, we compare the frequency of "the Great War" to the frequencies of "World War I" and "World War II". References to "the Great War" peak between 1915 and 1941. But although its frequency drops thereafter, interest in the underlying events had not disappeared; instead, they are referred to as "World War I" (Fig. 1C).

These examples highlight two central factors that contribute to culturomic trends. Cultural change guides the concepts we discuss (such as "slavery"). Linguistic change, which, of course, has cultural roots, affects the words we use for those concepts ("the Great War" versus "World War I"). In this paper, we examine both linguistic changes, such as changes in the lexicon and grammar, and cultural phenomena, such as how we remember people and events.

The full data set, which comprises over two billion culturomic trajectories, is available for download or exploration at www.culturomics.org and ngrams.googlelabs.com.

The size of the English lexicon. How many words are in the English language (*9*)?

We call a 1-gram "common" if its frequency is greater than one per billion. [This corresponds to the frequency of the words listed in leading dictionaries (*7*) (fig. S3).] We compiled a list of all common 1-grams in 1900, 1950, and 2000, based on the frequency of each 1-gram in the preceding decade. These lists contained 1,117,997 common 1-grams in 1900, 1,102,920 in 1950, and 1,489,337 in 2000.

Not all common 1-grams are English words. Many fell into three nonword categories: (i) 1-grams with nonalphabetic characters ("l8r", "3.14159"), (ii) misspellings ("becuase", "abberation"), and (iii) foreign words ("sensitivo").

To estimate the number of English words, we manually annotated random samples from the lists of common 1-grams (*7*) and determined what fraction were members of the above nonword categories. The result ranged from 51% of all common 1-grams in 1900 to 31% in 2000.

Using this technique, we estimated the number of words in the English lexicon as 544,000 in 1900, 597,000 in 1950, and 1,022,000 in 2000. The lexicon is enjoying a period of enormous growth: The addition of ~8500 words/year has increased the size of the language by over 70% during the past 50 years (Fig. 2A).

Notably, we found more words than appear in any dictionary. For instance, the 2002 *Webster's Third New International Dictionary* (W3), which keeps track of the contemporary American lexicon, lists approximately 348,000 single-word wordforms (*10*); the *American Heritage Dictionary of the English Language, Fourth Edition* (AHD4) lists 116,161 (*11*). (Both contain additional multiword entries.) Part of this gap is because dictionaries often

[1]Program for Evolutionary Dynamics, Harvard University, Cambridge, MA 02138, USA. [2]Cultural Observatory, Harvard University, Cambridge, MA 02138, USA. [3]Institute for Quantitative Social Sciences, Harvard University, Cambridge, MA 02138, USA. [4]Department of Psychology, Harvard University, Cambridge, MA 02138, USA. [5]Department of Systems Biology, Harvard Medical School, Boston, MA 02115, USA. [6]Laboratory-at-Large, Harvard University, Cambridge, MA 02138, USA. [7]Computer Science and Artificial Intelligence Laboratory, Massachusetts Institute of Technology (MIT), Cambridge, MA 02139, USA. [8]Harvard Medical School, Boston, MA, 02115, USA. [9]Harvard College, Cambridge, MA 02138, USA. [10]Google, Mountain View, CA 94043, USA. [11]Houghton Mifflin Harcourt, Boston, MA 02116, USA. [12]Encyclopaedia Britannica, Chicago, IL 60654, USA. [13]Department of Organismic and Evolutionary Biology, Harvard University, Cambridge, MA 02138, USA. [14]Department of Mathematics, Harvard University, Cambridge, MA 02138, USA. [15]Broad Institute of Harvard and MIT, Harvard University, Cambridge, MA 02138, USA. [16]School of Engineering and Applied Sciences, Harvard University, Cambridge, MA 02138, USA. [17]Harvard Society of Fellows, Harvard University, Cambridge, MA 02138, USA.

*These authors contributed equally to this work.
†To whom correspondence should be addressed. E-mail: jb.michel@gmail.com (J.-B.M.); erez@erez.com (E.L.A.)

exclude proper nouns (fig. S4) and compound words ("whalewatching"). Even accounting for these factors, we found many undocumented words, such as "aridification" (the process by which a geographic region becomes dry), "slenthem" (a musical instrument), and, appropriately, the word "deletable."

This gap between dictionaries and the lexicon results from a balance that every dictionary must strike: It must be comprehensive enough to be a useful reference but concise enough to be printed, shipped, and used. As such, many infrequent words are omitted. To gauge how well dictionaries reflect the lexicon, we ordered our year-2000 lexicon by frequency, divided it into eight deciles (ranging from 10^{-9} to 10^{-8}, to 10^{-2} to 10^{-1}) and sampled each decile (*7*). We manually checked how many sample words were listed in the *Oxford English Dictionary* (OED) (*12*) and in the *Merriam-Webster Unabridged Dictionary* (MWD). (We excluded proper nouns, because neither the OED nor MWD lists them.) Both dictionaries had excellent coverage of high-frequency words but less coverage for frequencies below 10^{-6}: 67% of words in the 10^{-9} to 10^{-8} range were listed in neither dictionary (Fig. 2B). Consistent with Zipf's famous law, a large fraction of the words in our lexicon (63%) were in this lowest-frequency bin. As a result, we estimated that 52% of the English lexicon—the majority of the words used in English books—consists of lexical "dark matter" undocumented in standard references (*12*).

To keep up with the lexicon, dictionaries are updated regularly (*13*). We examined how well these changes corresponded with changes in actual usage by studying the 2077 1-gram headwords added to AHD4 in 2000. The overall frequency of these words, such as "buckyball" and "netiquette", has soared since 1950: Two-thirds exhibited recent sharp increases in frequency (>2× from 1950 to 2000) (Fig. 2C). Nevertheless, there was a lag between lexicographers and the lexicon. Over half the words added to AHD4 were part of the English lexicon a century ago (frequency $>10^{-9}$ from 1890 to 1900). In fact, some newly added words, such as "gypseous" and "amplidyne", have already undergone a steep decline in frequency (Fig. 2D).

Not only must lexicographers avoid adding words that have fallen out of fashion, they must also weed obsolete words from earlier editions. This is an imperfect process. We found 2220 obsolete 1-gram headwords ("diestock", "alkalescent") in AHD4. Their mean frequency declined throughout the 20th century and dipped below 10^{-9} decades ago (Fig. 2D, inset).

Our results suggest that culturomic tools will aid lexicographers in at least two ways: (i) finding low-frequency words that they do not list, and (ii) providing accurate estimates of current frequency trends to reduce the lag between changes in the lexicon and changes in the dictionary.

The evolution of grammar. Next, we examined grammatical trends. We studied the English irregular verbs, a classic model of grammatical change (*14*–*17*). Unlike regular verbs, whose past tense is generated by adding -ed (jump/jumped), irregular verbs are conjugated idiosyncratically (stick/stuck, come/came, get/got) (*15*).

All irregular verbs coexist with regular competitors (e.g., "strived" and "strove") that threaten to supplant them (Fig. 2E and fig. S5). High-frequency irregulars, which are more readily remembered, hold their ground better. For instance, we found "found" (frequency: 5×10^{-4}) 200,000 times more often than we finded "finded." In contrast, "dwelt" (frequency: 1×10^{-5}) dwelt in our data only 60 times as often as "dwelled" dwelled. We defined a verb's "regularity" as the percentage of instances in the past tense (i.e., the sum of "drived", "drove", and "driven") in which the regular form is used. Most irregulars have been stable for the past 200 years, but 16% underwent a change in regularity of 10% or more (Fig. 2F).

These changes occurred slowly: It took 200 years for our fastest-moving verb ("chide") to go from 10% to 90%. Otherwise, each trajectory was sui generis; we observed no characteristic shape. For instance, a few verbs, such as "spill", regularized at a constant speed, but others, such as "thrive" and "dig", transitioned in fits and starts (*7*). In some cases, the trajectory suggested a reason for the trend. For example, with "sped/speeded" the shift in meaning from "to move rapidly" and toward "to exceed the legal limit" appears to have been the driving cause (Fig. 2G).

Six verbs (burn, chide, smell, spell, spill, and thrive) regularized between 1800 and 2000 (Fig. 2F). Four are remnants of a now-defunct phonological process that used -t instead of -ed; they are members of a pack of irregulars that survived by virtue of similarity (bend/bent, build/built, burn/burnt, learn/learnt, lend/lent, rend/rent, send/sent, smell/smelt, spell/spelt, spill/spilt, and spoil/spoilt). Verbs have been defecting from this coalition for centuries (wend/went, pen/pent, gird/girt, geld/gelt, and gild/gilt all blend/blent into the dominant -ed rule). Culturomic analysis reveals that the collapse of this alliance has been the most significant driver of regularization in the past 200 years. The regularization of burnt, smelt, spelt, and spilt originated in the United States; the forms still cling to life in British English (Fig. 2, E and F). But the -t irregulars may be doomed in England too. Each year, a population the size of Cambridge adopts "burned" in lieu of "burnt".

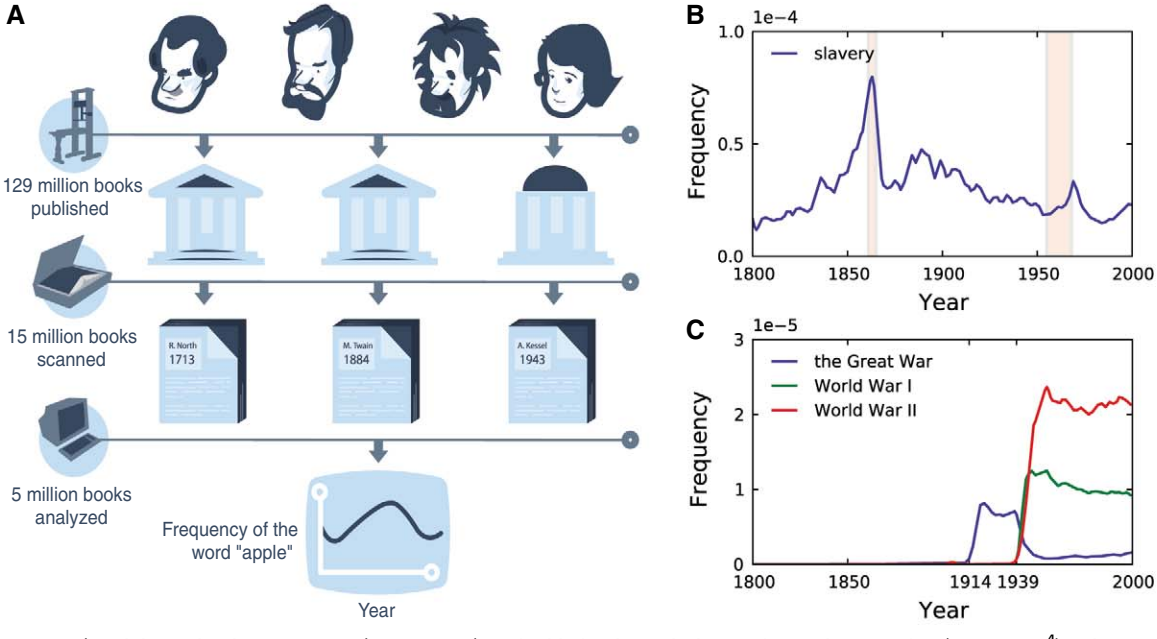

Fig. 1. Culturomic analyses study millions of books at once. (**A**) Top row: Authors have been writing for millennia; ~129 million book editions have been published since the advent of the printing press (upper left). Second row: Libraries and publishing houses provide books to Google for scanning (middle left). Over 15 million books have been digitized. Third row: Each book is associated with metadata. Five million books are chosen for computational analysis (bottom left). Bottom row: A culturomic time line shows the frequency of "apple" in English books over time (1800–2000). (**B**) Usage frequency of "slavery". The Civil War (1861–1865) and the civil rights movement (1955–1968) are highlighted in red. The number in the upper left (1e-4 = 10^{-4}) is the unit of frequency. (**C**) Usage frequency over time for "the Great War" (blue), "World War I" (green), and "World War II" (red).

Although irregulars generally yield to regulars, two verbs did the opposite: light/lit and wake/woke. Both were irregular in Middle English, were mostly regular by 1800, and subsequently backtracked and are irregular again today. The fact that these verbs have been going back and forth for nearly 500 years highlights the gradual nature of the underlying process.

Still, there was at least one instance of rapid progress by an irregular form. Presently, 1% of the English-speaking population switches from "sneaked" to "snuck" every year. Someone will have snuck off while you read this sentence. As before, this trend is more prominent in the United States but recently sneaked across the Atlantic: America is the world's leading exporter of both regular and irregular verbs.

Out with the old. Just as individuals forget the past (*18*, *19*), so do societies (*20*) (fig. S6). To quantify this effect, we reasoned that the frequency of 1-grams such as "1951" could be used to measure interest in the events of the corresponding year, and we created plots for each year between 1875 and 1975.

The plots had a characteristic shape. For example, "1951" was rarely discussed until the years immediately preceding 1951. Its frequency soared in 1951, remained high for 3 years, and then underwent a rapid decay, dropping by half over the next 15 years. Finally, the plots

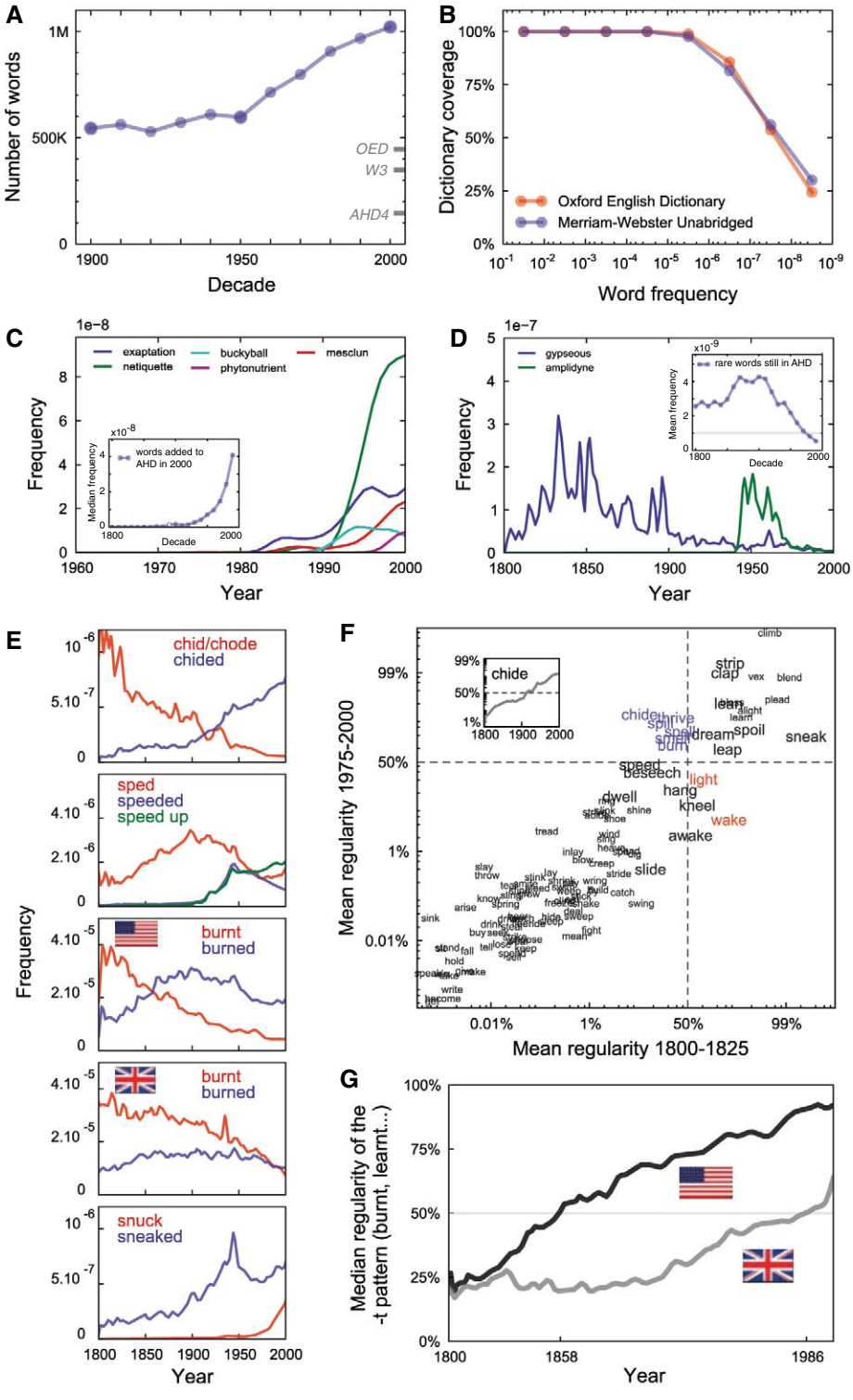

Fig. 2. Culturomics has profound consequences for the study of language, lexicography, and grammar. (**A**) The size of the English lexicon over time. Tick marks show the number of single words in three dictionaries (see text). (**B**) Fraction of words in the lexicon that appear in two different dictionaries as a function of usage frequency. (**C**) Five words added by the AHD in its 2000 update. Inset: Median frequency of new words added to AHD4 in 2000. The frequency of half of these words exceeded 10^{-9} as far back as 1890 (white dot). (**D**) Obsolete words added to AHD4 in 2000. Inset: Mean frequency of the 2220 AHD headwords whose current usage frequency is less than 10^{-9}. (**E**) Usage frequency of irregular verbs (red) and their regular counterparts (blue). Some verbs (chide/chided) have regularized during the past two centuries. The trajectories for "speeded" and "speed up" (green) are similar, reflecting the role of semantic factors in this instance of regularization. The verb "burn" first regularized in the United States (U.S. flag) and later in the United Kingdom (UK flag). The irregular "snuck" is rapidly gaining on "sneaked". (**F**) Scatterplot of the irregular verbs; each verb's position depends on its regularity (see text) in the early 19th century (*x* coordinate) and in the late 20th century (*y* coordinate). For 16% of the verbs, the change in regularity was greater than 10% (large font). Dashed lines separate irregular verbs (regularity < 50%) from regular verbs (regularity > 50%). Six verbs became regular (upper left quadrant, blue), whereas two became irregular (lower right quadrant, red). Inset: The regularity of "chide" over time. (**G**) Median regularity of verbs whose past tense is often signified with a -t suffix instead of -ed (burn, smell, spell, spill, dwell, learn, and spoil) in U.S. (black) and UK (gray) books.

enter a regime marked by slower forgetting: Collective memory has both a short-term and a long-term component.

But there have been changes. The amplitude of the plots is rising every year: Precise dates are increasingly common. There is also a greater focus on the present. For instance, "1880" declined to half its peak value in 1912, a lag of 32 years. In contrast, "1973" declined to half its peak by 1983, a lag of only 10 years. We are forgetting our past faster with each passing year (Fig. 3A).

We were curious whether our increasing tendency to forget the old was accompanied by more rapid assimilation of the new (*21*). We divided a list of 147 inventions into time-resolved cohorts based on the 40-year interval in which they were first invented (1800–1840, 1840–1880, and 1880–1920) (*7*). We tracked the frequency of each invention in the *n*th year after it was invented as compared to its maximum value and plotted the median of these rescaled trajectories for each cohort.

The inventions from the earliest cohort (1800–1840) took over 66 years from invention

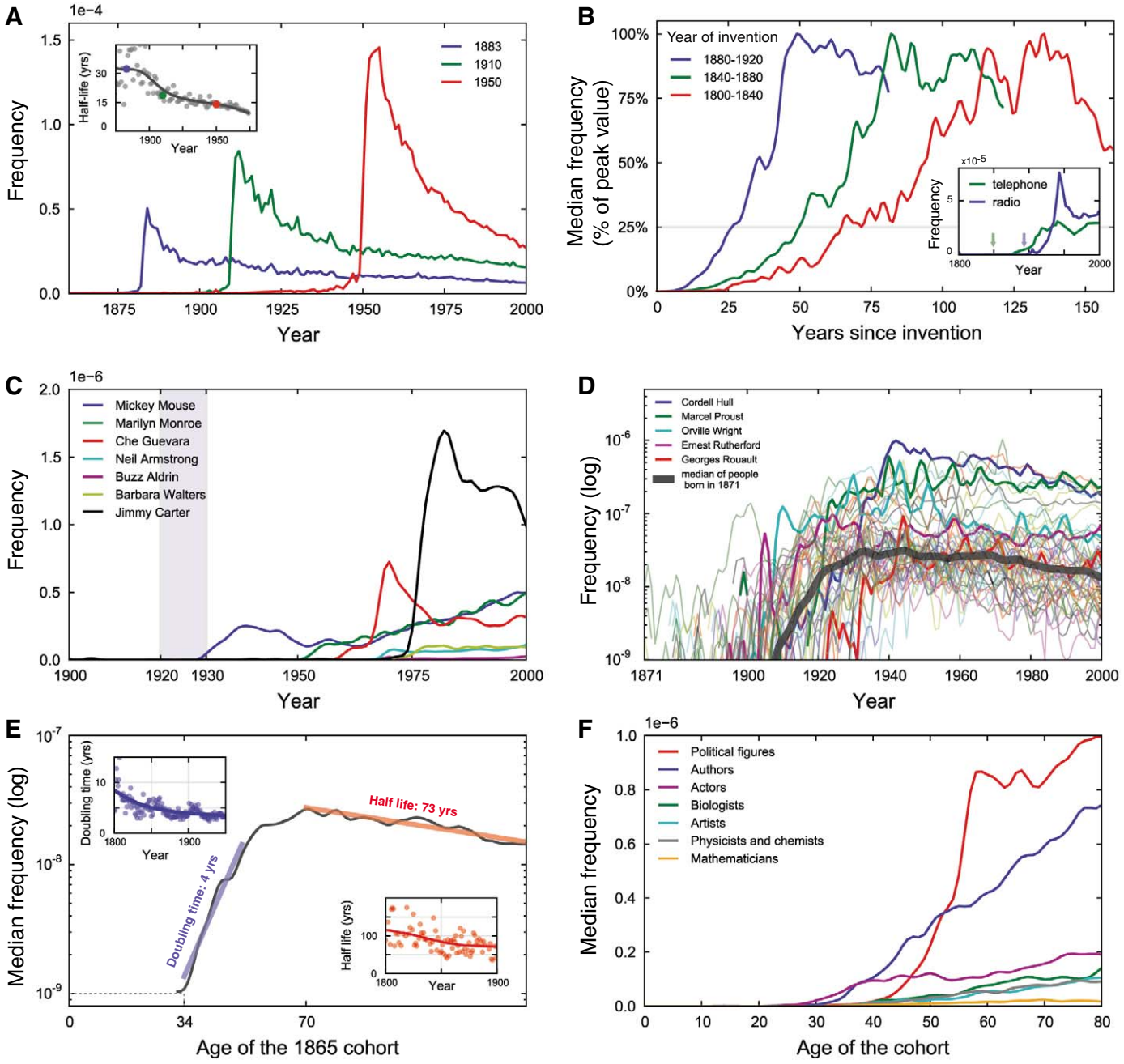

Fig. 3. Cultural turnover is accelerating. (**A**) We forget: frequency of "1883" (blue), "1910" (green), and "1950" (red). Inset: We forget faster. The half-life of the curves (gray dots) is getting shorter (gray line: moving average). (**B**) Cultural adoption is quicker. Median trajectory for three cohorts of inventions from three different time periods (1800–1840, blue; 1840–1880, green; 1880–1920, red). Inset: The telephone (green; date of invention, green arrow) and radio (blue; date of invention, blue arrow). (**C**) Fame of various personalities born between 1920 and 1930. (**D**) Frequency of the 50 most famous people born in 1871 (gray lines; median, thick dark gray line). Five examples are highlighted. (**E**) The median trajectory of the 1865 cohort is characterized by four parameters: (i) initial age of celebrity (34 years old, tick mark); (ii) doubling time of the subsequent rise to fame (4 years, blue line); (iii) age of peak celebrity (70 years after birth, tick mark), and (iv) half-life of the post-peak forgetting phase (73 years, red line). Inset: The doubling time and half-life over time. (**F**) The median trajectory of the 25 most famous personalities born between 1800 and 1920 in various careers.

to widespread impact (frequency >25% of peak). Since then, the cultural adoption of technology has become more rapid. The 1840–1880 invention cohort was widely adopted within 50 years; the 1880–1920 cohort within 27 (Fig. 3B and fig. S7).

"In the future, everyone will be famous for 7.5 minutes" – *Whatshisname*. People, too, rise to prominence, only to be forgotten (*22*). Fame can be tracked by measuring the frequency of a person's name (Fig. 3C). We compared the rise to fame of the most famous people of different eras. We took all 740,000 people with entries in Wikipedia, removed cases where several famous individuals share a name, and sorted the rest by birth date and frequency (*23*). For every year from 1800 to 1950, we constructed a cohort consisting of the 50 most famous people born in that year. For example, the 1882 cohort includes "Virginia Woolf" and "Felix Frankfurter"; the 1946 cohort includes "Bill Clinton" and "Steven Spielberg". We plotted the median frequency for the names in each cohort over time (Fig. 3, D and E). The resulting trajectories were all similar. Each cohort had a pre-celebrity period (median frequency $<10^{-9}$), followed by a rapid rise to prominence, a peak, and a slow decline. We therefore characterized each cohort using four parameters: (i) the age of initial celebrity, (ii) the doubling time of the initial rise, (iii) the age of peak celebrity, and (iv) the half-life of the decline (Fig. 3E). The age of peak celebrity has been consistent over time: about 75 years after birth. But the other parameters have been changing (fig. S8). Fame comes sooner and rises faster. Between the early 19th century and the mid-20th century, the age of initial celebrity declined from 43 to 29 years, and the doubling time fell from 8.1 to 3.3 years. As a result, the most famous people alive today are more famous—in books—than their predecessors. Yet this fame is increasingly short-lived: The post-peak half-life dropped from 120 to 71 years during the 19th century.

We repeated this analysis with all 42,358 people in the databases of the *Encyclopaedia Britannica* (*24*), which reflect a process of expert curation that began in 1768. The results were similar (*7*) (fig. S9). Thus, people are getting more famous than ever before but are being forgotten more rapidly than ever.

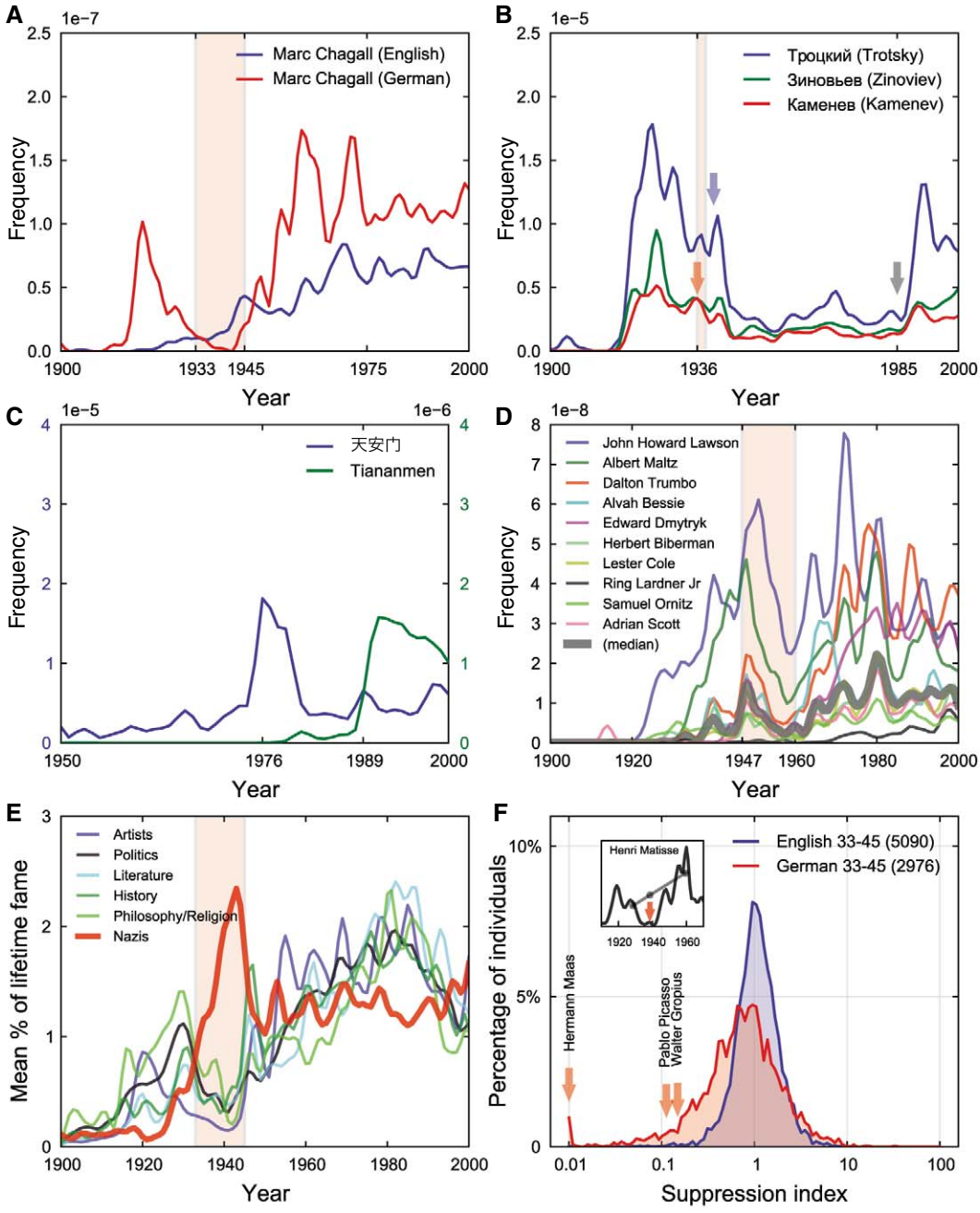

Fig. 4. Culturomics can be used to detect censorship. (**A**) Usage frequency of "Marc Chagall" in German (red) as compared to English (blue). (**B**) Suppression of Leon Trotsky (blue), Grigory Zinoviev (green), and Lev Kamenev (red) in Russian texts, with noteworthy events indicated: Trotsky's assassination (blue arrow), Zinoviev and Kamenev executed (red arrow), the Great Purge (red highlight), and perestroika (gray arrow). (**C**) The 1976 and 1989 Tiananmen Square incidents both led to elevated discussion in English texts (scale shown on the right). Response to the 1989 incident is largely absent in Chinese texts (blue, scale shown on the left), suggesting government censorship. (**D**) While the Hollywood Ten were blacklisted (red highlight) from U.S. movie studios, their fame declined (median: thick gray line). None of them were credited in a film until 1960's (aptly named) *Exodus*. (**E**) Artists and writers in various disciplines were suppressed by the Nazi regime (red highlight). In contrast, the Nazis themselves (thick red line) exhibited a strong fame peak during the war years. (**F**) Distribution of suppression indices for both English (blue) and German (red) for the period from 1933–1945. Three victims of Nazi suppression are highlighted at left (red arrows). Inset: Calculation of the suppression index for "Henri Matisse".

Occupational choices affect the rise to fame. We focused on the 25 most famous individuals born between 1800 and 1920 in seven occupations (actors, artists, writers, politicians, biologists, physicists, and mathematicians), examining how their fame grew as a function of age (Fig. 3F and fig. S10).

Actors tend to become famous earliest, at around 30. But the fame of the actors we studied, whose ascent preceded the spread of television, rises slowly thereafter. (Their fame peaked at a frequency of 2×10^{-7}.) The writers became famous about a decade after the actors, but rose for longer and to a much higher peak (8×10^{-7}). Politicians did not become famous until their 50s, when, upon being elected president of the United States (in 11 of 25 cases; 9 more were heads of other states), they rapidly rose to become the most famous of the groups (1×10^{-6}).

Science is a poor route to fame. Physicists and biologists eventually reached a similar level of fame as actors (1×10^{-7}), but it took them far longer. Alas, even at their peak, mathematicians tend not to be appreciated by the public (2×10^{-8}).

Detecting censorship and suppression. Suppression of a person or an idea leaves quantifiable fingerprints (*25*). For instance, Nazi censorship of the Jewish artist Marc Chagall is evident by comparing the frequency of "Marc Chagall" in English and in German books (Fig. 4A). In both languages, there is a rapid ascent starting in the late 1910s (when Chagall was in his early 30s). In English, the ascent continues. But in German, the artist's popularity decreases, reaching a nadir from 1936 to 1944, when his full name appears only once. (In contrast, from 1946 to 1954, "Marc Chagall" appears nearly 100 times in the German corpus.) Such examples are found in many countries, including Russia (Trotsky), China (Tiananmen Square), and the United States (the Hollywood Ten, blacklisted in 1947) (Fig. 4, B to D, and fig. S11).

We probed the impact of censorship on a person's cultural influence in Nazi Germany. Led by such figures as the librarian Wolfgang Hermann, the Nazis created lists of authors and artists whose "undesirable", "degenerate" work was banned from libraries and museums and publicly burned (*26*–*28*). We plotted median usage in German for five such lists: artists (100 names) and writers of literature (147), politics (117), history (53), and philosophy (35) (Fig. 4E and fig. S12). We also included a collection of Nazi party members [547 names (*7*)]. The five suppressed groups exhibited a decline. This decline was modest for writers of history (9%) and literature (27%), but pronounced in politics (60%), philosophy (76%), and art (56%). The only group whose signal increased during the Third Reich was the Nazi party members [a 500% increase (*7*)].

Given such strong signals, we tested whether one could identify victims of Nazi repression de novo. We computed a "suppression index" (s) for each person by dividing their frequency from 1933 to 1945 by the mean frequency in 1925–1933 and in 1955–1965 (Fig. 4F, inset). In English, the distribution of suppression indices is tightly centered around unity. Fewer than 1% of individuals lie at the extremes ($s < 1/5$ or $s > 5$).

In German, the distribution is much wider, and skewed to the left: Suppression in Nazi Germany was not the exception, but the rule (Fig. 4F). At the far left, 9.8% of individuals showed strong suppression ($s < 1/5$). This population is highly enriched in documented victims of repression, such as Pablo Picasso ($s = 0.12$), the Bauhaus architect Walter Gropius ($s = 0.16$), and Hermann Maas ($s < 0.01$), an influential Protestant minister who helped many Jews flee (*7*). (Maas was later recognized by Israel's Yad Vashem as one of the "Righteous Among the Nations.") At the other extreme, 1.5% of the population exhibited a dramatic rise ($s > 5$). This subpopulation is highly enriched in Nazis and Nazi-supporters, who benefited immensely from government propaganda (*7*).

These results provide a strategy for rapidly identifying likely victims of censorship from a large pool of possibilities, and highlight how culturomic methods might complement existing historical approaches.

Culturomics. Culturomics is the application of high-throughput data collection and analysis to the study of human culture. Books are a beginning, but we must also incorporate newspapers (*29*), manuscripts (*30*), maps (*31*), artwork (*32*), and a myriad of other human creations (*33*, *34*). Of course, many voices—already lost to time—lie forever beyond our reach.

Culturomic results are a new type of evidence in the humanities. As with fossils of ancient creatures, the challenge of culturomics lies in the interpretation of this evidence. Considerations of space restrict us to the briefest of surveys: a

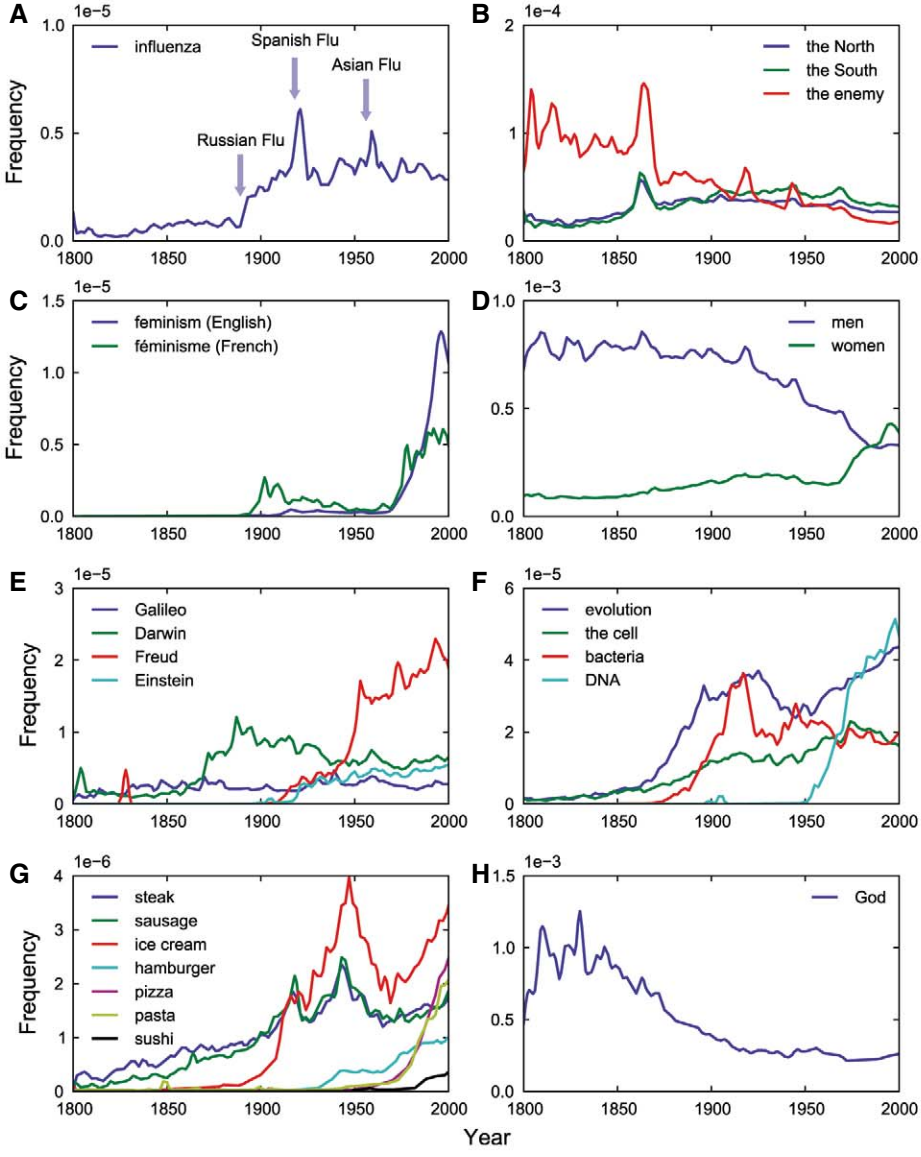

Fig. 5. Culturomics provides quantitative evidence for scholars in many fields. (**A**) Historical epidemiology: "influenza" is shown in blue; the Russian, Spanish, and Asian flu epidemics are highlighted. (**B**) History of the Civil War. (**C**) Comparative history. (**D**) Gender studies. (**E** and **F**) History of science. (**G**) Historical gastronomy. (**H**) History of religion: "God".

handful of trajectories and our initial interpretations. Many more fossils (Fig. 5 and fig. S13), with shapes no less intriguing, beckon:

(i) Peaks in "influenza" correspond with dates of known pandemics, suggesting the value of culturomic methods for historical epidemiology (*35*) (Fig. 5A and fig. S14).

(ii) Trajectories for "the North", "the South", and finally "the enemy" reflect how polarization of the states preceded the descent into the Civil War (Fig. 5B).

(iii) In the battle of the sexes, the "women" are gaining ground on the "men" (Fig. 5C).

(iv) "féminisme" made early inroads in France, but the United States proved to be a more fertile environment in the long run (Fig. 5D).

(v) "Galileo", "Darwin", and "Einstein" may be well-known scientists, but "Freud" is more deeply ingrained in our collective subconscious (Fig. 5E).

(vi) Interest in "evolution" was waning when "DNA" came along (Fig. 5F).

(vii) The history of the American diet offers many appetizing opportunities for future research; the menu includes "steak", "sausage", "ice cream", "hamburger", "pizza", "pasta", and "sushi" (Fig. 5G).

(viii) "God" is not dead but needs a new publicist (Fig. 5H).

These, together with the billions of other trajectories that accompany them, will furnish a great cache of bones from which to reconstruct the skeleton of a new science.

References and Notes

1. E. O. Wilson, *Consilience* (Knopf, New York, 1998).
2. D. Sperber, *Man (London)* **20**, 73 (1985).
3. S. Lieberson, J. Horwich, *Sociol. Methodol.* **38**, 1 (2008).
4. L. L. Cavalli-Sforza, W. Marcus, X. Feldman, *Cultural Transmission and Evolution* (Princeton Univ. Press, Princeton, NJ, 1981).
5. P. Niyogi, *The Computational Nature of Language Learning and Evolution* (MIT, Cambridge, MA, 2006).
6. G. K. Zipf, *The Psycho-biology of Language* (Houghton Mifflin, Boston, 1935).
7. Materials and methods are available as supporting material on *Science* Online.
8. E. S. Lander *et al.*; International Human Genome Sequencing Consortium, *Nature* **409**, 860 (2001).
9. A. W. Read, *Am. Speech* **8**, 10 (1933).
10. *Webster's Third New International Dictionary of the English Language, Unabridged*, P. B. Gove, Ed. (Merriam-Webster, Springfield, MA, 1993).
11. *The American Heritage Dictionary of the English Language, Fourth Edition*, J. P. Pickett, Ed. (Houghton Mifflin, Boston, 2000).
12. *Oxford English Dictionary*, J. A. Simpson, E. S. C. Weiner, M. Proffitt, Eds. (Clarendon, Oxford, 1993).
13. J. Algeo, A. S. Algeo, *Fifty Years among the New Words: A Dictionary of Neologisms, 1941–1991* (Cambridge Univ. Press, Cambridge, 1991).
14. S. Pinker, *Words and Rules* (Basic Books, New York, 1999).
15. Anthony S. Kroch, *Language Variation Change* **1**, 199 (1989).
16. J. L. Bybee, *Language* **82**, 711 (2006).
17. E. Lieberman, J. B. Michel, J. Jackson, T. Tang, M. A. Nowak, *Nature* **449**, 713 (2007).
18. B. Milner, L. R. Squire, E. R. Kandel, *Neuron* **20**, 445 (1998).
19. H. Ebbinghaus, *Memory: A Contribution to Experimental Psychology* (Dover Publications, New York, 1987).
20. M. Halbwachs, *On Collective Memory*, Lewis A. Coser, transl. (Univ. of Chicago Press, Chicago, 1992).
21. S. Ulam, *Bull. Am. Math. Soc.* **64**, 1 (1958).
22. L. Braudy, *The Frenzy of Renown: Fame & Its History* (Vintage Books, New York, 1997).
23. Wikipedia, 23 August 2010, www.wikipedia.org/.
24. *Encyclopaedia Britannica*, D. Hoiberg, Ed. (Encyclopaedia Britannica, Chicago, 2002).
25. *Censorship: 500 Years of Conflict*, V. Gregorian, Ed. (New York Public Library, New York, 1984).
26. W. Treß, *Wider Den Undeutschen Geist: Bücherverbrennung 1933* (Parthas, Berlin, 2003).
27. G. Sauder, *Die Bücherverbrennung: 10. Mai 1933* (Ullstein, Frankfurt am Main, Germany, 1985).
28. S. Barron, P. W. Guenther, *Degenerate Art: The Fate of the Avant-garde in Nazi Germany* (Los Angeles County Museum of Art, Los Angeles, 1991).
29. Google News Archive Search, http://news.google.com/archivesearch.
30. Digital Scriptorium, www.scriptorium.columbia.edu.
31. Visual Eyes, www.viseyes.org.
32. ARTstor, www.artstor.org.
33. Europeana, www.europeana.eu.
34. Hathi Trust Digital Library, www.hathitrust.org.
35. J. M. Barry, *The Great Influenza: The Epic Story of the Deadliest Plague in History* (Viking Press, New York, 2004).

36. J.-B.M. was supported by the Foundational Questions in Evolutionary Biology Prize Fellowship and the Systems Biology Program (Harvard Medical School). Y.K.S. was supported by internships at Google. S.P. acknowledges support from NIH grant HD 18381. E.L.A. was supported by the Harvard Society of Fellows, the Fannie and John Hertz Foundation Graduate Fellowship, a National Defense Science and Engineering Graduate Fellowship, an NSF Graduate Fellowship, the National Space Biomedical Research Institute, and National Human Genome Research Institute grant T32 HG002295. This work was supported by a Google Research Award. The Program for Evolutionary Dynamics acknowledges support from the Templeton Foundation, NIH grant R01GM078986, and the Bill and Melinda Gates Foundation. Some of the methods described in this paper are covered by U.S. patents 7463772 and 7508978. We are grateful to D. Bloomberg, A. Popat, M. McCormick, T. Mitchison, U. Alon, S. Shieber, E. Lander, R. Nagpal, J. Fruchter, J. Guldi, J. Cauz, C. Cole, P. Bordalo, N. Christakis, C. Rosenberg, M. Liberman, J. Scheidlower, B. Zimmer, R. Darnton, and A. Spector for discussions; to C.-M. Hetrea and K. Sen for assistance with *Encyclopaedia Britannica*'s database; to S. Eismann, W. Treß, and the City of Berlin Web site (berlin.de) for assistance in documenting victims of Nazi censorship; to C. Lazell and G. T. Fournier for assistance with annotation; to M. Lopez for assistance with Fig. 1; to G. Elbaz and W. Gilbert for reviewing an early draft; and to Google's library partners and every author who has ever picked up a pen, for books.

Supporting Online Material

www.sciencemag.org/cgi/content/full/science.1199644/DC1
Materials and Methods
Figs. S1 to S19
References

27 October 2010; accepted 6 December 2010
Published online 16 December 2010;
10.1126/science.1199644

A Biological Solution to a Fundamental Distributed Computing Problem

Yehuda Afek,[1]* Noga Alon,[1,2]* Omer Barad,[3]* Eran Hornstein,[3] Naama Barkai,[3]† Ziv Bar-Joseph[4]†

Computational and biological systems are often distributed so that processors (cells) jointly solve a task, without any of them receiving all inputs or observing all outputs. Maximal independent set (MIS) selection is a fundamental distributed computing procedure that seeks to elect a set of local leaders in a network. A variant of this problem is solved during the development of the fly's nervous system, when sensory organ precursor (SOP) cells are chosen. By studying SOP selection, we derived a fast algorithm for MIS selection that combines two attractive features. First, processors do not need to know their degree; second, it has an optimal message complexity while only using one-bit messages. Our findings suggest that simple and efficient algorithms can be developed on the basis of biologically derived insights.

Computational and mathematical methods are extensively used to analyze and model biological systems (*1*–*3*). We provide an example of the reverse of this strategy, in which a biological process is used to derive a solution to a long-standing computational problem.

In distributed computing, a large number of processors jointly and distributively solve a task, without any of the processors getting all of the inputs or observing all of the outputs (*4*). All large-scale computing efforts, from web search to airplane control systems, use distributed computing algorithms to reach agreement, overcome failures, and decrease response times. Biological processes are also distributed. Parallel pathways are used to transform environmental signals to gene expression programs, and several tasks are jointly performed by independent cells without clear central control.

A long-standing distributed computing problem is that of electing a set of local leaders [the maximal independent set (MIS)] in a network of connected processors (*4*). The MIS is used to determine a backbone for wireless networks, for routing, and in several other network protocols (*5*). Formally, a MIS is defined as a set of processors (nodes) A so that every node in the network is either in A or directly connected to a node in A, and no two nodes in A are connected (Fig. 1A). Distributively electing a MIS has been considered a challenging problem for three decades (*6*). In particular, when all nodes are initially identical constructing a MIS by using deterministic algorithms is impossible (*7*), necessitating probabilistic approaches. Luby (*8*) and Alon *et al*. (*9*) presented fast probabilistic algorithms for electing a MIS. In these algorithms, nodes change their probability of being elected based on the number of active neighbors they have (nodes that are not yet connected to nodes in A), and they require processors to send messages the sizes of which are a function of the number of nodes in the network. Recent methods were proposed that partially remove either of these assumptions (*10*, *11*), but to date, no method has been able to efficiently reduce message complexity without assuming knowledge of the number of neighbors. These are important requirements for deployment of large, ad hoc sensor networks.

The selection of neural precursors during the development of the nervous system resembles the MIS election problem. The precursors of the fly's sensory bristles [sensory organ precursors (SOPs)] are selected during larvae and pupae development from clusters of equivalent cells. The selection of the small bristles precursors (microchaetes) (Fig. 1B) is initiated 8 to 10 hours after pupae formation, when several elongated clusters of proneural cells, containing between 20 and 30 cells each, appear at specific positions in the imaginal discs, which will later become the fly's wings and notum. During the next 3 hours, SOPs begin to appear within these clusters. A cell that is selected as a SOP inhibits its neighbors by expressing high levels of the membrane-bound protein Delta, which binds and activates the transmembrane receptor protein Notch on adjacent cells (*12*). This lateral-inhibition process is highly accurate (*13*), resulting in a regularly spaced pattern in which each cell is either selected as SOP or is inhibited by a neighboring SOP (Fig. 1C). Thus, as in the MIS problem every proneural cluster must elect a set of SOPs (A) so that every cell in the cluster is either in A or connected to a SOP in A, and no two SOPs in A are adjacent.

Extensive studies and mathematical modeling were used to define the molecular components mediating SOP selection and the mechanism underlying selection. These studies suggest several similarities between the mechanism underlying SOP selection and current algorithms for MIS election (*14*). First, the selection of a particular cell as a SOP is a random event governed by an underlying stochastic process (*15*, *16*). Second, similar to computational requirements SOP selection is probably constrained in time because the default of all cluster cells is to become SOPs unless they are inhibited (*17*). Lastly, in computational algorithms (*8*, *9*) processors send messages only when they propose their

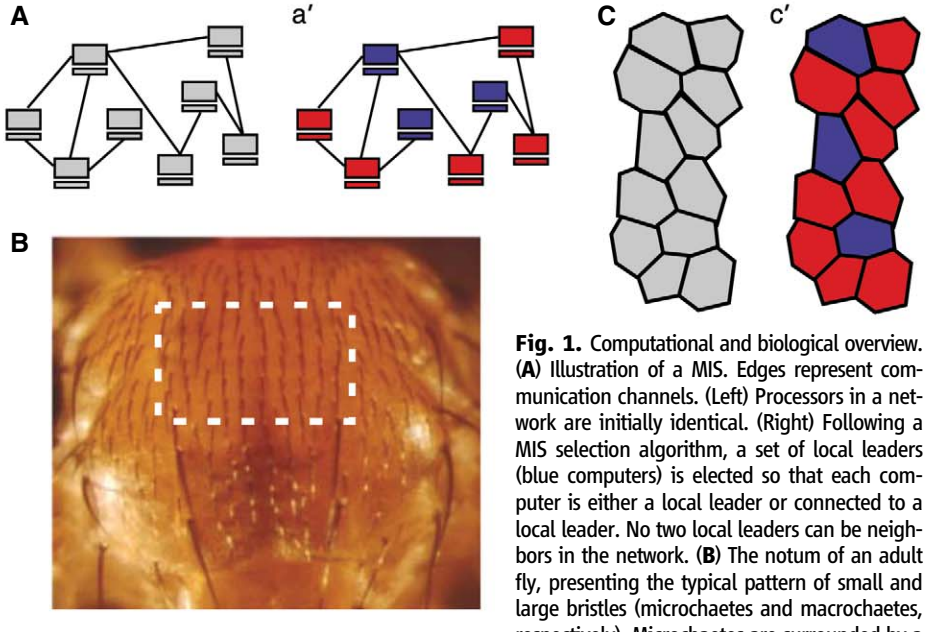

Fig. 1. Computational and biological overview. (**A**) Illustration of a MIS. Edges represent communication channels. (Left) Processors in a network are initially identical. (Right) Following a MIS selection algorithm, a set of local leaders (blue computers) is elected so that each computer is either a local leader or connected to a local leader. No two local leaders can be neighbors in the network. (**B**) The notum of an adult fly, presenting the typical pattern of small and large bristles (microchaetes and macrochaetes, respectively). Microchaetes are surrounded by a dashed line. (**C**) Illustration of SOPs in flies. (Left) Cells in a cluster are initially equivalent. (Right) Following a SOP selection process, selected SOPs (blue cells) inhibit their physical neighbors (red cells), and so for the cluster depicted in this figure, no more SOPs can be selected.

[1]Blavatnik School of Computer Science and Sackler School of Mathematics, Tel Aviv University, Tel Aviv 69978, Israel. [2]Institute for Advanced Study, Princeton, NJ 08544, USA. [3]Department of Molecular Genetics, Weizmann Institute of Science, Rehovot 76100, Israel. [4]School of Computer Science, Carnegie Mellon University, Pittsburgh, PA 15213, USA.

*These authors contributed equally to this work.
†To whom correspondence should be addressed. E-mail: naama.barkai@weizmann.ac.il (N.B.); zivbj@cs.cmu.edu (Z.B.-J.)

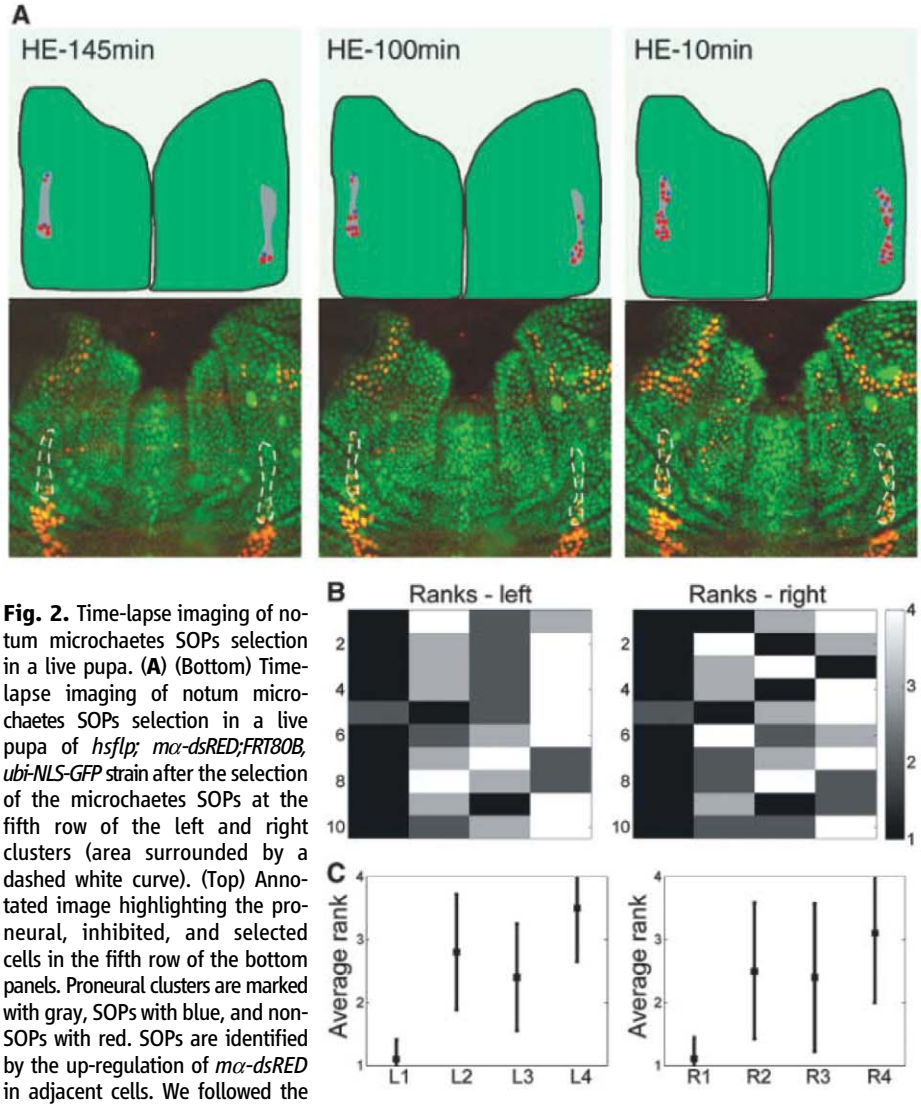

Fig. 2. Time-lapse imaging of notum microchaetes SOPs selection in a live pupa. (**A**) (Bottom) Time-lapse imaging of notum microchaetes SOPs selection in a live pupa of *hsflp; mα-dsRED;FRT80B, ubi-NLS-GFP* strain after the selection of the microchaetes SOPs at the fifth row of the left and right clusters (area surrounded by a dashed white curve). (Top) Annotated image highlighting the proneural, inhibited, and selected cells in the fifth row of the bottom panels. Proneural clusters are marked with gray, SOPs with blue, and non-SOPs with red. SOPs are identified by the up-regulation of *mα-dsRED* in adjacent cells. We followed the selection process from 145 min before head eversion (HE) to HE, corresponding to ~9.5 to 12 hours after pupa formation. (**B** and **C**) Statistics of SOP selection order from time-lapse imaging of ten pupae. The *y* axis represents the movie number. The *x* axis corresponds to the four SOPs selected in each row on the left and right sides (L1 to L4 and R1 to R4) ordered from bottom to top. Color in each (*x*, *y*) coordinate represents the order (1 to 4) in which this SOP was selected (see color legend on the right) (C) Average and SD of SOP selection order for L1 to L4 and R1 to R4; *x* axis is the same as in (B).

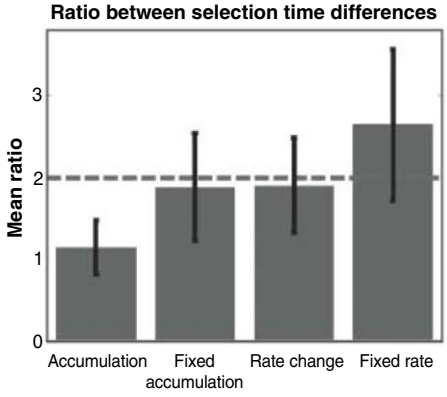

Fig. 3. Comparison of experimental and simulated results. We computed the average ratio for the difference between the selection times of SOPs in the movies we analyzed. The dashed line represents the average observed in our experiments (1.98). We simulated four stochastic models. In the accumulation model, cells accumulate random amounts of Delta at each step until reaching a threshold. The fixed accumulation and rate change models are described in the paper. In the fixed rate model, cells use the same burst distribution throughout the process (*14*). Values are based on 20,000 runs for each model. Error bars represent SD.

candidacy to become leaders, thus reducing communication complexity. Mathematical modeling by us and others suggests that this might also be the case during SOP selection: Before being selected, the ability of Delta to activate Notch on adjacent cells is inhibited by their interaction within the same cell, enabling communication between cells only after selection (*18*–*20*).

Although similar, the biological solution differs from computational algorithms in at least two aspects. First, SOP selection is probably performed without relying on knowledge of the number of neighbors that are not yet selected. Second, mathematical analysis demonstrated that SOP selection requires nonlinear inhibition that in effect reduces communication to the simplest set of possible messages (binary) (*21*, *22*).

These last two aspects of the biological process are attractive because they could greatly simplify applications of MIS selection. We thus examined SOP selection more closely in order to determine whether better understanding of this process can lead to an efficient algorithm for MIS selection. To verify the stochastic nature of this process, we first monitored the in vivo selection using a fluorescence reporter for Notch activity (*17*). We focused on the selection of SOPs in two symmetrical rows of pro-neural clusters [the fifth rows of notum microchaetes (Fig. 2A)], which occur before head eversion. These clusters consist of 10 rows with two cells each, giving rise to four SOPs per cluster. Measuring the SOP selection times in 10 different pupae (20 distinct clusters) revealed a bias for early selection of the lowest SOP, probably reflecting an earlier initiation of this part of the cluster. However, the upper three SOPs appeared at seemingly random order (Fig. 2B), supporting previous evidences for stochastic selection (*23*).

A defining aspect of algorithms for MIS selection is the per-round probability that a node joins the MIS. Current algorithms (*8*, *9*) optimize this rate by dynamically increasing it when the number of active neighbors a node has decreases. During SOP selection, cells do not know the number of nonselected neighbors. However, the temporal selection rate may still be optimized by cell-autonomous mechanisms, for example by stochastically accumulating a protein (such as Delta) until it passes some threshold. Characterizing the stochastic accumulation rate is thus a key for understanding the biological selection strategy. To determine this rate, we compared statistics derived from the observed SOP selection times with several in silico stochastic accumulation models. The models differ in the way by which stochasticity is introduced (*14*). Results of two of these models were consistent with our experimental data (Fig. 3). The first consistent model assumed a fixed rate of accumulation over time, and we concluded that it is not appropriate for computer networks (*14*). In contrast, the second model assumed a burst-like protein production in which the likelihood of bursting increases in time, resembling a com-

Table 1. MIS algorithm.

1. Algorithm: MIS (n, D) at node u
2. For i = 0: log D
   3. For j = 0: $M \log n$ // M is constant derived below
      4. * exchange 1*
      5. v = 0
      6. With probability $\frac{1}{2^{\log D - i}}$ broadcast $\boldsymbol{B}$ to neighbors and set v = 1 // $\boldsymbol{B}$ is one bit
      7. If received message from neighbor, then v = 0
      8. * exchange 2 *
      9. If v = 1 then
         10. Broadcast B; join MIS; exit the algorithm
      11. Else
         12. If received message B in this exchange, then mark node u inactive; exit the algorithm
      13. End
   14. End
15. End

putational algorithm for MIS in which the selection probability also increases in time as the number of active processors decreases. We thus asked whether we can develop an algorithm for MIS selection on the basis of this stochastic rate change model that would not require knowledge about the number of active neighbors and would only use threshold (binary) communication.

We assumed a collection of identical processors placed at nodes of an arbitrary synchronous communication network. Nodes can only broadcast one-bit messages. A message broadcasted by a node reaches all of its neighbors that are still active in the algorithm. In each round, a processor can only tell whether or not a message was sent to it. When a processor receives a message, it cannot tell which of its neighboring processors sent it, and it cannot count the number of messages received in a round. Hence, our model is appropriate for radio networks with collision detection. We assumed that nodes receive as input an upper bound on the number of nodes in the network (n) and an upper bound D, on the number of neighbors any node can have (if no such bound is known, we set D to n). We further assumed that no failures occur. The algorithm, presented in Table 1, is synchronously executed by all nodes.

The algorithm proceeds in $\log D$ phases, each consisting of $M \log n$ steps, where M is a constant; its value is given in (*14*). Initially, all nodes are active. Each step in each phase i consists of two exchanges. In the first exchange, each active node broadcasts a message to its neighbors with probability p_i. Such as in the biological model, the probability p_i increases with i. In the second exchange, a node that has broadcasted a message in the first exchange joins the MIS if none of its neighbors had broadcasted at the first exchange. Such node broadcasts again a message to its neighbors, telling them to become inactive, and exit the algorithm.

We proved that when the algorithm terminates, no two neighboring nodes are in A (the MIS set), and that every node that has become inactive has a neighbor in A [the proof can be found in (*14*)]. We thus conclude that the only way the algorithm may err is by terminating while leaving some nodes that are not in A and are also not connected to nodes in A. Next, we show that when the algorithm terminates all nodes are, with high probability, either in A or connected to a node in A, which solves the MIS problem.

The proof and the complete analysis are provided in (*14*). Briefly, the proof relies on an inductive argument to show that with high probability, by the time phase i ends (*14*) there are no active nodes with more than $\frac{D}{2^i}$ active neighbors. Thus, nodes with many neighbors either leave the algorithm (joining A or eliminating when a neighbor joins A) or lose many of their neighbors at each phase as these neighbors exit the algorithm. By the time the algorithm ends, i equals $\log D$, and so all nodes that have not joined A are, with high probability, not connected to any active node (and are also not connected to any node in A) and thus can join A with no collisions.

The running time of the algorithm is $O(\log n \log D)$, which is the number of rounds required to execute the two nested loops. The worst-case running time is $O(\log^2 n)$. All messages in the algorithm are one bit. We prove in (*14*) that the expected number of messages sent to active nodes in our algorithm is linear in the number of nodes of the network, which is optimal because each node is required to at least receive a message from its local leader.

Taken together, by studying a developmental process in flies we devised a solution to an important distributed computing problem. The new algorithm does not require knowledge of the degree of individual processors, uses one-bit messages, and has an optimal message complexity. These features are useful for many applications, including wireless communication systems and ad hoc sensor networks.

Biologists are increasingly relying on advanced modeling techniques. The other direction—using insights from biology to advance computational systems—has mainly focused on optimization techniques inspired by biological observations, including neural networks, genetic algorithms, and routing (*24*). We have shown that areas of computer science that require strict, provable guarantees can also benefit from knowledge regarding how biological systems operate. Better understanding of these biological systems can lead to further improvement in the design of complex distributed computing systems.

References and Notes

1. P. Flicek, E. Birney, *Nat. Methods* **6**, (11s), S6 (2009).
2. S. F. Altschul *et al.*, *Nucleic Acids Res.* **25**, 3389 (1997).
3. U. Alon, *An Introduction to Systems Biology: Design Principles of Biological Circuits* (Chapman & Hall/CRC, Boca Raton, FL, 2006).
4. N. Lynch, *Distributed Algorithms* (Morgan Kaufmann, San Francisco, 1996).
5. P. J. Wan, K. M. Alzoubi, O. Frieder, *Mobile Netw. Appl.* **9**, 141 (2004).
6. L. G. Valiant, *Proceedings of the 7th IBM Symposium on Mathematical Foundations of Computer Science* (IBM, New York, 1982).
7. S. Cohen, D. Lehmann, A. Pnueli, *Theor. Comput. Sci.* **34**, 215 (1984).
8. M. Luby, *SIAM J. Comput.* **15**, 1036 (1986).
9. N. Alon, L. Babai, A. Itai, *J. Algorithms* **7**, 567 (1986).
10. Y. Métivier, J. M. Robson, N. Saheb-Djahromi, A. Zemmari, "An optimal bit complexity randomized distributed MIS algorithm," in *Proceedings of the 16th International Colloquium on Structural Information and Communication Complexity (SIROCCO),* pp. 323–337 (2009).
11. T. Moscibroda, R. Wattenhofer, "Maximal independent sets in radio networks," in *Proceedings of the Twenty-Fourth Annual ACM SIGACT-SIGOPS Symposium on Principles of Distributed Computing (PODC)*, pp. 148–157 (2005).
12. S. J. Bray, *Nat. Rev. Mol. Cell Biol.* **7**, 678 (2006).
13. J. M. Rendel, B. L. Sheldon, D. E. Finlay, *Genetics* **52**, 1137 (1965).
14. Materials and methods are available as supporting material on *Science* Online.
15. P. Simpson, *Curr. Opin. Genet. Dev.* **7**, 537 (1997).
16. M. E. Fortini, *Dev. Cell* **16**, 633 (2009).
17. B. Castro *et al.*, *Development* **132**, 3333 (2005).
18. A. C. Miller, E. L. Lyons, T. G. Herman, *Curr. Biol.* **19**, 1378 (2009).
19. O. Sprinzak *et al.*, *Nature* **465**, 86 (2010).
20. O. Barad, D. Rosin, E. Hornstein, N. Barkai, *Sci. Signal.* **3**, ra51 (2010).
21. J. R. Collier, N. A. Monk, P. K. Maini, J. H. Lewis, *J. Theor. Biol.* **183**, 429 (1996).
22. E. Plahte, *J. Math. Biol.* **43**, 411 (2001).
23. K. Usui, K.-i. Kimura, *Rouxs Arch. Dev. Biol.* **203**, 151 (1993).
24. A. Tero *et al.*, *Science* **327**, 439 (2010).

25. We thank J. W. Posakony for fly stock and D. Rosin for help in experiments. This work was supported by a European Research Council (ERC) Advanced grant, the Oswald Veblen Fund, and the Bell Companies Fellowship (N.A.), the Azrieli Foundation (O.B.), the Israel Science Foundation (E.H. and N.B.), ERC (IDEA), the Hellen and Martin Kimmel award for innovative investigations (N.B.), NIH grant 1RO1 GM085022, and NSF CAREER award 0448453 (Z.B.-J.).

Supporting Online Material

www.sciencemag.org/cgi/content/full/331/6014/183/DC1
Materials and Methods
SOM Text
Figs. S1 to S7
Table S1
References
Movies S1 and S2

10.1126/science.1193210

Observation of Half-Height Magnetization Steps in Sr_2RuO_4

J. Jang,[1] D. G. Ferguson,[1] V. Vakaryuk,[1,2] R. Budakian,[1]* S. B. Chung,[3] P. M. Goldbart,[1] Y. Maeno[4]

Spin-triplet superfluids can support exotic objects, such as half-quantum vortices characterized by the nontrivial winding of the spin structure. We present cantilever magnetometry measurements performed on mesoscopic samples of Sr_2RuO_4, a spin-triplet superconductor. With micrometer-sized annular-shaped samples, we observed transitions between integer fluxoid states as well as a regime characterized by "half-integer transitions"—steps in the magnetization with half the height of the ones we observed between integer fluxoid states. These half-height steps are consistent with the existence of half-quantum vortices in superconducting Sr_2RuO_4.

Most known superconductors are characterized by the spin-singlet pairing of the electrons that constitute the superconducting flow. An exception is Sr_2RuO_4 (SRO), which much like the A-phase of superfluid ^{3}He may exist in the equal-spin pairing (ESP) phase (*1*). This phase has been proposed to host half-quantum vortices (HQVs), which are characterized by the relative winding of the phase of the spin-up and spin-down components of the superfluid order parameter (*2*, *3*). In addition to being of basic scientific interest, HQVs are expected to give rise to zero-energy Majorana quasiparticles (*4*, *5*), which have been suggested as a resource for topological quantum computation (*6*).

The ESP state may be thought of as comprising two weakly interacting condensates, having Cooper-pair spin configurations, $|\uparrow\uparrow\rangle$ and $|\downarrow\downarrow\rangle$, defined with respect to a common (ESP) axis. An HQV corresponds to the winding of the phase of only one of these condensates around a contour that encircles the HQV core, such as $(\Delta\theta_\uparrow, \Delta\theta_\downarrow) = (\pm 2\pi, 0)$ or $(0, \pm 2\pi)$, producing half of the magnetic moment of a conventional, full-quantum vortex (FQV), for which $\Delta\theta_\uparrow = \Delta\theta_\downarrow = \pm 2\pi$. The Meissner response of the superconductor screens charge currents over the length scale of the London penetration depth λ; however, any (charge-neutral) spin currents go unscreened. Consequently, the kinetic energy of an isolated HQV diverges logarithmically with the system size, whereas the kinetic energy of a FQV would remain finite. Hence, a single HQV may not be energetically stable in a macroscopic sample, whereas according to (*7*), a single HQV could be stable in a mesoscopic SRO sample of size comparable with or smaller than λ.

We used cantilever magnetometry to measure the magnetic moment of micrometer-sized SRO samples, with the aim of distinguishing between HQV and FQV states via changes in magnetic moment associated with the entry of single vortices. To facilitate this aim, we have fabricated annular samples by drilling a hole in the center of each particle with a focused ion beam. This geometry yields a discrete family of equilibrium states, in which the order parameter winds around the annulus as it would around a vortex core, but evades complications arising from the vortex core.

For an annular conventional superconductor, the fluxoid Φ', defined via $\Phi' = \Phi + (4\pi/c) \times \oint \lambda^2 \vec{j}_s \cdot d\vec{s} = n\Phi_0$, must be an integer multiple n of the flux quantum $\Phi_0 = hc/2e$ for any path encircling the hole (*8*), where h is Planck's constant, c is the speed of light, and e is the electron charge. Here, $\vec{j}_s$ is the supercurrent density, $\Phi = \oint \vec{A} \cdot d\vec{s}$ is the magnetic flux enclosed by the path, $\vec{A}$ is the vector potential, and $n = \oint \vec{\nabla}\theta \cdot d\vec{s}\,/2\pi$ is the order-parameter winding-number along the path. In the regime in which the wall thickness of the annulus becomes comparable with or smaller than λ, $\vec{j}_s$ will not necessarily vanish in the interior of the annulus; hence, it is the fluxoid and not the flux that is quantized. The quantized winding of the order parameter, however, produces observable effects in the magnetic response of the annulus. In the regime in which the magnetization is piecewise linear in the magnetic field, the supercurrents that flow around the hole produce a magnetic moment $\mu_z = \Delta\mu_z n + \chi_M H_z$, where χ_M is the Meissner susceptibility and H_z is the component of the magnetic field that controls the flux through the hole (Fig. 1). In equilibrium, changes in the fluxoid are associated with transitions in the winding number in single units ($n \rightarrow n + 1$), corresponding to the changes in the magnetic moment in increments of $\Delta\mu_z$.

For an ESP superconductor, the two condensates bring the two integer-valued winding numbers: $n_\uparrow$ and $n_\downarrow$. Then, the role of n is played by the half-sum $n = (n_\uparrow + n_\downarrow)/2$. The integer-fluxoid (IF) state of the annulus—the coreless analog of the FQV state—corresponds to the common winding of the condensates ($n_\uparrow = n_\downarrow$), whereas the half-fluxoid (HF) state—the coreless

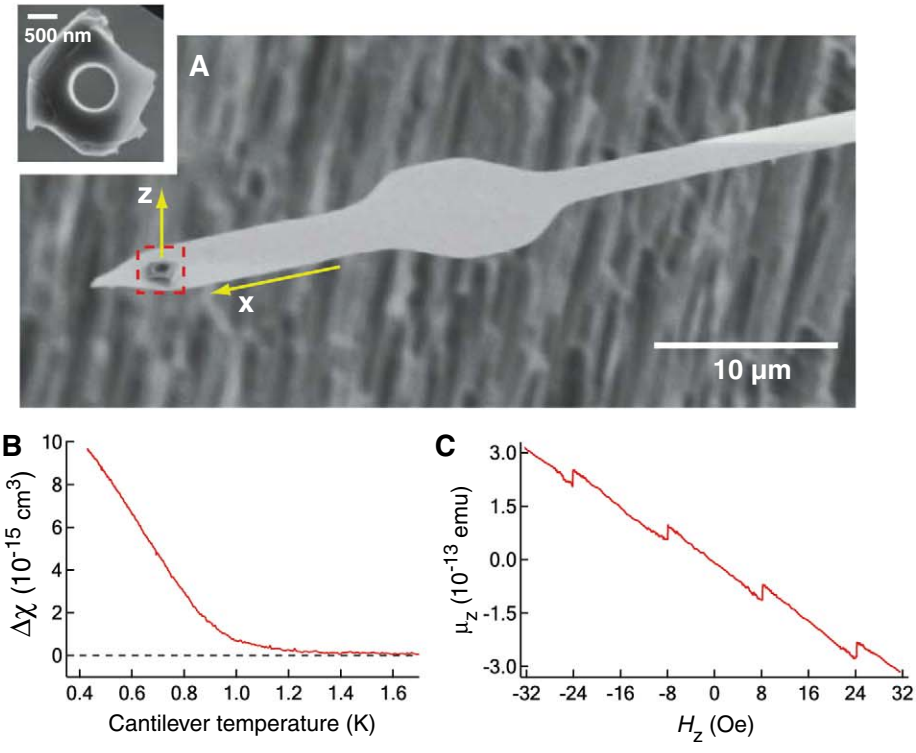

Fig. 1. Image of cantilever with attached annular SRO particle. (**A**) The 80 μm by 3 μm by 100 nm single-crystal silicon cantilever has natural frequency $\omega_0/2\pi = 16$ kHz, spring constant $k = 3.6 \times 10^{-4}$ N/m, and quality factor $Q = 65{,}000$ and exhibits a thermal-limited force sensitivity of $S_F^{1/2} \approx 1.0 \times 10^{-18}$ N/$\sqrt{Hz}$ at $T = 0.5$ K. (Inset) Scanning electron microscopy of the 1.5 μm by 1.8 μm by 0.35 μm annular SRO sample attached to the cantilever. The orientation of the *ab* planes is clearly visible from the layering observed near the edges of the SRO particle. (**B**) Anisotropic component of the susceptibility $\Delta\chi = \chi_c - \chi_{ab}$ as a function of temperature. Here, χ_c and χ_{ab} are the *c* axis and in-plane susceptibilities, respectively. (**C**) Field-cooled data was measured at $T = 0.45$ K for $H_x = 0$.

[1]Department of Physics, University of Illinois at Urbana-Champaign, Urbana, IL 61801–3080, USA. [2]Materials Science Division, Argonne National Laboratory, Argonne, IL 60439, USA. [3]Department of Physics, McCullough Building, Stanford University, Stanford, CA 94305–4045, USA. [4]Department of Physics, Kyoto University, Kyoto 606-8502, Japan.

*To whom correspondence should be addressed. E-mail: budakian@illinois.edu

analog of the HQV state—corresponds to winding numbers that differ by unity ($n_\uparrow = n_\downarrow \pm 1$). Thus, equilibrium transitions between the IF and HF states would change n by half a unit ($n \rightarrow n \pm 1/2$), and this would produce a change $\Delta\mu_z/2$ of the magnetic moment—half of that produced for an equilibrium transition between two IF states (insofar as the corrections produced by nonzero spin polarization are negligible).

To measure the magnetic response of the superconductor, we used a recently developed phase-locked cantilever magnetometry technique (*9*) operating inside a ^{3}He refrigerator with a base temperature of 300 mK (Fig. 1A). In our setup, the displacement of the cantilever was measured by using a fiber optic interferometer operating at a wavelength of 1510 nm. The optical power was maintained at 5 nW in order to minimize heating of the sample from optical absorption. To exclude the potential fortuitous effects of geometry, we present data for three annular SRO particles, of different sizes, fabricated from a high-quality SRO single crystal with a bulk transition temperature T_c = 1.43 K, grown using the floating-zone method (*10*).

We start with the particle shown in Fig. 1A. To characterize its equilibrium fluxoid state, the particle is heated above T_c by momentarily increasing the laser power and then cooled below T_c in the presence of a static magnetic field (field cooling). The field-cooled data (Fig. 1C) exhibits periodic steps in the magnetic moment of nearly constant magnitude $\Delta\mu_z = (4.4 \pm 0.1) \times 10^{-14}$ electromagnetic units (emu), period ΔH_z = (16.1 ± 0.1) Oe, and susceptibility $\chi_M = -6.0 \times 10^{-15}$ cm^3. The measured period ΔH_z is in reasonable agreement with theoretical estimates for the equilibrium fluxoid transitions of a hollow superconducting cylinder having the dimensions of the SRO sample (estimated value of $\Delta H_z \approx 20$ Oe) (*11*). Thus, we conclude that the periodic events observed in Fig. 1C correspond to equilibrium transitions between IF states of the annular SRO particle.

The presence of an in-plane magnetic field H_x brings two new features: (i) For $H_z = 0$, the in-plane magnetic response of the sample exhibits a Meissner behavior for $H_x < 250$ Oe. At $H_x = 250$ Oe, we observed a step in the in-plane magnetic moment with magnitude $\Delta\mu_x \approx 2 \times 10^{-14}$ emu; both the magnitude of the step and the value of H_x at which it occurs are consistent with those expected for the critical field $H_{c1} \parallel ab$ and $\Delta\mu_{ab}$ of an in-plane vortex for our micrometer-sized sample (fig. S3). (ii) For $H_x < H_{c1} \parallel ab$, where no in-plane vortices are expected to penetrate the sample, and in the presence of H_z, we observed the appearance of half-integer (HI) states, for which the change in the magnetic moment of the particle is half that of the IF states.

Figure 2A shows data taken at T = 0.6 K for in-plane fields H_x ranging from –200 to 200 Oe. The data in Fig. 2A were obtained by cooling the sample through T_c in zero field and performing a cyclic field sweep starting at H_z = 0 (zero-field cooling). At this temperature, the zero-field cooled and field cooled data are nearly identical, indicating that the equilibrium response is well-described by the zero-field cooled data. Figure 2B shows the data after subtracting the Meissner response; Fig. 2C shows a histogram of the data in Fig. 2B. The steps, which remain, indicate that the change in magnetic moment associated with HI → IF transitions is half of that associated with transitions between two IF states (Table 1). Shown in fig. S4 are zero-field cooled data taken at T = 0.5 K for a direction of the in-plane field having been rotated by 35° in the *ab* plane of the sample. The half-step features remain, and furthermore, the range of H_z values for which the HI state is the equilibrium state is influenced by the magnitude but not the direction of the in-plane field.

To verify that the HI features we observed correspond to fluxoid states and not tilted or kinked vortex lines that pierced the sample walls, we performed an additional series of measurements on a particular SRO annulus in order to determine the dependence of the HI state on the sample geometry. Before each of these measurements, we cut away more of the annulus, using the focused ion beam. The motivation for this study was the following: The location and stability of a vortex line passing through the bulk of the sample should be sensitive to the sample geometry (such as the thickness of the walls of the annulus or the location of pinning sites). In contrast, if the currents responsible for the half-step features are generated by a HI fluxoid—and thus

Table 1. The calculated fractional step heights for the data shown in Fig. 2C. The average value of a given fractional step is indicated by the quantity ⟨…⟩.

H_x (Oe)	$\Delta_1/(\Delta_1 + \Delta_2)$	$\Delta_3/(\Delta_3 + \Delta_4)$
200	0.46 ± 0.06	0.46 ± 0.06
140	0.47 ± 0.05	0.47 ± 0.05
80	0.48 ± 0.06	0.51 ± 0.04
–80	0.45 ± 0.06	0.53 ± 0.09
–140	0.52 ± 0.07	0.51 ± 0.06
–200	0.46 ± 0.07	0.43 ± 0.07
	$\langle\Delta_1/(\Delta_1 + \Delta_2)\rangle$	$\langle\Delta_3/(\Delta_3 + \Delta_4)\rangle$
	0.47 ± 0.03	0.48 ± 0.03

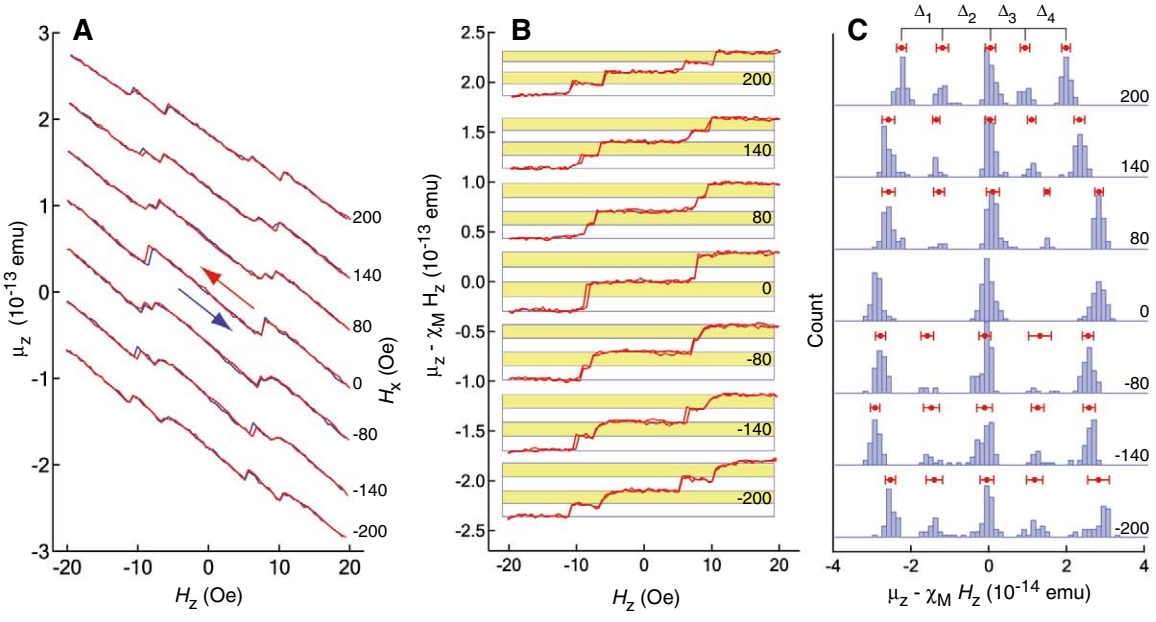

Fig. 2. Evolution of the HI state with in-plane magnetic field. (**A**) Zero-field cooled data obtained at T = 0.6 K. (**B**) Data shown in (A) after subtracting the linear Meissner response; curves have been offset for clarity. (**C**) Histogram of the Meissner-subtracted data. The red points show the mean value of each cluster in the histogram, corresponding to the mean value of a given plateau; the horizontal error bars represent the SD of a given cluster. The change in moment corresponding to the *i*th transition is labeled Δ_i.

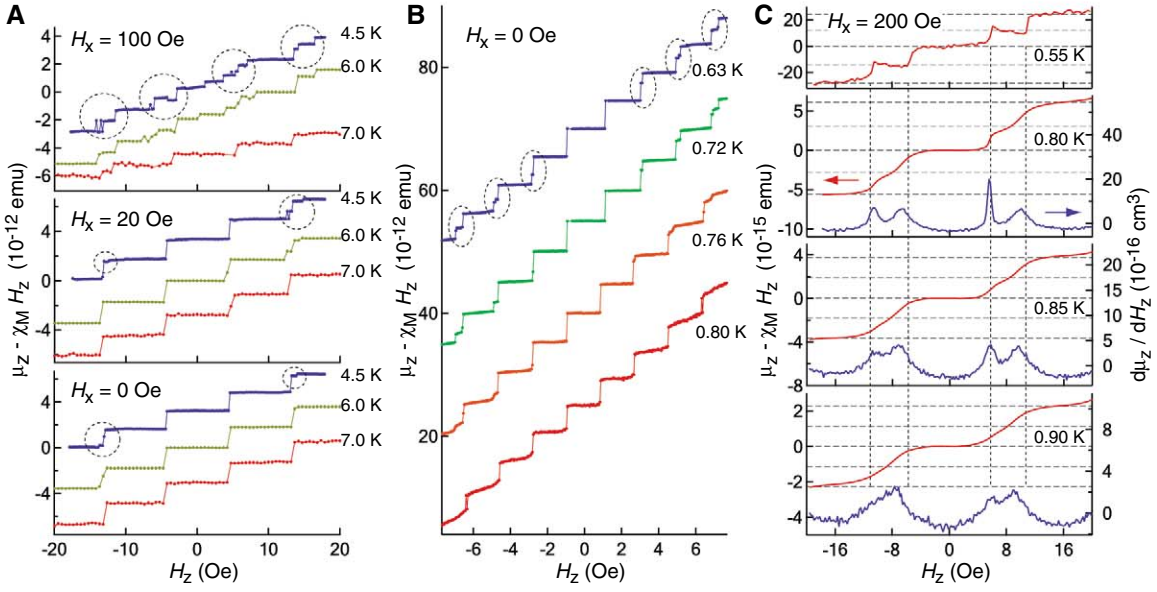

Fig. 3. Temperature evolution of the fractional and HI states. The data were acquired at the value of the in-plane field indicated on the top left-hand corner of each panel; all data were measured by field-cooling the samples. The Meissner response has been subtracted from all data; curves have been offset for clarity. (**A**) Data obtained for the $NbSe_2$ sample (fig. S10). The data are scaled by 4.5 K, 1.0×; 6.0 K, 1.7×; and 7.0 K, 10×. (**B**) Data obtained for the large SRO sample (fig. S9). The data are scaled by 0.63 K, 1.0×; 0.72 K, 1.5×; 0.76 K, 2.3×; and 0.80 K, 6.0×. (**C**) Data obtained for the SRO sample in Fig. 1. The $T = 0.55$ K data are a plot of the *c* axis moment acquired by applying the phase-locked modulation of $\delta H_x = 1.0$ Oe perpendicular to the *c* axis. For the $T \geq 0.80$ K data, we measured $d\mu_z/dH_z$ by applying the phase-locked modulation ($\delta H_z = 0.25$ Oe) parallel to the *c* axis (*9*). The magnetic moment curves are calculated by integrating the measured derivative signal.

only circulate the hole—the observed fractions should not be affected by the sample dimensions. Measurements on a second SRO annulus are shown in fig. S7; the in-plane magnetic field stabilizes an HI state in which the observed fraction is very nearly a half (0.50 ± 0.02). Shown in fig. S8B is the image of the sample presented in fig. S7 (black outline) as well as the outline after reshaping (purple outline). After reshaping, the sample volume was reduced to 44% of the original volume; however, the HI fraction was not affected (0.50 ± 0.01). Half-height step features observed in these samples are robust and not sensitive to the wall thickness or the shape of the boundary.

We have also studied annular samples for which the HI state is not expected to occur: (i) an SRO particle whose dimensions are considerably larger than λ (fig. S9) and (ii) a micrometer-sized particle fabricated from $NbSe_2$—a spin-singlet, layered superconductor (fig. S10). For both of these samples, as the applied field is increased a complicated set of fractional steps in the magnetic moment emerges; their fraction need not be one-half, and it changes with field. Furthermore, the pattern of fractional steps depends on the direction of the in-plane field (changes when $H_x \rightarrow -H_x$). The irregular pattern of fractional steps found for these particles is consistent with the presence of vortices in the bulk of the sample.

The temperature dependence of the fractional steps measured for the large SRO (Fig. 3A) and $NbSe_2$ (Fig. 3B) samples show qualitatively different behavior from that of the HI steps observed for the smaller SRO sample, shown in Fig. 1 (Fig. 3C). As the temperature is raised toward T_c, the fractional steps observed in Fig. 3, A and B, become less pronounced, and most eventually disappear, leaving only the periodic fluxoid transitions. Numerical simulations for thin superconducting discs containing a circular hole (*12*) show that as λ and the coherence length ξ become comparable with or larger than the wall thickness of the ring, the fluxoid states become favored energetically over bulk vortices (vortices penetrating the walls of the superconductor). Thus, at higher temperatures bulk vortices should be less stable—in part because near T_c, ξ and λ will increase and eventually become large (relative to the wall thickness) and also because of increased thermal fluctuations. This behavior is consistent with the temperature dependence observed for the large SRO and $NbSe_2$ samples. In contrast, the HI transitions persist at higher temperature, and the relative contribution to the magnetic moment from each HI transition does not change appreciably with temperature. The HI transitions measured for the SRO sample shown in Fig. 1 exhibit a qualitatively similar temperature dependence to the fluxoid transitions: Near T_c, the HI transitions become reversible and broaden (Fig. 3C), indicating that ξ is comparable with the wall thickness in a portion of the ring. The HI transitions are clearly identified by the two double peaks in the derivative signal.

The HI states observed in magnetometry measurements performed on mesoscopic rings of SRO are consistent with the existence of half-quantum fluxoid states in this system. Our key findings—the reproducibility of the half-height steps in the *c* axis magnetic moment in multiple samples and their evolution with the applied magnetic field—demonstrate that the HI states are intrinsic to the small SRO annuli. These findings can be understood qualitatively on the basis of existing theoretical models of HQVs [supporting online material (SOM) text]. In addition to the magnetic response, further studies will probe characteristics that are particular to the HQV state, such as spin currents or vortices obeying non-abelian statistics (*13*, *14*).

References and Notes

1. A. P. Mackenzie, Y. Maeno, *Rev. Mod. Phys.* **75**, 657 (2003).
2. G. E. Volovik, V. P. Mineev, *JETP Lett.* **24**, 561 (1976).
3. M. C. Cross, W. F. Brinkman, *J. Low Temp. Phys.* **27**, 683 (1977).
4. N. B. Kopnin, M. M. Salomaa, *Phys. Rev. B* **44**, 9667 (1991).
5. N. Read, D. Green, *Phys. Rev. B* **61**, 10267 (2000).
6. A. Y. Kitaev, *Ann. Phys.* **303**, 2 (2003).
7. S. B. Chung, H. Bluhm, E.-A. Kim, *Phys. Rev. Lett.* **99**, 197002 (2007).
8. F. London, *Superfluids.* (Dover, New York, ed. 2, 1961).
9. Materials and methods are available as supporting material on *Science* Online.
10. Y. Maeno *et al.*, *Nature* **372**, 532 (1994).
11. R. M. Arutunian, G. F. Zharkov, *J. Low Temp. Phys.* **52**, 409 (1983).
12. B. J. Baelus, F. M. Peeters, V. A. Schweigert, *Phys. Rev. B* **61**, 9734 (2000).
13. D. A. Ivanov, *Phys. Rev. Lett.* **86**, 268 (2001).
14. S. Das Sarma, C. Nayak, S. Tewari, *Phys. Rev. B* **73**, 220502 (2006).

15. We thank D. Van Harlingen, M. Stone, E. Fradkin, E.-A. Kim, and H. Bluhm for valuable discussions and M. Ueda for helpful suggestions regarding the data analysis. In particular, the authors thank A. J. Leggett for his theoretical guidance. This work was supported by the U.S. Department of Energy Office of Basic Sciences, grant DEFG02-07ER46453 through the Frederick Seitz Materials Research Laboratory at the University of Illinois at Urbana Champaign and the grants-in-aid for the Global Centers of Excellence "Next Generation of Physics" programs from the Ministry of Education, Culture, Sports, Science and Technology of Japan.

Supporting Online Material

www.sciencemag.org/cgi/content/full/331/6014/186/DC1
Materials and Methods
SOM Text
Figs. S1 to S10
Tables S1 and S2
References

16 June 2010; accepted 8 December 2010
10.1126/science.1193839

Light-Induced Superconductivity in a Stripe-Ordered Cuprate

D. Fausti,[1,2]*†‡ R. I. Tobey,[2]†§ N. Dean,[1,2] S. Kaiser,[1] A. Dienst,[2] M. C. Hoffmann,[1] S. Pyon,[3] T. Takayama,[3] H. Takagi,[3,4] A. Cavalleri[1,2]*

One of the most intriguing features of some high-temperature cuprate superconductors is the interplay between one-dimensional "striped" spin order and charge order, and superconductivity. We used mid-infrared femtosecond pulses to transform one such stripe-ordered compound, nonsuperconducting $La_{1.675}Eu_{0.2}Sr_{0.125}CuO_4$, into a transient three-dimensional superconductor. The emergence of coherent interlayer transport was evidenced by the prompt appearance of a Josephson plasma resonance in the *c*-axis optical properties. An upper limit for the time scale needed to form the superconducting phase is estimated to be 1 to 2 picoseconds, which is significantly faster than expected. This places stringent new constraints on our understanding of stripe order and its relation to superconductivity.

High-temperature cuprate superconductors are synthesized by chemically doping the parent compound, an antiferromagnetic Mott insulator. An example of a parent compound is La_2CuO_4, which turns into an unconventional metal as holes are doped into its CuO_2 planes by substitution of La by Ba or Sr. $La_{2-x}(Ba/Sr)_xCuO_4$ becomes superconducting for $x > 0.05$, reaching the highest critical temperatures near $x = 0.16$. The $x = 1/8$ compound deserves special attention, because it hosts one-dimensional (1D) modulations of charge and spin (*1*) and exhibits sharp reduction in critical temperature T_c (superconducting transition temperature). In the Ba-doped system, these "stripes" become static, enhanced by the buckled Cu-O planes in the so-called low-temperature tetragonal (LTT) phase (*2*, *3*). Static stripes, LTT phases (*4*), and suppressed superconductivity are also detected in $La_{1.48}Nd_{0.4}Sr_{0.12}CuO_4$ (*5*, *6*) and $La_{1.675}Eu_{0.2}Sr_{0.125}CuO_4$ ($LESCO_{1/8}$) (*7*). Figure 1 shows a schematic phase diagram of $La_{1.8-x}Eu_{0.2}Sr_xCuO_4$, in which T_c is strongly reduced in the stripe region, for all doping values below $x = 0.2$ (*8*, *9*).

The transition between a doped Mott insulator and a superconductor has long been at the heart of research into cuprate superconductivity. Virtually all studies have explored this transition by changing static doping or by adiabatically tuning an external parameter, such as pressure, to demonstrate that superconductivity can be restored if the equilibrium crystallographic structure is perturbed (*10*).

We dynamically perturbed the nonsuperconducting $LESCO_{1/8}$ with mid-infrared (mid-IR) radiation (*11*, *12*), inducing superconductivity on the ultrafast time scale. Optical excitation in the visible or near-IR has been used in the past to study (*13*–*18*), and sometimes even enhance (*19*), superconductivity. However, in all these cases, superconductivity could be achieved only after the relaxation of hot incoherent carriers back to the ground state and was not triggered directly by the light field.

Nonsuperconducting $LESCO_{1/8}$, held at a base temperature of 10 K, was excited with 15-μm–wavelength pulses (80 meV of photon energy), made resonant with an in-plane, near–600 cm^{-1}, Cu-O stretch. The time-dependent intensity reflectivity, $R = I_{refl}/I_{inc}$ (refl, reflected; inc, incident), was measured in the near-IR (1.5 eV), a photon energy at which the optical properties are indirectly related to the appearance of superconductivity (*20*–*22*). A prompt reflectivity change, remaining constant up to the longest time delays probed (100 ps), was observed (Fig. 2). Photoexcitation with the electric field polarized orthogonal to the planes resulted in only a small reflectivity change during the pump pulse and no long-lived response.

The long-lived photoinduced state of $LESCO_{1/8}$, can be shown to be superconducting by time-resolved terahertz spectroscopy. At equilibrium, superconductivity in cuprates is reflected in the appearance of a Josephson plasma resonance (JPR) in the *c*-axis terahertz optical properties. This is a general feature of cuprate superconductors (*23*–*25*), well understood by noting that 3D superconductivity in these compounds can be explained by Josephson coupling between capacitively coupled stacks of quasi-2D superconducting layers (*26*). This effect is shown in Fig. 3A for optimally doped $La_{1.84}Sr_{0.16}CuO_4$. A plasma edge in the reflectance appears near 60 cm^{-1} when the temperature is reduced below $T_c = 38$ K.

Figure 3C reports mid-IR pump, terahertz reflectance-probe measurements in nonsuperconducting $LESCO_{1/8}$. The equilibrium electric field reflectance, as in other striped cuprates (*27*),

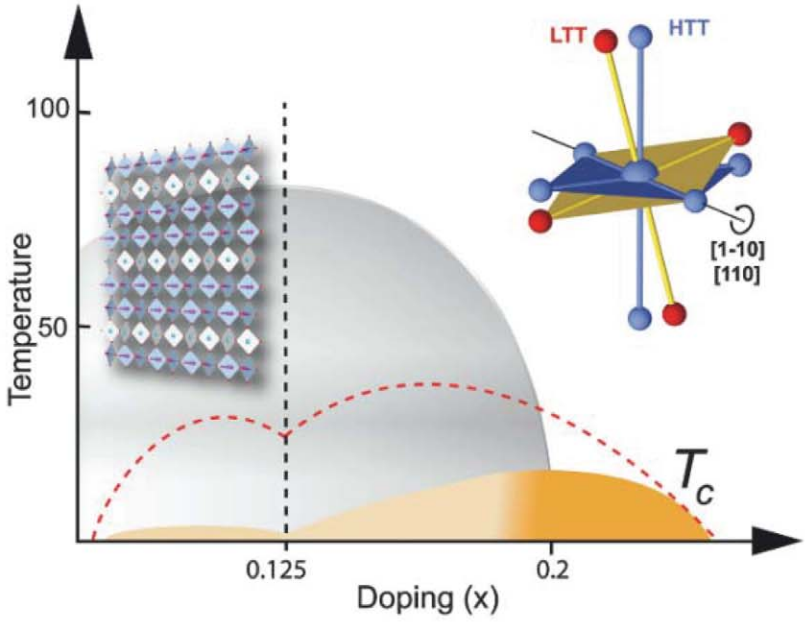

Fig. 1. Schematic phase diagram for $La_{1.8-x}Eu_{0.2}Sr_xCuO_4$. Superconductivity (yellow area) is quenched at all doping levels (gray area) below 0.2, emerging only at very low temperatures. At 0.125 doping, a static 1D modulation of charges and spins, the stripe state, emerges in the planes. This stripe phase (left inset) is associated with a LTT distortion, in which the oxygen octahedrals in the crystal are tilted (right inset). The red dashed curve marks the boundary for superconductivity in compounds of the type $La_{2-x}Sr_xCuO_4$, in which the LTT structural modulation is less pronounced.

[1]Max Planck Research Department for Structural Dynamics, University of Hamburg–Centre for Free Electron Laser Science–Hamburg, Germany. [2]Department of Physics, Clarendon Laboratory, University of Oxford, Oxford, UK. [3]Department of Advanced Materials Science, University of Tokyo, Tokyo, Japan. [4]IKEN Advanced Science Institute, Hirosawa 2-1, Wako 351-0198, Japan.

*To whom correspondence should be addressed. E-mail: andrea.cavalleri@mpsd.cfel.de (A.C.); daniele.fausti@mpsd.cfel.de (D.F.)
†These authors contributed equally to this work.
‡Present address: University of Trieste, Trieste, Italy.
§Present address: Physics Division, Brookhaven National Laboratory, Upton, NY, USA.

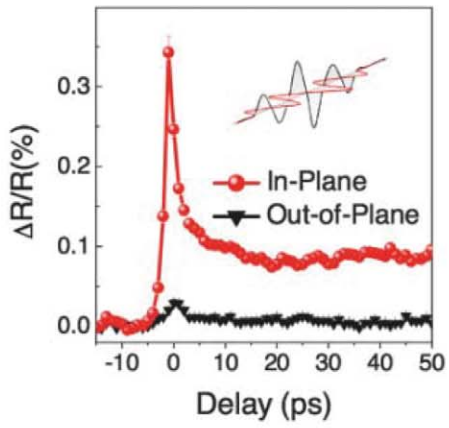

Fig. 2. Time-dependent 800-nm intensity reflectivity changes after excitation with IR pulses at 16 μm wavelength and ~1mJ/cm^2 intensity. Photoexcitation along the Cu-O planes results in the appearance of a long-lived meta-stable phase lasting longer than 100 ps. Excitation with the electric field polarized orthogonal to the Cu-O plane results in minimal reflectivity changes.

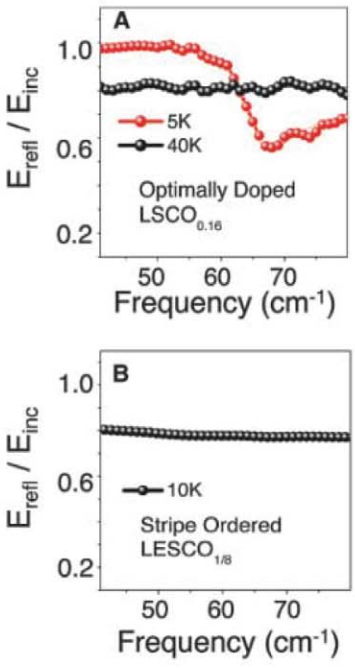

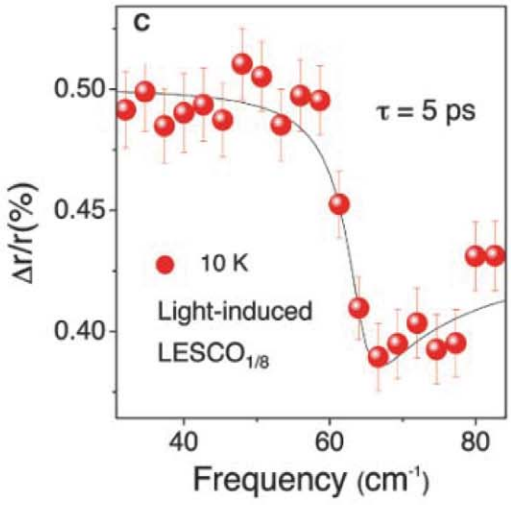

Fig. 3. (**A**) Static *c*-axis electric field reflectance ($r = E_{refl}/E_{inc}$) of $LSCO_{0.16}$, measured at a 45° angle of incidence above (black dots) and below (red dots) T_c = 38 K. Here field reflectances $r = E_{refl}/E_{inc}$ are measured, as opposed to intensity reflectivities in the near-IR, because the time domain detection scheme for short terahertz transients is sensitive to the electric field. In the equilibrium low-temperature superconducting state, a Josephson plasma edge is clearly visible, reflecting the appearance of coherent transport. This edge is fitted with a two-fluid model (continuous line). Above T_c, incoherent ohmic transport is reflected in a featureless conductivity. (**B**) Static *c*-axis reflectance of $LESCO_{1/8}$ at 10 K. The optical properties are those of a nonsuperconducting compound down to the lowest temperatures. (**C**) Transient *c*-axis reflectance of $LESCO_{1/8}$, normalized to the static reflectance. Measurements are taken at 10 K, after excitation with IR pulses at 16 μm wavelength. The appearance of a plasma edge at 60 cm^{-1} demonstrates that the photoinduced state is superconducting.

exhibits a featureless terahertz response reminiscent of that of $LSCO_{0.16}$ above T_c (Fig. 3B). Five picoseconds after excitation, a plasma edge at a frequency comparable to that of the $LSCO_{0.16}$ JPR is observed, indicating the emergence of coherent transport in the *c* axis. This is the most important observation of our work, evidencing ultrafast photoinduced superconductivity in $LESCO_{1/8}$.

The measured change in the absolute terahertz field reflectance is less than 1%, which is suggestive of an incomplete transformation of the probed volume. This is well explained by noting that the pump field penetration depth is about 200 nm, whereas the terehertz probe samples a depth of nearly 10 μm. The raw data of Fig. 3C was processed assuming a total terahertz reflectance resulting from a homogeneously transformed surface layer and an unperturbed bulk beneath. Relying on the knowledge of both amplitude and phase of the static and transient field reflectance, we could isolate the real and imaginary part of the time- and frequency-dependent optical conductivity $\sigma_1(\omega,\tau) + i\sigma_2(\omega,\tau)$ in the surface layer. In Fig. 4, we plot the imaginary part $\sigma_2(\omega,\tau)$, after subtracting a component originating from higher-frequency oscillators, which are also perturbed by photoexcitation and give a negative contribution to the conductivity change (*28*). The imaginary time-dependent conductivity $\sigma_2(\omega,\tau)$ acquires a $1/\omega$ frequency dependence immediately after excitation. A divergent imaginary conductivity at low frequencies is a defining characteristic of a superconductor. The real part $\sigma_1(\omega) = \pi/2(n_s e^2/m^*)\delta(0)$ reflects vanishing DC resistivity, and $\sigma_2(\omega) = n_s e^2/m^*\omega$ is connected to the diamagnetic response, and to the Meissner effect as $\omega \rightarrow 0$ (*29*) Here n_s is the superfluid density, *e* is the electron charge, and m^* is the electron effective mass (*30*). The quantity $\omega\sigma_2(\omega \rightarrow 0^*,\tau)$ (*31*), defined as the low-frequency limit of the measured terahertz transient for various pump-probe time delays, provides a measure of the formation time of the superconducting state (Fig. 4B). The prompt appearance of finite superconducting density, overshooting before relaxing into a plateau at a 5-ps time delay, reflects the transition dynamics between the striped state and the 3D superconductor. The temperature dependence of $\sigma_2(\omega,\tau)$, for time delays τ = 5 ps shows that the signatures of the transient superconducting state are lost above a base temperature of 20 K, at least for the 1 mJ/cm^2 excitation fluence used here (Fig. 4C).

In Fig. 4D we plot the wavelength-dependent susceptibility for photoinduced superconductivity, operationally defined as the inverse of the fluence F_{sat} at which the photoinduced optical properties start saturating (see supporting online material). The key observation is that the photosusceptibility has a pronounced peak at the frequency of the phonon. In comparison, at the same frequency, the reflectivity and the extinction coefficient change only marginally. As shown in Fig. 4D, the photosusceptibility (red dots) follows the phonon-resonance line shape (dashed curve), plotted as a "partial" extinction coefficient α_{phonon} and associated with a single oscillator extracted from a Drude-Lorentz fit of the broadband reflectivity (*28*). This observation suggests that direct coupling to the crystal structure may be responsible for the ultrafast transition into the superconducting phase.

The detailed microscopic pathway that leads to the superconducting state deserves further discussion. As a working hypothesis, it is helpful to relate our work to recent studies in striped cuprates, in which evidence for low-temperature 2D superconductivity was found (*32*). A plausible explanation for the decoupling between different striped planes follows directly from the crystallographic structure of the LTT phase (*33*), in which stripes of neighboring planes are oriented in perpendicular directions, whereas the next-nearest planes exhibit a shift of a half stripe period. This leads to a superconducting order that is in antiphase between stripes within each plane, and to canceling of the lowest-order Josephson coupling between planes (*34*).

In our experiment, the Josephson effect is reestablished when mid-IR pulses perturb the stripe state, which we attribute to a direct distortion of the LTT structure by the mid-IR radiation. The data of Fig. 4B provides a rise time for the formation of the superconducting state $\tau_{SC} < 1$ to 2 ps, limited by the temporal resolution of our measurement. This is a surprisingly short time scale, and it is difficult to imagine how mutually incoherent planes could synchronize so rapidly. At 5 K, only the 100-GHz modes are

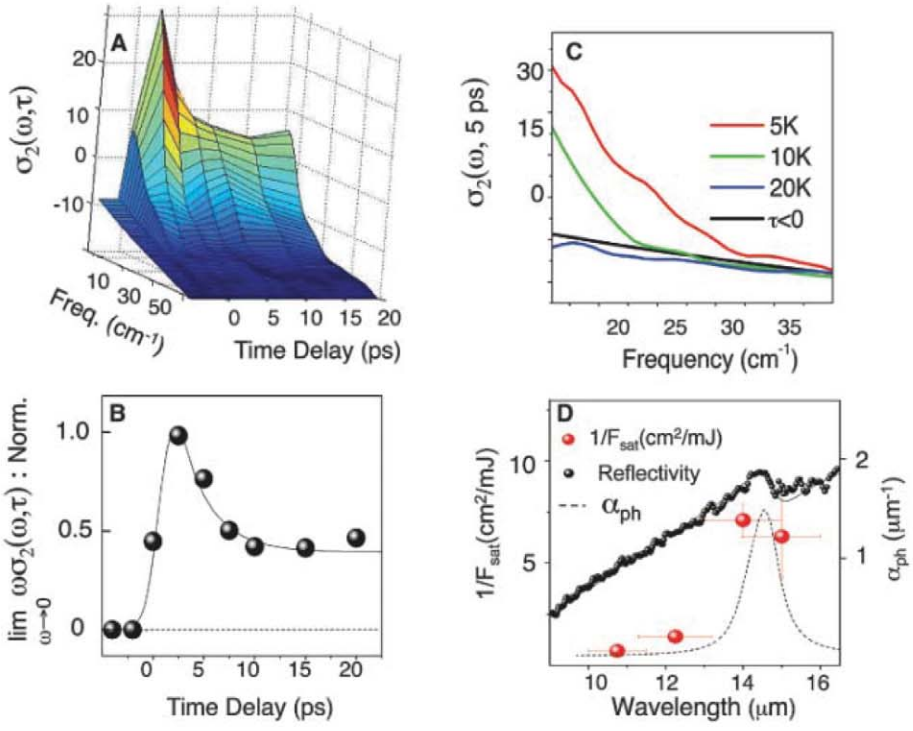

Fig. 4. (**A**) Time- and frequency-dependent imaginary conductivity $\sigma_2(\omega,\tau)$ of $LESCO_{1/8}$ at 10 K after excitation with IR pulses at 16 μm wavelength. The appearance of a 1/ω dispersion demonstrates that the system becomes superconducting on the shortest time scales accessible here. (**B**) Time-dependent plot of the normalized function $\omega\sigma_2(\omega - >0,\tau)$, proportional to the condensate density. (**C**) Transient measurement of the imaginary conductivity $\sigma_2(\omega,5\ ps)$, demonstrating that for the fluence used here (<1 mJ/cm^2), photoinduced superconductivity can only be induced for base temperatures T_b < 20 K. (**D**) Photosusceptibility, defined as the inverse of the saturation fluence plotted as a function of wavelength (red dots) compared to the reflectivity (black dots) of $LESCO_{1/8}$ measured in the *ab* plane. By means of a Drude-Lorentz fitting, the partial extinction coefficient for the α_{phonon} is extracted (dashed curve) and compared to the photosusceptibility.

thermally populated, and no spontaneous fluctuation could drive a process on time scales shorter than 10 ps.

This short time scale supports a picture in which information about the superconducting state is already present in the system before excitation. Indeed, if the planes were simply anticorrelated at equilibrium, recoupling could occur on a time scale needed to change the interplane order parameter phase difference, reestablishing the Josephson effect. This time scale may be very fast, commensurate with the Josephson plasmon period $T_{JPR} \sim 600$ fs.

The temperature at which photoinduced superconductivity disappears is near 10 to 20 K, significantly below $T_c = 35$ K in $LSCO_{0.16}$ and similar to the Berezinskii-Kosterlitz-Thouless temperature ($T_{BKT} = 16$ K) found from transport measurements in other striped compounds (*3*). One can speculate that the disappearance of 2D fluctuations for $T < T_{BKT}$ may be a necessary condition for photoinduced recoupling.

At the earliest time scales, a key question relates to the fate of stripe order once the Josephson coupling has been established. Time-resolved measurements of the stripe order, possible by extending soft x-ray scattering techniques (*35*) to the time domain, could clarify whether superconductivity emerges only in response to stripe melting, or, in contrast, the two can coexist.

Our measurements have not probed the dynamics beyond 100-ps time delays, although no relaxation was found on that time scale. We can thus deduce that the transient superconducting phase does not relax back for many nanoseconds, possibly more. The long lifetime can be understood by noting that once the 3D superconducting state is formed, the new broken symmetry leads to rigidity and to the formation of a kinetic barrier, which stabilizes the superconducting state.

The present paper has demonstrated that light can be used to affect phase competition in the underdoped cuprates, allowing for the emergence of a transient superconducting state at temperatures where the striped phase is the true ground state of the system. Similar photostimulation could be used to explore a broader region of the underdoped phase diagram, especially at doping levels and temperatures for which the electronic structure is already gapped (*36*) and signatures of quantum coherence are already present, but 3D superconductivity is not established (*37*).

References and Notes

1. J. Zaanen, O. Gunnarsson, *Phys. Rev. B* **40**, 7391 (1989).
2. T. Suzuki, T. Fujita, *Physica C* **159**, 111 (1989).
3. M. K. Crawford *et al.*, *Phys. Rev. B* **44**, 7749 (1991).
4. M. Fujita, H. Goka, K. Yamada, M. Matsuda, *Phys. Rev. Lett.* **88**, 167008 (2002).
5. J. Tranquada, B. J. Sternlieb, J. D. Axe, Y. Nakamura, S. Uchida, *Nature* **375**, 561 (1995).
6. Y. Nakamura, S. Uchida, *Phys. Rev. B* **46**, 5841 (1992).
7. J. Fink *et al.*, *Phys. Rev. B* **79**, 100502 (2009).
8. H. H. Klauss *et al.*, *Phys. Rev. Lett.* **85**, 4590 (2000).
9. Suryadijaya *et al.*, *Physica C* **426**, 402 (2005).
10. N. Takeshita, T. Sasagawa, T. Sugioka, Y. Tokura, H. Takagi, *J. Phys. Soc. Jpn.* **73**, 1123 (2004).
11. M. Rini *et al.*, *Nature* **449**, 72 (2007).
12. R. I. Tobey, D. Prabakharan, A. T. J. Boothroyd, A. Cavalleri, *Phys. Rev. Lett.* **101**, 197404 (2008).
13. R. D. Averitt *et al.*, *Phys. Rev. B* **63**, 140502 (2001).
14. J. Demsar, B. Podobnik, V. Kabanov, T. Wolf, D. Mihailovic, *Phys. Rev. Lett.* **82**, 4918 (1999).
15. R. A. Kaindl *et al.*, *Science* **287**, 470 (2000).
16. N. Gedik, D. S. Yang, G. Logvenov, I. Bosovic, A. H. Zewail, *Science* **300**, 1410 (2003).
17. L. Perfetti *et al.*, *Phys. Rev. Lett.* **99**, 197001 (2007).
18. A. Pashkin *et al.*, *Phys. Rev. Lett.* **105**, 067001 (2010).
19. G. Nieva *et al.*, *Appl. Phys. Lett.* **60**, 2159 (1992).
20. G. P. Segre *et al.*, *Phys. Rev. Lett.* **88**, 137001 (2002).
21. N. Gedik *et al.*, *Phys. Rev. Lett.* **95**, 117005 (2005).
22. C. Giannetti *et al.*, *Phys. Rev. B* **79**, 224502 (2009).
23. V. Z. Kresin, H. Morawitz, *Phys. Rev. B* **37**, 7854 (1988).
24. H. A. Fertig, S. Das Sarma, *Phys. Rev. Lett.* **65**, 1482 (1990).
25. K. Tamasaku, Y. Nakamura, S. Uchida, *Phys. Rev. Lett.* **69**, 1455 (1992).
26. N. Basov, T. Timusk, B. Dabrowski, J. D. Jorgensen, *Phys. Rev. B* **50**, 3511 (1994).
27. T. Tajima, T. Noda, H. Eisaki, S. Uchida, *Phys. Rev. Lett.* **86**, 500 (2001).
28. See supporting material on *Science* Online.
29. J. F. Annett, *Superconductivity, Superfluids and Condensates* (Oxford Master Series in Condensed Matter Physics, Oxford, 2004).
30. D. N. Basov, T. Timusk, *Rev. Mod. Phys.* **77**, 721 (2005).
31. N. Basov *et al.*, *Science* **283**, 49 (1999).
32. Q. Li, M. Hücker, G. Gu, A. Tsvelik, J. Tranquada, *Phys. Rev. Lett.* **99**, 067001 (2007).
33. M. von Zimmermann *et al.*, *Europhys. Lett.* **41**, 629 (1998).
34. E. Berg *et al.*, *Phys. Rev. Lett.* **99**, 127003 (2007).
35. P. Abbamonte *et al.*, *Nat. Phys.* **1**, 155 (2005).
36. T. Timusk, B. Statt, *Rev. Mod. Phys.* **62**, 61 (1999).
37. Z. A. Xu, N. P. Ong, Y. Wang, T. Kakeshita, S. Uchida, *Nature* **406**, 486 (2000).

38. This research was supported by a 2004 European Young Investigator Award, by core support from the Max Planck Society and the University of Hamburg, and by a Japanese Ministry of Education, Culture, Sports, Science and Technology (MEXT) Grant-in-Aid for Scientific Research (S) (19104008).

Supporting Online Material

www.sciencemag.org/cgi/content/full/331/6014/189/DC1
Materials and Methods
Figs. S1 to S3

2 September 2010; accepted 7 December 2010
10.1126/science.1197294

Electron Vortex Beams with High Quanta of Orbital Angular Momentum

Benjamin J. McMorran,[1]* Amit Agrawal,[1,2] Ian M. Anderson,[3] Andrew A. Herzing,[3] Henri J. Lezec,[1] Jabez J. McClelland,[1] John Unguris[1]

Electron beams with helical wavefronts carrying orbital angular momentum are expected to provide new capabilities for electron microscopy and other applications. We used nanofabricated diffraction holograms in an electron microscope to produce multiple electron vortex beams with well-defined topological charge. Beams carrying quantized amounts of orbital angular momentum (up to 100$\hbar$) per electron were observed. We describe how the electrons can exhibit such orbital motion in free space in the absence of any confining potential or external field, and discuss how these beams can be applied to improved electron microscopy of magnetic and biological specimens.

The discovery that optical vortices—light beams with a spiral phase singularity at the center of helical wavefronts—carry orbital angular momentum (OAM) (*1*) has led to appreciable advances in optical microscopy (*2*, *3*), astronomy (*4*), micromanipulation (*5*), quantum state manipulation (*6*, *7*), and other diverse applications (*8*). In an effort to extend these applications to other types of beams, we demonstrate the production of well-separated electron vortex beams with large quantized angular momentum. Electron vortices provide novel opportunities in electron microscopy.

An optical vortex beam can be characterized by the topological charge, m, describing the magnitude of the phase singularity at the center of the vortex. The wave functions of all such optical vortices include a phase winding factor, $\exp(im\varphi)$, where φ is the azimuthal angle about the optical axis z. This phase factor can be imprinted onto a conventional Gaussian beam, described in cylindrical coordinates as

$$G(\rho,z) \propto \frac{1}{w(z)}\exp\left\{-i\left[\frac{2\pi z}{\lambda}+\frac{\pi\rho^2}{\lambda R(z)}-\zeta(z)\right]\right\} \times \exp\left[\frac{-\rho^2}{w(z)^2}\right] \quad (1)$$

where ρ is the radial distance from the optical axis, $w(z)$ is the beam width, $R(z)$ is the radius of wavefront curvature, $\zeta(z)$ is the Guoy phase, and λ is the wavelength. When this imprinting occurs, the result is a particularly simple kind of optical vortex called a Laguerre-Gaussian (LG) beam, described by the wave function

$$\psi_{LG}(\rho,\varphi,z) = G(\rho,z)\left[\frac{\sqrt{2}\rho}{w(z)}\right]^{|m|}\exp\left\{i\left[m\varphi+|m|\zeta(z)\right]\right\} \quad (2)$$

For $m \neq 0$, complete destructive interference at the vortex core yields an intensity node along the entire optical axis of the vortex, such that LG beams are hollow and form characteristic ring-shaped (annular) intensity distributions when projected on a planar detector. An application of the angular momentum operator $\hat{L}_z = -i\hbar\partial_\varphi$ to this wave function shows that the optical vortex carries a quantized projection of OAM onto the optical axis, such that $L_z = m\hbar$ (where $\hbar$ is Planck's constant divided by 2π). The optical vortex is an orbital eigenstate for the individual particles that make up the beam (*6*).

Massive particles, such as free electrons, can also occupy such vortex states. The similarity between the Schrödinger equation describing the evolution of free-particle wave functions and the Helmholtz equation describing the propagation of light suggests that matter waves can be manipulated and applied in similar ways to light waves. The fact that LG beams are stable paraxial solutions of both the Helmholtz equation and the Schrödinger equation led to predictions (*9*, *10*) that free electron vortices were not only physically realizable but they could also be produced and applied in analogous ways to optical vortices. The first demonstration of electron vortex beams used a nanoscale spiral phase plate (*11*), formed by three pieces of thin graphite. However, it is very difficult to generate smooth helical wavefronts

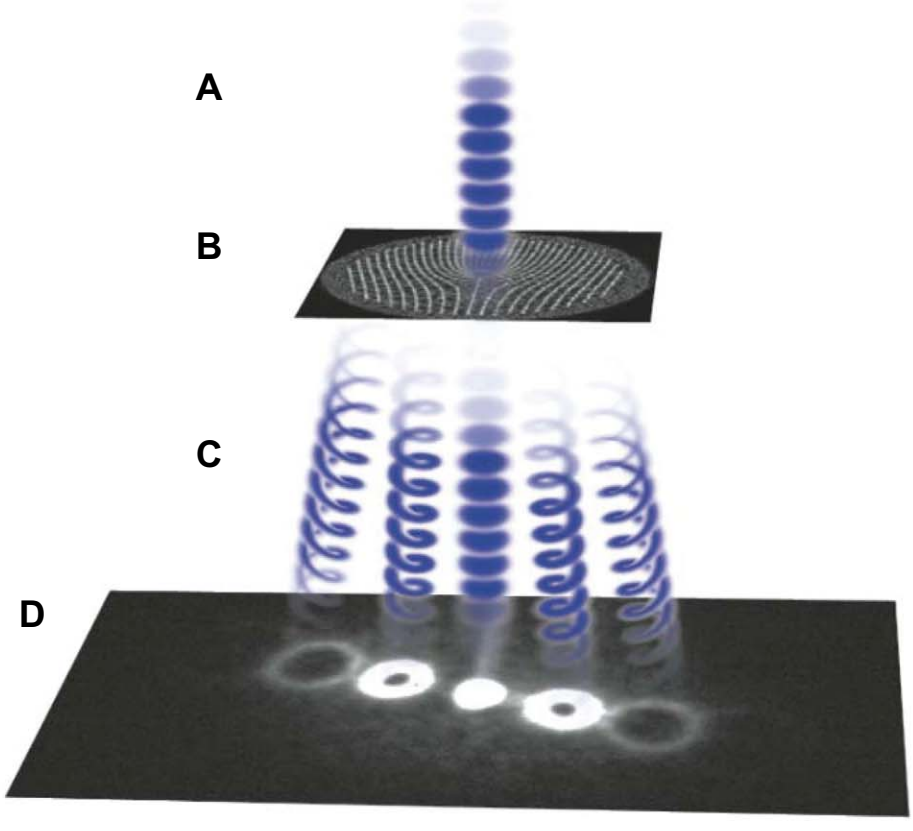

Fig. 1. Representation of the formation of electron vortices. (**A** to **D**) A spatially coherent plane wave of electrons (A) illuminates a nanofabricated hologram (B) and then diffracts into multiple electron vortex beams (C), which are then imaged (D) using a CCD (charge-coupled device). The depictions of the vortex beams shown at (C) simulate the wavefronts of the electrons, not their trajectories. The beam cross section shown in (D) is a measured diffracted electron intensity distribution. For simplicity, the TEM imaging optics used to demagnify the diffraction pattern are not shown here.

[1]Center for Nanoscale Science and Technology, National Institute of Standards and Technology, Gaithersburg, MD 20899, USA. [2]Maryland NanoCenter, University of Maryland, College Park, MD 20742, USA. [3]Surface and Microanalysis Science Division, National Institute of Standards and Technology, Gaithersburg, MD 20899, USA.

*To whom correspondence should be addressed. E-mail: mcmorran@nist.gov

using this approach, and it was noted that the resulting electron vortices had noninteger topological charge, such that the electrons occupied mixed quantized orbital states (*12*). Microscale gratings were recently used to create electron vortex beams with topological charge $m = 1$ (*13*).

We use nanoscale diffraction holograms to produce free electrons with large angular momentum in pure quantized orbital states (Fig. 1). Our work is based on earlier demonstrations using nanofabricated gratings for coherent electron interferometry (*14*–*16*), which led to a proposal to apply similar techniques to generate electron vortices (*10*). This approach, also adopted by (*13*), uses a grating mask with a fork dislocation to holographically imprint a phase vortex onto a diffracted beam (*17*, *18*). Advantages of this technique over spiral phase plates are that the diffracted beam automatically possesses integer topological charge, regardless of the wavelength, and it can be scaled to generate vortices with large quanta of OAM by including a higher-order fork dislocation. Transmission of a beam with wavelength λ through a binary hologram with slit spacing d (the grating period) and a fork dislocation defined by b additional half-slits produces multiple diffracted vortex beams. The nth diffraction order has distinct topological charge $m = nb$, such that negative diffraction orders propagating to one side of the central order beam have quantized OAM that is antiparallel to the propagation direction, and vice versa for positive diffraction orders. The diffracted beams propagate at discrete angles $\alpha = \lambda/d$ relative to one another, so for applications requiring isolated electron vortex beams it is necessary to use holograms with sufficiently small grating periods.

With a view toward future applications requiring high-quality isolated electron vortex beams, we have placed a particular emphasis on fabricating diffraction holograms with nanoscale feature sizes. Using a focused ion beam to mill silicon nitride membranes (*19*), we made multiple transmission holograms with grating periods of 50, 75, and 100 nm over circular areas 5 μm in diameter, featuring fork dislocations that encode various amounts of topological charge, from $b = 1$ to $b = 25$ (Fig. 2, A and B). These holograms have grating periods that are an order of magnitude smaller than those demonstrated in (*13*); this provides a correspondingly larger separation angle between beams. The smaller feature size also allows higher topological charge to be encoded within the same finite aperture area, enabling us to demonstrate electron beams with OAM up to $100\hbar$.

The electron vortices are produced by diffraction from the holograms in a transmission electron microscope (TEM) operating at 300 keV (*19*). Images of the diffraction patterns (Fig. 2 and Fig. 3) show the ring-shaped projections of electron vortex beams onto the detector plane. Electron vortex beams with distinct topological charge are selectively generated in particular diffraction orders from different holograms. In Fig. 3, one can discern the fourth diffraction order produced by a grating with dislocation number $b = 25$ (Fig. 2B). The corresponding topological charge in this beam is $m = 100$, and it is composed of individual electrons that each carry $100\hbar$ quanta of OAM. Electrons that have such high OAM are localized to a thin annulus around a large hollow core.

The free-space evolution of a hollow core in a wave function can be used to determine the existence of a vortex. A wave function with OAM has zero amplitude at the vortex core because of the repulsive centrifugal barrier. This is manifested in an LG beam by a central node that persists through the focus and increases in diameter as a function of distance from the beam waist. On the other hand, an initially ring-shaped wave function without OAM, such as that formed with an annular beam-defining aperture, will spread radially both inward and outward, such that the hole at the center of the wave becomes smaller and eventually disappears. We measured the hollow structure of the electron vortex beam by focusing it in space and then imaging the beam at multiple transverse planes relative to the beam waist (Fig. 4A) (*19*). The dark core can be observed throughout the Rayleigh range of each diffracted electron beam. Intensity line profiles through the first diffraction order, an $m = 15$ beam, show that the dark vortex core increases in diameter with distance from the focus (Fig. 4B). A quantitative analysis shows that over this range the vortex core diameter increases away from the beam waist by a factor of 2.8 ± 0.4 (fig. S1), which indicates that the diffracted electron

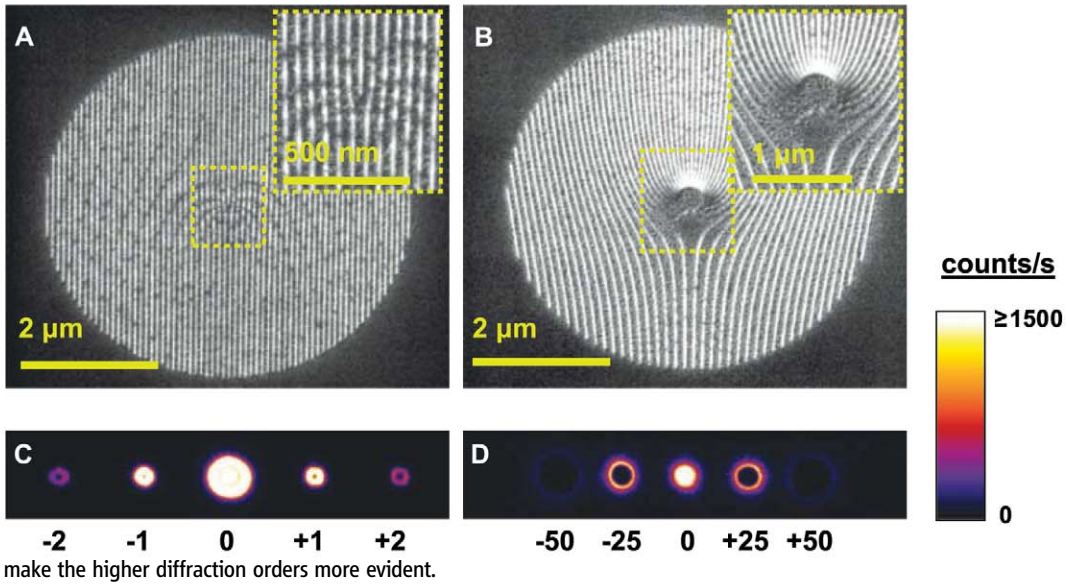

Fig. 2. Nanofabricated gratings with fork dislocations (top row) used to create electron beams with quantized phase vortices (bottom row). (**A** and **B**) A spatially coherent beam of 300-keV electrons transmitted through (A) a grating with period of 75 nm and $b = 1$, and (B) a grating with period of 100 nm and $b = 25$ (dislocations magnified in insets). The area around the central dislocation in (B) has been masked off to preserve structural integrity. (**C** and **D**) The diffraction patterns formed by (A) and (B), respectively. Each ring-shaped spot in (C) and (D) is the transverse intensity profile of an electron vortex beam. The topological charge is indicated below each diffracted beam. The diffracted electron intensity distributions are shown in false color to make the higher diffraction orders more evident.

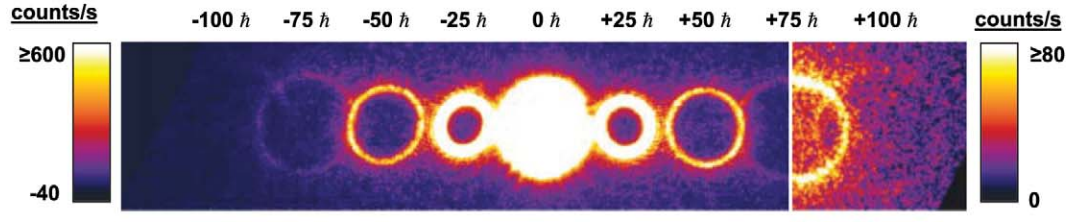

Fig. 3. Electron vortices with large OAM. The false-color image shows transverse intensity profiles of electron vortex beams produced using the hologram shown in Fig. 2C. The labels indicate the associated values of L_z possessed by each electron in an order. An electron vortex with $L_z = +100\hbar$ ($m = 100$) is evident with a different color scale applied to the right side of the image, containing the fourth and part of the third diffraction orders.

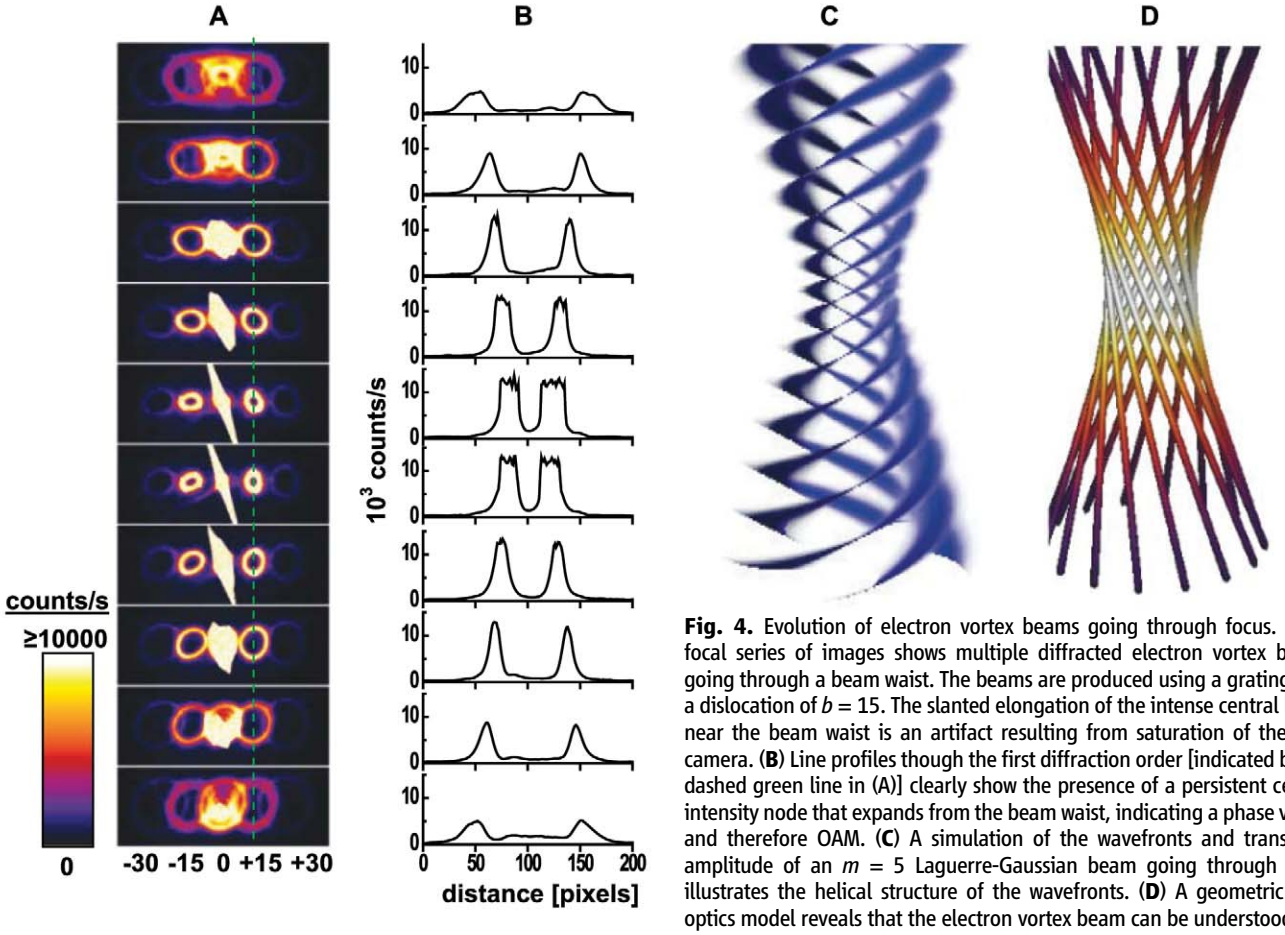

Fig. 4. Evolution of electron vortex beams going through focus. (**A**) A focal series of images shows multiple diffracted electron vortex beams going through a beam waist. The beams are produced using a grating with a dislocation of $b = 15$. The slanted elongation of the intense central beam near the beam waist is an artifact resulting from saturation of the CCD camera. (**B**) Line profiles though the first diffraction order [indicated by the dashed green line in (A)] clearly show the presence of a persistent central intensity node that expands from the beam waist, indicating a phase vortex and therefore OAM. (**C**) A simulation of the wavefronts and transverse amplitude of an $m = 5$ Laguerre-Gaussian beam going through focus illustrates the helical structure of the wavefronts. (**D**) A geometric (ray) optics model reveals that the electron vortex beam can be understood as a superposition of semiclassical straight-line trajectories.

beams possess angular momentum. An interference experiment between the electron vortex beam and a plane wave confirmed that this OAM is due to a helical phase (fig. S2).

These results show that electrons can be prepared in quantized orbital states with large OAM, in free space devoid of any central potential, electromagnetic field (*20*), or medium that confines the orbits. The electron vortex state is nonradiative in free space, as it must be, because emission of a photon would violate the simultaneous conservation of energy and linear momentum. Unlike a classical vortex, this orbital motion cannot be attributed to the collective behavior of many electrons in the beam; at the low beam currents of this experiment, the separation between individual electrons along the optical axis is several orders of magnitude larger than the longitudinal extent of each wave packet (*21*). Such high-OAM electron vortex states can exist at rest, too, because (unlike in a beam of photons) one can produce, using a decelerating electric field, a reference frame in which the forward motion of the electron vortex is zero along the optical axis.

The electron vortex is understandable in terms of semiclassical physics, provided the correct model is used for how these states evolve in time. In the reference frame where the electron vortex has no forward motion, the wave function is uniformly delocalized in a ring. The radius of this ring-shaped vortex wave function may change with time, but the centroid of the wave function is stationary. Thus, there is no acceleration associated with the electron's center of mass, and so no external force is necessary to preserve or define the orbital motion. A picture of this wave function evolving in space is provided by the simulation of a focused LG beam (Fig. 4C). The helical wavefronts of the beam are slightly tilted both azimuthally and radially, such that their locus of peak amplitude sweeps out a hyperboloid surface that can be described as a family of straight lines (Fig. 4D). Thus, the electron vortex can be modeled simply as a coherent superposition of classical straight trajectories that are slightly skewed and offset from the optical axis of the vortex (*22*).

Electron vortex beams are expected to provide new capabilities for electron energy-loss spectroscopy (EELS) in a TEM (*23*). Computed scattering cross sections between electron vortices and atoms show that it is possible for the electron vortex to transfer both quantized OAM and energy to the atoms. This transfer could be used to induce atomic transitions that were previously inaccessible in conventional EELS, such that an OAM-dependent signal could provide new chemical, crystallographic, optical, electronic, and magnetic information about a sample. This finding was recently confirmed experimentally (*13*). We are particularly interested in developing this technique for magnetic imaging, which will require the use of well-separated electron vortex beams.

Electron vortices can also enable spiral phase microscopy (*2*, *24*) in a TEM, enhancing the visibility of edges in samples with low absorption contrast, such as unstained biological specimens, without sacrificing spatial resolution. Computer-generated holograms have been used to implement spiral phase measurements in transmission light microscopes (*24*). Nanofabricated holograms could be implemented in a similar way in a TEM, provided that the hologram provides sufficient angular separation between vortex beams. This technique could provide some advantages over emerging TEM phase plate technologies (*25*, *26*), because the spiral phase provides additional information (*2*). This improved phase contrast will be relevant for TEM imaging of electron-transparent samples, such as biological specimens, macromolecules, carbon nanotubes, and polymers.

References and Notes

1. L. Allen, M. W. Beijersbergen, R. J. C. Spreeuw, J. P. Woerdman, *Phys. Rev. A* **45**, 8185 (1992).
2. S. Fürhapter, A. Jesacher, S. Bernet, M. Ritsch-Marte, *Opt. Lett.* **30**, 1953 (2005).

3. S. W. Hell, *Nat. Biotechnol.* **21**, 1347 (2003).
4. G. Foo, D. M. Palacios, J. Swartzlander Jr., *Opt. Lett.* **30**, 3308 (2005).
5. D. G. Grier, *Nature* **424**, 810 (2003).
6. A. Mair, A. Vaziri, G. Weihs, A. Zeilinger, *Nature* **412**, 313 (2001).
7. M. F. Andersen *et al.*, *Phys. Rev. Lett.* **97**, 170406 (2006).
8. S. Franke-Arnold, L. Allen, M. Padgett, *Laser Photon. Rev.* **2**, 299 (2008).
9. K. Bliokh, Y. Bliokh, S. Savel'ev, F. Nori, *Phys. Rev. Lett.* **99**, 190404 (2007).
10. B. J. McMorran, thesis, University of Arizona (2009).
11. M. Uchida, A. Tonomura, *Nature* **464**, 737 (2010).
12. J. Leach, E. Yao, M. J. Padgett, *N. J. Phys.* **6**, 71 (2004).
13. J. Verbeeck, H. Tian, P. Schattschneider, *Nature* **467**, 301 (2010).
14. B. McMorran, J. D. Perreault, T. A. Savas, A. Cronin, *Ultramicroscopy* **106**, 356 (2006).
15. A. Cronin, B. McMorran, *Phys. Rev. A* **74**, 061602(R) (2006).
16. B. J. McMorran, A. D. Cronin, *N. J. Phys.* **11**, 033021 (2009).
17. V. Y. Bazhenov, M. V. Vasnetsov, M. S. Soskin, *JETP Lett.* **52**, 429 (1990).
18. N. R. Heckenberg, R. McDuff, C. P. Smith, H. Rubinsztein-Dunlop, M. J. Wegener, *Opt. Quantum Electron.* **24**, S951 (1992).
19. See supporting material on *Science* Online.
20. Although the beams in this experiment do traverse magnetic fields in the lenses, the fields are confined to very small intervals relative to the entire path of the electrons.
21. Assuming a 1-nA, 300-keV electron beam with 0.3-eV energy spread, the longitudinal extent of a electron's wave packet along the optical axis is about 3 μm, whereas the average separation distance between consecutive electrons is 4 cm.
22. A. V. Volyar, V. G. Shvedov, T. A. Fadeeva, *Tech. Phys. Lett.* **25**, 203 (1999).
23. R. F. Egerton, *Electron Energy-Loss Spectroscopy in the Electron Microscope* (Springer, New York, 1996).
24. A. Jesacher, S. Fürhapter, S. Bernet, M. Ritsch-Marte, *Phys. Rev. Lett.* **94**, 233902 (2005).
25. R. Danev, H. Okawara, N. Usuda, K. Kametani, K. Nagayama, *J. Biol. Phys.* **28**, 627 (2002).
26. K. Schultheiß, F. Pérez-Willard, B. Barton, D. Gerthsen, R. R. Schröder, *Rev. Sci. Instrum.* **77**, 033701 (2006).
27. We thank S. Adam, G. Gallatin, M. Stiles, and J. H. Scott for useful discussions. Supported by the NIST-CNST NanoFab, NIST Division 637 FIB-SEM, and the NIST-CNST/UMD-NanoCenter Cooperative Agreement. The authors declare no competing financial interests.

Supporting Online Material

www.sciencemag.org/cgi/content/full/331/6014/192/DC1
Materials and Methods
Figs. S1 and S2

7 October 2010; accepted 23 November 2010
10.1126/science.1198804

Solvent-Free Oxidation of Primary Carbon-Hydrogen Bonds in Toluene Using Au-Pd Alloy Nanoparticles

Lokesh Kesavan,[1] Ramchandra Tiruvalam,[2] Mohd Hasbi Ab Rahim,[1] Mohd Izham bin Saiman,[1] Dan I. Enache,[1] Robert L. Jenkins,[1] Nikolaos Dimitratos,[1] Jose A. Lopez-Sanchez,[1] Stuart H. Taylor,[1] David W. Knight,[1] Christopher J. Kiely,[2] Graham J. Hutchings[1]*

Selective oxidation of primary carbon-hydrogen bonds with oxygen is of crucial importance for the sustainable exploitation of available feedstocks. To date, heterogeneous catalysts have either shown low activity and/or selectivity or have required activated oxygen donors. We report here that supported gold-palladium (Au-Pd) nanoparticles on carbon or TiO_2 are active for the oxidation of the primary carbon-hydrogen bonds in toluene and related molecules, giving high selectivities to benzyl benzoate under mild solvent-free conditions. Differences between the catalytic activity of the Au-Pd nanoparticles on carbon and TiO_2 supports are rationalized in terms of the particle/support wetting behavior and the availability of exposed corner/edge sites.

Selective oxidation of primary carbon-hydrogen bonds is of crucial importance in activating raw materials to form intermediates and final products for use in the chemical, pharmaceutical, and agricultural business sectors (*1*). One class of raw materials is alkyl aromatics; toluene, for example, the simplest member of this class, can be oxidized to benzyl alcohol, benzaldehyde, benzoic acid, and benzyl benzoate. These products are commercially significant as versatile intermediates in the manufacture of pharmaceuticals, dyes, solvents, perfumes, plasticizers, dyestuffs, preservatives, and flame retardants. Commercially, benzaldehyde is produced by the chlorination of toluene followed by saponification (*2*), and benzoic acid is produced by the liquid-phase cobalt-catalyzed reaction of toluene using oxygen at 165°C with acetic acid as solvent, but the conversion has to be limited to <15% to retain high selectivities (*3*–*9*). The use of halogens and acidic solvents makes these processes environmentally unfriendly. Vapor-phase oxidation has been considered, but the conversion must be limited to avoid overoxidation to CO_2 and other byproducts (*10*). Attempts to overcome these problems have prompted investigation of the use of supercritical CO_2 and ionic liquids, but these unfortunately resulted in low conversions (*11*, *12*).

Often, heterogeneous catalysts are preferred over homogeneous catalysts, because these materials can be readily separated from the reaction mixture. Heterogeneous catalysts can also be readily used in flow reactors, facilitating the efficient production of materials using continuous processes. For the oxidation of toluene, there have been many attempts to find a suitable oxidation catalyst, and to date these have used copper and manganese (*13*–*15*), cobalt (*16*), or chromium (*17*) catalysts, but all of these perform very poorly with turnover numbers (TONs: mole of product per mole of metal catalyst) of less than 100, even at temperatures in excess of 190°C (table S1) (*18*). There is clearly a need to develop heterogeneous catalysts for toluene oxidation that have greatly improved activity while retaining selectivity.

Recently, we have shown that Au-Pd alloy nanoparticles are very effective for the direct synthesis of hydrogen peroxide (*19*) and the oxidation of primary alcohols using oxygen (*20*). This catalyst operates by establishing a reactive hydroperoxy intermediate. Because these intermediates are known to be involved in the enzymatic oxidation of primary carbon-hydrogen bonds (*21*), we reasoned that it should be feasible for Au-Pd nanoparticles to be active for the oxidation of the primary carbon-hydrogen bonds in toluene. Here we show that Au-Pd alloy nanoparticles prepared by a sol immobilization technique can give significantly improved activity for the oxidation of toluene under mild solvent-free conditions. These catalysts have TONs that are a factor of ~30 greater than those of previous heterogeneous catalysts for this reaction and also display a remarkably high selectivity to benzyl benzoate.

We started by investigating the oxidation of toluene in an autoclave reactor with O_2 in the absence of catalyst in order to determine the blank baseline rate. O_2 is a di-radical and can initiate homogeneous oxidation processes at elevated temperatures and pressures. We found that such processes become substantial at 190°C under our conditions (fig. S1) (*18*). This important observation suggests that the earlier studies conducted at 190°C (table S1) (*18*) may not in fact have been heterogeneously catalyzed. In view of the potential role of O_2 di-radicals, the maximum reaction temperature in our studies has been restricted to 160°C; at this temperature, the blank reaction in the absence of catalyst but in the presence of support is negligible for short reaction times (Table 1, entries 1, 3, and 4) and is very low at longer reaction times (Table 1, entry 2). We initially investigated Au-Pd/TiO_2 catalysts, prepared by impregnation, because these had previously been shown to be very active for H_2O_2 synthesis (*19*) and alcohol oxidation (*20*); however, these catalysts were not found to be particularly active for toluene oxidation, although they did not produce any CO_2 (table S2) (*18*).

The Au-Pd nanoparticles synthesized by the impregnation method can be relatively large (typically >6 nm) and have substantial compositional variations, which limits their reactivity. Therefore, in order to design more effective catalysts, we decided to investigate Au-Pd nanoparticles with smaller median particle sizes (2 to

[1]Cardiff Catalysis Institute, School of Chemistry, Cardiff University, Main Building, Park Place, Cardiff CF10 3AT, UK. [2]Department of Materials Science and Engineering, Lehigh University, 5 East Packer Avenue, Bethlehem, PA 18015–3195, USA.

*To whom correspondence should be addressed. E-mail: hutch@cardiff.ac.uk

5 nm) and a more controlled composition. These were prepared by sol immobilization of Au-Pd colloids, with carbon and TiO_2 as supports (*18*), a method that afforded tightly controlled particle size distributions and composition. We investigated the effect of the Au-Pd molar ratio (Table 1, entries 5 to 12) using these sol-immobilized materials supported on carbon. For all catalysts, no CO_2 formation was observed; the only products were benzyl alcohol, benzaldehyde, benzoic acid, and benzyl benzoate. By itself, Au was not active for this reaction, but the addition of Pd significantly enhanced the conversion, demonstrating a clear synergistic effect for the Au-Pd catalysts as compared with the monometallic species.

Table 1. Comparison of catalytic activity for the oxidation of toluene in the absence of solvent with O_2. Catalyst mass varied between 0.2 and 0.6 g to give a substrate/metal molar ratio of 6500. Toluene, 10 to 20 ml; stirring rate, 1500 rpm; TON calculated on the basis of the total metal. All metal catalysts were prepared using the sol immobilization method (*18*). *T*, temperature.

								Selectivity (%)			
Entry	Catalyst	Metal (%)	Au:Pd molar ratio	*T* (°C)	P_{O_2} (bar)	Time (hours)	Conversion (%)	Benzyl alcohol	Benzaldehyde	Benzoic acid	Benzyl benzoate	TON
1	None*	-	-	160	10	7	0.2	18.3	69.4	1.9	10.4	-
2	None*	-	-	160	10	48	2.9	5.8	43.6	38.2	12.4	-
3	Carbon*	-	-	160	10	7	0.1	11.4	72.6	0.1	16.0	-
4	TiO_2*	1	-	160	10	7	0.2	0.1	6.0	85.1	8.9	-
5	Au/C*	1	1:0	160	10	7	0.2	9.0	81.9	0	8.1	11
6	Au-Pd/C*	1	7:1	160	10	7	0.3	28.4	57.6	6.2	7.8	17
7	Au-Pd/C*	1	3:1	160	10	7	1.5	1.8	63.4	3.1	31.4	95
8	Au-Pd/C*	1	1:1.85	160	10	7	4.8	0.9	12.7	10.3	76.1	310
9	Au-Pd/C*	1	1:2	160	10	7	5.3	1.2	8.3	11.1	79.3	350
10	Au-Pd/C*	1	1:3	160	10	7	5.2	1.9	8.5	10.3	79.3	340
11	Au-Pd/C*	1	1:7	160	10	7	4.3	9.6	13.6	7.3	69.5	280
12	Pd/C*	1	0:1	160	10	7	1.6	3.9	56.4	3.3	36.4	105
13	Au/C+Pd/C†	1	1:1.85	160	10	7	1.6	0.8	26.2	11.4	61.6	105
14	Au-Pd/TiO_2*	1	1:1.85	160	10	7	2.1	2.9	6.6	1.0	89.5	135
15	Au-Pd/TiO_2*	1	1:1.85	160	10	7	2.2	2.2	6.5	2.3	89.0	141
16	Au-Pd/C‡	1	1:1.85	160	10	48	50.8	0.1	1.1	4.5	94.3	3300
17	Au-Pd/TiO_2‡	1	1:1.85	160	10	48	24.1	0.5	1.2	2.8	95.5	1570
18	Au-Pd/C‡	1	1:1.85	120	10	48	10.6	0.2	7.1	13.1	79.7	690
19	Au-Pd/TiO_2‡	1	1:1.85	120	10	48	4.0	1.1	6.0	4.8	88.1	260
20	Au-Pd/C‡	1	1:1.85	80	10	48	0.9	8.6	34.2	0.1	57.2	60
21	Au-Pd/C‡	1	1:1.85	160	6	48	4.9	0.1	5.7	2.9	91.4	320
22	Au-Pd/C§	1	1:1.85	160	10	0.5	1.8	2.1	11.6	0.8	85.5	29
23	Au-Pd/C§	1	1:1.85	160	10	7	21.5	0.3	1.8	3.1	94.8	350
24	Au-Pd/C§	1	1:1.85	160	10	24	82.9	0.1	0.8	7.3	91.8	1347
25	Au-Pd/C§	1	1:1.85	160	10	27	94.4	0.2	1.0	13.3	85.5	1534

*Reaction conditions: toluene, 20 ml; substrate/metal molar ratio, 6500; mass of catalyst, variable. †Reaction of a physical mixture composed of 1 wt % Au/C and 1 wt % Pd/C. Toluene, 20 ml; substrate/metal molar ratio, 6500. ‡Reaction conditions: toluene, 10 ml; substrate/metal molar ratio, 6500; mass of catalyst, 0.2 g. §Reaction conditions: toluene, 20 ml; substrate/metal molar ratio, 1625; mass of catalyst, 1.6 g.

Table 2. Comparison of the catalytic activity for oxidation of substituted toluenes in the absence of solvent with O_2. Catalyst mass, 0.4 g; substrate, 20 ml; stirring rate, 1500 rpm; 160°C; 10 bar O_2; TOF and TON calculated on the basis of the total metal. Au-Pd/C (1:1.85 Au:Pd molar ratio), 1 wt % total metal was prepared using the sol immobilization method (*18*).

			Selectivity (%)							
Substrate	Time (hours)	Conversion (%)	Benzyl alcohol	Benzaldehyde	Benzoic acid	Benzyl benzoate				TON
Toluene	1	1.1	2.7	27.5	6.9	62.9				
	4	2.2	2.2	18.7	8.6	70.5				
	7	4.4	1.0	12.4	10.4	76.2				284
			n-*Methoxy benzyl alcohol*	n-*Methoxy benzaldehyde*	n-*Methoxy benzoic acid*	n-*Methoxybenzyl* n-*methoxybenzoate*	*Toluene*	*Esters*	*C-C products*	
4- Methoxytoluene	1	2.3	0.8	18.7	30.3	24.1	0.9	7.1	18.1	
	4	6.1	0.8	11.8	25.8	43.5	0.2	5.0	12.9	
	7	10.6	0.5	7.4	26.9	49.0	0.1	4.5	11.6	581
3-Methoxytoluene	1	1.7	1.4	16.4	46.5	8.1	7.4	1.2	19.0	
	4	2.0	1.1	33.3	30.6	2.2	19.5	0.8	12.5	
	7	3.7	0.9	12.6	43.3	17.0	6.8	1.2	19.0	204
2-Methoxytoluene	1	3.6	1.4	8.8	63.8	0.7	22.7	0.3	2.3	
	4	6.4	1.0	10.0	66.8	3.6	15.7	0.4	2.5	
	7	11.1	0.8	13.0	61.1	7.3	11.8	0.8	5.2	619

A physical mixture of the separate Au/C and Pd/C catalysts showed no enhancement (Table 1, entry 13), highlighting the molecular-scale nature of the synergy. The observed synergy is due to electronic and morphological features because transmission electron microscopy (TEM) shows that the mean particle size of the nanoparticles decreases slightly on the addition of Au to Pd (table S3). When Au-rich catalysts were used, some benzyl alcohol was formed, but this was readily oxidized to the main product benzaldehyde, as this sequential oxidation is rapid at this temperature (*20*). We consider the initial oxidation of toluene to involve a surface hydroperoxy intermediate formed from the interaction of the metal with oxygen and toluene. However, as the fraction of Pd in the alloy was increased, the selectivity to benzyl benzoate became dominant. The optimum catalyst composition found was a 1:2 Au:Pd molar ratio (approximately 1:1 by weight). For this catalyst, the turnover frequency (TOF: mole of product formed per mole of metal per hour) of toluene oxidation after 7 hours of reaction was ~50. We also investigated this Au-Pd composition using a TiO_2-supported material (Table 1, entry 14) and found that it was also active, but less so than the carbon-supported material, displaying a TOF of 20 $hour^{-1}$ after 7 hours of reaction.

To demonstrate the general applicability of the AuPd/C catalyst, we oxidized 2-, 3-, and 4-methoxytoluene (Table 2), and 2-, 3-, and 4-nitrotoluene (table S4) (*18*). No CO_2 was observed, and the reactivity trend (4-methoxy- ~ 2-methoxy- >3-methoxy ~ toluene > 2-nitro- > 3-nitro ~ 4-nitro) is indicative of the involvement of electron-deficient intermediate(s). Additional products formed were identified as a family of esters and C-C coupling products (table S5) (*18*). We have also investigated the reaction of xylenes; the catalysts are equally effective for the oxidation of this substrate and formed the aldehyde, acid, and esters as products, with the relative amounts being dependent on the conversion (table S6) (*18*), confirming the wider applicability of our catalysts.

Given these initial promising results, we investigated the oxidation of toluene at longer reaction times (Table 1, entries 16 and 17). In this regime, much higher toluene conversions were attained and no CO_2 was observed. Once again only four products were observed: benzyl alcohol, benzaldehyde, and benzoic acid in trace amounts and benzyl benzoate as the dominant product (~95%) for both catalysts. The carbon-supported catalyst was typically twice as active over this longer time scale, exhibiting a TON of 3300 with ~3150 mol of benzyl benzoate per mole of metal produced over the reaction period. We investigated the use of lower reaction temperatures (Table 1, entries 18 though 20) and observed some activity, albeit slight, even at 80°C. In a further set of experiments, we attempted to enhance the activity of the catalyst at 80°C by using *t*-butyl hydroperoxide as a co-oxidant (table S7) and found that the conversion increased appreciably when both the carbon- and TiO_2-supported catalysts were used; TON values of 850 to 1200 can be achieved even under these mild conditions. However, using this hydroperoxide as a co-oxidant generated a different product profile. At long reaction times and high conversions, benzoic acid became the main product, together with appreciable amounts of benzaldehyde and benzyl alcohol; only negligible amounts of benzyl benzoate were formed. As with O_2 as the sole oxidant, when using the hydroperoxide co-oxidant, the carbon-supported catalyst was about twice as active as the TiO_2-supported Au-Pd nanoparticles.

The reaction profile over an initial 7-hour reaction period was investigated using a higher substrate-to-metal ratio at 160°C (fig. S2). This experiment showed that the toluene conversion increases linearly over this time scale and that the selectivity to benzyl benzoate increases as the selectivity to benzaldehyde decreases. The reaction profile over a longer time scale was also investigated using a lower substrate/metal molar ratio and showed that the conversion continued to increase steadily, fully depleting the toluene after 110 hours (Fig. 1), while the selectivity to benzyl benzoate also increased. Monometallic Au and Pd catalysts showed very low conversion (8%) over 110 hours (table S8) (*18*). The toluene conversion was also found to increase linearly with catalyst mass (fig. S3). Hence, with appropriate tuning of catalyst loading and reaction conditions, we are confident that complete and selective conversion of toluene to desirable products can be achieved (Table 1, entries 22 to 25 show results of an initial optimization). Furthermore, by increasing the reaction time at 140°C, we can obtain a 95% yield of benzyl benzoate (table S9) (*18*).

We consider that the high selectivity to benzyl benzoate **6** could result from four possible mechanisms: (i) coupling of the aldehyde **3** and the alcohol **2** to give the hemiacetal **5**, followed by oxidation to the ester (Scheme 1); (ii) direct thermal (catalyzed) dehydrative esterification between acid **4** and alcohol **2** (Scheme 1); (iii) Cannizzaro reaction between alcohol **2** and aldehyde **3** via alkoxide **7** (Scheme 2); and (iv) Tishchenko coupling of two aldehydes **3** via "dimer" **8** directly to the ester **6** (Scheme 3).

Recently, Bäumer and co-workers (*22*) have shown that methyl formate is formed on an Au catalyst when methanol is oxidized with O_2 under very dilute conditions; we consider that this precedent favors mechanism (i) in the present case. We performed several control experiments to rule out the other three possible pathways. Heating the oxidized intermediates with O_2 in the absence of catalyst gave little ester (table S10), establishing the involvement of the catalyst in steps beyond the initial toluene-to-alcohol oxidation. Heating mixtures of alcohol **2** and acid **4** in the absence of O_2, with and without catalyst, did not result in ester formation (tables S11 and S12), ruling out direct esterification (**4** → **6**; Scheme 1). Similarly, treating alcohol **2** with aldehyde **3** also failed to produce ester **6** (tables S11 and S12), ruling out the Cannizzaro mechanism (Scheme 2). Finally, we investigated reactions of the aldehyde **3** alone in the absence of O_2, with and without catalyst, and again observed no ester **6** formation (tables S11 and S12), precluding the Tishchenko mechanism (Scheme 3). Hence we conclude that the high selectivities observed are consistent with the involvement of the hemiacetal **5** (Scheme 1).

To determine the origin of the differences in activity between the two catalysts, we have characterized the common starting sol (*18*) and the two sol-immobilized materials using EM. Figure S4 (*18*) shows a representative scanning TEM (STEM) high-angle annular dark field (HAADF) image of the starting colloidal particles deposited onto a carbon film. The nanoparticles have a mean particle size of 2.9 nm (fig. S5A) and were found to be homogeneous Au-Pd alloys. More than 80% of the particles were icosahedral or decahedral (multiply twinned), with the remain-

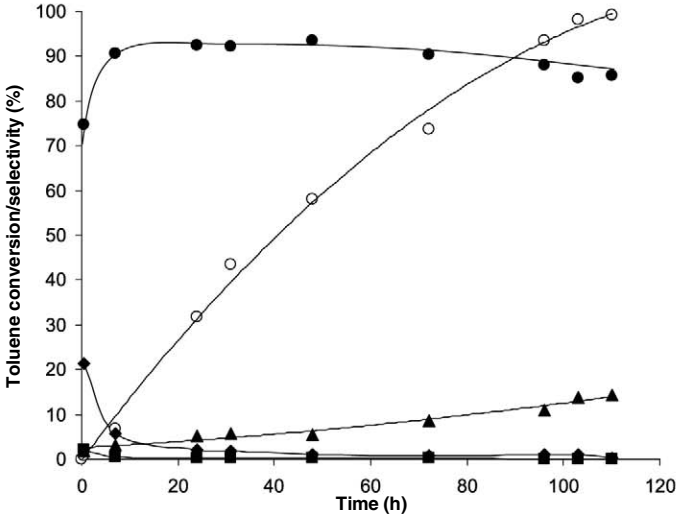

Fig. 1. Toluene conversion and selectivity to benzyl alcohol, benzaldehyde, benzoic acid, and benzyl benzoate: reaction temperature, 160°C (433 K); 0.1 MPa partial pressure of oxygen (P_{O_2}); 20 ml of toluene; 0.8 g of catalyst [1 weight % (wt %) Au-Pd/C prepared by sol immobilization with a 1:1.85 Au/Pd ratio]; toluene/metal molar ratio of 3250; and reaction time, 110 hours. Open circles indicate conversion, squares indicate selectivity to benzyl alcohol, diamonds indicate selectivity to benzaldehyde, triangles indicate selectivity to benzoic acid, and solid circles indicate selectivity to benzyl benzoate.

der being cub-octahedral or just single/double-twinned in character. They were also distinctly rounded in shape because they were still coated with protective polyvinyl alcohol ligands. After deposition of the colloids onto either activated amorphous carbon or TiO_2, the sol-immobilized material was dried at 120°C for 3 hours. The low-temperature drying process in each case caused a very modest size increase in the Au-Pd particles, leading to HAADF-measured mean sizes for the TiO_2- and carbon-supported catalysts of 3.9 and 3.7 nm, respectively (fig. S5 B and C).

The most important difference noted between the two samples relates to the morphology of the Au-Pd particles. In contrast to the starting colloid, many of the smaller particles were now found to be highly faceted, and primarily cub-octahedral (Fig. 2, A to D) or singly twinned (Fig. 2E) in character. Such particles preferentially exposed distinct {111}- and {200}-type facets. The larger particles (Fig. 2F) still tended to be multiply twinned and exclusively exposed {111}-type facet planes. In addition, the Au-Pd particles tended to form an extended flat interface structure with the crystalline TiO_2 substrate (fig. S6), which could serve to improve particle adhesion and inhibit sintering at higher temperatures.

In contrast, the corresponding HAADF images (Fig. 2, G to I) from the carbon-supported samples show that the Au-Pd particles are more rounded and have a much lower ability to wet the amorphous carbon support. The distribution of Au-Pd particle morphologies on the carbon support was much closer to that of the starting colloid, with icosahedral and decahedral (five-fold-twinned) particles predominating (Fig. 2, G to J) and comparatively few single/double-twinned (Fig. 2K) and cub-octahedral (Fig. 2L) particles present. It is plausible that the strong interaction of the Au-Pd metal with the TiO_2 support in the former case templates many of the smaller multiply twinned particles to restructure as cub-octahedral particles or simple single/double-twinned crystals during the drying step. X-ray photoelectron spectroscopy (XPS) analysis of the Au-Pd catalysts immobilized on carbon and TiO_2 showed them to have a Pd/Au ratio of 2.1 and 2.2, respectively, and confirmed that in both cases, the Pd was predominantly in the metallic state (*23*).

The AuPd/C sample had approximately double the catalytic activity of the AuPd/TiO_2 sample, despite having a very similar size distribution of Au-Pd particles. This suggests that simple metal surface area considerations are not dominating the catalytic activity in this instance, because the total numbers of exposed surface atoms are almost identical (*24*), and the TONs per surface-exposed atoms for the most-active catalysts are 1.03×10^4 for Au-Pd/C (Table 1, entry 16) and 0.56×10^4 for Au-Pd/TiO_2 (Table 1, entry 17) (tables S14 and S15) (*18*). In addition, the similarity in surface composition, as evidenced by XPS, does not provide a clue as to the source of the activity difference. The Au-Pd/TiO_2 catalyst does clearly have more support/particle periphery sites relative to the Au-Pd/C catalyst, by virtue of its flatter, better wetting interface. However, such periphery sites are probably not implicated in the catalytic process in this instance, because the Au-Pd/TiO_2 catalyst displays the lower activity. It is possible that the disparity in catalytic activity may be related to subtle differences in the number of low coordination facet-edge and corner sites in the two cases. The flatter, more faceted, Au-Pd particles have fewer of these low coordination number sites, whereas the more irregular, rougher Au-Pd

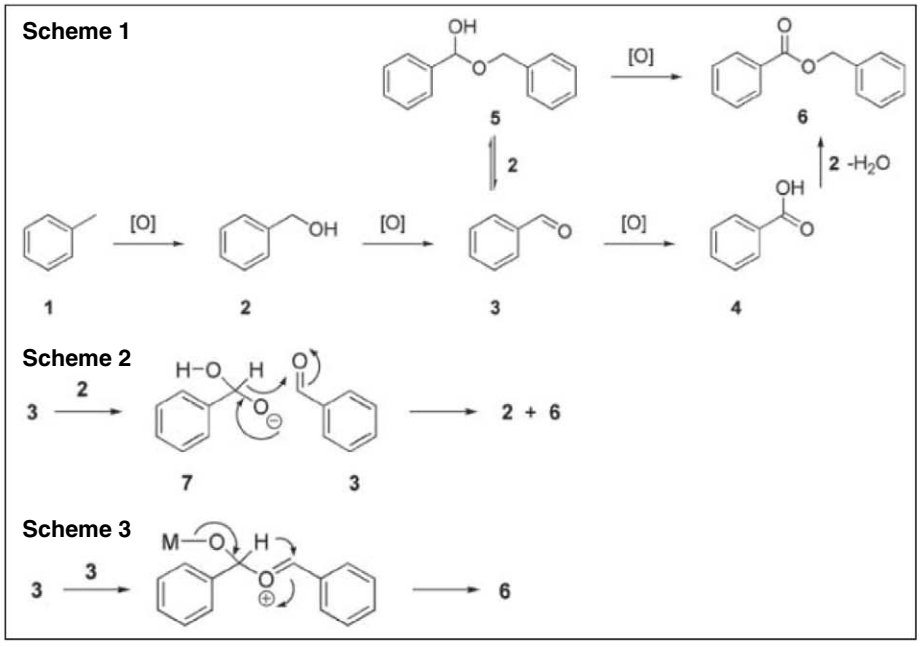

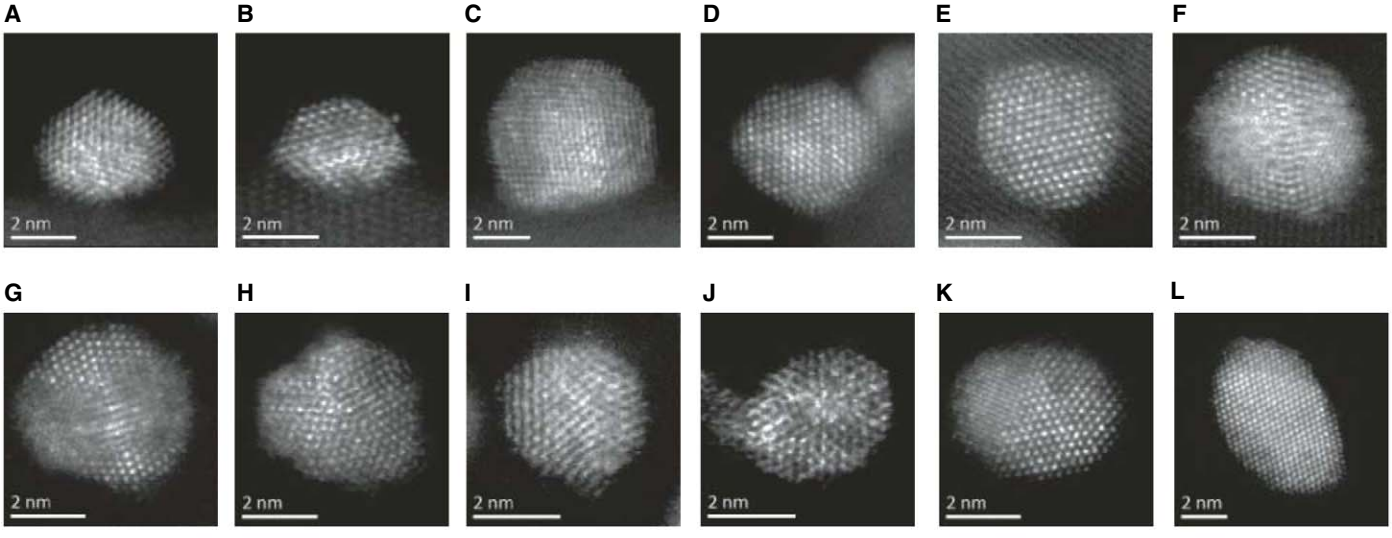

Fig. 2. Representative (**A** to **F**) STEM HAADF micrographs of Au-Pd nanoparticles in the Au-Pd/TiO_2 sol-immobilized sample. Representative (**G** to **L**) STEM HAADF micrographs of Au-Pd nanoparticles in the Au-Pd/C sol-immobilized sample.

particles have substantially more of them. If these low coordination number corner and/or edge positions are implicated as active sites for toluene oxidation, then their relatively higher occurrence in the Au-Pd/C sample could account for the superior performance displayed by this catalyst. Another possible explanation could lie in the difference in the distribution of Au-Pd particle morphologies found in the two catalyst samples. The Au-Pd/C catalyst predominantly has multiply twinned (icosahedral and decahedral) particles, which tend to have {111} facet terminations. In comparison, the Au-Pd/TiO_2 materials show an increased fraction of cuboctahedral and singly/doubly twinned particles, which exhibit mixed {100}/{111} facet terminations. Hence, the increasing proportion of {100}-type facets in the Au-Pd/TiO_2 sample correlates with a lowering of the catalytic activity, and preparation strategies need to avoid them.

In a final set of experiments, we investigated the stability of the catalysts, because it is crucial to confirm that high-activity catalysts can be reused. With the Au-Pd/TiO_2 catalyst, the reaction was stopped after 7 hours, and the catalyst was recovered by decantation. Identical conversion was obtained on reuse of the Au-Pd/TiO_2 catalyst (Table 1, entries 14 and 15). For the Au-Pd/C catalyst, the reaction was stopped after 7 hours and the catalyst was allowed to settle. The liquid phase was then carefully removed by decantation and fresh toluene was added. No metal was observed to have leached into the liquid phase during reaction, and the decanted liquid showed no further reaction in the absence of catalyst (fig. S7 and table S16). The reaction was then allowed to proceed for a further 7 hours, and the whole process was repeated a further two times. The reaction profile obtained with the decantation experiments was identical to that obtained with the fresh catalyst (fig. S8). Detailed STEM characterization shows that there is minimal particle growth or morphology change for the Au-Pd/C catalysts when studied over an extended reaction period (Fig. 1), during which catalysts were recovered after 31 and 65 hours of reaction, followed by two reuse cycles of 7 hours (figs. S9 and S10). Therefore, it is clear that any sintering or structural modification of these highly active catalysts is minimal, and we consider them to be stable and reusable.

References and Notes

1. R. A. Sheldon, J. K. Kochi, *Metal-Catalyzed Oxidations of Organic Compounds* (Academic Press, New York, 1981).
2. W. Partenheimer, *Catal. Today* **23**, 69 (1995).
3. Y. Ishii, S. Sakaguchi, T. Iwahama, *Adv. Synth. Catal.* **343**, 393 (2001).
4. K. Nomiya, K. Hashino, Y. Nemoto, M. Watanabe, *J. Mol. Catal. Chem.* **176**, 79 (2001).
5. T. G. Carrell, S. Cohen, G. C. Dismukes, *J. Mol. Catal. Chem.* **187**, 3 (2002).
6. S. Saravanamurugan, M. Palanichany, V. Murugesan, *Appl. Catal. A Gen.* **273**, 143 (2004).
7. H. V. Borgaonkar, S. R. Raverkar, S. B. Chandalia, *Ind. Eng. Chem. Prod. Res. Dev.* **23**, 455 (1984).
8. M. L. Kantam *et al.*, *Catal. Lett.* **81**, 223 (2002).
9. Snia-Viscosa, *Hydrocarbon Proc.* **134**, 210 (1977).
10. F. Konietzni, U. Kolb, U. Dingerdissen, W. F. Maier, *J. Catal.* **176**, 527 (1998).
11. J. Zhu, A. Robertson, S. C. Tsang, *Chem. Commun. (Camb.)* **18**, 2044 (2002).
12. K. R. Seddon, A. Stark, *Green Chem.* **4**, 119 (2002).
13. X. Li *et al.*, *Catal. Lett.* **110**, 149 (2006).
14. F. Wang *et al.*, *Adv. Synth. Catal.* **347**, 1987 (2005).
15. J. Gao, X. Tong, X. Li, H. Miao, J. Xu, *J. Chem. Technol. Biotechnol.* **2002**, 620 (2007).
16. R. L. Brutchey, I. J. Drake, A. T. Bell, T. Tilley, *Chem. Commun. (Camb.)* **2005**, 3736 (2005).
17. A. P. Singh, T. Selvam, *J. Mol. Catal. Chem.* **113**, 489 (1996).
18. See supporting on *Science* Online for detailed methods.
19. J. K. Edwards *et al.*, *Science* **323**, 1037 (2009).
20. D. I. Enache *et al.*, *Science* **311**, 362 (2006).
21. J. Colby, D. I. Stirling, H. Dalton, *Biochem. J.* **165**, 395 (1977).
22. A. Wittstock, V. Zielasek, J. Biener, C. M. Friend, M. Bäumer, *Science* **327**, 319 (2010).
23. N. Dimitratos *et al.*, *Phys. Chem. Chem. Phys.* **11**, 5142 (2009).
24. A. Borodziński, M. Bonarowska, *Langmuir* **13**, 5613 (1997).

25. We acknowledge the support of the Dow Chemical Company through the Dow Methane Challenge.

Supporting Online Material

www.sciencemag.org/cgi/content/full/331/6014/195/DC1
Materials and Methods
Figs. S1 to S10
Tables S1 to S16
References

29 September 2010; accepted 14 December 2010
10.1126/science.1198458

Supracolloidal Reaction Kinetics of Janus Spheres

Qian Chen,[1] Jonathan K. Whitmer,[1,2] Shan Jiang,[1] Sung Chul Bae,[1] Erik Luijten,[3,4]* Steve Granick[1,2,5]*

Clusters in the form of aggregates of a small number of elemental units display structural, thermodynamic, and dynamic properties different from those of bulk materials. We studied the kinetic pathways of self-assembly of "Janus spheres" with hemispherical hydrophobic attraction and found key differences from those characteristic of molecular amphiphiles. Experimental visualization combined with theory and molecular dynamics simulation shows that small, kinetically favored isomers fuse, before they equilibrate, into fibrillar triple helices with at most six nearest neighbors per particle. The time scales of colloidal rearrangement combined with the directional interactions resulting from Janus geometry make this a prototypical system to elucidate, on a mechanistic level and with single-particle kinetic resolution, how chemical anisotropy and reaction kinetics coordinate to generate highly ordered structures.

Clusters, an intermediate level of matter between building block (atom, molecule, or particle) and bulk phase, are found ubiquitously in nature and technology—for example, in the nucleation of bulk phases (*1*), nanoparticles (*2*), and protein aggregates in biology (*3*, *4*). Whereas structures that result from isotropic interactions between building blocks are well understood (*5*–*8*), it is more challenging to understand clusters formed from the common case of directional noncovalent interactions (*9*–*17*). On this question, we note that for molecular amphiphiles, such as surfactants, phospholipids, and many block copolymers, the segregation of their polar and nonpolar portions is a major mechanism steering the spontaneous formation of microstructured mesophases with fascinating and useful structures (*9*–*11*). Similarly, colloidal particles, larger than molecules but small enough to sustain Brownian motion, also assemble into clusters owing to directional noncovalent interactions (*12*–*17*). A largely unsolved problem is the question of commonality between these fields. Therefore, combining amphiphilicity with colloidal rigidity, we study "Janus spheres" that are hydrophobic on one hemisphere and negatively charged on the other. An earlier publication from this laboratory described some structures that these hybrid materials form (*18*). Here, we address the kinetics of self-assembly at the single-particle level, showing that small, kinetically favored isomers join to form highly ordered but nonequilibrium large-scale structures.

A critical design rule is that the range of interparticle interactions (hydrophobic attraction and electrostatic repulsion) must be short relative to particle size and that the interactions must be reversible. Clustering then favors densely packed structures with at most six nearest neighbors per particle, in contrast to the more open and less ordered structures formed by particles whose interaction range is larger (*13*). At very low salt concentrations, particles repel one another electrostatically, whereas at high salt concentrations, van der Waals forces cause the particles to aggregate irreversibly (*19*). Therefore, we consider intermediate concentrations of monovalent salt at which amphiphilic clusters self-assemble (*20*).

If the hydrophobic patch is too small, assembly admits clusters composed of at most four particles. However, increase in patch size allows such clusters to grow into larger assemblies, with two constraints: First, particles must approach closely enough to experience hydrophobic attrac-

[1]Department of Materials Science and Engineering, University of Illinois, Urbana, IL 61801, USA. [2]Department of Physics, University of Illinois, Urbana, IL 61801, USA. [3]Department of Materials Science and Engineering, Northwestern University, Evanston, IL 60208, USA. [4]Department of Engineering Sciences and Applied Mathematics, Northwestern University, Evanston, IL 60208, USA. [5]Department of Chemistry, University of Illinois, Urbana, IL 61801, USA.

*To whom correspondence should be addressed. E-mail: luijten@northwestern.edu (E.L.); sgranick@illinois.edu (S.G.)

tion; second, the number of nearest neighbors must not exceed six. For Janus particles whose hydrophobic domains are hemispheres, Fig. 1A displays pathways of reversible self-assembly, all of which we observed. They form a complex network in which multiple cluster possibilities emanate from every point and, likewise, routes from every point can meet. The hydrophobic patches lend appreciable orientational freedom to individual particles within the clusters. This promotes dynamical interconversion between clusters through three major mechanisms: step-by-step addition of individual particles, fusion of smaller clusters into a larger one, and isomerization. The clusters in this regime, with a size range $N = 2$ to 7 (fig. S1), are similar to those formed in depletion-induced assembly of homogeneous particles (*5*), except that for homogeneous particles the clusters must be kept isolated to avoid further aggregation. Here, cluster aggregation is prevented by electrostatic repulsion between the charged surface regions, allowing clusters to live in close proximity without fusing.

The ability to control the long-range repulsion makes it possible to switch on clustering at will by adding salt to Janus spheres in deionized water. We found that after the distribution of cluster sizes equilibrated (fig. S2), their shapes continued to change. For example, the capped trigonal bipyramid (CTBP) shape with cluster size $N = 6$ formed first, then gradually isomerized to the more symmetric octahedral shape (Fig. 1B). These kinetic data are consistent with a reversible first-order reaction with rate constants given in the figure caption. In this system, the octahedral shape is more stable. Nonetheless, the CTBP isomer forms first, because growth proceeds via rotation of a particle in a feeder cluster. Particles located at the cluster ends have the largest rotational freedom and thus act as the points where additional particles join the cluster, causing elongated structures to form. In a cluster, particles constantly jiggle about their mean positions; this process is analogous to highly excited vibrational motion in molecules, where the vibrations occasionally cause collective rearrangements. Molecular reaction dynamics occur on picosecond or faster time scales (*21*), whereas these colloidal transformations occur on the time scale of seconds and can be visualized one by one without ensemble averaging. These reaction dynamics are illustrated in movie S1, showing cluster growth from smaller clusters, and movies S2 and S3, showing cluster isomerization via different pathways. Unlike micelles formed from molecules, whose predominant growth mechanism is through addition of monomers to preexisting micelles (*10*), the rigid, spherical shape of these colloidal building blocks allows them to rotate without change of position such that clusters grow at their ends by fusing with other clusters. A second difference is that, unlike molecular micelles whose fluidity encourages shape to equilibrate rapidly, these colloidal clusters possess definite configurations. For the same number of particles in a cluster, there are distinctly different, long-lived shapes.

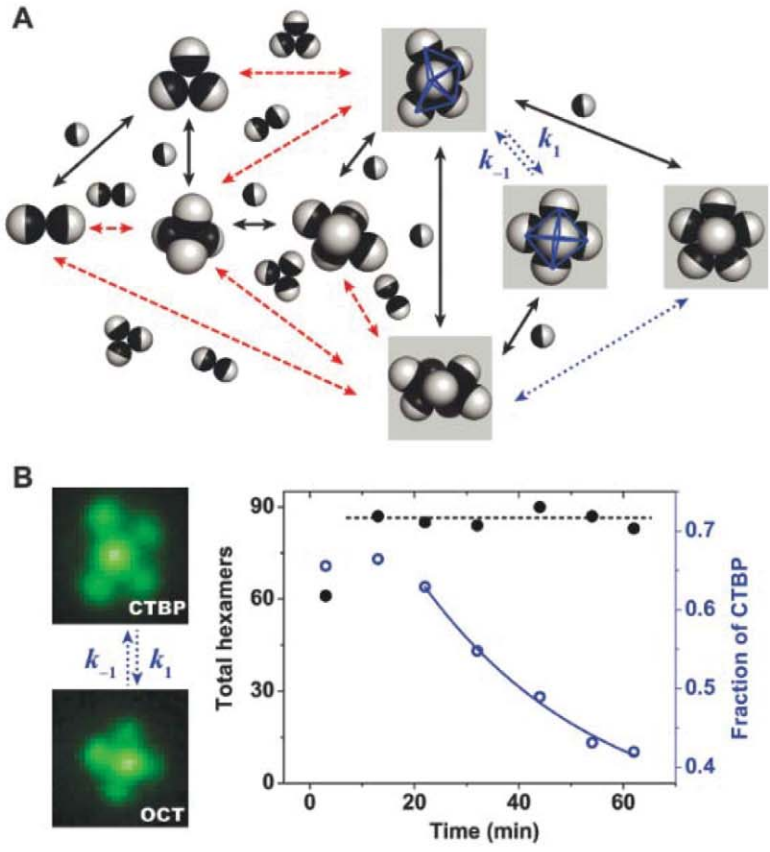

Fig. 1. Clusters formed from Janus spheres with one hydrophobic hemisphere. (**A**) Network of reaction pathways, all of which we have observed in experiments at 3.8 mM NaCl. Reaction mechanisms of monomer addition, cluster fusion, and isomerization are denoted by black, red, and blue arrows, respectively. Isomers with $N = 6$ and $N = 7$ elemental spheres are highlighted in boxes. Movie S1 shows a simple example of cluster growth by the fusion of two clusters. (**B**) A study of isomerization between two types of $N = 6$ clusters, the capped trigonal bipyramid (CTBP) and the octahedron (OCT). Here and in all other images, the Janus spheres have a diameter of 1 μm. After initiating the cluster process by setting the NaCl concentration at 3.8 mM, the partition of Janus spheres between clusters of different size equilibrates after 20 min (see fig. S2) but isomerization continues. Once the total number of hexamers (black filled circles) has stabilized, isomerization (fraction of CTBP, blue open circles) is consistent with first-order reaction kinetics in time t, $d[\mathrm{OCT}]/dt = k_1[\mathrm{CTBP}] - k_{-1}[\mathrm{OCT}]$, time constant 34 min, $k_1/k_{-1} = 2.2$, and $k_1 = 0.02\ \mathrm{min}^{-1}$. Here the calculation is based on the ensemble behavior of many clusters, among which individual ones can follow different reaction pathways. Movies S2 and S3 compare different pathways of isomerization.

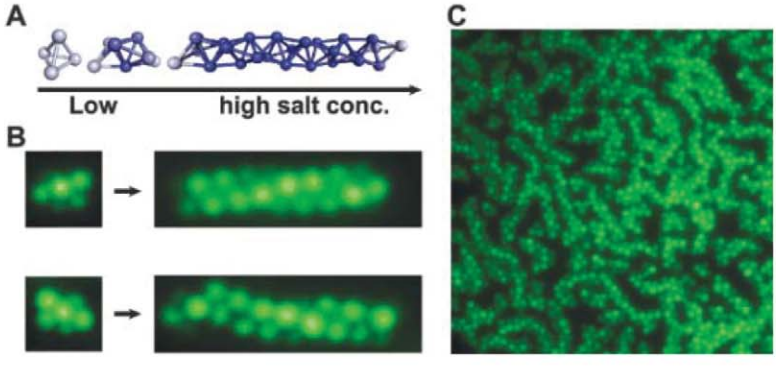

Fig. 2. Triple helices formed at higher salt concentration and higher particle concentration. (**A**) Geometrical representation of helix growth by face-sharing tetrahedra. (**B**) Comparison of a small chiral cluster (3.8 mM NaCl) and a longer helical cluster (5 mM NaCl). For both cases, fluorescence images of both right-handed and left-handed structures are shown. (**C**) Fluorescence image illustrating the stability of wormlike structures at high volume fraction. Movie S6 shows the fusion of two chiral chains by Brownian motion.

A minor increase of the salt concentration to 5 mM reduced the electrostatic repulsion to permit the growth of striking helical structures (Fig. 2). Closer inspection showed these to be Boerdijk-Coxeter (BC) helices (*22*), sometimes called Bernal spirals. The formation and stability of helices per se is a consequence of the directionality of the pairwise interactions, which allows them to persist up to the highest particle concentrations (60% after sedimentation), unlike homogeneous particles, which at lower particle concentrations form BC helices that become unstable when the concentration is higher (*6*, *7*).

All dense packings of spheres on a cylindrical surface have the same internal energy, because each sphere except those at the ends of the chain interacts with six nearest neighbors (*4*). This remains true for Janus spheres, provided that each hydrophobic side faces the corresponding hemispheres of all neighbors—a constraint that is satisfied in the very structures that arise from the anisotropic interaction. This is analogous to carbon nanotubes, whose variety of rolled structures result from the same threefold coordinated graphene sheet (*23*). Thus, the absence of helical structures other than the BC helix indicates that either entropic or kinetic effects matter here.

To clarify the relative stability of a range of helical structures (*4*), we calculated their relative free energy as a function of Janus balance, taking into account the rotational entropy of individual Janus particles as well as vibrational modes; a related free-energy landscape is known for spheres with isotropic interactions (*5*). As plotted in Fig. 3A, the 3(0,1,1) helix is in fact thermodynamically favored over the BC helix by a modest amount; here we use the notation proposed when this structure was identified (*4*). Strict quantitative correspondence to the experimental situation is not expected, as a full calculation including collective excitations and chain bending would be formidable to execute, but we can safely conclude that thermodynamically the BC helix is not strongly favored over the 3(0,1,1) helix (other tubular forms have a higher free energy).

Instead, we believe that the BC helices are the observed structure up to the highest particle concentrations because they are selected by kinetics. The preferred initial formation of CTBP $N = 6$ isomers, the basic building block of the BC helix, rather than octahedral $N = 6$ clusters, the basic unit of the 3(0,1,1) helix, causes the former helices to form first. Subsequent transformation relaxation of a BC helix into a 3(0,1,1) helix would require a massive collective change where, in the long-chain limit, one bond must be broken for every group of three spheres. This metastability explains why 3(0,1,1) helices are never observed in the experiment.

We confirmed the preferred formation of polytetrahedral over polyoctahedral clusters in molecular dynamics (MD) simulations, in particular at high attraction strengths where configurations tend to get trapped. Two further experimental observations strengthen this scenario. Although stable against relaxation into a 3(0,1,1) helix, the BC helices occasionally display a spontaneous switch of handedness (movies S4 and S5). This is energetically slightly less costly, because only one bond needs to be broken for every four particles. More important, the possible pathway for chirality switching is simpler. Both chirality switching and relaxation to the 3(0,1,1) helix require unfavorable intermediate structures in which one particle has seven nearest neighbors. For the chirality switch, this pivotal particle has four bonds with reduced stability owing to large bond angles. If any of these bonds is broken, the chirality switching either proceeds or the chain returns to its original chirality. For the change from BC to 3(0,1,1), there are three bonds of reduced stability, and breaking any of these interrupts the transition; instead, it is one of the stable bonds that needs to be broken for the change to proceed, which is comparatively harder (fig. S3). Lastly, in both experiments (Fig. 3B) and MD simulations (Fig. 3C) we observe defects in which an $N = 7$ cluster is incorporated into a helix, reconfirming the kinetically arrested state of these structures, even though individual constituent spheres display considerable mobility. As expected for reversible self-assembly, these fibrillar clusters reform (heal) spontaneously after being torn apart by strong shear. They also fuse with one another through Brownian motion (movie S6) because the ends, which are most free to rotate, are more reactive than the middle.

Our results underscore the importance of kinetic selection when colloidal amphiphiles cluster. Unlike the rapid shape equilibration of molecular amphiphiles, Janus spheres present transient isomeric structures whose lifetime is so long that before isomers equilibrate they fuse to form the stable, highly ordered nonequilibrium helices described here. Their generalization to colloidal blocks of asymmetric shape (rods, ellipsoids, chains, etc.) presents an agenda for future work. This work on a prototypical system offers a direction in which to look for the design of new reconfigurable materials from the interplay between equilibration time scale and packing allowed by orientation-specific attraction.

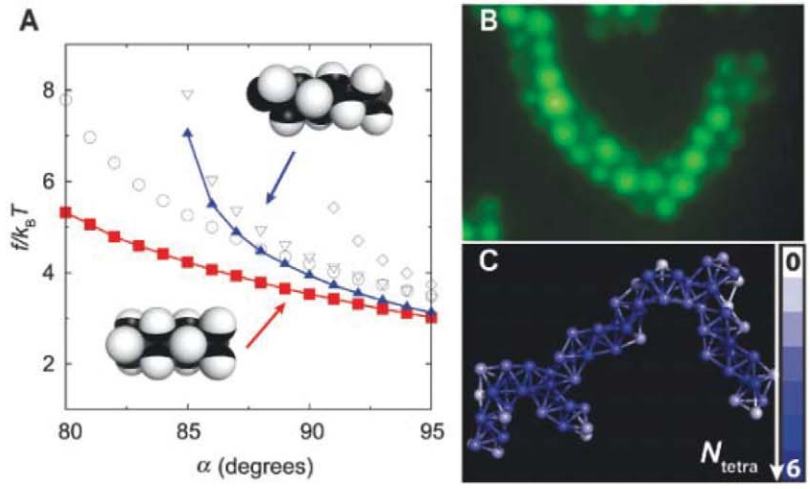

Fig. 3. Consideration of alternative tubular packings and defective structures. (**A**) Free energy per particle as a function of Janus balance α, half the opening angle of the hydrophobic patch. These tubular structures (*4*) are the 3(0,1,1) structure whose building block is the octahedral $N = 6$ isomer (red squares); the BC helix whose building block is the capped trigonal bipyramidal $N = 6$ isomer (blue triangles); also, for completeness, the 4(0,1,1) (circles), the (1,3,4) (inverted triangles), and the 2(1,1,2) (diamonds) structures, which have a higher free energy at the experimental Janus balance ($\alpha = 90°$). Including vibrational entropy (*5*) reduces the free-energy difference between the 3(0,1,1) and the BC helix by 0.19 k_BT per particle for a representative chain length ($N = 24$). At $\alpha = 90°$ this reduces the total free-energy difference by a factor of 2. The insets show schematic structures of the 3(0,1,1) and the BC helix. (**B**) Example of a kinked chain observed in experiments, in which an $N = 7$ cluster structure intercalates the predominant BC helix. (**C**) Similar structure, now with several intercalating $N = 7$ clusters, observed in molecular dynamics simulation. Particles are colored from white to blue depending on the number of tetrahedra in which they participate, N_{tetra}.

References and Notes

1. A. Cacciuto, S. Auer, D. Frenkel, *Nature* **428**, 404 (2004).
2. B. Yoon *et al.*, *ChemPhysChem* **8**, 157 (2007).
3. T. P. Knowles *et al.*, *Science* **318**, 1900 (2007).
4. R. O. Erickson, *Science* **181**, 705 (1973).
5. G. Meng, N. Arkus, M. P. Brenner, V. N. Manoharan, *Science* **327**, 560 (2010).
6. A. I. Campbell, V. J. Anderson, J. S. van Duijneveldt, P. Bartlett, *Phys. Rev. Lett.* **94**, 208301 (2005).
7. F. Sciortino, P. Tartaglia, E. Zaccarelli, *J. Phys. Chem. B* **109**, 21942 (2005).
8. J. Groenewold, W. K. Kegel, *J. Phys. Chem. B* **105**, 11702 (2001).
9. S. A. Safran, *Statistical Thermodynamics of Surfaces, Interfaces, and Membranes* (Addison-Wesley, Reading, MA, 1994).
10. I. A. Nyrkova, A. N. Semenov, *Macromol. Theory Simul.* **14**, 569 (2005).
11. S. Jain, F. S. Bates, *Science* **300**, 460 (2003).
12. S. C. Glotzer, M. J. Solomon, *Nat. Mater.* **6**, 557 (2007).
13. F. Sciortino, A. Giacometti, G. Pastore, *Phys. Rev. Lett.* **103**, 237801 (2009).

14. W. L. Miller, A. Cacciuto, *Phys. Rev. E* **80**, 021404 (2009).
15. S. Whitelam, S. A. F. Bon, *J. Chem. Phys.* **132**, 074901 (2010).
16. K. Liu *et al.*, *Science* **329**, 197 (2010).
17. Z. Mao, H. Xu, D. Wang, *Adv. Funct. Mater.* **20**, 1053 (2010).
18. L. Hong, A. Cacciuto, E. Luijten, S. Granick, *Langmuir* **24**, 621 (2008).
19. J. W. Goodwin, *Colloids and Interfaces with Surfactants and Polymers* (Wiley, Chichester, UK, ed. 2, 2009), pp. 163–181.
20. See supporting material on *Science* Online.
21. J. Mikosch *et al.*, *Science* **319**, 183 (2008).
22. A. H. Boerdijk, *Philips Res. Rep.* **7**, 303 (1952).
23. H. Dai, *Surf. Sci.* **500**, 218 (2002).
24. We thank J. Yan for discussions. Supported by the U.S. Department of Energy (S.G., Q.C., S.J.); Division of Materials Science, under award DE-FG02-07ER46471 through the Frederick Seitz Materials Research Laboratory at the University of Illinois at Urbana-Champaign (to S.G.); and by NSF grants CBET-0853737 (S.C.B.) and DMR-0346914 and DMR-1006430 (J.K.W. and E.L., to E.L.).

Supporting Online Material

www.sciencemag.org/cgi/content/full/331/6014/199/DC1
Materials and Methods
Figs. S1 to S3
Movies S1 to S6
References

7 September 2010; accepted 9 December 2010
10.1126/science.1197451

The Deglacial Evolution of North Atlantic Deep Convection

David J. R. Thornalley,[1,2]* Stephen Barker,[1] Wallace S. Broecker,[3] Henry Elderfield,[2] I. Nick McCave[2]

Deepwater formation in the North Atlantic by open-ocean convection is an essential component of the overturning circulation of the Atlantic Ocean, which helps regulate global climate. We use water-column radiocarbon reconstructions to examine changes in northeast Atlantic convection since the Last Glacial Maximum. During cold intervals, we infer a reduction in open-ocean convection and an associated incursion of an extremely radiocarbon (^{14}C)–depleted water mass, interpreted to be Antarctic Intermediate Water. Comparing the timing of deep convection changes in the northeast and northwest Atlantic, we suggest that, despite a strong control on Greenland temperature by northeast Atlantic convection, reduced open-ocean convection in both the northwest and northeast Atlantic is necessary to account for contemporaneous perturbations in atmospheric circulation.

Vertical density gradients within the global ocean limit the exchange of surface and deep waters. Only in a limited number of locations, characterized by weak stratification of the water column and intense surface buoyancy losses, can surface water be converted into deep water by open-ocean convection (*1*). Through its control on deepwater formation, open-ocean convection sets the properties of the deep global ocean and forms an essential component of the global overturning circulation (*1*).

Open-ocean deep convection in the North Atlantic occurs in the Labrador and Greenland Seas (*1*), transforming well-ventilated, nutrient-poor surface waters into North Atlantic Deep Water (NADW), which spreads southward to occupy much of the deep Atlantic. Paleoceanographic studies suggest that deep convection in the North Atlantic was altered during the last ice age as compared with today [e.g., (*2*, *3*)]. Glacial convection was shallower, forming Glacial North Atlantic Intermediate Water (GNAIW), and possibly weaker, leading to poorer ventilation of the deep Atlantic. Rapid fluctuations between weak and strong modes of deep convection could also be linked with abrupt climate changes across the North Atlantic region because of the associated changes in the poleward flux of warm surface waters. Furthermore, mode switches in deep convection might be triggered by changes in the input of fresh water, with the Younger Dryas (YD)

[1]School of Earth and Ocean Sciences, Cardiff University, Cardiff, CF10 3YE, UK. [2]The Godwin Laboratory for Palaeoclimate Research, Department of Earth Sciences, University of Cambridge, Cambridge, CB2 3EQ, UK. [3]Lamont-Doherty Earth Observatory of Columbia University, Palisades, NY 10964–8000, USA.

*To whom correspondence should be addressed. E-mail: d.thornalley@cantab.net

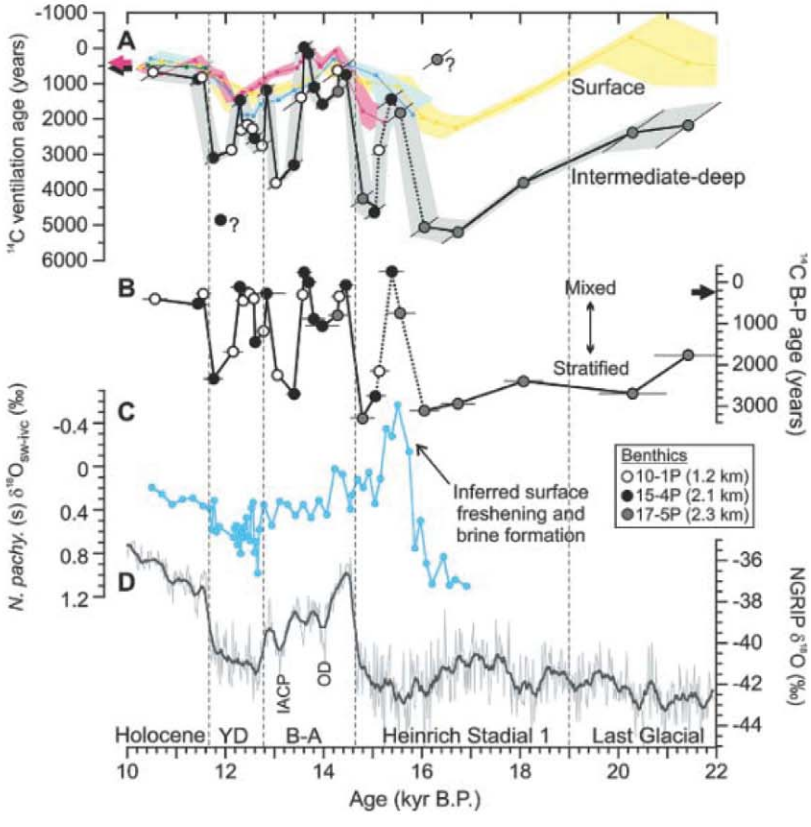

Fig. 1. (**A**) Surface and intermediate/deep ocean ^{14}C ventilation ages, with estimated uncertainty. Surface ocean estimates are from planktic foraminifera samples picked from the sediment cores: 12-1K, green line; 10-1P, blue line; 15-4P, red line; 17-5P, yellow line. Modern ventilation ages for the surface ocean and NADW are shown by the red and black arrow, respectively. Anomalous benthic ^{14}C dates are indicated by question marks. The date at 12 ka may contain reworked material because it is taken from within the Vedde Ash layer, the base of which consists of a basaltic turbidite. The anomalously young benthic ^{14}C date at 16.3 ka suggests contamination by modern carbon; we cannot, however reject this date with certainty, and it is possible that the young age is indicative of a brief interval of local convection, likely brine-induced. (**B**) Benthic-planktic foraminifera ^{14}C difference. Black arrow, modern surface-to-deep ^{14}C age difference. Dashed line in (A) and (B) indicates an interval of inferred local brine-induced convection. (**C**) Reconstructed surface seawater δ^{18}O, corrected for global ice-volume changes, based on *N. pachyderma* (s) Mg/Ca-δ^{18}O in 10-1P (*22*). (**D**) NGRIP δ^{18}O (*11*).

cold reversal being the archetypal example [e.g., (*4*)]. Yet there is growing evidence that the YD may be part of an intrinsic oscillation associated with deglaciation, rather than peculiar to the last termination [e.g., (*5*, *6*)]. To test these hypotheses, we require precise constraints on the timing (and rate) of deep convection changes relative to abrupt climate events and freshwater perturbations.

High-resolution evidence for past North Atlantic mode changes has come primarily from stable isotope and nutrient proxy records [e.g., (*2*, *7*)]. However, these proxies are complicated by biological processes and isotopic fractionation during air-sea gas exchange, which may overprint variations caused by water mass changes. Here, we reconstruct seawater ^{14}C activities to investigate past changes in deep convection. Our results suggest extremely large variations in water column ventilation and substantial differences compared to the mid-latitude northwest (NW) Atlantic (*8*), allowing us to assess the relative role of northeast (NE) and NW Atlantic convection changes on deglacial climate.

Radiocarbon (^{14}C) is produced in the upper atmosphere by cosmogenic interaction with nitrogen and is taken up by the ocean through air-sea gas exchange. After equilibration with the atmosphere, the radioactive decay of ^{14}C to ^{12}C allows determination of the apparent time elapsed since a water mass was last in equilibrium with the atmosphere (^{14}C ventilation age). Because of mixing with "older" underlying water, the modern average ventilation age, or reservoir age, for tropical and North Atlantic surface waters is ~400 years (*9*). Modern deep convection in the North Atlantic quickly transfers surface waters to depth, forming well-ventilated NADW and resulting in a minimal surface-to-deep gradient in ^{14}C. [Newly formed NADW has a ventilation age of ~500 years, just 100 years older than surface waters (*9*)].

To reconstruct past surface and intermediate/deep (I/D) water ^{14}C ventilation ages in the NE Atlantic, we measured planktic and benthic foraminifera $^{14}C/^{12}C$ ratios from four sediment cores located on the South Iceland Rise (spanning a range of water depths from 1237 to 2303 m), adjacent to the modern open-ocean deep convection site of the Greenland Sea and directly under the overflow path of recently formed deep water [Iceland-Scotland Overflow Water (ISOW)]. Independent age models for the cores (*10*) were constructed by correlating Icelandic tephra layers and abrupt changes in the abundance of polar foraminifera, *Neogloboquadrina pachyderma* sinistral (indicative of cooling/warming) with equivalent events in the annual-layer–counted North Greenland Ice Core Project (NGRIP) (*11*) [see Supporting Online Material (SOM)]. The original radiocarbon content ($\Delta^{14}C$) of the ambient water masses were determined by correcting for the radioactive decay of ^{14}C since deposition. These values were then compared with the $\Delta^{14}C$ of the contemporaneous atmosphere (*12*) to yield ^{14}C ventilation ages (equivalent to reservoir ages for the surface ocean) (Fig. 1).

Deglacial I/D ventilation ages from all cores show similar trends throughout the deglaciation. I/D ^{14}C ventilation ages alternated rapidly (within ~100 to 200 years) between close-to-modern values (500 years or less) and extremely old ages (3000 to 5200 years), reflecting abrupt changes in deep convection during this period. In general, young I/D ventilation ages are seen during warm intervals [e.g., the Bølling-Allerød (B-A) and early Holocene] and reflect the rapid transfer of equilibrated surface waters to depth, similar to today's ocean. However, the occurrence of extremely ^{14}C-depleted waters between 1.2 and 2.3 km during cold intervals [e.g., Heinrich stadial 1 (HS1), the Intra-Allerød Cold Period (IACP), and YD] demands not only a shoaling of convection but also the incursion of a very depleted water mass that must already have been in existence.

During the last glacial period, dissolved inorganic carbon (DIC) is thought to have accumulated in the deep Southern Ocean (*13*). Correspondingly, glacial ^{14}C ventilation age estimates (with respect to the atmosphere) of up to ~4000 years have been reported from there (*14*). During deglaciation, intervals of reduced NADW formation (e.g., HS1 and the YD) (*7*) have been linked to enhanced vertical mixing within the Southern Ocean (*15*, *16*). Crucially, the formation of Antarctic Intermediate Water (AAIW) along the northern margin of the Southern Ocean could have allowed the northward migration of these DIC rich and ^{14}C-depleted waters via the surface Southern Ocean to intermediate waters of the global ocean. So far, such a migration has been invoked for the Pacific and Indian Oceans (*17*, *18*), although we note that this is a topic under current debate and that further work investigating the properties of deglacial AAIW throughout the global ocean is warranted (see SOM). Here, we argue that the influence of ^{14}C-depleted AAIW reached as far north as ~60°N in the North Atlantic.

Today, the influence of AAIW reaches 20 to 30°N in the Atlantic Ocean (*9*). A recent study, using Nd isotopes as a water mass tracer, suggested that penetration of AAIW into the Atlantic was enhanced during HS1 and the YD (*19*), and low-resolution $\delta^{13}C$-Cd/Ca data (*20*) hint that AAIW occasionally reached 60°N during cold intervals. Because of the Coriolis effect, NADW/GNAIW are concentrated into western boundary currents, causing the eastern basins of the North Atlantic to be subject to a greater influence of southern source I/D water than the western basins. Our benthic ^{14}C results reflect the incursion of extremely depleted AAIW to at least 60°N during cold intervals of the deglacial period. At these times, local deep convection decreased dramatically, allowing the buildup of extremely poorly ventilated I/D waters. Modeling studies [e.g., (*21*)] have demonstrated that, depending on their respective densities, AAIW may compete with NADW/GNAIW for occupation of the Atlantic between ~1- and 2.5-km depth. When

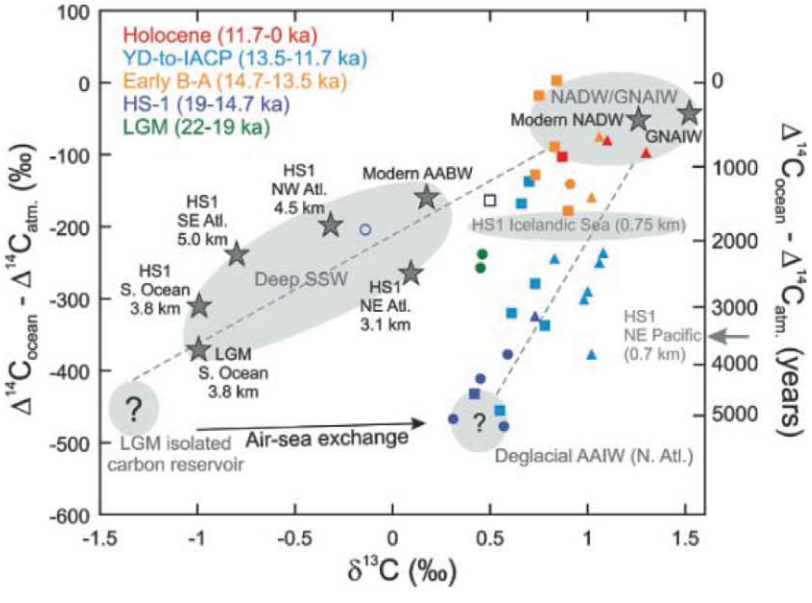

Fig. 2. Comparison of benthic $\delta^{13}C$ and ventilation age ($\Delta^{14}C$ offset from the contemporaneous atmosphere). No correction has been applied for the whole ocean glacial-interglacial shift in $\delta^{13}C$. Colored symbols, South Iceland Rise data; triangles, 10-1P (1237 m); squares, 15-4P (2133 m); circles, 17-5P (2303 m); open symbols indicate local brine-influenced convection during HS1. South Iceland Rise benthic $\delta^{13}C$ data (*10*); modern end-member values (*9*); GNAIW from the Denmark Strait (*3*, *25*); HS1 SE Atlantic (*13*, *26*); Last Glacial Maximum (LGM) and HS1 Southern Ocean (*16*, *27*); HS1 NE Atlantic (*28*); HS1 NW Atlantic (*8*, *29*); HS1 NE Pacific (*17*); HS1 Icelandic Sea (*3*, *25*). Large changes in the isotopic composition of seawater can occur during degassing of CO_2 from seawater to the atmosphere because CO_2 (aqueous) has an equilibrium isotopic offset from the bulk solution ($\Sigma CO2$) of ~10 per mil (‰) for $\delta^{13}C$ and ~20‰ for $\delta^{14}C$ (*30*). For a ΣCO_2 of ~2200 μmol/kg, the removal of 220 μmol/kg (10%), causes a positive shift of ~1 ‰ in $\delta^{13}C$ and ~2 ‰ shift in $\delta^{14}C$, the latter being negligible in comparison to typical ocean values of several tens to hundreds per mil. Additional kinetic fractionation effects may also contribute toward an enrichment of the residual phase (seawater) in ^{13}C and ^{14}C (*30*).

surface water at AAIW formation sites attains a density greater than that found at the deep convection sites in the North Atlantic (thereby crossing a threshold), NADW formation will decrease, AAIW formation will increase, and vice versa. In this manner, rapid fluctuations in the dominance of AAIW or NADW/GNAIW can occur.

Combining benthic $\delta^{13}C$ with our $\Delta^{14}C$ evidence from the South Iceland Rise also supports our assertion that the most ^{14}C-depleted water influencing our site was AAIW (Fig. 2). Plotting benthic $\delta^{13}C$ versus $\Delta^{14}C$, our measurements form a separate trend to that formed by measurements from sites influenced by deep Southern Source Water (SSW), with our data likely recording the influence of air-sea exchange processes associated with the formation of AAIW. Moreover, our reconstructed I/D ocean ventilation ages south of Iceland (up to ~5200 years) suggest that current estimates of the ventilation age of the glacial deep Southern Ocean (*14*) provide only a lower limit for the isolated carbon (Fig. 2).

An alternative source for the ^{14}C-depleted water observed south of Iceland during cold intervals may be the deep Nordic Seas and Arctic Ocean, possibly caused by brines flushing out deep waters. However, it is difficult to reconcile this hypothesis with our current knowledge of the region. We do not observe a consistent relationship between the timing of our ^{14}C-depleted benthic ventilation ages and Nordic Seas overflow, which has a distinctive low $\delta^{18}O$ signal during HS1 (attributed to brine formation processes) (*2*, *10*). Rather, we observe better ventilated I/D water during inferred peak brine formation at 15 to 16 thousand years ago (ka) (Fig. 1 and fig. S8). Furthermore, if the Nordic Seas were well ventilated during the Bølling, as is widely accepted, it cannot be the source for the 3000- to 4000-year-old water observed south of Iceland during the IACP because there was insufficient time for in situ decay of deep water in the Nordic Seas.

We compare our deglacial I/D ocean ventilation age estimates with other high-resolution reconstructions of Atlantic circulation and climate in Fig. 3. Increased ventilation ages and inferred incursions of AAIW to the NE Atlantic occurred during Northern Hemisphere cold intervals [HS1, Older Dryas (OD), IACP, and YD], which are associated with warming in the Southern Hemisphere via the bipolar seesaw mechanism (Fig. 3) [e.g., (*21*)]. There are two notable exceptions to this coupling between NE Atlantic ventilation and Greenland climate.

First, at ~15.9 to 15.2 ka, improved I/D ocean ventilation south of Iceland is not observed in other Atlantic records (Fig. 3). This ventilation event occurs during a pronounced minimum in seawater $\delta^{18}O$ recorded in *N. pachyderma* (sinistral) (Fig. 1), indicating surface freshening and/or sea-ice formation and brine rejection (*22*). Minima in benthic $\delta^{18}O$ records from south of Iceland and the Nordic Seas also occur during this interval, strongly suggesting that local convection occurred via sea-ice formation and brine rejection, which transferred better ventilated surface water (with low seawater $\delta^{18}O$ values) to the I/D ocean [e.g., (*2*, *10*)] (Fig. 1 and fig. S8).

Second, while poorer I/D ocean ventilation in the NE Atlantic occurred both at the onset (~12.8 to 12.6 ka) and culmination (~12.2 to 11.7 ka) of the YD, the mid-YD (~12.6 to 12.2 ka) was characterized by a well-mixed water column on the South Iceland Rise. It is possible that a decrease in freshwater input to the NE Atlantic during the mid-YD (*22*) reduced surface stratification and facilitated overturning of the water column close to Iceland, aided by coastal upwelling and interaction with seafloor topography. During the mid-YD, I/D ocean ventilation ages were reduced but surface ventilation ages were increased, suggesting that overturning of the water column south of Iceland involved upwelling of ^{14}C-depleted AAIW to the (near) surface ocean.

The large amplitude and abrupt changes recorded in benthic ^{14}C south of Iceland allow us to constrain the timing of convection changes in the NE Atlantic relative to deglacial climate events. A long-standing view of Northern Hemisphere deglaciation has been that the strong resumption of deep convection in the North Atlantic during the B-A was interrupted by a freshwater rerouting or flood event, which reduced convection and triggered the YD cold reversal (*4*). In contrast to this paradigm, our I/D ocean ventilation results show that after the vigorous convection of the early B-A (see SOM), there was a shutdown in open-ocean deep convection in the high-latitude NE Atlantic for a sustained interval beginning ~600 years before the onset of the YD, that is, during the IACP. The occurrence of an earlier shutdown in deep convection in the NE Atlantic before the YD suggests that in terms of NE Atlantic convection, the YD was not a unique event during the deglaciation. Instead, the amplified circulation associated with the Bølling warming was probably a transient feature of deglaciation, and the stability of deep convection in the NE Atlantic gradually weakened throughout the B-A, with

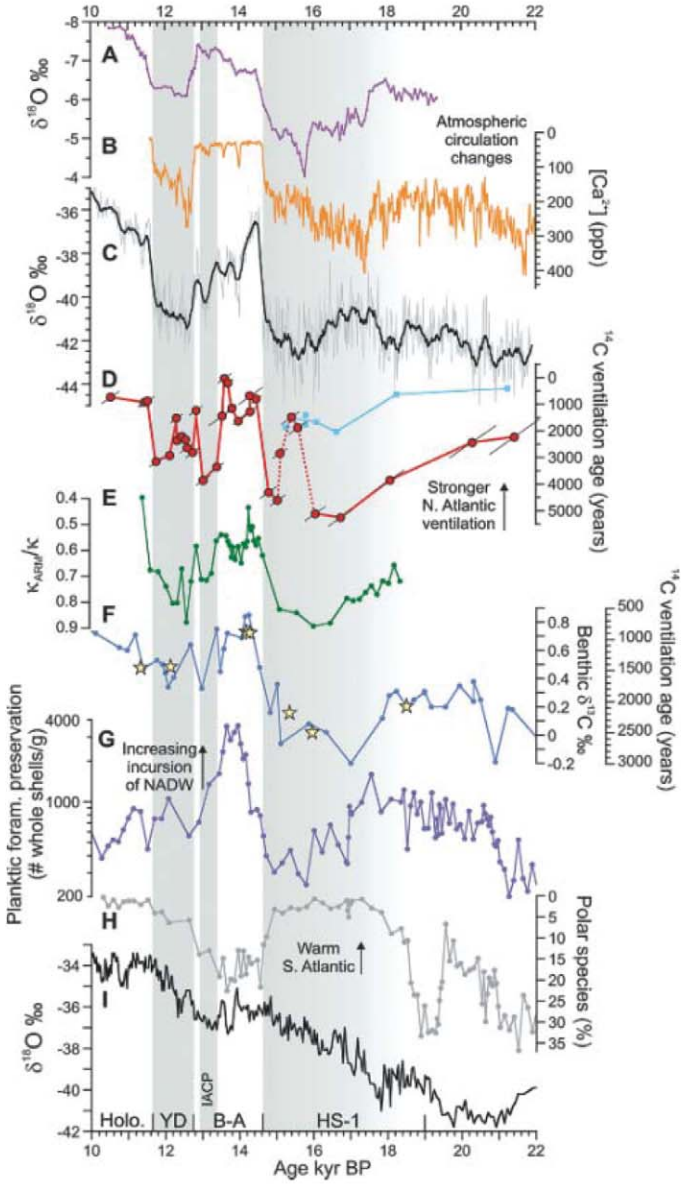

Fig. 3. Comparison of the timing of deep convection changes in the NE Atlantic to other Atlantic Ocean and climate records. (**A**) Hulu Cave (speleothem PD) $\delta^{18}O$ proxy for migration of the intertropical convergence zone (*31*). (**B**) NGRIP $[Ca^{2+}]$ proxy for atmosphere circulation changes (*11*). (**C**) NGRIP $\delta^{18}O$ (Greenland) (*11*). (**D**) South Iceland Rise benthic ^{14}C ventilation ages (red) and the Icelandic Seas at 0.6-km depth (*3*). (**E**) Eirik drift (1.9 km, NW Atlantic) flow speed proxy (magnetic mineral grain size) (*32*). (**F**) Iberian margin (3.1 km, NE Atlantic) benthic $\delta^{13}C$ (*28*) and radiocarbon ventilation ages (yellow stars) (*14*, *28*). (**G** and **H**) Cape basin (5.0 km South Atlantic) foraminifera preservation as a proxy for incursions of high $[CO_3^{2-}]$ NADW (*26*) (G), and the abundance of polar planktic foraminifera (*16*) (H). (**I**) Byrd $\delta^{18}O$ (Antarctica) (*33*).

intervals of vigorous deep convection being punctuated by several freshwater events [e.g., (*22*)]. This interpretation is consistent with the recent recognition of "YD equivalents" during earlier terminations of the Late Pleistocene (*5*, *6*).

The shutdown of deep convection in the NE Atlantic during the IACP contrasts with less pronounced changes in I/D ocean ventilation in the NW Atlantic, which monitors the combined deep waters formed by convection in both the NE and NW Atlantic (Fig. 3 and 4). Therefore, continued open-ocean convection in the Irminger and/or Labrador Sea (*2*) was probably sustained throughout the IACP but weakened substantially during the YD (*8*).

The observed difference in North Atlantic convection between the IACP (weakened NE convection) and the YD (weakened NE and NW convection) allows us to examine the broader climate implications for regional differences in convection in the North Atlantic. Cooling over Greenland is inferred for both the IACP and YD (Fig. 3C), and because model studies (*23*) indicate that Greenland ice core $\delta^{18}O$ is largely controlled by sea-ice cover in the Nordic Seas (but relatively insensitive to NW Atlantic ice cover), it is very likely that these cold events were caused by decreased NE Atlantic convection and an associated increase in sea-ice cover over the Nordic Seas. In contrast, atmospheric circulation proxies (Fig. 3, B and C) indicate only a modest change during the IACP, whereas a much larger shift occurs at the onset of the YD. It therefore seems, that, although NE Atlantic convection was crucial for determining conditions within the NE Atlantic and over Greenland, it was only with further weakening of North Atlantic convection (i.e., by reducing deep convection within the NW Atlantic) that the major atmospheric circulation changes of the YD were achieved.

Regional differences in convection and sea-ice coverage may also be implicated in the two-fold division of the "Mystery Interval" (17.5 to 14.5 ka), which has been attributed to a shift in atmospheric circulation patterns at ~16 ka (*24*). Reconstructions suggest that there was enhanced freshwater discharge from the Laurentide ice sheet into the NW Atlantic and increased sea-ice cover at ~16 to 17.5 ka, which was followed by a later input of fresh water into the NE Atlantic from proximal ice sheets at ~15 to 16 ka, with an inferred increase in sea-ice and brine formation (*22*). This change in freshwater input and sea-ice cover at ~16 ka may be related to the contemporaneous atmospheric circulation shift.

In this study, we have demonstrated that the deglacial NE Atlantic underwent abrupt decreases in deep convection that were associated with the incursion of an extremely ^{14}C-depleted water mass, interpreted to be AAIW. Major differences in the convective activity of the NE versus the NW Atlantic have been revealed. Of particular note is the strong reduction in NE Atlantic convection for a sustained interval (i.e., during the IACP) beginning ~600 years before the onset of the YD. We have suggested that differences in the timing of changes in open-ocean convection and sea-ice coverage between the NE and NW Atlantic may be an important control on atmospheric circulation and, therefore, further investigation into the nature of the atmospheric reorganizations associated with this heterogeneity is warranted.

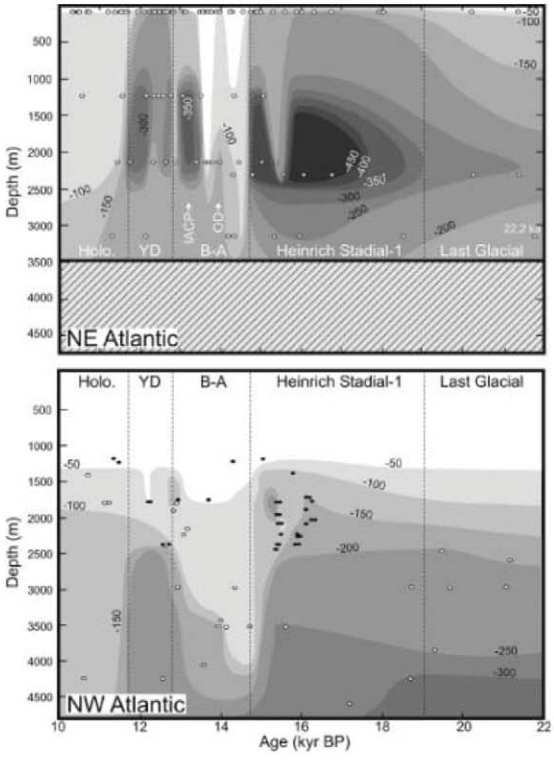

Fig. 4. Cartoon contour plots for the ventilation age (expressed as $\Delta^{14}C$ offset from the atmosphere in ‰) for the NE Atlantic and mid-latitude NW Atlantic (*8*). Data for the NE Atlantic from 3.1-km depth is from the Iberian margin (*14*). Closed circles, coral data; open circles, foraminifera data. (Foraminifera data from the NW Atlantic assume a constant surface reservoir age of 400 years.) Darker shading, poorly ventilated water; lighter shading, better ventilated water.

References and Notes

1. J. Marshall, F. Schott, *Rev. Geophys.* **37**, 1 (1999).
2. M. S. Sarnthein *et al.*, in *The Northern North Atlantic: A Changing Environment,* P. R. Schafer, W. Schluter, J. Thiede, Eds. (Springer, Berlin, 2000), pp. 365–410.
3. M. Sarnthein, P. Grootes, J. Kennett, M.-J. Nadeau, *Geophys. Monogr. Ser.* **173**, 175 (2007).
4. W. S. Broecker *et al.*, *Nature* **341**, 318 (1989).
5. W. S. Broecker *et al.*, *Quat. Sci. Rev.* **29**, 1078 (2010).
6. M. Sarnthein, R. Tiedemann, *Paleoceanography* **5**, 1041 (1990).
7. T. Marchitto, W. Curry, D. Oppo, *Nature* **393**, 557 (1998).
8. L. F. Robinson *et al.*, *Science* **310**, 1469 (2005).
9. W. S. Broecker, T. H. Peng, *Tracers in the Sea* (Eldigio Press, Palisades, NY, 1982).
10. D. J. R. Thornalley, H. Elderfield, I. N. McCave, *Paleoceanography* **25**, PA1211 (2010).
11. S. O. Rasmussen *et al.*, *J. Geophys. Res.* **111** (D6), D06102 (2006).
12. P. J. Reimer *et al.*, *Radiocarbon* **51**, 1111 (2009).
13. D. A. Hodell *et al.*, *Geochem. Geophys. Geosyst.* **4**, 1004 (2003).
14. L. C. Skinner, S. Fallon, C. Waelbroeck, E. Michel, S. Barker, *Science* **328**, 1147 (2010).
15. R. F. Anderson *et al.*, *Science* **323**, 1443 (2009).
16. S. Barker *et al.*, *Nature* **457**, 1097 (2009).
17. T. M. Marchitto, S. J. Lehman, J. D. Ortiz, J. Fluckiger, A. van Geen, *Science* **316**, 1456 (2007).
18. S. Bryan, T. Marchitto, S. Lehman, *Earth Planet. Sci. Lett.* **298**, 244 (2010).
19. K. Pahnke, S. L. Goldstein, S. R. Hemming, *Nat. Geosci.* **1**, 870 (2008).
20. R. E. M. Rickaby, H. Elderfield, *Geochem. Geophys. Geosyst.* **6**, Q05001 (2005).
21. R. Keeling, B. Stephens, *Paleoceanography* **16**, 112 (2001).
22. D.J.R. Thornalley, H. Elderfield, I. N. McCave, *Glob. Planet. Change* (2010), 10.1016/j.gloplacha.2010.06.003.
23. C. Li, D. S. Battisti, C. Bitz, *J. Clim.* (2010).
24. W. S. Broecker *et al.*, *Quat. Sci. Rev.* **28**, 2557 (2009).
25. C. Millo, M. Sarnthein, A. Voelker, H. Erlenkeuser, *Boreas* **35**, 50 (2006).
26. S. Barker, G. Knorr, M. J. Vautravers, P. Diz, L. C. Skinner, *Nat. Geosci.* **3**, 567 (2010).
27. N. Vázquez Riveiros *et al.*, *Earth Planet. Sci. Lett.* **298**, 323 (2010).
28. L. C. Skinner, N. J. Shackleton, *Paleoceanography* **19**, PA2005 (2004).
29. L. D. Keigwin, G. A. Jones, S. J. Lehman, E. A. Boyle, *J. Geophys. Res.* **96** (C9), 16,811 (1991).
30. J. Lynch-Stieglitz, T. F. Stocker, W. S. Broecker, R. G. Fairbanks, *Global Biogeochem. Cycles* **9**, 653 (1995).
31. Y. J. Wang *et al.*, *Science* **294**, 2345 (2001).
32. J. D. Stanford *et al.*, *Paleoceanography* **21**, PA4103 (2006).
33. T. Blunier, E. J. Brook, *Science* **291**, 109 (2001).

34. We thank L. Booth for help in picking planktic ^{14}C dates. D.T. thanks S. Bryan, I. Hall, L. Keigwin, G. Knorr, T. Marchitto, and L. Skinner for useful discussions. Radiocarbon dates were analyzed by Natural Environment Research Council (NERC, UK) and National Ocean Sciences Accelerator Mass Spectrometry (NOSAMS, USA) facilities. This work was funded by NERC grants NER/T/S/2002/00436 and NE/F002734/1 and National Science Foundation grant OCE 04-35703.

Supporting Online Material

www.sciencemag.org/cgi/content/full/331/6014/202/DC1
Materials and Methods
SOM Text
Figs. S1 to S8
Tables S1 to S3
References

23 August 2010; accepted 29 November 2010
10.1126/science.1196812

A Basal Dinosaur from the Dawn of the Dinosaur Era in Southwestern Pangaea

Ricardo N. Martinez,[1] Paul C. Sereno,[2]* Oscar A. Alcober,[1] Carina E. Colombi,[1,3] Paul R. Renne,[4,5] Isabel P. Montañez,[6] Brian S. Currie[7]

Upper Triassic rocks in northwestern Argentina preserve the most complete record of dinosaurs before their rise to dominance in the Early Jurassic. Here, we describe a previously unidentified basal theropod, reassess its contemporary *Eoraptor* as a basal sauropodomorph, divide the faunal record of the Ischigualasto Formation with biozones, and bracket the formation with $^{40}Ar/^{39}Ar$ ages. Some 230 million years ago in the Late Triassic (mid Carnian), the earliest dinosaurs were the dominant terrestrial carnivores and small herbivores in southwestern Pangaea. The extinction of nondinosaurian herbivores is sequential and is not linked to an increase in dinosaurian diversity, which weakens the predominant scenario for dinosaurian ascendancy as opportunistic replacement.

An arid valley in northeastern Argentina called Ischigualasto contains a well-exposed fossiliferous Upper Triassic section from the dawn of the dinosaur era. Some 50 years of intensive collecting have yielded nearly complete skeletons of the basal dinosaurs, *Eoraptor* (Fig. 1A) and *Herrerasaurus* (*1*, *2*), and hundreds of additional fossil vertebrates. Recent finds include several previously unidentified dinosaurs based on partial skeletons (*3*–*5*), and recent geologic work has detailed stratigraphic and paleoclimatic variation across the formation (*6*).

We describe here a nearly complete basal dinosaur, *Eodromaeus murphi* nov. gen. nov. sp. (*7*, *8*), which helps to reveal skeletal form and function at the root of Theropoda, a clade that includes all predatory dinosaurs (Fig. 2A) (*9*). The skull is relatively low and lightly built with a relatively spacious antorbital fenestra, which is emarginated anteriorly by a relatively broad antorbital fossa (Fig. 1B). On the snout, an accessory pneumatic opening, the promaxillary fenestra, is present near the anterior margin of the antorbital fossa (specimen number PVSJ 560) (Fig. 1B). The promaxillary fenestra is present in the basal theropod *Herrerasaurus* (*10*) and in most later theropods, although it is secondarily closed in the early North American theropod *Tawa* and some coelophysoids (*11*, *12*). The premaxilla-maxilla suture is long and akinetic, and the jugal ramus under the orbit is shallow (Fig. 1B). The sidewall and ventral aspects of the braincase are marked by well-defined tympanic and basisphenoid recesses, respectively, and the basipterygoid processes are transversely compressed (Fig. 1C). In the lower jaw, the dentary is slender, and the retroarticular process is well developed posteriorly (Fig. 1B).

There are 4 premaxillary and 11 maxillary teeth, which are separated medially by interdental plates. All crowns are laterally compressed, recurved, and very finely serrated mesially and distally (nine serrations per millimeter), unlike the more numerous maxillary teeth in *Eoraptor*, which have larger denticles, less recurvature, and a constriction at the base of the crown (Fig. 1, D and E). Anterior maxillary crowns are caniniform, their ventral reach increased by a ventrally convex alveolar margin (Fig. 1, B and E). Dentary teeth, on the other hand, are relatively uniform in size, and the first tooth is located at the anterior tip of the dentary, unlike the condition in *Eoraptor* (Fig. 1, A and B). A row of very small rudimentary teeth crosses the palatal ramus of the pterygoid in *Eodromaeus* (PVSJ 560), as in *Eoraptor*, the only dinosaurs known to retain palatal teeth.

The cervical column is composed of proatlantal neural arches followed by 10 cervical vertebrae. Cervical vertebrae have spool-shaped centra that are more elongate than in *Eoraptor*; many centra have lengths more than three times the centrum diameter (Fig. 2, A and B). Cervical vertebrae have a low ventral keel and projecting epipophyseal processes. Invaginated pleurocoels are present in posterior cervicals, indicative of the presence of pneumatic invasion by parasagittal cervical air sacs (Fig. 2B). The pleurocoels open posteriorly into a lateral groove, which is present in most other vertebrae in the axial column. Thus, the cervical air sac system may have extended into the trunk, unlike in extant avians. There are 14 dorsal vertebrae in the trunk, the posterior of which are stabilized by hyposphene-hypantrum articulations (Fig. 2D). There appear to be three sacral vertebrae—a dorsosacral followed by two primordial sacrals with robust ribs—although the dorsosacral rib is not preserved in articulation. The elongate tail, which is composed of ~45 caudal vertebrae, has long anterior chevrons (Fig. 2A). Mid and distal caudal centra are cylindrical and have elongate prezygapophyses (Fig. 2, A and E).

Table 1. Skull and long-bone lengths (in millimeters, upper portion of table) and proportions (in percent, lower portion) of *Eodromaeus murphi*, *Eoraptor lunensis*, and other basal dinosaurs (*32*, *33*). Parentheses indicate estimate. Skull length is measured from the anterior tip of the premaxilla to the posterior extremity of the occipital condyle. Measurements average long-bone lengths when both sides are available.

Measure or ratio	*Eodromaeus* PVSJ 562	*Herrerasaurus* PVSJ 373	*Eoraptor* PVSJ 512	*Heterodontosaurus* SAM-PK-K337
Skull*	(120)	282‖	114	115
Humerus	85	(175)	85	83
Radius	64	153	63	58
Metacarpal 3	28	62	21	22
Femur	160	345	152	112
Tibia	165	315	156	145
Metatarsal 3	(100)§	165	81	68
Humerus/forelimb†	48%	45%	50%	51%
Radius/forelimb	36%	39%	37%	36%
Metacarpal 3/forelimb	16%	16%	12%	14%
Tibia/femur	106%¶	91%	103%	130%
Femur/hind limb‡	38%	42%	39%	35%
Tibia/hind limb	39%	38%	40%	45%
Metatarsal 3/hind limb	24%	20%	21%	21%
Humerus/femur	53%	51%	56%	74%
Forelimb/hind limb	42%	47%	43%	50%

*Skull length was measured between the anterior tip of the premaxilla and posterior extremity of the occipital condyle. †Forelimb length equals the sum of the lengths of the humerus, radius, and metacarpal 3. ‡Hind-limb length equals sum of the femur, tibia, and metatarsal 3 lengths. §Metatarsal 3 is not preserved in PVSJ 562. In PVSJ 560, the distal end is missing; the length estimate is based on a comparison to digit I (plus 10% to account for the size differential for the major long bones of the hind limb). ‖Skull length is based on the comparably sized specimen PVSJ 407, because the skull is not preserved in PVSJ 373. ¶Average of 103 and 109%, based on PVSJ 560 and 562, respectively.

[1]Instituto y Museo de Ciencias Naturales, Universidad Nacional de San Juan, San Juan 5400, Argentina. [2]Department of Organismal Biology and Anatomy and Committee of Evolutionary Biology, University of Chicago, Chicago, IL 60637, USA. [3]Consejo Nacional de Investigaciones Científicas y Técnicas, Buenos Aires, Argentina. [4]Berkeley Geochronology Center, 2455 Ridge Road, Berkeley, CA 94709, USA. [5]Department of Earth and Planetary Science, University of California, Berkeley, CA 94720, USA. [6]Department of Geology, University of California, Davis, CA 95616, USA. [7]Department of Geology, Miami University, Oxford, OH 45056, USA.

*To whom correspondence should be addressed. E-mail: dinosaur@uchicago.edu

In the pectoral girdle, the coracoid has deep proportions with a relatively short posterior process, and the scapula has a relatively narrow neck between a prominent acromial process and a distally expanded blade (Fig. 2C). The straight-shafted humerus has a broad proximal end, a subrectangular deltopectoral crest, and a distal end with a hemispherical radial condyle (Fig. 2F). The ulna and radius have shafts in close contact, the former with a prominent olecranon process unlike the condition in *Eoraptor* (Fig. 2G). The well-ossified carpus is composed of a radiale, ulnare, centrale, and four distal carpals (Fig. 1G). There are five manual digits with a phalangeal formula of 2-3-4-1-1 (Fig. 1G). The manus has a pronounced lateral metacarpal arch, distal extensor depressions on metacarpals 1 to 3, and elongate penultimate phalanges on digits I to III.

In the pelvic girdle, the preacetabular process is proportionately deep, and the postacetabular process has an arched brevis fossa (Fig. 1A). The pubic blades taper distally, where a small parasagittal pubic foot is located (Fig. 2H). Proximally, the femur has a dorsally projecting anterior trochanter and trochanteric shelf (Fig. 2, K and L). Distally, the end of the femur is marked by a broad rugose depression for femoral extensor musculature (Fig. 2M). The tibia is slightly longer than the femur, which, like other intra- and interlimb proportions, is similar to that in *Eoraptor* (Table 1). The fibula has a raised scar proximally for strong ligamentous attachment to the tibia (Fig. 2I). The astragalus has a rectangular medial margin and a wedge-shaped ascending process, and the calcaneum retains a prong-shaped posterior heel (Fig. 2J).

Phylogenetic analysis of basal dinosaurs positions the contemporaneous and similar-sized *Eodromaeus* and *Eoraptor* at the base of Theropoda and Sauropodomorpha, respectively (Fig. 3) (*8*). Basal theropod status for *Eodromaeus* is supported by a suite of derived attributes in the skull (promaxillary fenestra, basisphenoid fossa), axial skeleton (cervical pleurocoels, elongate caudal prezygapophyses), forelimb (radioulnar shaft apposition, elongate penultimate phalanges), pelvic girdle (distally tapering pubic blade, pubic foot), and hind limb (femoral extensor depression, tibial crest for fibula) (*8*). Whereas herrerasaurids appear to be more basal in position among theropods (Fig. 3), *Eodromaeus* is only marginally more derived, has few specializations (autapomorphies) (*8*), and thus approximates the hypothetical ancestral theropod in body size and morphology. The North American basal theropod *Tawa* is allied with coelophysoids in our analysis but with a single added step can be repositioned outside Neotheropoda as originally proposed (*11*).

Not only does *Eoraptor* lack all of the aforementioned theropod attributes in *Eodromaeus*, but it also exhibits features previously seen only among basal sauropodomorphs. In the skull, these features include an enlarged narial opening, a

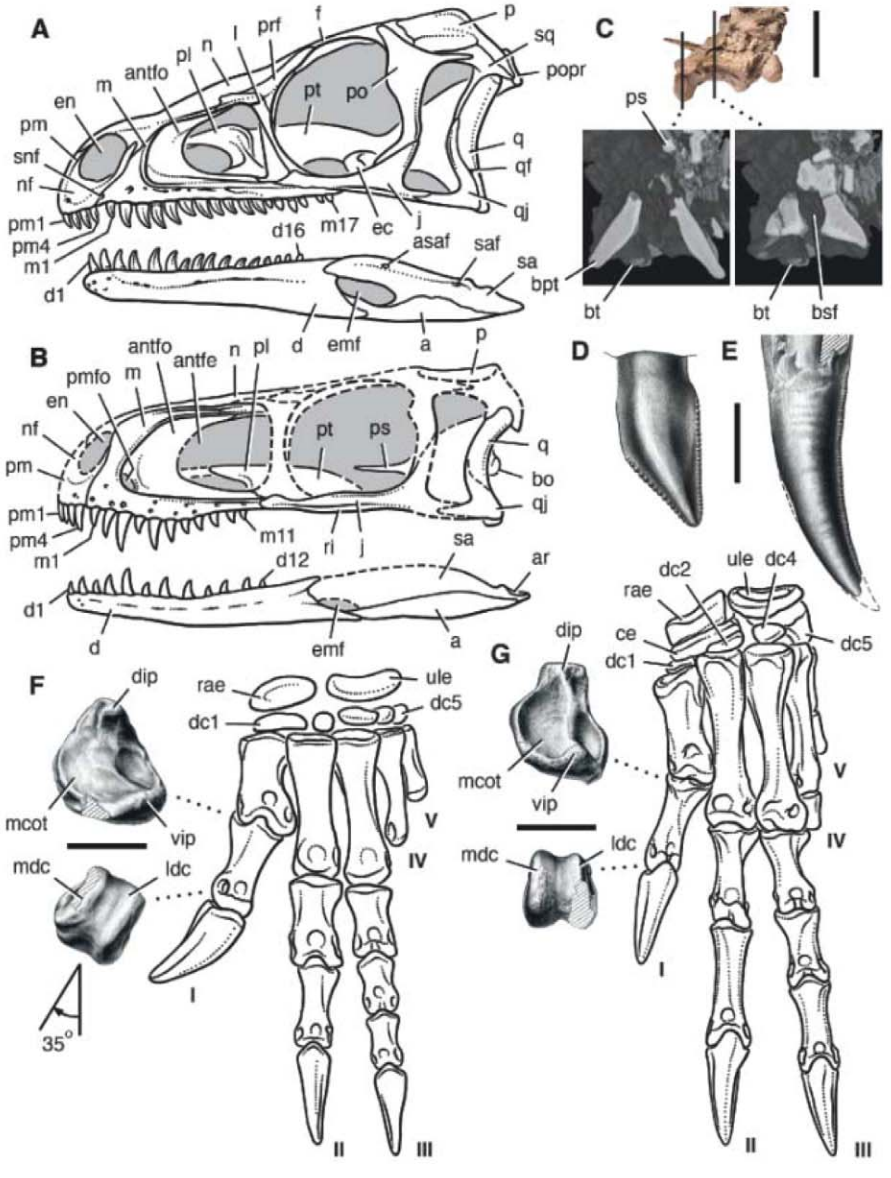

Fig. 1. Skull, carpus, and manus of the basal dinosaurs *Eoraptor lunensis* and *Eodromaeus murphi*. Skull reconstruction in lateral view of (**A**) *E. lunensis* (based on PVSJ 512) and (**B**) *E. murphi* (based on PVSJ 560 to 562). (**C**) Braincase of *E. murphi* (PVSJ 562) in ventrolateral view (reversed) and in two computed-tomographic (CT) cross sections (at vertical lines). Anterior left maxillary teeth are shown at the same scale in (**D**) *E. lunensis* [PVSJ 512, drawing of right maxillary tooth 2 in lateral view (reversed)] and (**E**) *E. murphi* [PVSJ 561, cast of left maxillary tooth 3 in medial view (reversed)]. Reconstruction of the left carpus and manus in dorsal view with enlarged views of the proximal and distal ends of phalanx 1 of digit I in (**F**) *E. lunensis* (based on PVSJ 512) and (**G**) *E. murphi* (based on PVSJ 560 and 562). The distal condyles in *E. lunensis* show 35° clockwise rotation with the proximal dorsal extensor process positioned dorsally. Abbreviations: I to V, manual digits I to V; a, angular; antfe, antorbital fenestra; antfo, antorbital fossa; ar, articular; asaf, anterior surangular foramen; bo, basioccipital; bpt, basipterygoid process; bsf, basisphenoid fossa; bt, basal tubera; ce, centrale; d, dentary; d1, d12, and d16, dentary teeth 1, 12, and 16; dc1 to dc5, distal carpals 1 to 5; dip, dorsal intercondylar process; ec, ectopterygoid; emf, external mandibular fenestra; en, external naris; f, frontal; j, jugal; l, lacrimal; ldc, lateral distal condyle; m, maxilla; m1, m11, and m17, maxillary teeth 1, 11, and 17; mcot, medial cotylus; mdc, medial distal condyle; n, nasal; nf, narial fossa; p, parietal; pl, palatine; pm, premaxilla; pm1 and pm4, premaxillary teeth 1 and 4; pmfo, promaxillary fossa; po, postorbital; popr, paroccipital process; prf, prefrontal; ps, parasphenoid; pt, pterygoid; q, quadrate; qf, quadrate foramen; qj, quadratojugal; rae, radiale; ri, ridge; sa, surangular; saf, surangular foramen; snf, subnarial foramen; sq, squamosal; ule, ulnare; vip, ventral intercondylar process. Dashed lines indicate a missing margin; hatching indicates a broken surface. Scale bars, 2 cm in (C) (for braincase); 3 mm in (D) and (E); 5 mm in (F) and (G) (enlarged views).

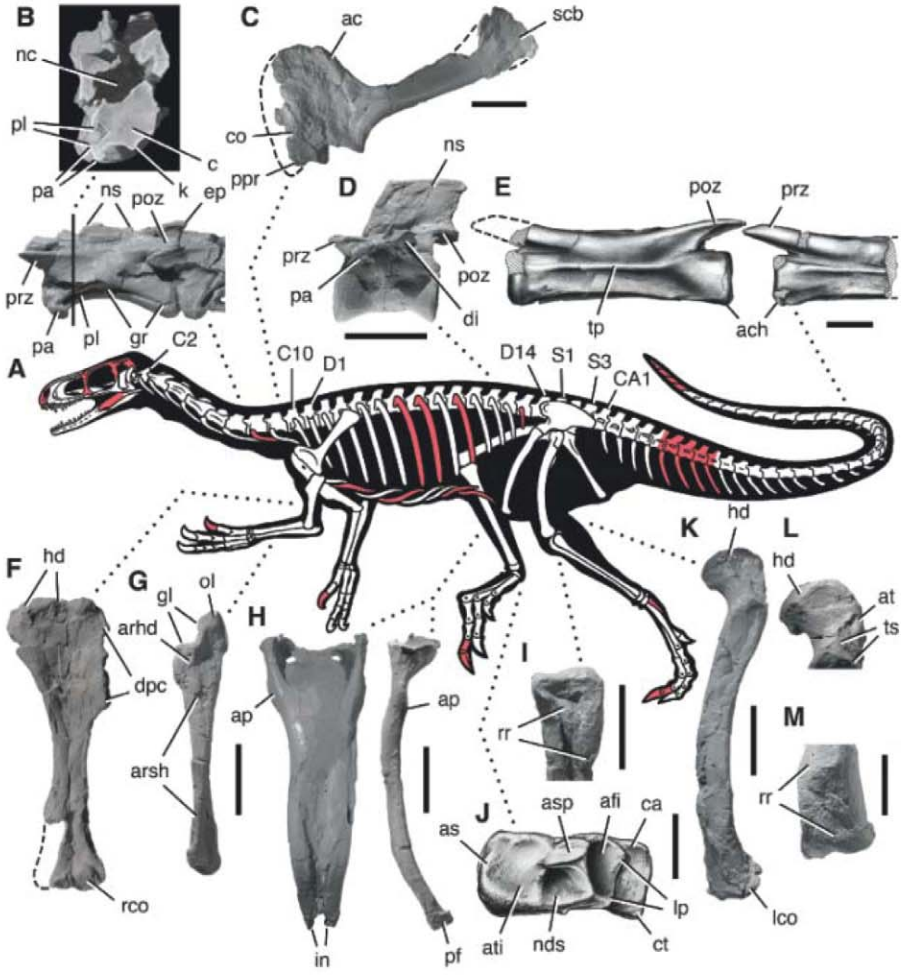

Fig. 2. Postcranial features of the Late Triassic basal theropod *Eodromaeus murphi*. Skeletal silhouette based on PVSJ 534, 560, and 562; postcranial bones are from PVSJ 562, except where indicated; bone casts and pencil drawings were used to eliminate color distraction and reversed as needed to left lateral view. (**A**) Skeletal silhouette showing preserved bones (missing portions in red). (**B**) Posterior cervical vertebrae (C7 and C8 anterior part) in lateral view (reversed) with enlarged cross-sectional view across the pleurocoel from a CT scan (at vertical line). (**C**) Scapulocoracoid in lateral view. (**D**) Posterior dorsal vertebra (~D11) in lateral view. (**E**) Distal caudal vertebrae (CA27 and CA28) in lateral view (PVSJ 560). (**F**) Humerus in anterior view. (**G**) Ulna in lateral view. (**H**) Pubes in anterior and lateral (reversed) views. (**I**) Proximal fibula in medial view. (**J**) Astragalus and calcaneum (right) in dorsal view (PVSJ 534). (**K** to **M**) Femur in lateral view, proximal end in lateral view, and distal end in anterior view, respectively. Abbreviations: ac, acromion; ach, articular surface for the chevron; afi, articular surface for the fibula; ap, ambiens process; arhd, articular surface for the radial head; arsh, articular surface for the radial shaft; as, astragalus; asp, ascending process; at, anterior trochanter; ati, articular surface for the tibia; c, centrum; C2 and C10, cervical vertebrae 2 and 10; ca, calcaneum; CA1, caudal vertebra 1; co, coracoid; ct, calcaneal tuber; D1 and D14, dorsal vertebrae 1 and 14; di, diapophysis; dpc, deltopectoral crest; ep, epipophysis; gl, glenoid; gr, goove; hd, head; in, interpubic notch; k, keel; lco, lateral condyle; lp, lateral process; nc, neural canal; nds, nonarticular dorsal surface; ns, neural spine; ol, olecranon; pa, parapophysis; pf, pubic foot; pl, pleurocoel; poz, postzygapophysis; ppr, posterior process; prz, prezygapophysis; rco, radial condyle; rr, raised rugosity for attachment; S1 and S3, sacral vertebrae 1 and 3; scb, scapular blade; tp, transverse process; ts, trochanteric shelf. Dashed lines indicate a missing margin; hatching indicates a broken surface. Scale bars, 2 cm in (B) and (D); 2 cm in (C); 5 mm in (E); 2 cm in (F) and (G); 3 cm in (H); 2 cm in (I); 1 cm in (J); 3 cm in (K); 2 cm in (L) and (M).

slender ventral process of the squamosal, and the inset position of the first dentary tooth (Fig. 1B). The toothless anterior end of the dentary, which is flanked by a conspicuous pair of vascular foramina, may have supported a small lower bill as in other basal sauropodomorphs (*13*). In addition, the form of the crowns (basal constriction, lateral crest, larger inclined denticles) strongly suggests that *Eoraptor* had an omnivorous, if not wholly herbivorous, diet. In the postcranial skeleton, sauropodomorph features include substantial medial rotation in the shaft of the first phalanx of the thumb (digit I) that directs the tip of the ungual inward (Fig. 1F) (*13*) and an astragalus with a characteristic shape (anteriorly projecting anteromedial corner) (*3*).

Reinterpretation of *Eoraptor* as a basal sauropodomorph closely related to *Panphagia* (Fig. 3) differs from previous phylogenetic assessments of this early dinosaur as a basal saurischian (*3*, *5*, *14*–*16*) or basal theropod (*1*, *11*, *12*, *17*). The phylogenetic analysis is decisive in this regard, requiring nine additional steps to reposition *Eoraptor* at the base of Theropoda. With *Eoraptor* as a basal sauropodomorph, the three principal clades of dinosaurs (ornithischians, sauropodomorphs, theropods) now appear to be converging on an ancestral skeletal plan—a bipedal cursor (tibia longer than femur) with body length less than 2 m. (Fig. 2A and Table 1). In our analysis, heterodontosaurids remain nested among basal ornithischians (Fig. 3). If heterodontosaurids are repositioned as basalmost ornithischians (*18*), which is only slightly less parsimonious, the ancestral body plan for dinosaurs would have included a proportionately long forelimb (~45% hind-limb length) and sharp-

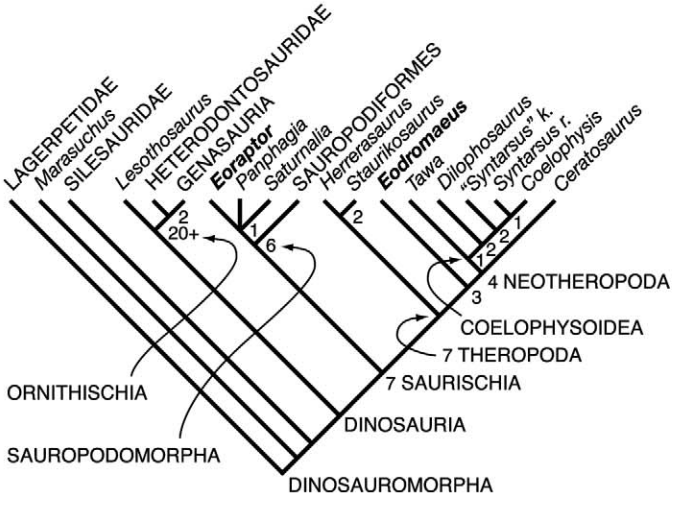

Fig. 3. Phylogenetic relationships among basal dinosaurs. Consensus cladogram summarizing three minimum-length trees based on maximum-parsimony analysis of 139 characters in successive outgroups (Lagerpetidae, *Marasuchus*, Silesauridae) and 16 basal dinosaur taxa (246 steps; consistency index = 0.618, retention index = 0.800). Outgroup taxa were constrained as shown; numbers at nodes indicate decay index. Suprageneric terminal taxa are scored on the basis of two or more included species. Suprageneric taxa that label the cladogram are positioned on the basis of phylogenetic definitions (*8*).

clawed manus with pits to accommodate digital hyperextension.

The Ischigualasto Formation, a richly fossiliferous fluvial succession within a Triassic continental rift basin (*6*, *19*), provides a window to faunal dynamics at the dawn of the dinosaur era. To quantify and temporally calibrate faunal abundance in the Ischigualasto Formation, we logged nearly 800 vertebrate specimens and obtained radioisotopic ages that bracket the formation between 231.4 and 225.9 million years ago (Ma) (Fig. 4) (*8*, *20*).

All of the early dinosaurs from the Ischigualasto Formation thrived during what we identify here as the *Scaphonyx-Exaeretodon-Herrerasaurus* biozone, a narrow temporal interval from 231.5 to 229 Ma in the latter half of the Carnian stage (Fig. 4). During this interval, dinosaurs account for 11% of recorded vertebrate specimens, which is about twice that previously estimated (*20*). This biozone is dominated by mid-sized non-dinosaurian herbivores (rhynchosaurs, traversodontid cynodonts) (Fig. 4). Herrerasaurids and *Eodromaeus*, however, represent ~70% of all nonaquatic carnivores in the faunal assemblage. Similarly, all small-bodied omnivores or herbivores (<2 m in body length and/or <15 kg) are dinosaurs (*Pisanosaurus*, *Eoraptor*, *Panphagia*, *Chromogisaurus*). Dinosaurs are also taxonomically diverse within this biozone, making up 33% of recorded genera, a percentage equaling that in the overlying Los Colorados Formation near the close of the Late Triassic (late Norian) (Fig. 4, top pie chart).

A major faunal change seems to have occurred near the Carnian-Norian boundary ~229 Ma, when humidity increased as inferred from sedimentological (argillic paleosols) and paleofloral (palynomorph-cuticle-trunk) evidence (*8*). The rhynchosaur *Scaphonyx*, most therapsids, and all dinosaurs disappeared, leaving a depauperate fauna dominated by the traversodontid cynodont *Exaeretodon* (*Exaeretodon* biozone). A less constrained but consistent faunal record from southern Brazil (*21*, *22*) suggests that this may have been a regional extinction event across southwestern Pangaea. Higher in the section, *Exaeretodon* is not present, and the mid-sized dicynodont *Jachaleria* is the dominant vertebrate (*Jachaleria* biozone). Although taphonomic bias against preservation of smaller vertebrates may play some role in the upper biozone, *Exaeretodon* is clearly not the dominant large vertebrate herbivore.

The discovery of *Eodromaeus*, the reinterpretation of *Eoraptor* as a sauropodomorph, and the faunal record of the Ischigualasto Formation provide additional evidence that, by mid Carnian time (~232 Ma), the earliest dinosaurs had already evolved the most functionally important trophic and locomotor features characterizing ornithischians, sauropodomorphs, and theropods (*17*, *23*). These attributes are thus unlikely to have functioned as the competitive

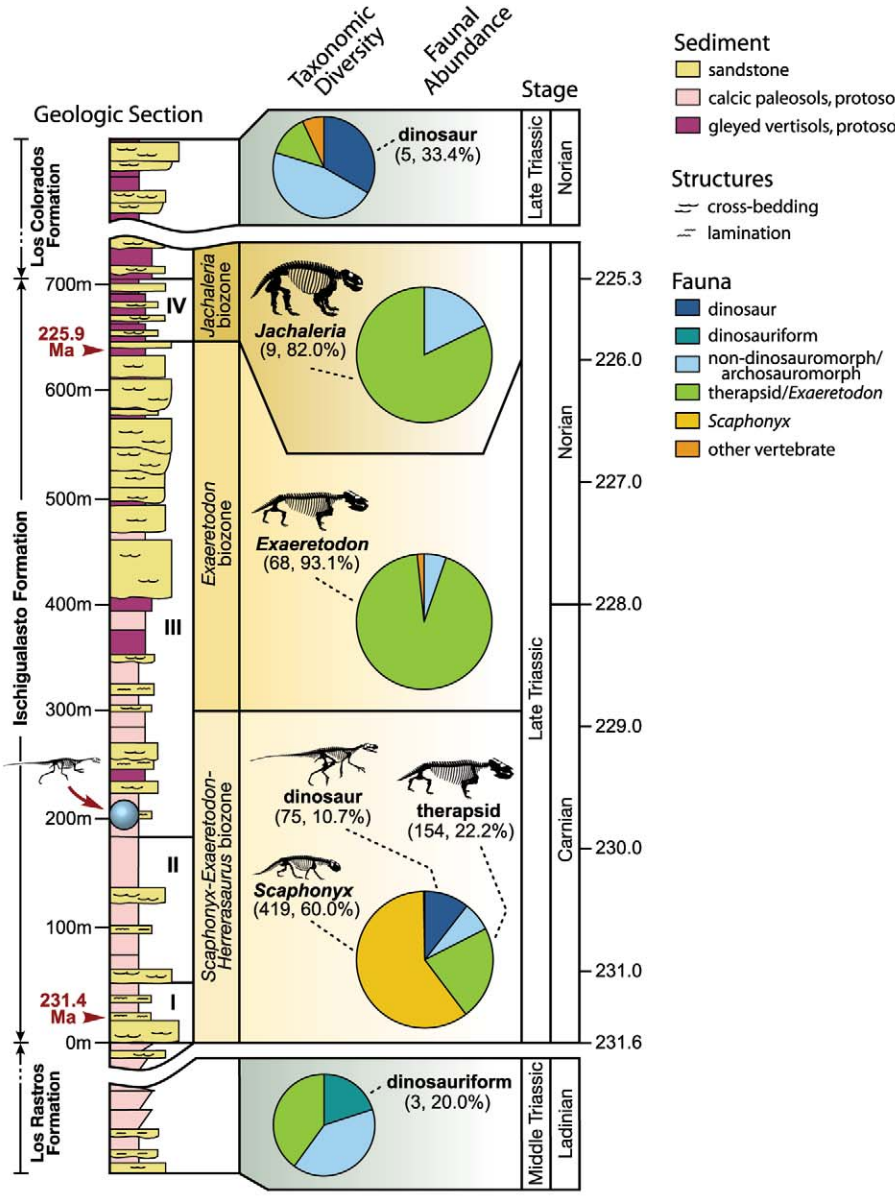

Fig. 4. Calibrated stratigraphic profile across the Ischigualasto Formation (northwest Argentina) showing tetrapod diversity and abundance. (**Left**) The chart shows a simplified stratigraphic section divided into four formational members (Roman numerals I to IV) as well as the stratigraphic positions of the holotype of *Eodromaeus murphi* and a bracketing pair of radiometric dates using recently revised radioisotopic decay constants (*30*). (**Middle**) Three biozones, three large pie charts summarizing faunal abundance for each biozone, and two smaller pie charts pie showing taxonomic diversity before (Los Chañares Fm.) and after (Los Colorados Fm.) the Ischigualasto Formation. (**Right**) A current geologic time scale (*31*), which assumes an average rate of sedimentation between radioisotopically dated horizons.

advantage to account for the dominance of dinosaurs in abundance and diversity in terrestrial habitats some 30 million years later in the earliest Jurassic (~202 Ma). *Eodromaeus* increases the range of salient theropod features present in the earliest dinosaurs, and *Eoraptor* shows that the enlarged naris, basally constricted crowns, and a twisted pollex were present in the earliest sauropodomorphs.

One explanation for the rise of dinosaurs has been that a few key features led gradually to the competitive dominance of dinosaurs (*20*, *24*). This view has been overtaken by a hypothesis of noncompetitive replacement, in which their rise is split into two successive episodes of extinction and noncompetitive infilling of vacant ecospace (*25*, *26*). In the replacement hypothesis, the earliest dinosaurs are regarded as particularly rare (1 to 3% of terrestrial vertebrates), their abundance and diversity increasing successively at the Carnian-Norian and Triassic-Jurassic boundaries coincident with mass extinction of rhynchosaurs, traversodontid cynodonts, and dicynodonts and later of (noncrocodyliform) crurotarsal archosaurs.

In contrast, the fossil record from Ischigualasto indicates that early dinosaurs in the latter half of the Carnian (231 to 228 Ma) were more common and diverse than previously thought, equaling the percentage of dinosaurian genera in the late Norian fauna from the overlying Los Colorados Formation (Fig. 4). Thus, in terms of taxonomic diversity, dinosaurs did not increase their percentage among terrestrial vertebrates toward the end of the Triassic in southwestern Pangaea.

The record also shows that extinction of rhynchosaurs and other large-bodied herbivores was not synchronous but rather spread out across 4 to 5 million years (Fig. 4). The disappearance of rhynchosaurs at the Carnian-Norian boundary was not linked to an increase in dinosaur diversity but rather coincided with the local extinction of dinosaurs. The most substantial change between the earliest dinosaurs in the Carnian and those in the late Norian is that the latter have expanded into the upper register of body size as both carnivores (*Zupaysaurus*) and herbivores (*Lessemsaurus*). Increased body size probably enhanced the preservation potential of late Norian dinosaurs, which are also recorded from many more sites than late Carnian dinosaurs (*6*, *27*). We cannot evaluate whether the increase in body size was gradual or rapid, as there are no dinosaurs in the section between late Carnian and late Norian faunas. Furthermore, increasing body size among dinosaurs was not limited to the Triassic but continued throughout the Jurassic (*23*, *28*) long after the extinction of Triassic synapsids and (noncrocodyliform) crurotarsal archosaurs.

The earliest dinosaurs are currently restricted to late Carnian sites in southern Pangaea (Argentina, Brazil). The earliest dinosaur from northern Pangaea (*Tawa*, western North America) has recently been dated to the mid Norian (~214 Ma) (*11*), making it some 15 million years younger in age. This has led to the view that the major dinosaurian clades (Ornithischia, Sauropodomorpha, Theropoda) may have originated in southern Pangaea (*14*, *16*). The paleogeographic importance of this distribution, however, is compromised by the absence of well-preserved skeletal remains of Carnian age from northern locales (northern Africa, Europe, North America) (*14*, *21*, *29*). Discerning global patterns of replacement or areas of paleogeographic origin for particular groups in terrestrial ecosystems in the Triassic requires greater temporal and geographic control than is currently available.

References and Notes

1. P. C. Sereno, C. A. Forster, R. R. Rogers, A. M. Monetta, *Nature* **361**, 64 (1993).
2. P. C. Sereno, F. E. Novas, *Science* **258**, 1137 (1992).
3. R. N. Martinez, O. A. Alcober, *PLoS ONE* **4**, e4397 (2009).
4. O. A. Alcober, R. N. Martinez, *ZooKeys* **63,** 55 (2010).
5. M. D. Ezcurra, *J. Syst. Palaeontology* **8**, 371 (2010).
6. B. S. Currie, C. E. Colombi, N. J. Tabor, T. C. Shipman, I. P. Montañez, *J. S. Am. Earth Sci.* **27**, 74 (2009).
7. **Etymology**: *eos*, dawn (Greek); *dromaeus*, runner (Greek); *murphi*; in allusion to its early age, slender axial and appendicular proportions, and the Earthwatch volunteer who discovered the holotypic specimen (J. Murphy). **Holotype**: PVSJ 560, articulated skeleton lacking only the scapulocoracoids, most of the right forelimb, some cervical and dorsal ribs, gastralia, four anterior caudal vertebrae, and most chevrons. Fusion of all neurocentral sutures suggests that the holotype has reached adult size. This specimen is cataloged in the collection of the Instituto y Museo de Ciencias Naturales (San Juan, Argentina). **Type locality**: 30°04′3.5″S, 67°56′11.4″W; Valle de la Luna, Ischigualasto Provincial Park, San Juan, Argentina. **Horizon**: Ischigualasto Formation, Valle de la Luna Member (PVSJ 560 to 563), ~200 m from base of the formation. Two referred specimens (PVSJ 534, 877) were found in the underlying La Peña and Cancha de Bochas Members, overlapping the range of several other dinosaurs (Fig. 3). **Age**: Ages range from ~232 to 229 Ma (Fig. 4) (*8*, *20*). **Diagnosis**: Basal theropod with no more than 11 maxillary teeth, caniniform maxillary crowns more than three times the basal mesiodistal width near the anterior end of the tooth row, fine serrations (~nine per millimeter) on mesial and distal margins, ventrally convex maxillary alveolar margin, very shallow jugal suborbital ramus, centrale in carpus between the radiale and distal carpal 1, large distal carpal 5 overlapping distal carpal 4 with a posteroventral heel; pubic apron with sinuous lateral margin, and pubic foot with squared posterior margin.
8. See supporting material on *Science* Online.
9. Higher taxa cited in the text are defined as follows (www.taxonsearch.org): **Dinosauria**, the least inclusive clade containing *Tyrannosaurus rex* Osborn 1905 and *Passer domesticus* (Linnaeus 1758); **Ornithischia**, the most inclusive clade containing *Tyrannosaurus rex* Osborn 1905 but not *Ornithomimus edmontonicus* Sternberg 1933, *Troodon formosus* Leidy 1856, *Velociraptor mongoliensis* Osborn 1924; **Saurischia**, the least inclusive clade containing *Tyrannosaurus rex* Osborn 1905 and *Gorgosaurus libratus* Lambe 1914, *Albertosaurus sarcophagus* Osborn 1905; **Sauropodomorpha**, the most inclusive clade containing *Saltasaurus loricatus* Bonaparte and Powell 1980 but not *Passer domesticus* (Linnaeus 1758), *Triceratops horridus* Marsh 1889; **Sauropodiformes**, the least inclusive clade containing *Mussaurus patagonicus* Bonaparte and Vince 1979 and *Saltasaurus loricatus* Bonaparte and Powell 1980; **Theropoda**, the most inclusive clade containing *Passer domesticus* (Linnaeus 1758) but not *Saltasaurus loricatus* Bonaparte and Powell 1980; **Neotheropoda**, the least inclusive clade containing *Coelophysis bauri* (Cope 1889) and *Passer domesticus* (Linnaeus 1758); **Coelophysoidea**, the most inclusive clade containing *Coelophysis bauri* (Cope 1889) but not *Carnotaurus sastrei* Bonaparte 1985, *Ceratosaurus nasicornis* Marsh 1884, *Passer domesticus* (Linnaeus 1758).
10. P. C. Sereno, *Hist. Biol.* **19**, 145 (2007).
11. S. J. Nesbitt *et al*., *Science* **326**, 1530 (2009).
12. R. S. Tykoski, thesis, University of Texas at Austin, Austin, TX (2005).
13. P. C. Sereno, in *Evolution and Paleobiology of Sauropodomorph Dinosaurs*, P. M. Upchurch, D. J. Batten, Eds. (Palaeontological Association, London, 2007), pp. 261–289.
14. M. C. Langer, M. D. Ezcurra, J. S. Bittencourt, F. E. Novas, *Biol. Rev. Camb. Philos. Soc.* **85**, 55 (2010).
15. M. C. Langer, in *The Dinosauria*, D. B. Weishampel, P. Dodson, H. Osmólska, Eds. (Univ. of California Press, Berkeley, CA, 2004), pp. 25–46.
16. S. L. Brusatte *et al*., *Earth Sci. Rev.* **101**, 68 (2010).
17. P. C. Sereno, *Science* **284**, 2137 (1999).
18. R. J. Butler, P. Upchurch, D. B. Norman, *J. Syst. Palaeontology* **6**, 1 (2008).
19. J. F. Bonaparte, *J. Vert. Paleo.* **2**, 362 (1982).
20. R. R. Rogers *et al*., *Science* **260**, 794 (1993).
21. M. C. Langer, *J. S. Am. Earth Sci.* **19**, 219 (2005).
22. M. C. Langer, A. M. Ribeiro, C. L. Schultz, J. Ferigolo, in *The Global Triassic*, S. G. Lucas, J. A. Speilmann, Eds. (New Mexico Museum of Natural History, Albuquerque, NM, 2007).
23. P. C. Sereno, *Annu. Rev. Earth Planet. Sci.* **25**, 435 (1997).
24. A. J. Charig, *Zool. Soc. London Symp.* **57**, 597 (1984).
25. M. J. Benton, in *In the Shadow of the Dinosaurs*, N. C Fraser, H.-D. Sues, Eds. (Cambridge Univ. Press, Cambridge, 1994), pp. 366–397.
26. M. J. Benton, "The origin of the dinosaurs," in *Actas de las III Jornadas sobre Dinosaurios y su Entorno* (Colectivo Arqueol'ogico-Paleontol'ogico Salense, Burgos, Spain, 2006), pp. 11–19.
27. P. D. Mannion, P. Upchurch, M. T. Carrano, P. M. Barrett, *Biol. Rev. Camb. Philos. Soc.*, published online 16 April 2010 (10.1111/j.1469-185X.2010.00139.x).
28. D. W. E. Hone, T. M. Keesey, D. Pisani, A. Purvis, *J. Evol. Biol.* **18**, 587 (2005).
29. S. J. Nesbitt, R. B. Irmis, W. G. Parker, *J. Syst. Palaeontology* **5**, 209 (2007).
30. P. R. Renne, R. Mundil, G. Balco, K. Min, K. R. Ludwig, *Geochim. Cosmochim. Acta* **74**, 5349 (2010).
31. J. D. Walker, J. W. Geissman, *GSA Today* **19**, 60 (2009).
32. F. E. Novas, *J. Vert. Paleo.* **13**, 400 (1994).
33. A. P. Santa Luca, *Ann. S. Afr. Mus.* **79**, 159 (1980).

34. We thank C. Abraczinskas for final drafts of all figures, personnel of the Fossil Lab at the Univ. of Chicago for preparation of fossil material, personnel of the High-Resolution X-ray Computed Tomography Facility at The Univ. of Texas at Austin for assistance with computed tomography imaging, and S. Nesbitt and R. Irmis for examination of fossil material in their care. This work was supported by the Whitten-Newman Foundation, the Island Fund of the New York Community Trust, Earthwatch Institute, Consejo Nacional de Investigaciones Científicas y Técnicas, the Ann and Gordon Getty Foundation, and the National Geographic Society.

Supporting Online Material

www.sciencemag.org/cgi/content/full/331/6014/206/DC1
Materials and Methods
Fig. S1
Tables S1 to S6
References

29 September 2010; accepted 8 December 2010
10.1126/science.1198467

Writing About Testing Worries Boosts Exam Performance in the Classroom

Gerardo Ramirez and Sian L. Beilock*

Two laboratory and two randomized field experiments tested a psychological intervention designed to improve students' scores on high-stakes exams and to increase our understanding of why pressure-filled exam situations undermine some students' performance. We expected that sitting for an important exam leads to worries about the situation and its consequences that undermine test performance. We tested whether having students write down their thoughts about an upcoming test could improve test performance. The intervention, a brief expressive writing assignment that occurred immediately before taking an important test, significantly improved students' exam scores, especially for students habitually anxious about test taking. Simply writing about one's worries before a high-stakes exam can boost test scores.

For many students, the desire to perform their best in academics is strong. Consequences for poor performance, especially on exams, include poor evaluations by mentors, teachers, and peers; lost scholarships; and relinquished educational opportunities. Yet despite the fact that students are often motivated to perform their best, the pressure-filled situations in which important tests occur can cause students to perform below their ability instead (*1*).

The expression "choking under pressure" is used to describe what happens when people perform more poorly than expected given their skill level when there are large incentives for optimal performance and negative consequences for poor performance (*2*). Choking is a serious problem given that poor exam performance affects students' subsequent academic opportunities. It also limits potentially qualified students from participating in the talent pool tapped to fill advanced jobs in disciplines where the workforce is dwindling [e.g., science, technology, engineering, and mathematics workforce in the United States (*3*)]. Here we demonstrate how a 10-min. pre-exam intervention, derived from psychological theories of stress and performance, can prevent choking and enhance exam scores, particularly for students who habitually become anxious in testing situations.

Several studies have shown that, when students feel an anxious desire to perform at a high level [i.e., performance pressure (*4*)], they worry about the situation and its consequences (*5*, *6*). These worries compete for the working memory (WM) available for performance. WM is a short-term memory system involved in the control and regulation of a limited amount of information immediately relevant to the task at hand (*7*). If the ability of WM to maintain task focus is disrupted because of situation-related worries, performance can suffer (*8*).

Department of Psychology and Committee on Education, University of Chicago, Chicago, IL 60637, USA.

*To whom correspondence should be addressed. E-mail: beilock@uchicago.edu

Worries not only occur in intense academic situations but are a major component of depression and other clinical disorders (*9*). Expressive writing, in which people repeatedly write about a traumatic or emotional experience over several weeks or months, has been shown to be an effective technique for decreasing rumination in depressed individuals (*10*). Writing may alleviate the burden that worries place on WM by affording people an opportunity to reevaluate the stressful experience in a manner that reduces the necessity to worry altogether (*11*).

We reasoned that, if worries lead to poor test performance and writing helps regulate these worries, then giving students the opportunity to express their thoughts and feelings about an impending examination would enhance test performance. This is a somewhat counterintuitive idea given that drawing attention to negative information typically makes it more rather than less salient in memory (*12*, *13*). However, if expressive writing helps to reduce rumination, then it should benefit high-stakes test performance, especially for students who tend to worry in testing situations.

Moreover, the benefits of writing therapy are traditionally seen over multiple writing sessions spanning weeks or months. In these situations, people write about an event that occurred in the past (*11*), and thus substantial reflection time is likely necessary to bring different aspects of the event to mind and explore them in detail. However, we reasoned that, if a threatening situation is immediately forthcoming, the details should be salient. Thus, one bout of writing should be sufficient to impact performance. Such a finding would show that minimal class or exam time is needed to achieve expressive writing benefits.

Across two laboratory studies and two randomized field experiments, we investigated expressive writing as a test-taking intervention (*14*). In the laboratory studies, students took a math test under conditions designed to elicit either lower or higher levels of performance pressure. We predicted that math performance would be worse under high-pressure compared with low-pressure situations (*8*) but that allowing students to write about their exam-related thoughts immediately before the test would eliminate this choking-under-pressure effect (study 1). In study 2, we tested whether it is writing about the test per se that prevents choking or whether writing about any topic (e.g., a mundane event in one's life) can prevent choking under pressure. In studies 3 and 4, we extended our laboratory results to the classroom and asked for whom the benefits of expressive writing would be most pronounced. Ninth-grade students were randomly assigned to an expressive writing or control condition immediately before the first final exam of their high school career. If expressive writing alleviates the impact of worries on performance, then students most prone to worry during exams (i.e., students highest in test anxiety) should benefit most from the writing intervention.

We began by creating a high-stakes testing environment in the laboratory. In study 1, college students ($N = 20$) took two short tests composed of Gauss's modular arithmetic. Modular arithmetic is advantageous as a laboratory task because, although it is based on common mathematical

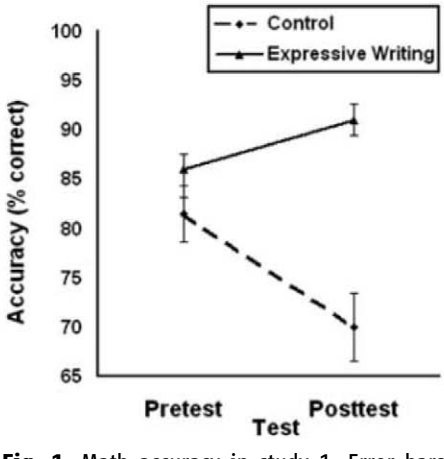

Fig. 1. Math accuracy in study 1. Error bars are SEM.

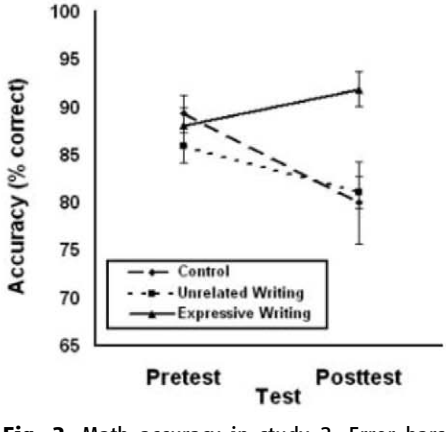

Fig. 2. Math accuracy in study 2. Error bars are SEM.

procedures, most students have not seen it before; thus, previous task experience is controlled.

Before taking the first math test (pretest), students were simply told to perform their best. After completing the pretest, students were given a high-pressure scenario based on common pressures: monetary incentives (which stand in for scholarships associated with high test scores) and peer pressure and social evaluation (which comes from judgments of test scores from admissions committees, teachers, parents, and peers).

Students were informed that, if they performed at a high level, they would receive a monetary reward. Students were also told that this award was dependent on high-level performance of both themselves and a partner they were paired with, a "team effort." Students were then informed that their partner had completed the experiment and improved. Thus, the current participant was entirely responsible for winning (or losing) the money. Students were also told that their performance would be videotaped and that teachers and students would watch the tapes. This scenario has been repeatedly demonstrated to increase feelings of pressure and anxiety (*8*). These feelings do not differ as a function of math ability, and thus this factor is not confounded with response to pressure.

After the high-pressure scenario was described, students spent 10 min either sitting quietly (control group) or engaged in our writing intervention (expressive writing group). The expressive writing group was asked to write as openly as possible about their thoughts and feelings regarding the math problems they were about to perform. Everyone then took the math posttest.

Our main performance measure was math accuracy. Problem-solving time did not differ as a function of group (*15*). Pretest math performance did not differ across the control and expressive writing groups as revealed by a *t* test [$t(18) = 1.14$, $P = 0.27$] (Fig. 1). However, in the posttest, the expressive writing group performed significantly better than the control group [$t(18) = 5.55$, $P < 0.01$, Cohen's $d = 2.48$]. Control participants choked under pressure, showing a 12% accuracy drop from pretest to posttest [$t(9) = 4.87$, $P < 0.01$, $d = 1.14$], whereas students who expressed their thoughts before the high-pressure test showed a significant 5% math accuracy improvement from the pretest to posttest [$t(9) = 2.74$, $P < 0.03$, $d = 0.58$] (*16*).

From study 1, it is unclear whether writing about one's test-related thoughts per se prevents pressure-induced failure or whether any writing might alleviate the relation between pressure and performance. Perhaps writing, regardless of content, distracts students' attention from the situation and thus benefits performance. We tested this notion in a second laboratory study ($N = 47$) that replicated study 1 and included another condition where some students wrote about an unrelated unemotional event (unrelated writing group) before the posttest.

Before receiving our high-pressure scenario, math performance did not differ as a function of group as revealed by a one-way analysis of variance (ANOVA) [$F_{2,44} = 0.74$, $P = 0.48$] (Fig. 2). However, this was not true in the posttest [$F_{2,44} = 5.56$, $P < 0.01$]. Students in the control and unrelated writing groups showed a significant 7% drop in accuracy from pretest to posttest [$t(30) = 3.35$, $P < 0.01$, $d = 1.17$]. This drop did not differ across groups [$t(29) = 1.07$, $P = 0.29$]. In contrast, the expressive writing group showed a significant 4% gain in accuracy from pretest to posttest [$t(15) = 2.09$, $P = 0.05$, $d = 0.47$].

Analysis of writing content showed that students in the expressive writing group revealed significantly more anxiety-related words (e.g., worried, fearful, nervous) than students in the unrelated writing group [$F_{1,29} = 6.31$, $P < 0.02$]. Students in the expressive writing group also had a significantly greater proportion of sentences expressing negative thoughts and worries (e.g., "I am afraid I am going to make a mistake") than students in the unrelated writing group [$F_{1,30} = 20.96$, $P < 0.01$]. If writing about negative thoughts and worries underlies performance differences among the expressive writing and unrelated writing groups, then taking these sentences into account should eliminate the differences in performance from the pretest to posttest seen for these writing groups. This is exactly what was found. Specifically, when the proportion of worry-related sentences was taken into account, the significant writing group (expressive writing, unrelated writing)–by–test (pretest, posttest) interaction [$F_{1,30} = 9.30$, $P < 0.005$], demonstrating that changes in math performance across test depend on writing group, became nonsignificant [$F_{1,29} = 2.88$, $P = 0.10$] (*17*). Writing about negative thoughts and worries accounts for choking-under-pressure differences across the unrelated and expressive writing groups.

If expressive writing benefits test performance by reducing intrusive thoughts and worries, then students most prone to worry during exams (i.e., students highest in test anxiety) should show the largest writing benefit. Moreover, if test anxiety, over and above knowledge and ability, causes some students to score poorly on exams, then expressive writing should eliminate the negative relation commonly seen between test anxiety and performance. Obtaining this latter result would highlight the importance of introducing classroom interventions that ensure all students (regardless of test anxiety) have the opportunity to demonstrate their knowledge on important tests.

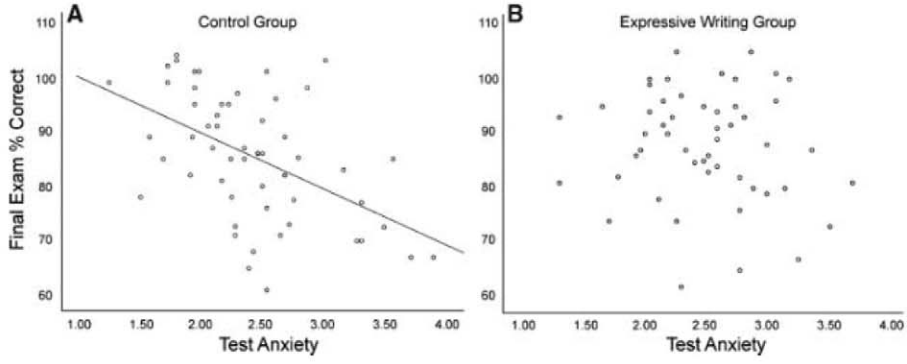

Fig. 3. Scatterplot of the relation between test anxiety and final exam performance for students in the control condition (**A**) and the expressive writing condition (**B**) combined across studies 3 and 4. Some scores top 100% because of possible extra credit.

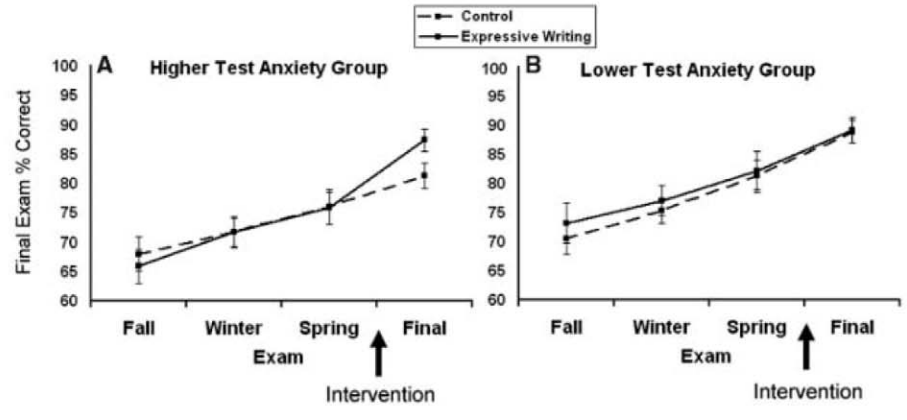

Fig. 4. Exam performance for students higher (**A**) and lower (**B**) in test anxiety. Error bars are SEM.

We tested these predictions in studies 3 and 4, immediately before ninth-grade students' first final high-school exam. This is an especially pressure-filled exam, because year-end grades often serve as the first data point in averages used for college admissions, and final exams contribute substantially to this grade point.

We performed the same intervention twice, 1 year apart, with separate ninth-grade cohorts in the same school. Students taking ninth-grade biology participated (study 3 had 51 students across three biology teachers; study 4, 55 students across three teachers).

Six weeks before the final exam, we measured students' test anxiety, the degree to which students worry in reaction to evaluative situations. In their home rooms (independent of biology), students were given a standard measure of test anxiety designed to tap into their habitual tendency to feel tension, apprehension, or anxiety in testing situations (*18*). Students were asked to rate items such as "During tests, I find myself thinking about the consequences of failing" (1 was "not typical of me," and 4 was "very typical of me").

Conveniently, within each year, all biology exams were administered in one final exam session in the same room. Students were randomly assigned (within teacher) to either an expressive writing or a control condition. Immediately before the exam, proctors asked students to put away their materials and prepare for a short assignment. Students received an envelope with their name on it. These envelopes contained a sheet of paper with specific instructions.

About half of the students were given instructions to write about their thoughts about the upcoming exam (expressive writing condition). The other half were asked to think about a topic that would not be covered on the exam (control condition). This particular control was chosen because students often report introspecting on possible exam topics immediately before a test (*19*), and we were attempting to mimic normal exam conditions as closely as possible. Students were given 10 min to complete the assignment. They then returned the instruction sheet to the envelope and gave the envelope to a proctor (*20*). Everyone then began their exams.

We obtained students' final exam scores as well as their midterm exam scores for the fall, winter, and spring quarters. We first examined the correlations between test anxiety and final exam performance separately in each study and then combined across both studies. The higher students' test anxiety, the lower their final exam score in the control condition [for study 3, $r(26) = -0.45$ and $P < 0.02$; study 4, $r(30) = -0.48$ and $P < 0.01$; combined, $r(56) = -0.51$ and $P < 0.01$] (*21*) but not in the expressive writing condition [study 3, $r(25) = -0.07$ and $P = 0.73$; study 4, $r(25) = -0.19$ and $P = 0.36$; combined, $r(50) = -0.14$ and $P = 0.33$]. Across both studies, the correlations between test anxiety and final exam scores were significantly different from each other in the expressive writing and control conditions [Z(two-tailed) = –2.09, $P < 0.04$ (*22*)] (Fig. 3).

Why was there a negative relation between test anxiety and exam performance in the control, but not the expressive writing, condition? If writing alleviates the impact of worries on performance, then highly test anxious students should benefit most from writing. If so, then writing about one's worries may allow those higher in test anxiety to perform up to the level of low-test-anxious students, eliminating the relation commonly seen between test anxiety and performance.

To test this possibility, we next divided students across both studies into groups (median split) on the basis of whether they were lower or higher in test anxiety. In terms of higher test anxious students, there was no difference in fall, winter, or spring midterm exam scores [all P values > 0.60] before our writing intervention (Fig. 4A). However, after the intervention, on the final exam, those who expressively wrote outperformed controls by 6% [$t(52) = 2.08$, $P < 0.05$, $d = 0.57$] (*23*) and performed similarly to lower-test-anxious students, regardless of writing condition [$t(78) = 0.66$, $P = 0.52$]. Higher-test-anxious students in the expressive writing condition received a B+ on a standard grading scale; those in the control condition received a B–. In contrast, lower-test-anxious students showed no difference as a function of writing condition across the midterms [P values > 0.53] or final exam [$t(50) = 0.09$, $P = 0.93$] (Fig. 4B). The differential impact of writing on lower- and higher-test-anxious students is similar to study 1's finding, whereby writing did not affect performance in a low-pressure situation. If lower- as compared to higher-test-anxious students worry less about exams and thus express fewer worries in their writing, worry less during the exam, or both, their performance should be less influenced by expressive writing.

We demonstrate that a short expressive writing intervention reduces performance deficits commonly associated with high-pressure testing situations. The benefits of expressive writing are especially apparent for students who are habitually anxious about taking tests. Expressive writing eliminates the relation commonly seen between test anxiety and poor test performance. Moreover, it is not any writing that benefits performance, but expressing worries about an upcoming high-pressure situation that accounts for enhanced exam scores under pressure.

Past work in school settings demonstrates that asking African American students to reaffirm their values across the school year reduces the racial achievement gap by year's end (*24*, *25*). This is true for women and the gender gap in science classes as well (*26*). Moreover, helping students repeatedly make connections between the curriculum and their personal lives has been shown to increase motivation and academic success in science classes among students who profess low interest to begin with (*27*). The current research shows that interventions designed to boost school performance are not restricted to students who are members of stigmatized groups or who are already disengaged from course material. Rather, for those students who are most anxious about success, one short writing intervention that brings testing pressures to the forefront enhances the likelihood of excelling, rather than failing, under pressure.

References and Notes

1. S. L. Beilock, *Curr. Dir. Psychol. Sci.* **17**, 339 (2008).
2. R. F. Baumeister, *J. Pers. Soc. Psychol.* **46**, 610 (1984).
3. S. L. Beilock, *Choke: What the Secrets of the Brain Reveal About Getting It Right When You Have To* (Free Press, New York, 2010).
4. L. Hardy, R. Mullen, G. Jones, *Br. J. Psychol.* **87**, 621 (1996).
5. S. L. Beilock, C. A. Kulp, L. E. Holt, T. H. Carr, *J. Exp. Psychol. Gen.* **133**, 584 (2004).
6. M. Cadinu, A. Maass, A. Rosabianca, J. Kiesner, *Psychol. Sci.* **16**, 572 (2005).
7. P. Miyake, P. Shah, Eds., *Models of Working Memory: Mechanisms of Active Maintenance and Executive Control* (Cambridge Univ. Press, New York, 1999).
8. S. L. Beilock, T. H. Carr, *Psychol. Sci.* **16**, 101 (2005).
9. J. Joormann, B. T. Taran, *Cognit. Emotion* **23**, 1223 (2009).
10. J. M. Smyth, *J. Consult. Clin. Psychol.* **66**, 174 (1998).
11. K. Klein, A. Boals, *J. Exp. Psychol. Gen.* **130**, 520 (2001).
12. T. Schmader, M. Johns, *J. Pers. Soc. Psychol.* **85**, 440 (2003).
13. D. M. Wegner, D. J. Schneider, S. R. Carter, T. L. White, *J. Pers. Soc. Psychol.* **53**, 5 (1987).
14. Materials and methods are available as supporting material on *Science* Online.
15. See tables S1 and S2 for reaction time data.
16. We also ran another group of participants ($N = 20$) in study 1 who did not receive a high-pressure scenario before the posttest. Math accuracy was relatively high and did not differ from the pretest to posttest, nor did it differ as a function of whether students expressively wrote before the posttest. Thus, an accuracy drop from the pretest to posttest occurred only for students given our high-pressure scenario who did not write. See supporting online material (SOM) text for details.
17. See table S4 for details.
18. J. C. Cassady, R. E. Johnson, *Contemp. Educ. Psychol.* **27**, 270 (2002).
19. M. S. DeCaro, K. E. Rotar, M. S. Kendra, S. L. Beilock, *Q. J. Exp. Psychol.* **63**, 1619 (2010).
20. Proctors were two biology teachers. Teachers and students were blind to the study purpose. Teachers were blind to the particular instructions students received.
21. Correlations remained significant when controlling for prior midterms and teacher (SOM text).
22. K. J. Preacher, http://quantpsy.org (2002).
23. One might wonder whether, rather than expressive writing boosting students' scores, the control condition hurt performance. A comparison with students who did not participate in either condition and spent the exercise time studying for the final shows no difference with the control condition [$F_{1,78} = 0.59$, $P = 0.44$], supporting the idea that expressive writing improved scores. This analysis controls for prior midterm exams.
24. G. L. Cohen, J. Garcia, N. Apfel, A. Master, *Science* **313**, 1307 (2006).
25. G. L. Cohen, *Science* **324**, 400 (2009).
26. A. Miyake *et al.*, *Science* **330**, 1234 (2010).
27. C. S. Hulleman, J. M. Harackiewicz, *Science* **326**, 1410 (2009).

28. Supported by NSF CAREER DRL-0746970 and NSF Spatial Intelligence and Learning Center SBE-0541957 to S.L.B. and Institute of Educational Science predoctoral training fellowship R305C050076 to G.R. We thank F. Spaltro for coordination of study 3 and 4 logistics and S. Goldin-Meadow for comments on a draft manuscript.

Supporting Online Material

www.sciencemag.org/cgi/content/full/331/6014/211/DC1
Materials and Methods
SOM Text
Tables S1 to S6
References

22 October 2010; accepted 17 December 2010
10.1126/science.1199427

Genomic Signatures Predict Migration and Spawning Failure in Wild Canadian Salmon

Kristina M. Miller,[1,2]* Shaorong Li,[1] Karia H. Kaukinen,[1] Norma Ginther,[1] Edd Hammill,[3] Janelle M. R. Curtis,[3] David A. Patterson,[4] Thomas Sierocinski,[5] Louise Donnison,[5] Paul Pavlidis,[5] Scott G. Hinch,[2] Kimberly A. Hruska,[2] Steven J. Cooke,[6] Karl K. English,[7] Anthony P. Farrell[8]

Long-term population viability of Fraser River sockeye salmon (*Oncorhynchus nerka*) is threatened by unusually high levels of mortality as they swim to their spawning areas before they spawn. Functional genomic studies on biopsied gill tissue from tagged wild adults that were tracked through ocean and river environments revealed physiological profiles predictive of successful migration and spawning. We identified a common genomic profile that was correlated with survival in each study. In ocean-tagged fish, a mortality-related genomic signature was associated with a 13.5-fold greater chance of dying en route. In river-tagged fish, the same genomic signature was associated with a 50% increase in mortality before reaching the spawning grounds in one of three stocks tested. At the spawning grounds, the same signature was associated with 3.7-fold greater odds of dying without spawning. Functional analysis raises the possibility that the mortality-related signature reflects a viral infection.

For 60 years preceding the early 1990s, approximately 8 million sockeye salmon (*Oncorhynchus nerka*) returned annually from the Pacific Ocean to Canada's Fraser River basin to spawn. However, since then, sockeye salmon productivity has declined precipitously to the point that returns in 2009 were less than the replacement rate. Consequently, the long-term viability of the wild salmon resource in British Columbia, worth over $1 billion dollars annually, is in doubt. Indeed, several of these Canadian stocks are at risk of extinction (*1*, *2*). In 2009, the prime minister of Canada announced a judicial inquiry into this salmon collapse, which has occurred despite substantial reductions in fisheries harvest. Contributing to the collapse have been massive (40 to 95%) mortalities of adult sockeye salmon before spawning, both in the Fraser River en route to spawning areas and on spawning grounds (*3*). The causal mechanisms of this premature mortality have eluded multidisciplinary research by scientists and fisheries managers (*4*). However, the three functional genomics studies presented here reveal a striking and consistent association between a powerful genomic signature and salmon mortality.

Seven of the last 10 summers have been the warmest on record for the Fraser River, and biotelemetry has revealed high losses of migrating sockeye in regions of elevated river temperature (*5*). Warmer water reduces the delivery of oxygen to the tissues (aerobic scope) of salmon (*6*) and allows more rapid development of infections (*7*). Our preliminary studies also suggest that some fish are stressed before they reach the river, further impairing their survival (*8*). The current study was undertaken to advance our mechanistic understanding of the role of salmon condition (before mortality events occur) on migration and spawning success in the river. We combined established methodologies of nonlethal biopsy of ocean- and river-caught salmon with watershed-scale biotelemetry to follow the fate of tagged fish migrating upstream (*9*, *10*). Functional genomics and tracking of individuals were used to correlate physiological profiles with failed migrations and reproduction. Gene expression was profiled in gill tissue, a respiratory and ionoregulatory organ that is highly responsive to stress, chemical exposure, and disease.

Returning adult salmon caught in the ocean and river were gastrically implanted with a radio transmitter—or a Peterson disc tag if caught at spawning areas—and biopsied for blood, gill, muscle, and fin tissues (*10*); fin tissue was used to genetically identify sockeye stocks (*11*). We tracked individual fish with radio-receivers deployed

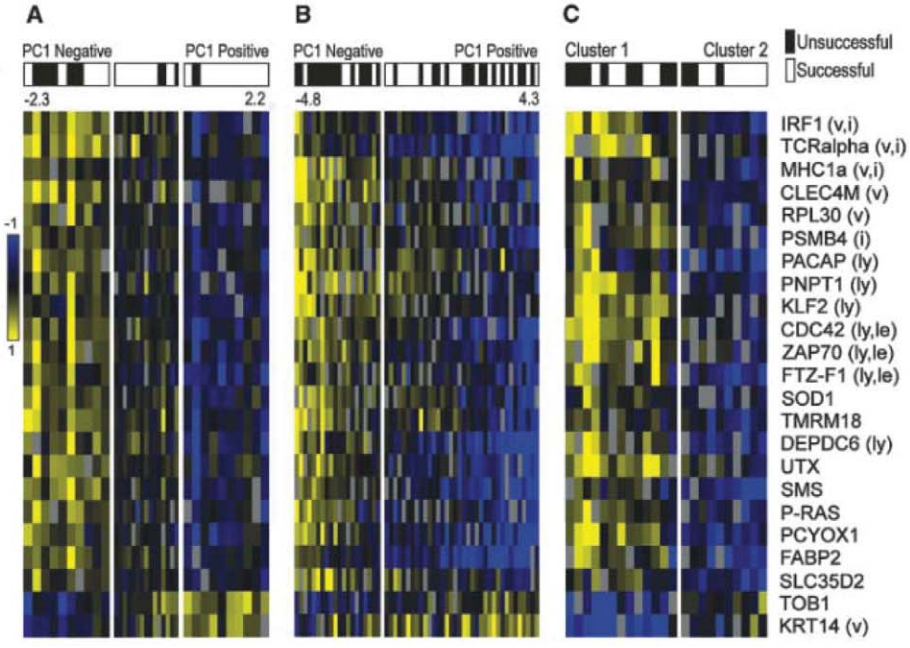

Fig. 1. Heatmaps of 23 annotated genes significantly associated with survivorship in all three studies. For (**A**) ocean-tagging and (**B**) freshwater-tagging studies, heatmaps reflect the ranking of individuals along the PC1 axis (rotational values shown above the heatmap), in which the associations with fate were strongest at the ends of the PC1 distribution, which are demarcated by white blocks. Migration success, depicted in the top bar, was reduced at the PC1-negative end of the axis for both studies. (**C**) For the spawning study, the heatmap reflects the relationships depicted by clustering significant genes from the freshwater PC1-based *t* test, with the white block differentiating the two emergent clusters and the black/white bar reflecting unsuccessful and successful spawners, respectively. (Right) Literature associations of genes with viruses (v), immune response (i), lymphocytes (ly), and leukemia (le) are depicted with letter codes in parentheses next to gene names. (Left) Expression levels are indicated by the color scale ranging from (up-regulated) yellow to (down-regulated) blue. Missing values are shown in light gray.

[1]Molecular Genetics Section, Pacific Biological Station, 3190 Hammond Bay Road, Fisheries and Oceans Canada, Nanaimo, BC V9T 6N7, Canada. [2]Department of Forest Sciences, University of British Columbia, Vancouver, BC V6T 1Z4, Canada. [3]Conservation Biology Section, Pacific Biological Station, 3190 Hammond Bay Road, Fisheries and Oceans Canada, Nanaimo, BC V9T 6N7, Canada. [4]Fisheries and Oceans Canada, Cooperative Resource Management Institute, School of Resource and Environmental Management, Simon Fraser University, Burnaby, BC V5A 1S6, Canada. [5]Department of Psychiatry, Centre for High-Throughput Biology, University of British Columbia, Vancouver, BC V6T 1Z4, Canada. [6]Fish Ecology and Conservation Physiology Laboratory, Department of Biology, Carleton University, Ottawa, ON K1S 5B6, Canada. [7]LGL Limited Environmental Research Associates, Sidney, BC V8L 3Y8, Canada. [8]Department of Zoology and Faculty of Land and Food Systems, University of British Columbia, Vancouver, BC V6T 1Z4, Canada.

*To whom correspondence should be addressed. E-mail: kristi.miller@dfo-mpo.gc.ca

throughout the Fraser watershed (fig. S1) to identify date of river entry (for ocean-tagged fish) and in-river fate (location the fish was last detected). Expression profiles were compared between fish that arrived at spawning areas (successful migrants) with those that perished en route. Previous biotelemetry data showed that large losses of sockeye in the upper river (above Hells Gate) (fig. S1) cannot be attributed to river fisheries, which are largely restricted to the lower river (*12*). Thus, to minimize interference from fisheries activities we contrasted expression profiles only for survivors and fish disappearing above Hells Gate in the ocean-tagging study (n = 35 salmon), comprising Late Shuswap Adams fish released 215 and 300 km from the river mouth, in Johnstone Strait and Juan de Fuca Strait, respectively (fig. S1 and table S1). The larger freshwater-tagging study (n = 104 salmon) occurred 69 km upstream of the river mouth on Late Shuswap (largely Adams), Chilko, and Scotch Creek stocks that perished throughout the Fraser River drainage but survived at least 2 days after tagging (to minimize tagging and handling effects). Because large numbers of fish [for example, >80% (*3*)] can die on the spawning areas before spawning, we tagged fish at the Weaver Creek spawning area (fig. S1) and compared the genomic signatures of 11 failed and 12 successful spawners. The ocean and freshwater studies used a salmonid 16K feature cDNA microarray (*13*, *14*), in which 11,535 of the 16,008 genes have gene annotations, whereas the spawning study used a salmonid 32K feature cDNA microarray (*15*), which contained an additional 16K genes, 7513 with gene annotations (*16*, *17*).

Supervised analyses of the ocean-tagging data (analysis of variance and computer algorithm) to detect genes differentially expressed between successful and unsuccessful migrants did not yield a significant result, suggesting that a single physiological mechanism was not likely to be responsible for all river mortality. Alternately, by taking an unsupervised principal component (PC) analysis approach we identified the underlying gene expression patterns in the data and assessed the top five PCs for associations with fate. Among the top five PCs, only PC1 (explaining 12% of the variance in the data) yielded a ranking of fish that showed a significant correlation with survival (Mann-Whitney U = 183, with P = 0.03). Further data inspection revealed a complex relationship between fate and PC1, with enrichment at the negative and positive ends of the PC1 distribution, encompassing approximately 60% of the fish in the study (Fig. 1A). Upper river mortalities were twice as common in the PC1 negative and three times less common in the PC1 positive ends, corresponding to an odds ratio (OR) of 13.5. Moreover, arrival at the receiver adjacent to Adams River spawning areas was on average 15 days faster for successful PC1-negative migrants than successful PC1-positive migrants, 10 days faster after river entry. In 2006, successful spawners also swam upstream slower than fish that failed [20.0 versus 15.5 km/day (*18*)]. Taken together, these results showed that up to 60% of fish contained a gene expression signature in seawater >200 km from the river that was predictive of in-river fate, which in 2006 represented over 2.4 million Late Shuswap fish.

We hypothesized that a similar pattern would exist in the freshwater-tagging study. Comparing only successful migrants and upper-river mortalities (n = 56 salmon), the first PC of the freshwater-tagging data was related to PC1 of the ocean-tagging data (see below). Again, an over-representation of unsuccessful migrants was apparent on the extreme PC1-negative end of the distribution, with the odds of successful migration five times lower in the first third of PC1-negative fish as compared with all remaining fish in the study (χ^2, $P < 0.05$) (Fig. 1B). PC2 to PC5 showed no correlation with survival, and supervised analyses did not yield a significant result (*17*).

The larger freshwater-tagging study included fish that went missing throughout the Fraser River and sufficient sample sizes from three salmon stocks so as to facilitate a more precise analytical

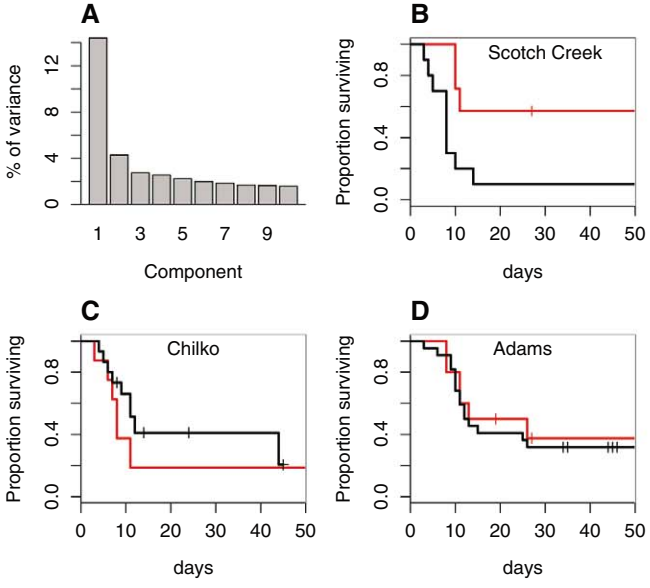

Fig. 2. Survivorship analysis revealed a significant interaction between stock and PC1 in fresh water. (**A**) Graphical representation of PC1 to PC10. (**B** to **D**) Survivorship curves for Scotch Creek, Chilko, and Late Shuswap Adams, respectively. Although in the analysis the value of PC1 was taken as a continuous variable, to graphically represent the correlation with survival the PC1 rotational values were divided into negative (<0, black line) and positive (>0, red line) categories.

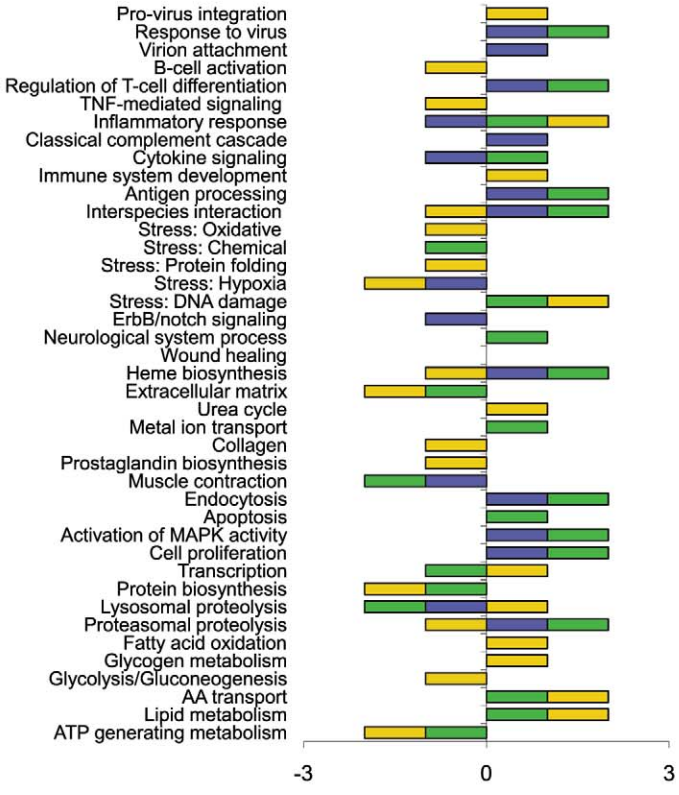

Fig. 3. Functional analysis of signatures associated with fate in (blue) saltwater, (green) freshwater, and (yellow) spawning studies. The axis indicates the number of studies in which a biological process (defined as a collection of molecular events with a defined beginning and end) was (positive) up- or (negative) down-regulated in the mortality- versus survivor-related PC1 signature. Biological processes differentially regulated with no clear indication of overall direction are not shown. A more detailed presentation is available in table S3.

approach. Using all but known fisheries losses for these stocks [n = 72 salmon; see (*17*) for fisheries analyses], the first four PCs along with stock and sex were included as explanatory variables in survivorship analysis (*17*). Parametric survival analysis revealed a significant stock *PC1 interaction [$F_{2,65}$ = 7.30, P = 0.026]. Further analysis revealed a significant relationship between PC1 and survival for Scotch Creek fish [$F_{1,14}$ = 4.97, P = 0.026] but not for Chilko or Late Shuswap salmon (P > 0.05) (Fig. 2). Although the stock *PC3 interaction [$F_{2,65}$ = 6.44, P = 0.040] was also significant, the relationship was not significant when individual stocks were considered (*17*). PC2, PC4, and sex were not explanatory. Differences observed among stocks suggest that some are more severely affected than others. However, other influences could include stock-specific differences in travel time to the receiver adjacent to spawning tributaries (averaging 12, 17, and 24 days, respectively, for Chilko, Scotch, and Late Shuswap), travel time from last receiver to spawning areas (7 days Chilko versus 1 day Scotch/Late Shuswap), and levels of subsequent mortality on spawning areas.

To obtain groups of significant genes for functional analysis, we used t tests to compare samples in the extreme PC1-positive and -negative quartiles for both studies. A reproducible pattern of gene expression correlated with fate emerged. 1603 genes were significant at P < 0.001 in saltwater, and 2762 genes were significant in fresh water. 498 genes were common to both independent data sets, of which 97% were directionally congruent and 90% were up-regulated in PC1-negative fish (fig. S2).

To test the hypothesis that the same genomic signature was also associated with premature mortality at the Weaver Creek spawning area, we used the significant genes from the freshwater t test to cluster successful and unsuccessful spawners. Two well-differentiated clusters emerged, with >70% of unsuccessful spawners in the cluster associated with the PC1-negative mortality-related signature. Salmon with this signature were 3.7 times less likely to spawn than those with a PC1-positive–related signature, despite reaching the spawning area. To assess changes in the signature that may occur closer to spawning, we conducted a t test between the two clusters; 2507 significant genes were resolved (P < 0.001), of which 1136 were on the 16K array, with 36% overlap for freshwater and/or saltwater t test gene lists, 98% of which were directionally congruent (Fig. 1C and fig. S2). The correlation between genomic signatures associated with poor survival throughout return migration was further supported by quantitative reverse transcription polymerase chain reaction validation of six genes (APR-3, ATP6V1C1, FKBP2, C4B, SCHC, and CYP46A1) that showed even more consistent up-regulation in the mortality-related signature fish in all three tagging studies than revealed on microarrays (table S2).

Physiological differentiation along the PC1 axis escalated appreciably during migration into the river and toward spawning areas, with 25 biological processes differentially affected in the ocean, 34 in fresh water, and 47 at spawning (Fig. 3 and table S3) (*17*). Furthermore, an intensification of complement-mediated inflammatory and perforin-mediated apoptotic processes occurred for fish containing the mortality-related signature. Immune stimulation of these same fish was indicated by T-cell activation/proliferation and induction of a Th1 cellular immune response through interferon activation of the virus-specific innate JAK/STAT pathway. Some of the most consistent and/or significantly up-regulated genes (such as Mx, STAT1, IRF1, PRF1, MHC1a, PCSK5, and TCRα) have known linkages with viral activity (Fig. 1C and table S4). Moreover, 65% of affected biological processes were consistent with responses to viral infections (table S3); within these processes, many key regulators co-opted by or activated in response to viruses were differentially expressed (*17*). These data indicate that fish containing the genomic signature correlated with elevated mortality may be responding to viral infection [details are in (*17*)]. Linkages also existed with genes associated with leukemia, most notably cell lymphoblastic leukemia-lymphoma (fig. S3 and tables S3 and S4).

This correlative data set cannot be used to assign cause to the association between a preexisting signature and subsequent mortality. However, we can eliminate the possibility that this signature simply relates to the inevitable senescence of salmon after spawning because the mortality-survival–associated PC1 signature showed relatively stronger differentiation on the spawning area, when salmon were within 1 to 3 weeks of death, than in the ocean, when salmon were 3 to 10 weeks from death. The relatively stronger association with survival in the ocean-tagging study also suggests tagging effects did not appreciably influence the genomic relationships of PC1 with mortality (*17*). Moreover, because the mortality-related signature preexisted before river entry, it cannot reflect a response to stress of moving from seawater to fresh water. In fact, few indications of a general stress response existed within the mortality-related signature; DNA damage was the only stress-specific biological process up-regulated, as indicated by elevated expression of more than 20 genes (such as KIN, RAD51, CRY5, and NSMCE2) (Fig. 3). However, these fish could have experienced salinity stress in seawater induced by a premature transcriptional shift in osmoregulatory genes [Na^+/K^+ adenosine triphosphatase (ATPase) isoforms 1a, 1b, and a3 (fig. S5) and PRL, SHOP21, CIRBP, CLIC5 SLC5A1, and FXYD3] better suited for fresh water (*17*). Indeed, elevated chloride and osmolarity were anti-correlated with PC1 of ocean-tagged fish (Spearman rank = –0.33 and –0.27, respectively), supporting a 2006 tagging study that associated plasma ionic imbalances with coastal mortality (*19*) and salinity challenge experiments that revealed higher mortality for sockeye held in saltwater as compared with isoosmotic or fresh water (*20*). As a result, we speculate that osmoregulatory dysfunction of salmon containing the mortality-related signature may have contributed to ocean mortality and possibly stimulated faster entry into fresh water.

This combination of watershed-scale biotelemetry and functional genomics of wild salmon in nature has yielded new insight into one potential physiological mechanism associated with survivorship during return migration. Migrating salmon are expected to markedly transform gene expression, given the required physiological demands associated with upstream swimming, environmental shifts, maturation, fuel depletion, and senescence. Our study revealed a mechanistic signature associated with premature mortality of salmon measurable >1 month to <1 week ahead of death and throughout the river. Our hypothesis is that the genomic signal associated with elevated mortality is in response to a virus infecting fish before river entry and that persists to the spawning areas.

References and Notes

1. J. R. Irvine *et al.*, *Fisheries* **30**, 11 (2005).
2. P. S. Rand, *Oncorhyncus nerka*, in IUCN 2010: IUCN Red List of Threatened Species, version 2010.4 (www.iucnredlist.org).
3. S. J. Cooke *et al.*, *Fisheries (Bethesda, Md.)* **29**, 22 (2004).
4. S. G. Hinch, in Conference on Early Migration and Premature Mortality in Fraser River Late-Run Sockeye Salmon: Proceedings, Vancouver, BC, S.G. Hinch and J. Gardner, Eds. (Pacific Fisheries Resource Conservation Council, Vancouver, BC, 2009), pp. 8–14; www.psc.org/info_laterunsockeye.htm.
5. M. T. Mathes *et al.*, *Can. J. Fish. Aquat. Sci.* **67**, 70 (2010).
6. H. O. Pörtner *et al.*, *Science* **323**, 876 (2009).
7. G. N. Wagner *et al.*, *Can. J. Fish. Aquat. Sci.* **62**, 2124 (2005).
8. S. J. Cooke *et al.*, *Can. J. Fish. Aquat. Sci.* **63**, 1469 (2006).
9. K. A. English *et al.*, *Trans. Am. Fish. Soc.* **134**, 1342 (2005).
10. S. J. Cooke *et al.*, *Fisheries (Bethesda, Md.)* **33**, 321 (2008).
11. T. D. Beacham *et al.*, *Trans. Am. Fish. Soc.* **134**, 1124 (2005).
12. E. G. Martins *et al.*, *Glob. Change Biol.*, published online 26 April 2010 (10.1111/j.1365-2486.2010.02241.x).
13. K. R. von Schalburg *et al.*, *BMC Genomics* **6**, 126 (2005).
14. B. F. Koop, W. Davidson, www.uvic.ca/cbr/grasp.
15. B. F. Koop *et al.*, *BMC Genomics* **9**, 545 (2008).
16. K. M. Miller *et al.*, *Comp. Biochem. Physiol. D* **4**, 75 (2009).
17. Materials and methods are available as supporting material on *Science* Online.
18. G. T. Crossin *et al.*, *Physiol. Biochem. Zool.* **82**, 635 (2009).
19. G. T. Crossin *et al.*, *Can. J. Zool.* **86**, 127 (2008).
20. M. S. Cooperman *et al.*, *Physiol. Biochem. Zool.* **83**, 459 (2010).
21. Microarray data were deposited (according to Microarray Gene Expression Data Society Standard) in the National Center for Biotechnology Information Gene Expression Omnibus (GEO, www.ncbi.nlm.nih.gov/geo/) with the saltwater experimental accession number GSE22171, freshwater GSE22177, spawning GSE22347, and Superseries ID GSE22179. We thank the Pacific Salmon Commission Southern Endowment Fund, Department of Fisheries and Oceans Genomics Research and Development Fund, Genome British Columbia, and Natural Sciences and Engineering Research Council of Canada for research support. All procedures used were developed with approvals and guidance from the Canadian Council on Animal

Care administered by the University of British Columbia and Fisheries and Oceans Canada. We thank M. Donaldson, I. Olsson, G. Crossin, K. Hanson, R. Alexander, D. Robichaud, S. Tyerman, D. Welch, and J. Hills for tagging and biopsies; L. Stenhouse and A. Schulze for RNA extractions; M. Shrimpton for gill Na^+/K^+ ATPase activity levels; C. Wallace for figure preparation; M. Lapointe and C. McConnell for organizational assistance; and the skippers and crews of the ocean vessels *Sunfisher* and *Belina*.

Supporting Online Material
www.sciencemag.org/cgi/content/full/331/6014/214/DC1
Materials and Methods
Supplemental Results
Figs. S1 to S5
Tables S1 to S4

24 August 2010; accepted 1 December 2010
10.1126/science.1196901

The Structure of Human 5-Lipoxygenase

Nathaniel C. Gilbert,[1] Sue G. Bartlett,[1] Maria T. Waight,[1] David B. Neau,[2] William E. Boeglin,[3] Alan R. Brash,[3] Marcia E. Newcomer[1]*

The synthesis of both proinflammatory leukotrienes and anti-inflammatory lipoxins requires the enzyme 5-lipoxygenase (5-LOX). 5-LOX activity is short-lived, apparently in part because of an intrinsic instability of the enzyme. We identified a 5-LOX–specific destabilizing sequence that is involved in orienting the carboxyl terminus, which binds the catalytic iron. Here, we report the crystal structure at 2.4 angstrom resolution of human 5-LOX stabilized by replacement of this sequence.

Leukotrienes and lipoxins are potent mediators of the inflammatory response derived from arachidonic acid (AA). When leukocytes are activated, AA is released from the nuclear membrane by the action of cytosolic phospholipase A_2 and binds 5-lipoxygenase–activating protein (FLAP). The increased Ca^{2+} concentration of the activated cells simultaneously promotes translocation of 5-LOX to the nuclear membrane, where it acquires its substrate from FLAP (*1*, *2*). AA is converted to leukotriene A_4 in a two-step reaction that produces the 5*S*- isomer of hydroperoxyeicosatetraenoic acid (5*S*-HPETE) as an intermediate (*3*, *4*).

Autoinactivation of 5-LOX activity has been described, and this loss of activity is perhaps important in limiting the synthesis of its pro- and anti-inflammatory products (*5*). Previous reports indicate that non–turnover-based inactivation is a consequence of an O_2 sensitivity linked to the oxidation state of the catalytic iron (*6*). However, not all LOXs display this hypersensitivity to O_2. For example, 8*R*-LOX activity is stable despite a solvent-exposed iron coordination sphere equivalent to that in 5-LOX (*7*). In similar conditions, 50% of 5-LOX activity is lost in 10 hours (*8*). We reasoned that 5-LOX–specific destabilizing features may confer susceptibility to non–turnover-based inactivation. Regulatory mechanisms that facilitate transient activation include targeted degradation, phosphorylation, and allosteric control of enzyme activities. Autoinactivation as a consequence of intrinsic protein instability may play a similar role. For example, the instability of the tumor suppressor protein p53, relative to its orthologs such as p73, has been proposed to have a functional role (*9*).

On the basis of the crystal structures of two AA-metabolizing lipoxygenases [an 8*R*-LOX from *Plexaura homomalla* (*7*, *10*) and a 15-LOX from rabbit reticulocyte (*11*, *12*)], each with ~40% sequence identity to 5-LOX, we identified a 5-LOX–specific lysine-rich region near the C terminus of the enzyme that might confer instability (*13*). In the 8*R*- and 15-LOX structures, a turn centered on amino acid 655 (5-LOX numbering) leads from the C-terminal helix to the C-terminal segment and allows the terminal carboxylate to penetrate the LOX body and bind the catalytic iron (Fig. 1, A and B). In most LOXs, amino acid 655 is a highly conserved Leu, with its side chain pointing toward an invariant Arg (Arg^{651}). A striking 5-LOX–specific feature is Lys in place of Leu at this position as part of a di- or tri-Lys peptide (fig. S1). Although numerous salt links anchor the C-terminal helix to the

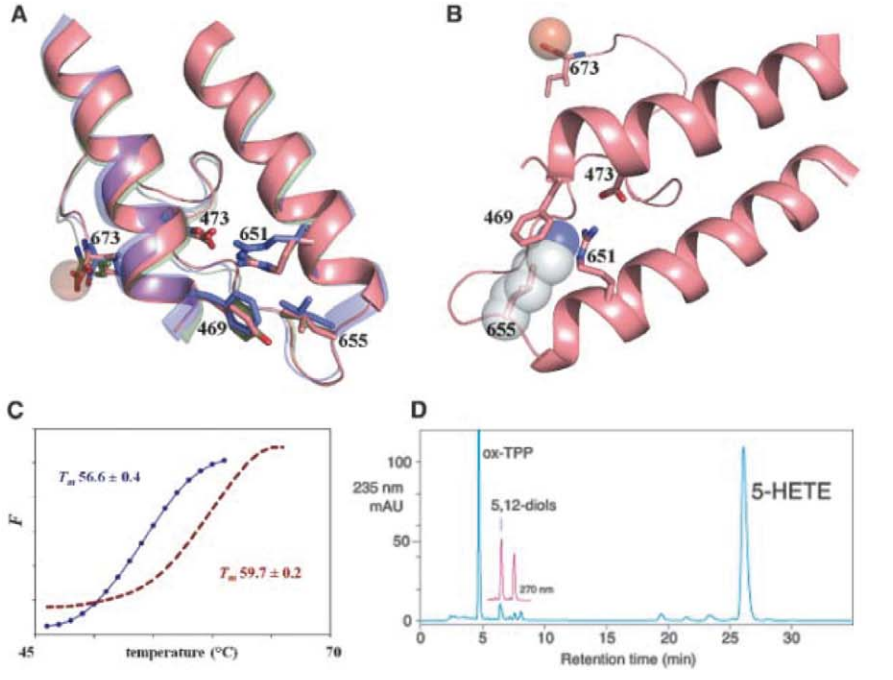

Fig. 1. Stabilization of human 5-LOX. (**A**) Superposition of the C-terminal regions of the structures of 15-, 8*R*-, and Stable-5-LOX. The C-terminal segment that leads to the catalytic Fe emanates from the helix that terminates at amino acid 655 (5-LOX numbering; Stable-5-LOX, pink; 8*R*-LOX green; 15-LOX, blue). Highly conserved amino acids (Leu and Phe/Tyr) and an invariant salt link (Asp-Arg) are depicted in stick rendering. (**B**) Detail of the turn at the end of the terminal helix. The 5-LOX–specific Lys (replaced in Stable-5-LOX with Leu) is modeled at position 655 as its most common rotamer (transparent sphere rendering). As positioned, it would interfere with the invariant salt-link and cation-π interactions. All figures were generated with Pymol (*31*). (**C**) Thermal denaturation of Stable-5-LOX (red) and the parent enzyme Sol-5-LOX (blue). Fluorescence (*F*) is monitored as a function of temperature. T_m (with SD) 56.6°C (±0.4°) and 59.7°C (±0.2°) for Sol-5-LOX and Stable-5-LOX, respectively. (**D**) High-performance liquid chromatography chromatogram. Product analysis of Stable-5-LOX reveals both 5-HETE (5-HPETE reduced by the addition of triphenylphosphine, TPP) and leukotriene A_4 hydrolysis products (5,12-diols).

[1]Department of Biological Sciences, Louisiana State University, Baton Rouge, LA 70803, USA. [2]Northeastern Collaborative Access Team, Argonne National Laboratory, 9700 South Cass Avenue, Argonne, IL 60439, USA. [3]Department of Pharmacology, Vanderbilt University School of Medicine, Nashville, TN 37232, USA.

*To whom correspondence should be addressed. E-mail: newcomer@lsu.edu

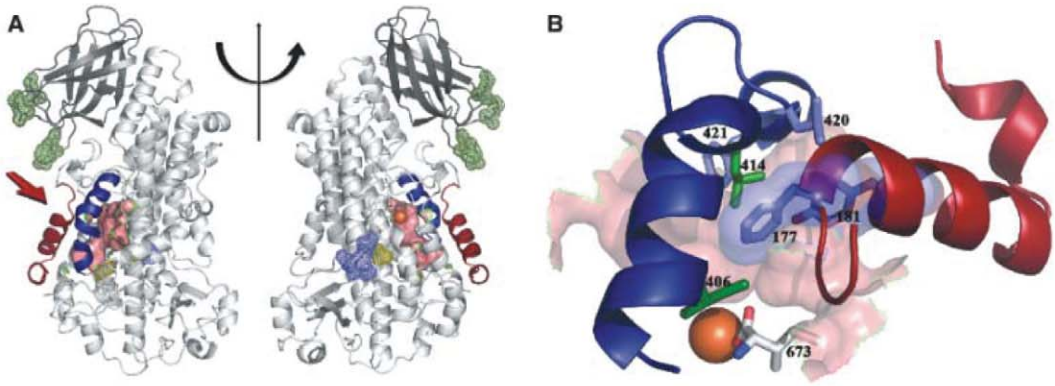

Fig. 2. The structure of Stable-5-LOX. (**A**) A cartoon rendering of 5-LOX. The two views differ by a 180° rotation about the vertical line. The N-terminal C2-like domain is in dark gray, and the catalytic domain in light gray. The distinctive arched helix is in blue, and helix α2 in red. The internal cavity, generated with CastP (*32*), is in pink, and the Fe is an orange sphere. The positions of the mutated amino acids are indicated in mesh rendering: green, putative membrane insertion residues; yellow, proximal cysteines; and blue, the KKK→ENL substitution. (**B**) Detail of the relation of the arched helix and helix α2 to the active site as viewed from the perspective indicated by the red arrow in (A). Shown in stick rendering are amino acids 406, 414, 420, and 421 of the arched helix and Phe^{177} and Tyr^{181} from helix α2 (with transparent surface rendering). The latter two bulky amino acids obstruct access to the cavity. The proximity of the C-terminal Ile^{673} to the corked portal is apparent.

body of the protein in the structures of the two homologs noted above, none of these salt links is conserved in the 5-LOX sequence. As a consequence of the lysine-rich sequence and the absence of helix-anchoring salt links, the orientation of the terminal helix is less favorable and the C-terminal ligand to the active site Fe is likely to be tenuously restrained. Conservative mutations in the C-terminal helix have been noted to reduce enzyme expression levels and activity (*14*). These observations led us to replace 5-LOX K^{653}KK^{655} with the corresponding sequence from 8*R*-LOX (ENL) in an effort to stabilize the enzyme for crystallographic studies (*15*).

The mutant human enzyme (herein referred to as Stable-5-LOX) was prepared in the context of a soluble 5-LOX (Sol-5-LOX) that lacks putative membrane-insertion amino acids (Δ40to 44GS, W13E, F14H, W75G, and L76S), as well as a pair of cysteines (C240A and C561A) predicted to be proximal in the 5-LOX structure. Substitution of the membrane insertion loops was based on a similar approach with the *P. homomalla* enzyme, which shares both these amino acids and Ca^{2+}-binding residues with 5-LOX in the N-terminal membrane-binding domain (*16*). The replacement of KKK with ENL in this context led to a ~3°C increase in the melting temperature (T_m) of the enzyme (Fig. 1C). Moreover, Stable-5-LOX has a longer half-life at 37°C (~16 hours versus ~7 hours) (fig. S2). Furthermore, Stable-5-LOX produces both the intermediate 5*S*-HPETE and the product leukotriene A_4 (Fig. 1D), as does its progenitor protein Sol-5-LOX (fig. S3). In addition, we measured an apparent dissociation constant (K_m) for AA of ~11 μM (fig. S4), equivalent to that of the wild-type enzyme (*17*). These observations are consistent with the proposal that the KKK sequence is destabilizing and that its substitution does not affect catalytic fidelity. The structure of Stable-5-LOX was determined to 2.4 Å resolution (Fig. 2A, fig. S5, and table S1).

The canonical LOX framework contains two distinct domains: the N-terminal "C2-like" domain (~120 amino acids), which in 5-LOX confers Ca^{2+}-dependent membrane binding (*18*–*21*), and the larger catalytic domain. The latter is primarily α-helical and harbors the nonheme catalytic iron. The iron is coordinated by three conserved histidines (histidines 367, 372, and 550), as well as the main-chain carboxylate of the C terminus (Ile^{673}). Another structurally distinct conserved feature in this domain, previously described in detail by Minor *et al* (*22*) for soybean LOX L-1, is an arched helix that shields access to the catalytic iron. At the vertex of the Stable-5-LOX arched helix is Leu^{414} (Fig. 2B), an invariant amino acid that in other lipoxygenases has been proposed to control access of O_2 to the substrate (*23*, *24*) or to position the substrate pentadiene for attack (*7*). Additional amino acids from the arched helix that help define the catalytic site are Leu^{420} and Phe^{421}. The crystal structure of Stable-5-LOX reveals a striking variation on the classic lipoxygenase fold in helix α2, which defines one edge of the active site. In the structures of 8*R*- and 15-LOX, helix α2 is six to seven turns, whereas in Stable-5-LOX, it is a short three-turn helix flanked by extended loops. The shortened helix is positioned at ~45° to its counterparts in the 8*R*- and 15*S*- enzymes (Fig. 3, A and B). The unique orientation of helix α2 in Stable-5-LOX greatly limits access to the catalytic iron and yields a distinctive active site cavity. Specifically, the side chains of Phe^{177} and Tyr^{181} are positioned inward and close off an access channel to the catalytic iron that is observed in both the 8*R*- and 15-LOX structures (Figs. 2B and 4A). The remainder of the secondary structural elements and their relative orientations are maintained (Fig. 3B). In addition, the structural context of the Lys-rich peptide also appears conserved as the C-terminal helices superimpose (Fig. 1A). However, it is apparent that a Lys at position 655 would interfere with invariant salt link and cation-π interactions (Fig. 1B).

In Stable-5-LOX, the active site is an elongated cavity, with no clear access to bulk solvent,

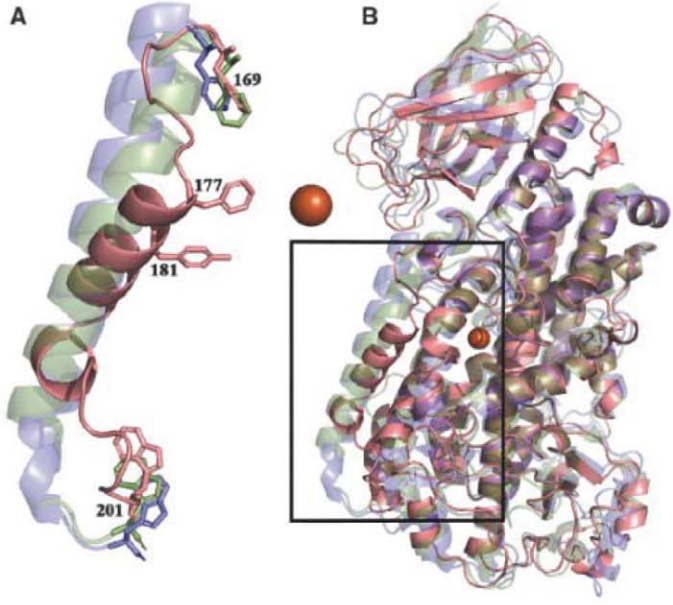

Fig. 3. The positioning of helix α2 is unique in 5-LOX. (**A**) A 5-LOX cartoon is rendered in pink, 15-LOX in blue and 8*R*-LOX in green. Conserved aromatic amino acids (Phe^{169} and Trp^{201}) that flank the region are in stick rendering. Phe^{177} and Tyr^{181}, which make up the cork that helps define the active site, are in stick. The catalytic iron is an orange sphere. (**B**) A full overlay of the three structures in which it is apparent that, with the exception of α2, the secondary structural elements in the enzymes are conserved. The box indicates the region amplified in (A).

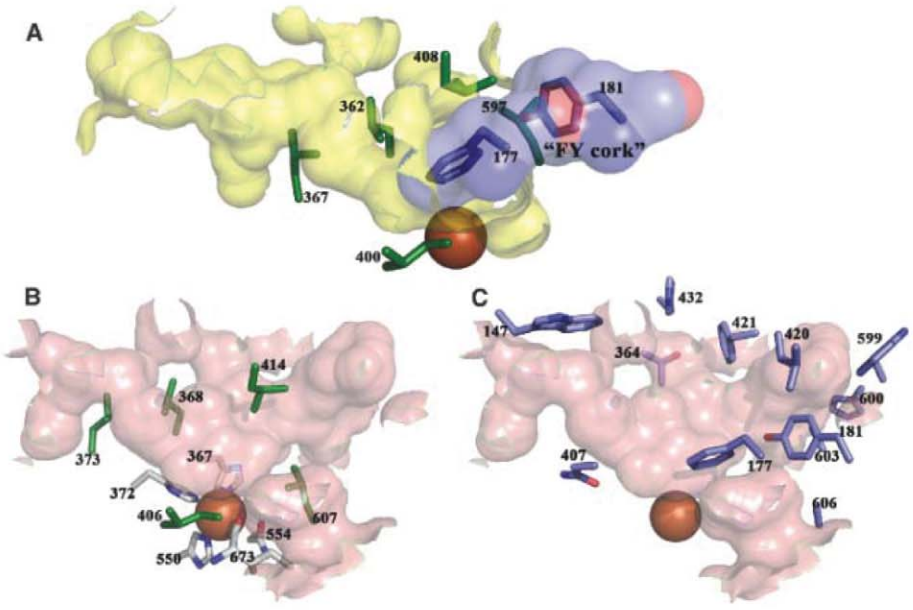

Fig. 4. The 5-LOX active site. Internal cavities calculated with CastP (*32*). (**A**) The active site cavity of 15-LOX (2P0M) is in yellow. Invariant Leu and Ile side chains are in green stick rendering. The 5-LOX FY cork is superposed on the 15-LOX cavity and plugs the entrance. (**B**) The equivalent orientation of the active site cavity of Stable-5-LOX in pink; invariant Leu and Ile side chains in green sticks. Note the similarity of the positions of these amino acids to their counterparts in 15-LOX (A). Iron coordination sphere amino acids (C, white) are in stick rendering, and the iron an orange sphere. (**C**) 5-LOX amino acids that contribute to the active site cavity. Entry into this cavity requires a conformational change.

lined with both invariant and 5-LOX–specific amino acids. Leucines 368, 373, 414, and 607 and Ile^{406} are conserved in all AA-metabolizing lipoxygenases (*7*) and form a structurally similar constellation of branched hydrophobic side chains that envelops the region where the pentadiene must be positioned for catalysis (Fig. 4, A and B). Tyr^{181}, Ala^{603}, Ala^{606}, His^{600}, and Thr^{364} are specific to 5-LOX sequences, and the small side chains of Ala^{603} and Ala^{606} appear to be required for the conformation of Tyr^{181}, which, along with Phe^{177}, "corks" the cavity at one end. Tyr^{181} is in van der Waals contact with Ala^{603}, and the small side chains of both 603 and 606 allow both bulky aromatics (Phe^{177} and Tyr^{181}) to point into the cavity where they can be shielded from solvent (Fig. 4C). An additional 5-LOX–specific amino acid, Trp^{599}, appears to buttress the FY cork from one side. Amino acids Asn^{407} and His^{432} also help define the active site.

The closed cavity (volume, 663 Å^3) raises the question of how substrate gains access to the catalytic iron. Two possibilities can be envisioned: (i) removal of the FY cork at one end of the cavity and/or movement of Trp^{599} that secures it, or (ii) a rotamer shift of Trp^{147} at the opposite end. A rotamer shift in Trp^{147} would require only rotation of the side chain, whereas the former may require both side-chain and main-chain movements in two amino acids. This observation suggests that AA may enter 5-LOX from the opposite direction as it does in the 15*S*- or 8*R*- enzymes, which lack the FY cork. This site of entry fits well with what is known about the catalytic mechanism: H abstraction and peroxidation occur on opposite sides of the pentadiene (*25*). The *S*-stereochemistry of the 5-LOX product is consistent with an "inverse" orientation of AA relative to that for the 15*S*- and 8*R*- enzymes (*26*, *27*). An opening at the Trp^{147} end would allow the AA to enter methyl end first and position the substrate for the production of the *S* isomer of 5-HPETE. While the above model is attractive, the structure does not rule out the alternative: that the AA enters the same portal it does in 8*R*- and 15*S*-enzymes. Carboxylate-first entry in the latter mode achieves the same binding orientation and reaction specificity.

The 2.4 Å structure of Stable-5-LOX reveals an active site which, despite a conserved constellation of five invariant amino acids, is clearly distinct from the active sites of the AA metabolizing lipoxygenases for which structures are available. The structure provides a context for the development of 5-LOX–specific inhibitors and, together with the crystal structures of FLAP (*28*) and the downstream enzyme leukotriene C_4 synthase (*29*, *30*), a molecular model for early events in leukotriene biosynthesis.

References and Notes

1. J. F. Evans, A. D. Ferguson, R. T. Mosley, J. H. Hutchinson, *Trends Pharmacol. Sci.* **29**, 72 (2008).
2. R. A. Dixon *et al.*, *Nature* **343**, 282 (1990).
3. O. Rådmark, B. Samuelsson, *J. Lipid Res.* **50** (suppl.), S40 (2009).
4. T. Shimizu, O. Rådmark, B. Samuelsson, *Proc. Natl. Acad. Sci. U.S.A.* **81**, 689 (1984).
5. R. C. Murphy, M. A. Gijón, *Biochem. J.* **405**, 379 (2007).
6. M. D. Percival, D. Denis, D. Riendeau, M. J. Gresser, *Eur. J. Biochem.* **210**, 109 (1992).
7. D. B. Neau *et al.*, *Biochemistry* **48**, 7906 (2009).
8. Y. Y. Zhang, M. Hamberg, O. Rådmark, B. Samuelsson, *Anal. Biochem.* **220**, 28 (1994).
9. J. M. Cañadillas *et al.*, *Proc. Natl. Acad. Sci. U.S.A.* **103**, 2109 (2006).
10. M. L. Oldham, A. R. Brash, M. E. Newcomer, *J. Biol. Chem.* **280**, 39545 (2005).
11. S. A. Gillmor, A. Villaseñor, R. Fletterick, E. Sigal, M. F. Browner, *Nat. Struct. Biol.* **4**, 1003 (1997).
12. J. Choi, J. K. Chon, S. Kim, W. Shin, *Proteins* **70**, 1023 (2008).
13. Materials and methods are available as supporting material on *Science* Online.
14. H. Kuhn, M. Anton, C. Gerth, A. Habenicht, *Arterioscler. Thromb. Vasc. Biol.* **23**, 1072 (2003).
15. Single-letter abbreviations for the amino acid residues are as follows: A, Ala; C, Cys; D, Asp; E, Glu; F, Phe; G, Gly; H, His; I, Ile; K, Lys; L, Leu; M, Met; N, Asn; P, Pro; Q, Gln; R, Arg; S, Ser; T, Thr; V, Val; W, Trp; and Y, Tyr.
16. D. B. Neau, N. C. Gilbert, S. G. Bartlett, A. Dassey, M. E. Newcomer, *Acta Crystallogr. Sect. F Struct. Biol. Cryst. Commun.* **63**, 972 (2007).
17. D. Aharony, R. L. Stein, *J. Biol. Chem.* **261**, 11512 (1986).
18. X. S. Chen, Y. Y. Zhang, C. D. Funk, *J. Biol. Chem.* **273**, 31237 (1998).
19. X. S. Chen, C. D. Funk, *J. Biol. Chem.* **276**, 811 (2001).
20. T. Hammarberg, K. V. Reddy, B. Persson, O. Rådmark, *Adv. Exp. Med. Biol.* **507**, 117 (2002).
21. S. Kulkarni, S. Das, C. D. Funk, D. Murray, W. Cho, *J. Biol. Chem.* **277**, 13167 (2002).
22. W. Minor *et al.*, *Biochemistry* **35**, 10687 (1996).
23. M. J. Knapp, J. P. Klinman, *Biochemistry* **42**, 11466 (2003).
24. M. J. Knapp, F. P. Seebeck, J. P. Klinman, *J. Am. Chem. Soc.* **123**, 2931 (2001).
25. C. Schneider, D. A. Pratt, N. A. Porter, A. R. Brash, *Chem. Biol.* **14**, 473 (2007).
26. M. Walther, I. Ivanov, G. Myagkova, H. Kuhn, *Chem. Biol.* **8**, 779 (2001).
27. G. Coffa, A. R. Brash, *Proc. Natl. Acad. Sci. U.S.A.* **101**, 15579 (2004).
28. A. D. Ferguson *et al.*, *Science* **317**, 510 (2007).
29. H. Ago *et al.*, *Nature* **448**, 609 (2007).
30. D. Martinez Molina *et al.*, *Nature* **448**, 613 (2007).
31. W. L. DeLano, www.pymol.org (2002).
32. J. Dundas *et al.*, *Nucleic Acids Res.* **34**, W116-8 (2006).

33. This work was funded in part by grants from the American Heart Association (MCB 08553920E) and NSF (0818387) to M.E.N. and from NIH (GM-15431) to A.R.B. Preliminary work was performed at the Center for Advanced Microstructures and Devices (Baton Rouge), funded in part by the Louisiana Governors' Biotechnology Initiative. X-ray data were collected at Beam Line 24-ID-E of NE-CAT at the Advanced Photon Source. Atomic coordinates and structure factors have been deposited in the Protein Data Bank under accession number 3O8Y. M.E.N., N.C.G., and S.G.B, have applied for a patent on the modified enzyme (Stable-5-LOX). For noncommercial use, the construct will be supplied subject to a material transfer agreement.

Supporting Online Material

www.sciencemag.org/cgi/content/full/331/6014/217/DC1
Materials and Methods
Figs. S1 to S5
Table S1
References

31 August 2010; accepted 7 December 2010
10.1126/science.1197203

Light-Driven Changes in Energy Metabolism Directly Entrain the Cyanobacterial Circadian Oscillator

Michael J. Rust,[1]* Susan S. Golden,[2] Erin K. O'Shea[1]†

Circadian clocks are self-sustained biological oscillators that can be entrained by environmental cues. Although this phenomenon has been studied in many organisms, the molecular mechanisms of entrainment remain unclear. Three cyanobacterial proteins and adenosine triphosphate (ATP) are sufficient to generate oscillations in phosphorylation in vitro. We show that changes in illumination that induce a phase shift in cultured cyanobacteria also cause changes in the ratio of ATP to adenosine diphosphate (ADP). When these nucleotide changes are simulated in the in vitro oscillator, they cause phase shifts similar to those observed in vivo. Physiological concentrations of ADP inhibit kinase activity in the oscillator, and a mathematical model constrained by data shows that this effect is sufficient to quantitatively explain entrainment of the cyanobacterial circadian clock.

Circadian clocks, based on self-sustained biological oscillators with a ~24-hour period, allow organisms to anticipate regular variations in the environment caused by Earth's rotation (*1*). For a circadian system to be most useful to the organism, it must function robustly in the face of fluctuations in the environment but also accept appropriate input signals to stay entrained with the true diurnal cycle. Therefore, a fundamental problem is to elucidate the molecular mechanisms that allow faithful transduction of timing information into the oscillator.

The cyanobacterium *Synechococcus elongatus* PCC 7942 has a core circadian oscillator that can be reconstituted in vitro from three purified proteins: KaiA, KaiB, and KaiC (*2*). KaiC is an enzyme that catalyzes the phosphorylation and dephosphorylation of two of its own residues in an ordered pattern (*3*). KaiA and KaiB work together to modulate the activity of KaiC in a phosphorylation-dependent manner, resulting in stable oscillations in the amount of phosphorylated KaiC (*4*–*6*). We sought to identify light-dependent clock input pathways in living cyanobacteria and to study their mechanism in the reconstituted in vitro oscillator.

Causal links between metabolic activity and circadian clocks have previously been described. The circadian clock in the rat liver can be entrained by feeding (*7*), and adenosine monophosphate–activated protein kinase has been implicated in clock function in liver tissue (*8*). A classical result connecting clocks and metabolism is Aschoff's Rule—the observation that varying the light intensity tends to have opposite effects on the circadian clocks of nocturnal versus diurnal organisms (*9*).

We reasoned that the link to metabolism might be especially important in photoautotrophic cyanobacteria, as these microorganisms are entirely reliant on photosynthesis to extract energy from the environment (*10*). Darkness elicits profound changes in the physiology of *S. elongatus*, beyond the direct effects on photosynthesis. When cultures are removed from the light, global transcription and translation rates drop and large changes in the superhelicity of endogenous DNA are observed (*11*, *12*).

Cyanobacteria growing in the light primarily synthesize adenosine triphosphate (ATP) by photophosphorylating adenosine diphosphate (ADP) at the thylakoid membrane (*13*), and changes in culture illumination have been reported to affect the relative abundance of adenine nucleotides (*14*–*16*). We therefore tested whether incubating synchronized cultures in the dark under conditions sufficient to cause a phase shift in the circadian clock would result in changes in the concentrations of ATP and ADP. We monitored changes induced by a dark pulse in the circadian rhythm of an engineered strain of *S. elongatus* with a bioluminescent reporter of clock-driven transcription (*17*). In agreement with previous studies, an 8-hour dark pulse applied during the subjective day (Fig. 1A) induced a phase shift in the circadian rhythm, and the clock was refractory to a dark pulse applied during the subjective night (Fig. 1B) (*18*–*20*). These phase shifts in the transcriptional reporter were mirrored by shifts in the rhythm of KaiC phosphorylation, as measured by immunoblotting (fig. S1). Irrespective of when the dark pulse was applied, these cultures experienced large changes in their adenine nucleotide pool (Fig. 1C). After 2 to 3 hours in the dark, the ATP/(ADP + ATP) ratio had fallen to nearly 50% and remained low for the duration of the dark pulse; when illumination was restored, this ratio returned to ~85% within 1 hour.

The mechanism of the KaiABC protein oscillator relies on ordered multisite phosphorylation of KaiC (*4*, *5*). Because ADP cannot serve as the phosphoryl donor in the kinase reaction, physiological changes in the relative amounts of ATP and ADP caused by changes in light have the potential to modulate the activity of enzymes that consume ATP, and might directly affect the function of the circadian clock (*21*). To test this, we developed an experimental system to mimic in vitro the changes in nucleotide ratio we had observed in living cyanobacteria. We initiated oscillator reactions with purified KaiA, KaiB,

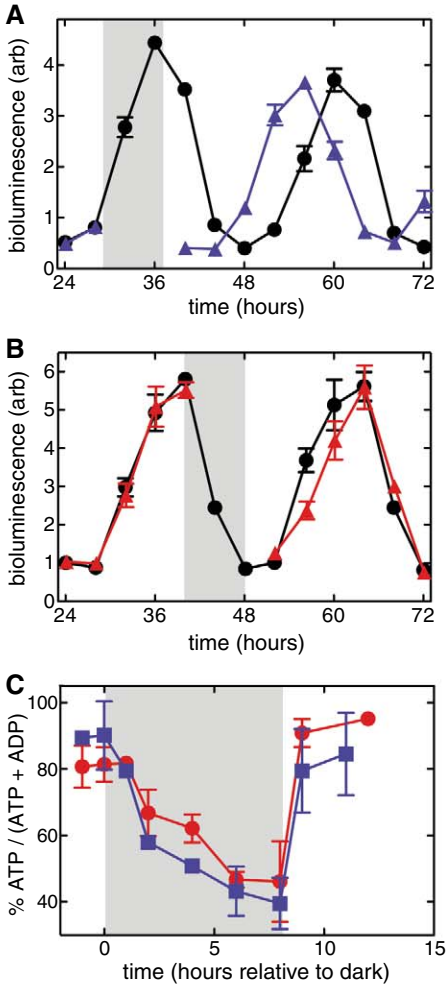

Fig. 1. Sustained drop in the ATP/ADP ratio and a phase shift in the circadian clock in response to a pulse of darkness. (**A**) Bioluminescence rhythms of a reporter under circadian control (P*kaiBC*::*luxAB*) in synchronized cultures either grown in constant light (black symbols) or subjected to an 8-hour pulse of darkness (shaded region) at t = 29 hours (blue symbols). Bars show the range of duplicate measurements from the same experiment. Time is measured from the release of cultures into constant light; arb, arbitrary units. (**B**) Same as (A) except that the dark pulse was applied at t = 40 hours. (**C**) Relative levels of ATP and ADP extracted from cultures before, during (shaded region), and after a dark pulse in the conditions shown in (A) (blue symbols) and in (B) (red symbols). Bars indicate the range from duplicate cultures.

[1]Howard Hughes Medical Institute, Center for Systems Biology, Department of Molecular and Cellular Biology, and Department of Chemistry and Chemical Biology, Harvard University, Cambridge, MA 02138, USA. [2]Center for Chronobiology, Division of Biological Sciences, University of California, San Diego, La Jolla, CA 92093, USA.

*Present address: Department of Molecular Genetics and Cell Biology and Institute for Genomics and Systems Biology, University of Chicago, Chicago, IL 60637, USA.

†To whom correspondence should be addressed. E-mail: eoshea@mcb.harvard.edu

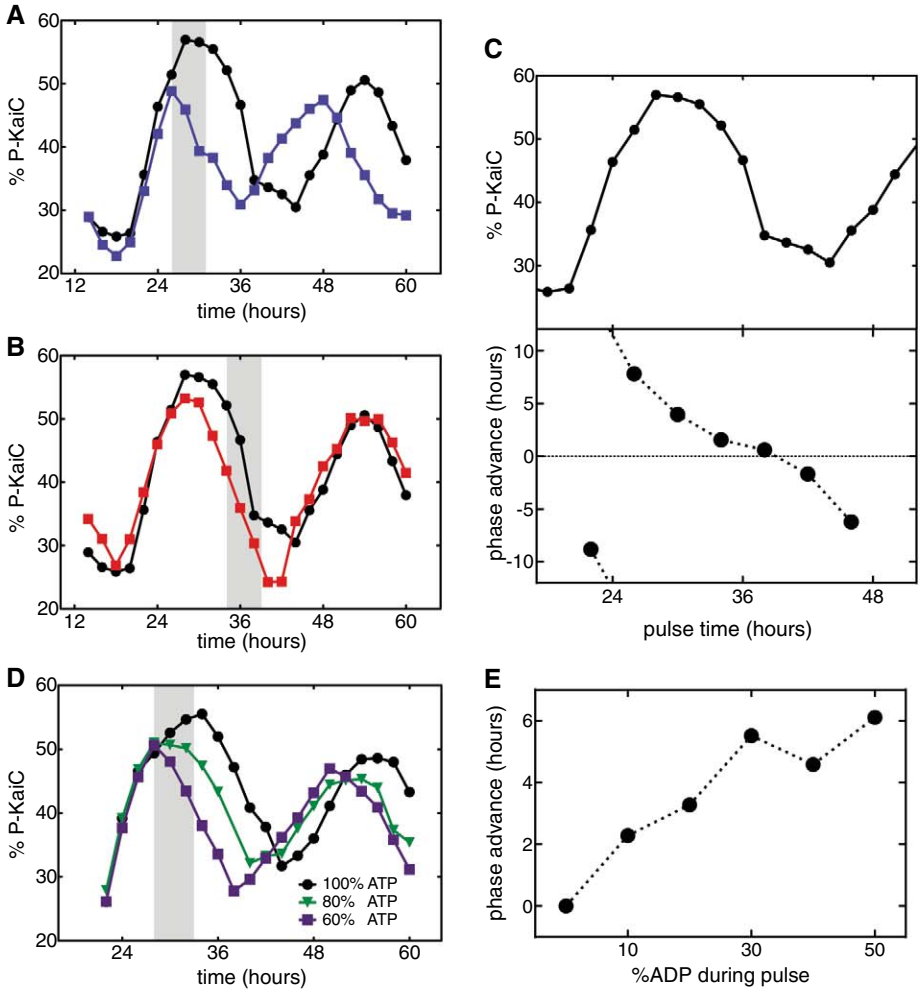

Fig. 2. Phase shifts in the in vitro KaiABC oscillator caused by changing the ATP/ADP ratio. (**A**) Phase shift induced by adding an amount of ADP equal to the amount of ATP in the reaction buffer ~6 hours before peak phosphorylation (blue symbols) relative to a control (black symbols). The shaded region indicates the time after addition of ADP but before the addition of pyruvate kinase to convert ADP to ATP. (**B**) Same as (A) except that ADP was added ~6 hours after peak phosphorylation (red symbols). (**C**) Phase shifts induced by a pulse of ADP in the in vitro oscillator reaction (lower panel) shown adjacent to the rhythm of KaiC phosphorylation in the control (upper panel) to indicate where in the cycle the pulses were applied. Differences in phase were measured by fitting the data to a sinusoidal function. (**D**) Effect of addition of mixtures of nucleotides to lower the ATP/ADP ratio (colored symbols) to various levels relative to a control that received only ATP (black symbols). Total adenine nucleotide concentration was the same across all reactions. The shaded region indicates the time before addition of pyruvate kinase. (**E**) Quantification of phase shifts from the experiment shown in (D). The phase shift when only ATP is added is zero by definition. Differences in phase were measured by fitting the data to a sinusoidal function.

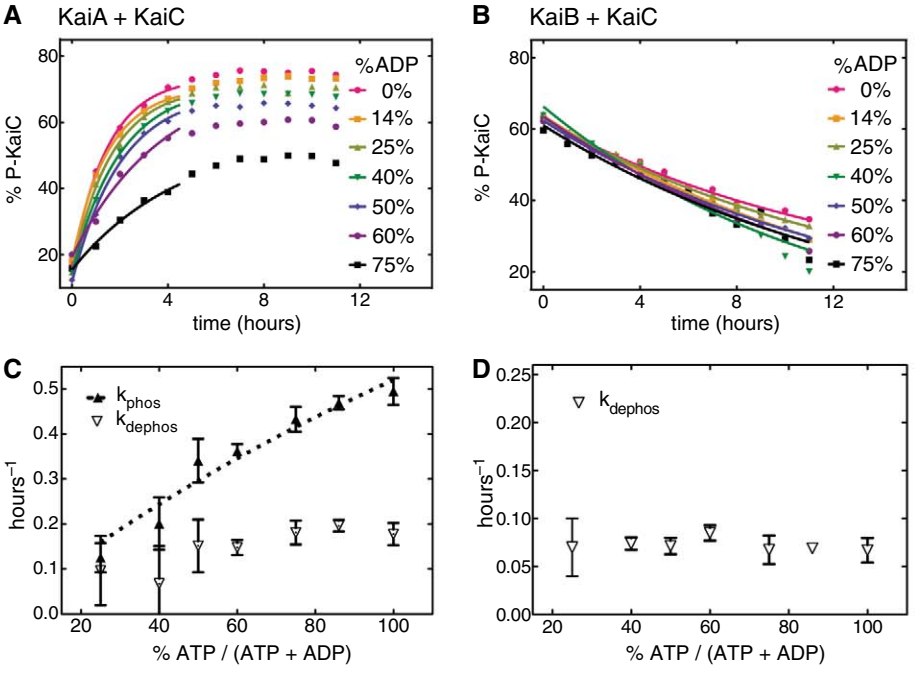

Fig. 3. Inhibition of KaiC phosphorylation by ADP. (**A**) KaiC phosphorylation in a KaiA-KaiC reaction with different ADP/(ATP + ADP) ratios. Solid lines are fits to the first 4 hours of data used to isolate the first phosphorylation step (*28*). (**B**) KaiC dephosphorylation in a KaiB-KaiC reaction with different ADP/(ATP + ADP) ratios. Solid lines are fit to a first-order reversible reaction. (**C**) Kinase (k_{phos}) and phosphatase (k_{dephos}) rate constants are obtained from the data in (A). The dashed line is a fit to the competitive inhibition model $k\{[ATP]/([ATP] + K_{rel}[ADP])\}$, where K_{rel} is an effective relative affinity for ADP versus ATP, fit to 0.76 ± 0.15. Error bars represent SE in the fit. (**D**) Phosphatase rate constants obtained from the data in (B). Error bars represent SE in the fit.

and KaiC in a buffer containing an excess of phosphoenolpyruvate and 4 mM ATP, similar to estimates of adenine nucleotide concentration in cyanobacterial cells in the millimolar range (*22*). After the oscillation had been established, we simulated the metabolic effects of darkness by adding ADP to bring the ATP/(ADP + ATP) ratio to ~50%. To then simulate the effects of a return to growth in light, we added pyruvate kinase to convert the ADP to ATP, a reaction that went to completion in ~1 hour (fig. S2). Because the ATP/ADP ratio in vivo initially falls gradually when cells are incubated in the dark for 8 hours in our liquid culture conditions (Fig. 1C), we used a 5-hour step-like pulse of ADP in vitro to approximate the amount of time that the in vivo cultures experience the lowest ATP/ADP ratio.

Transient manipulation of the ratio of ATP to ADP in the KaiABC oscillator created large phase shifts in the phosphorylation rhythm (Fig. 2A). Further, the phase response curve obtained by altering the ATP/ADP ratio in vitro was similar to that observed in live cells treated with pulses of darkness: The oscillator was most sensitive during the middle of subjective day (when KaiC phosphorylation was increasing) and nearly insensitive during subjective night (when KaiC phosphorylation was decreasing) (Fig. 2, B and C) (*18*, *19*, *23*). During the pulse of increased ADP, KaiC phosphorylation was decreased relative to that in the control reaction, similar to changes in KaiC phosphorylation in vivo when cells were subjected to a dark pulse (fig. S1) (*24*).

To determine the increase in the relative amount of ADP needed to produce this effect, we added varying amounts of ADP to several identical KaiABC reactions during a fixed portion of the oscillator cycle. The induced phase shift was a graded function of the amount of ADP added (Fig. 2, D and E). Similarly, the magnitude of the phase shift decreased when the length of the pulse of ADP was decreased (fig. S3). Thus, even small changes in the ATP/ADP ratio, smaller or shorter in duration than those induced by a rapid transition to prolonged darkness, adjusted the time specified by the circadian clock.

To investigate the molecular mechanism by which changes in the relative fraction of ADP are able to alter the oscillator phase, we studied the effect of the ATP/ADP ratio on nonoscillatory partial reactions in which one of the Kai proteins was absent. In the KaiA-KaiC reaction, KaiA chronically stimulates KaiC's autophosphorylation activity, resulting in a steady state in which KaiC is highly phosphorylated (*5*, *25*). Increasing the relative fraction of ADP present in the reaction resulted in both reduced steady-state phosphorylation and a slower approach to that steady state (Fig. 3A). In the KaiB-KaiC reaction, KaiC has very weak kinase activity and the fraction of phosphorylated KaiC slowly decreases, allowing us to isolate the dephosphorylation reaction (*5*). We did not detect any effect of varying the ATP/ADP ratio on KaiC's phosphatase activity (Fig. 3B), nor on the stability of KaiB-KaiC complexes (fig. S4).

Quantitative analysis of the kinetics of the partial reactions confirmed the above observations and was consistent with a model in which ADP acts as a competitive inhibitor of KaiC's kinase activity. In fitting the phosphorylation kinetics to an initial velocity approximation, we estimated an effective relative affinity for ATP and ADP that is close to unity ($K_{rel} = 0.76 \pm 0.15$) (Fig. 3C). This value is compatible with two simple mechanistic hypotheses: Either the true binding affinities for ATP and ADP are comparable in the CII lobe [the seat of KaiC autophosphorylation (*26*)], or the rate of ATP hydrolysis in CII is much faster than the rate of nucleotide dissociation, so that any difference in affinity is negligible. In either case, ADP acts in proportion to its relative abundance to decrease the KaiC phosphorylation rate.

To test whether the competitive inhibition mechanism we had identified was sufficient to explain the large phase shifts in the full oscillating reaction, we turned to a mathematical model of the circadian clock based on experimental measurements of the rates of phosphorylation and dephosphorylation at two sites on KaiC: Ser^{431} and Thr^{432} (*5*). In this model, stable oscillations arise because KaiC phosphorylated only on Ser^{431} interacts strongly with KaiB, trapping KaiA stoichiometrically and globally promoting dephosphorylation. In this sense, KaiC phosphorylated on Ser^{431} is autocatalytic, generating a nonlinearity that drives the oscillator.

We modified this model so that, in accord with our experimental observations, the kinase rates were modulated by the ATP/(ADP + ATP) ratio present in the reaction, as well as by the level of KaiA activity (Fig. 4A) (*5*). Thus, at each point in the oscillation, KaiC integrates clock information (through KaiA's kinase-stimulating activity) with metabolic information (through the adenosine pool). We simulated our in vitro experiments within this model by transiently lowering the ATP/(ADP + ATP) ratio from 100% to 50% at various times in the circadian cycle. In simulation, pulses of competitive inhibition by ADP were sufficient to generate large phase shifts in the oscillator when these pulses occurred during the phase of the cycle when KaiC phosphorylation was rising (Fig. 4B).

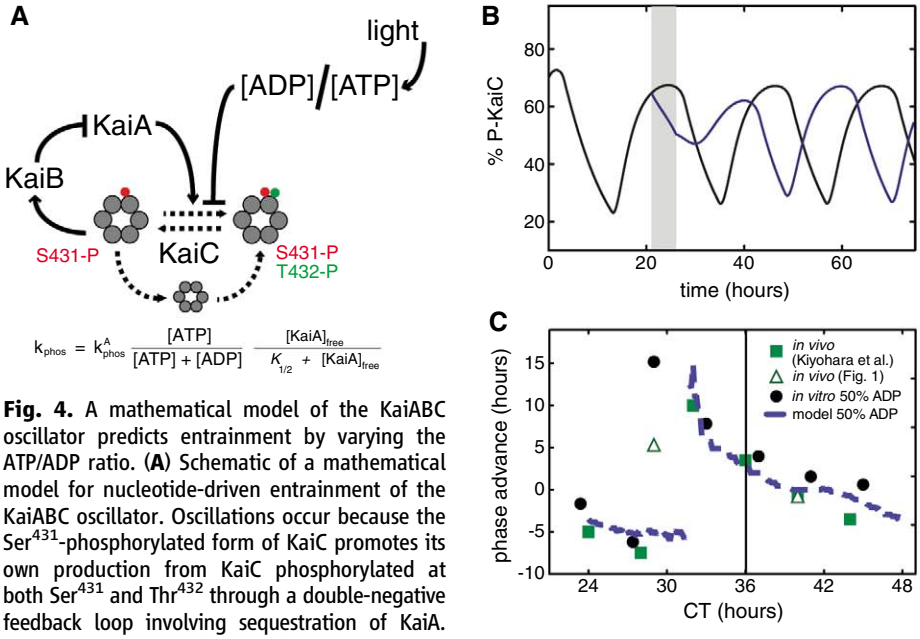

Fig. 4. A mathematical model of the KaiABC oscillator predicts entrainment by varying the ATP/ADP ratio. (**A**) Schematic of a mathematical model for nucleotide-driven entrainment of the KaiABC oscillator. Oscillations occur because the Ser^{431}-phosphorylated form of KaiC promotes its own production from KaiC phosphorylated at both Ser^{431} and Thr^{432} through a double-negative feedback loop involving sequestration of KaiA. Free KaiA promotes phosphorylation of KaiC and inhibits dephosphorylation. Changing illumination conditions in vivo drive changes in the adenosine pool, which in turn modulate phosphorylation rates (k_{phos}). Although the figure shows only the effect on Ser^{431}-phosphorylated KaiC, changes in KaiA activity and in the ATP/ADP ratio affect all phosphorylation steps in the model. K_{rel} is an effective relative affinity for ADP versus ATP. $[KaiA]_{free}$ is the free concentration of [KaiA], and $K_{1/2}$ is the concentration of [KaiA] needed to produce a half-maximal effect on KaiC. k^A_{phos} is the maximum phosphorylation rate with saturating KaiA and 100% ATP. See (*5*, *28*) for complete details. (**B**) Simulation of the effect of lowering the ATP/(ADP + ATP) ratio from 100% to 50% for 5 hours during the subjective day (shaded region) using equal affinities for ATP and ADP (blue curve) compared to a control in constant 100% ATP (black curve). (**C**) Phase response curve predicted by the model using equal affinities for ATP and ADP (blue dashed line) as in (B) compared with in vitro data (black circles) and in vivo data (green squares) from (*19*) (4-hour dark pulse, solid media) and from this study (open triangles) (8-hour dark pulse, liquid media). All data sets were aligned so that peak phosphorylation occurs at 36 hours (grid line), and the modeling results were scaled on both axes to make the period equal to 24 hours.

In order to obtain a strong resetting effect, KaiC must have sufficiently high sensitivity to ADP, at the upper end of the range of effective affinities we estimated experimentally (fig. S5). We used this model to predict a full phase-response curve based on this competitive inhibition mechanism and compared it to our experimental data and to measurements of the phase shift induced by darkness in vivo (Fig. 4C) (*19*). The agreement between these data and the model indicates that varying the relative nucleotide concentrations in the reconstituted oscillator approximates the response of the circadian clock in living cyanobacteria to changes in illumination, and an increase in the amount of ADP appears to alter the phase of the oscillator through inhibition of KaiC's kinase activity.

In the model, the ATP/ADP ratio describes a family of limit cycles that differ in the amplitude of the phosphorylation rhythm. Indeed, KaiABC reactions in buffers with tonically lowered ATP/ADP ratios continue to oscillate with a circadian period, but KaiC cycles through distinct patterns of phosphorylated states (fig. S6). If the ATP/ADP ratio is lowered abruptly, phosphorylation is inhibited, and the system must adjust to a new limit cycle. If this transition produces amounts of Ser^{431}-phosphorylated KaiC sufficient to block KaiA activity, a large phase shift can result.

We have described a simple entrainment mechanism for a circadian clock in which enzymatic activity is directly tied to the availability of biochemical energy in the cell. In this view, no signaling pathway that specifically targets the oscillator is required to couple the clock to the environment, and the core oscillator proteins interact directly with metabolites, as has been reported for KaiA in vitro (*27*). Although factors outside the Kai proteins have been implicated in light-driven input to the cyanobacterial circadian system, including LpdA and the histidine kinase CikA (*18*, *20*), strains lacking these proteins can be effectively entrained with repeated light-dark cycles, supporting the hypothesis that there exist basic synchronization mechanisms intrinsic to the KaiABC core oscillator itself. Because unexpected darkness will unavoidably lead to changes in the production and consumption of ATP in an obligate phototroph, KaiC's sensitivity to ADP represents a robust intrinsic mechanism for maintaining synchrony with the environment.

References and Notes

1. T. Roenneberg, R. G. Foster, *Photochem. Photobiol.* **66**, 549 (1997).
2. M. Nakajima *et al.*, *Science* **308**, 414 (2005).
3. Y. Xu *et al.*, *Proc. Natl. Acad. Sci. U.S.A.* **101**, 13933 (2004).
4. T. Nishiwaki *et al.*, *EMBO J.* **26**, 4029 (2007).
5. M. J. Rust, J. S. Markson, W. S. Lane, D. S. Fisher, E. K. O'Shea, *Science* **318**, 809 (2007); 10.1126/science.1148596.
6. X. Qin *et al.*, *Proc. Natl. Acad. Sci. U.S.A.* **107**, 14805 (2010).
7. K.-A. Stokkan, S. Yamazaki, H. Tei, Y. Sakaki, M. Menaker, *Science* **291**, 490 (2001).
8. K. A. Lamia *et al.*, *Science* **326**, 437 (2009).
9. J. Aschoff, *Cold Spring Harb. Symp. Quant. Biol.* **25**, 11 (1960).
10. R. Rippka, J. Deruelles, J. B. Waterbury, M. Herdman, R. Y. Stanier, *J. Gen. Microbiol.* **111**, 1 (1979).
11. H. Ito *et al.*, *Proc. Natl. Acad. Sci. U.S.A.* **106**, 14168 (2009).
12. M. A. Woelfle, Y. Xu, X. Qin, C. H. Johnson, *Proc. Natl. Acad. Sci. U.S.A.* **104**, 18819 (2007).
13. S. Scherer, H. Almon, P. Boger, *Photosynth. Res.* **15**, 95 (1988).
14. T. Bornefeld, W. Simonis, *Planta* **115**, 309 (1974).
15. T. Kallas, R. W. Castenholz, *J. Bacteriol.* **149**, 229 (1982).
16. H. J. Lubberding, W. Schroten, *FEMS Microbiol. Lett.* **22**, 93 (1984).
17. C. R. Andersson *et al.*, *Methods Enzymol.* **305**, 527 (2000).
18. O. Schmitz, M. Katayama, S. B. Williams, T. Kondo, S. S. Golden, *Science* **289**, 765 (2000).
19. Y. B. Kiyohara, M. Katayama, T. Kondo, *J. Bacteriol.* **187**, 2559 (2005).
20. M. Katayama, T. Kondo, J. Xiong, S. S. Golden, *J. Bacteriol.* **185**, 1415 (2003).
21. D. Atkinson, *Biochemistry* **7**, 4030 (1968).
22. M. J. Ihlenfeldt, J. Gibson, *Arch. Microbiol.* **102**, 13 (1975).
23. N. B. Ivleva, M. R. Bramlett, P. A. Lindahl, S. S. Golden, *EMBO J.* **24**, 1202 (2005).
24. N. B. Ivleva, T. Gao, A. C. LiWang, S. S. Golden, *Proc. Natl. Acad. Sci. U.S.A.* **103**, 17468 (2006).
25. H. Iwasaki, T. Nishiwaki, Y. Kitayama, M. Nakajima, T. Kondo, *Proc. Natl. Acad. Sci. U.S.A.* **99**, 15788 (2002).
26. R. Pattanayek *et al.*, *Mol. Cell* **15**, 375 (2004).
27. T. L. Wood *et al.*, *Proc. Natl. Acad. Sci. U.S.A.* **107**, 5804 (2010).
28. See supporting material on *Science* Online.

29. We thank G. Dong for advice on culture conditions, and K. Cook, V. Denic, Q. Justman, J. Markson, A. Rizvi, and V. Vijayan for valuable discussions and comments on the manuscript. E.K.O. is an investigator of the Howard Hughes Medical Institute. Supported by NIH grant GM62419 (S.S.G.), a Helen Hay Whitney Foundation postdoctoral fellowship (M.J.R.), and a Burroughs-Wellcome Foundation Career Award at the Scientific Interface (M.J.R.).

Supporting Online Material

www.sciencemag.org/cgi/content/full/331/6014/220/DC1
Materials and Methods
SOM Text
Table S1
Figs. S1 to S6
References

1 September 2010; accepted 9 December 2010
10.1126/science.1197243

Suppression of Avian Influenza Transmission in Genetically Modified Chickens

Jon Lyall,[1] Richard M. Irvine,[2] Adrian Sherman,[3] Trevelyan J. McKinley,[1] Alejandro Núñez,[2] Auriol Purdie,[3]* Linzy Outtrim,[2] Ian H. Brown,[2] Genevieve Rolleston-Smith,[3] Helen Sang,[3]† Laurence Tiley[1]†‡

Infection of chickens with avian influenza virus poses a global threat to both poultry production and human health that is not adequately controlled by vaccination or by biosecurity measures. A novel alternative strategy is to develop chickens that are genetically resistant to infection. We generated transgenic chickens expressing a short-hairpin RNA designed to function as a decoy that inhibits and blocks influenza virus polymerase and hence interferes with virus propagation. Susceptibility to primary challenge with highly pathogenic avian influenza virus and onward transmission dynamics were determined. Although the transgenic birds succumbed to the initial experimental challenge, onward transmission to both transgenic and nontransgenic birds was prevented.

The diversity of avian influenza viruses (AIVs) and their propensity for interspecies transmission make them a global threat to animal and public health communities. Cross-species transmission of influenza viruses may occur directly or be facilitated by intermediate host species that amplify and diversify virus populations, notably domestic chickens, ducks, and pigs (*1*). Although control of AIV infection in its wild aquatic bird reservoir is impractical, control of AIV in domesticated hosts is possible (*2*). The diversity of viral antigenic subtypes and their potential for evolutionary shift and drift are a challenge, particularly because current vaccines do not generally achieve sterile immunity even against antigenically well-matched viruses (*3*). One potential route to control AIVs in commercial poultry is to use genetic modification to introduce novel genes that confer resistance to infection (*4*, *5*). Here we evaluate transgenic expression of an RNA hairpin molecule capable of inhibiting influenza viral polymerase activity (*6*).

An RNA expression cassette (Fig. 1A) was designed to use a chicken U6 promoter (*7*) to express the short hairpin RNA molecule, decoy 5 (D5, Fig. 1B) (*8*). This decoy contains the conserved 3′- and 5′-terminal sequences of influenza virus genome segments that encompass the complementary RNA (cRNA) binding site for

[1]Department of Veterinary Medicine, University of Cambridge, Madingley Road, Cambridge CB3 0ES, UK. [2]Veterinary Laboratories Agency, Weybridge, Addlestone, Surrey KT15 3NB, UK. [3]The Roslin Institute and Royal (Dick) School of Veterinary Studies, University of Edinburgh, Edinburgh EH25 9PS, UK.

*Present address: Faculty of Veterinary Science, University of Sydney, NSW 2567, Australia.
†These authors contributed equally to this work.
‡To whom correspondence should be addressed. E-mail: Lst21@cam.ac.uk

influenza A virus polymerase (*9*, *10*) and has the potential to interfere with virus replication and packaging. A structurally similar decoy molecule (D7, Fig. 1B), containing specific mutations that prevent binding by the viral polymerase, provided the negative control. We confirmed the efficacy and specificity of the D5 expression cassette by expressing it in DF-1 chick embryo fibroblast (CEF) cells with a lentiviral vector plasmid (fig. S1A), cotransfected with an AIV-based minireplicon system (*8*, *11*) (Fig. 1C), in which activity of influenza polymerase is proportional to the amount of the reporter protein produced (*12*). The D5 lentivector was then used to generate transgenic chickens (*8*) carrying the D5 cassette inserted at a single location on chromosome 2 (fig. S1, B and C). One transgenic cockerel was crossed with stock hens, and the resulting ~1:1 transgenic (TG-D5) and nontransgenic (non-TG) progeny were used in the challenge studies described below. Expression of the green fluorescent protein (GFP) reporter gene, present in the integrated vector, was detected in all transgenic birds. Decoy RNA expression was below the limit of detection of Northern blot analysis, consistent with our experience in transiently transfected cells, in which we have found this RNA to be unstable in the absence of the viral polymerase. The minireplicon AIV polymerase assay, performed with CEFs isolated from TG-D5 and non-TG embryos, showed that expression of the reporter in the TG-D5 CEFs was on average 0.24 times that from the non-TG embryos ($P = 0.004$; 95% confidence interval 0.10 to 0.56), indicating that the D5 cassette in the transgenic CEFs was effective in this assay (Fig. 1C).

The susceptibility of the TG-D5 birds to highly pathogenic avian influenza (HPAI) infection was evaluated in two in vivo studies. In study 1, the susceptibility to direct infection and onward transmission in 3-week-old transgenic or nontransgenic birds was compared (*8*). Ten TG-D5 and 10 non-TG chickens were directly infected with a high dose [10^5 EID_{50} (50% egg infectious dose)] of H5N1 HPAI (A/turkey/Turkey/1/2005). One day post-infection (dpi), these challenged birds were housed with 10 uninfected birds (the "in-contact" group) of the same transgenic status, and the health of the birds was monitored over the next 11 days (fig. S2). All the directly infected birds died between 2 and 4 dpi, with negligible difference between the time to death for TG-D5 and the non-TG birds [$P = 0.50$; Bonferroni adjusted Mann-Whitney test (*8*)]. However, clear and statistically significant differences in mortality and time to death were apparent for the in-contact groups ($P = 0.017$), where 7 out of 10 non-TG in-contact birds died by the fifth day of the study, with a mean time to death (excluding survivors) of 3.3 (SD = 0.5) days after exposure. Only 2 out of 10 of the TG-D5 in-contact group died (on day 5 and 5.5 after exposure), whereas the others remained healthy for the duration of the study. These results suggest that susceptibility to a high dose of H5N1 HPAI virus challenge was similar for the TG-D5 and non-TG birds, but that there were clear differences in transmission and/or susceptibility after contact exposure.

Study 2 was designed to investigate whether the results obtained in study 1 reflected reduced levels of virus shedding from the transgenic challenge group and/or reduced susceptibility to infection via contact exposure to these infected birds. Ten TG-D5 and 10 non-TG sibling birds were directly infected as before, but with a dose of virus one-tenth that used in the earlier study (10^4 EID_{50}). Each of these groups was then split into two groups of five, and each group of five was housed with 12 TG-D5 or 12 non-TG birds (i.e., four groups of 17 birds housed together from dpi = 0; Fig. 2 and fig. S3), plus two unexposed control birds. Direct infection of the non-TG birds was again 100% lethal, with peak mortality at 2 dpi and the remaining birds succumbing to infection between days 4 and 6, consistent with this being caused by subsequent rounds of infection (Fig. 2, groups 1 and 2, "non-TG challenged"). In 6 out of 10 birds, mortality resulted directly from infection, and 4 out of 10 birds were euthanized on welfare grounds because of their severe clinical presentation. The infected TG-D5 birds also showed peak clinical signs at 2 dpi, when 1 out of 10 died directly from the infection and five were euthanized on welfare grounds (Fig. 2, groups 3 and 4, "TG-D5 challenged"). Four out of 10 of the birds survived to at least day 7. One of these (#4458) was euthanized on clinical grounds, with one healthy bird (#4446) for comparison. The sick bird (#4458) did not have viral antigen in any of its tissues and was not shedding detectable levels of viral RNA. The two remaining birds were healthy for the 10-day duration of the study. The pattern of mortality in the directly challenged birds is consistent with the TG-D5 birds having reduced transmission capacity that affected the successive waves of mortality apparent in the non-TG challenged birds. Although these data taken alone were not statistically significant, this hypothesis is supported by the analysis of the in-contact birds described later.

Direct infection of non-TG birds resulted in viral shedding from the cloaca and oropharynx and efficient transmission to the in-contact birds with 100% mortality, irrespective of whether these were TG-D5 or non-TG (Fig. 2 and fig. S3, groups 1 and 2, "in-contact"). However, the transmission dynamics to the TG-D5 birds were noticeably prolonged (Fig. 2, group 2, "in-contact"). This is an interesting observation but the effect was of marginal statistical significance ($P = 0.06$ before and $P = 0.18$ after adjustment; Mann-Whitney), if we accept that the power of the study to detect this difference is likely to be compromised at this level of aggregation. In marked contrast, contact with the directly infected TG-D5 birds did not result in clinical disease in either the TG-D5 or non-TG in-contact birds, because no in-contact birds died from influenza (Fig. 2, group 3 and 4 "in contact") and none of the birds sero-converted (as determined by enzyme-linked immunosorbent assay and hemagglutination inhibition assay performed with day 10 sera). Of the 24 in-contact birds, 14 remained healthy until the end of the study, 9 healthy birds were killed for postmortem examination (*8*) during the course of the study, and one bird (#5033) became sick

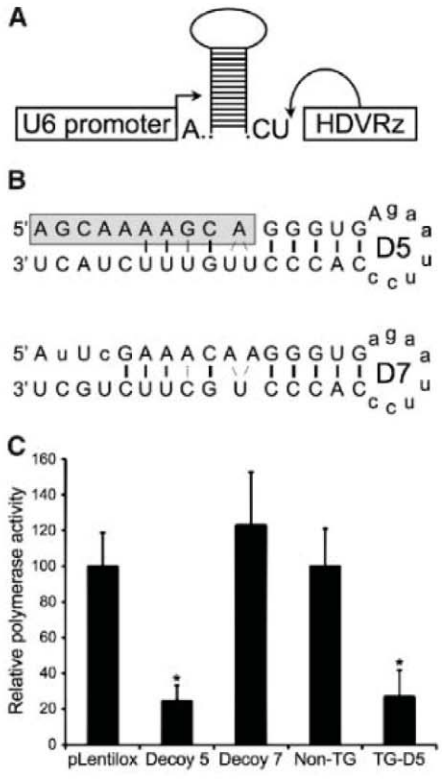

Fig. 1. Inhibition of influenza virus polymerase by decoy RNA hairpins. (**A**) The decoy hairpin RNA expression cassette comprised a chicken U6 RNA promoter, the decoy sequence, and hepatitis delta virus antigenomic ribozyme (*12*). (**B**) Structure of the RNA decoys: Decoy 5 (D5) comprises the conserved 5′- and 3′-terminal nucleotides from segment 8 cRNA with the polymerase primary binding site in the shaded box. Decoy 7 (D7) corresponds to the viral RNA sequence with mutations at position 2 and 4 of the 5′ end known to ablate polymerase binding. Lowercase letters indicate non–influenza-related sequences. (**C**) Polymerase activity in DF-1 and CEF cells determined by minireplicon-based luciferase expression assay. DF1 cells were transfected with plasmids expressing the 3P/NP genes (derived from A/turkey/England/50-92 H5N1) and chicken polymerase I–driven luciferase minireplicon. These were cotransfected with pLentilox, pL-D5, or pL-D7 expressing no decoy, decoy 5, or decoy 7, respectively, as indicated. Data are means ± SD from three replicate transfections. Similarly, the activity of the same minireplicon system was determined by transfection into CEFs prepared from decoy 5 transgenic (TG-D5, $n = 8$) or nontransgenic (non-TG, $n = 2$) embryos. Luciferase levels are plotted relative to the empty vector (pLentilox) and non-TG controls as appropriate. Polymerase activity in decoy 5 versus vector control transfected cells and non-TG versus TG-D5 CEFs were significantly different ($P = 0.02$ and $P = 0.004$, respectively).

from an apparently unrelated cause. Comparing the time to death for the in-contact birds between the non-TG and TG-D5 challenge birds (i.e., groups 1 and 2 versus 3 and 4) showed that these differences were highly statistically significant ($P = 0.0004$; Mann-Whitney test), indicating that the transgenic chickens have altered infection transmission dynamics for H5N1 HPA1 virus.

Figure 2 also shows the quantity of viral RNA [$\log_{10}$ RNA copies (*8*)] detected in buccal swabs sampled daily (parallel data for cloacal swabs are shown in fig. S3). The shedding patterns were typical of those observed for HPAI virus infection and transmission in poultry, with shedding from the oropharynx often preceding that from the cloaca (*13*). High levels of viral RNA were detected in 10 out of 10 buccal samples and 9 out of 10 cloacal samples from the directly infected non-TG challenge groups (Fig. 2 and fig. S3, groups 1 and 2). Shedding occurred in phases, with 60% of the birds shedding by 2 dpi, in parallel with the waves of mortality. The in-contact groups housed with the non-TG challenge birds showed an initial low level of viral RNA coincident with the peak shedding from the challenged birds (we interpret this as evidence of initial exposure at this time), followed by successive waves of shedding similar to that seen for the non-TG challenge birds but occurring ~2 days later. Similar levels of virus RNA were detectable in the buccal and cloacal swab samples from both the non-TG and TG-D5 in-contact groups (fig. S3).

In the directly infected TG-D5 birds (Fig. 2 and fig. S3, groups 3 and 4), viral RNA was detected by 2 dpi in 5 out of 10 buccal samples but in only 2 out of 10 cloacal samples (or maximally 4 out of 10, including the two for which H5 real-time reverse transcriptase–polymerase chain reaction (RRT-PCR) data are unavailable but that were positive in the immunohistochemical analysis). Half of the birds succumbed to the initial direct infection, but the virus shed by these birds was insufficient or not able to infect the remaining in-contact birds. Again, low levels of viral RNA were detected in the buccal samples from many birds in the in-contact groups at the time of peak shedding from the challenged birds. This low level of infection or exposure failed to establish a productive, systemic infection, as shown by the lack or very low level of viral RNA shed from the cloacae of these birds and by the absence of mortality.

Histopathology and immunohistochemistry of all major tissues and organs (table S1) revealed viral antigen and characteristic histopathological changes associated with AIV infection in 7 out of 13 directly infected (TG-D5 and non-TG) birds, consistent with their virus shedding status. The histopathological changes included multifocal necrosis in the spleen, bursa, thymus, brain, and pancreas, and interstitial pneumonia and perivascular and alveolar edema in the lung. There were no marked differences in the severity, nature, and distribution of histopathological changes or expression of viral antigen between the TG-D5 ($n = 5$) and non-TG ($n = 2$) directly infected birds examined. None of the birds (non-TG or TG-D5) that were in contact with the directly infected TG-D5 birds were positive for viral antigen or showed any typical histopathological changes (16 out of 16 birds tested on dpi 2, 8, or 10). Lymphoid hyperplasia was observed in the spleen, thymus, and bursa for most of these birds at later time

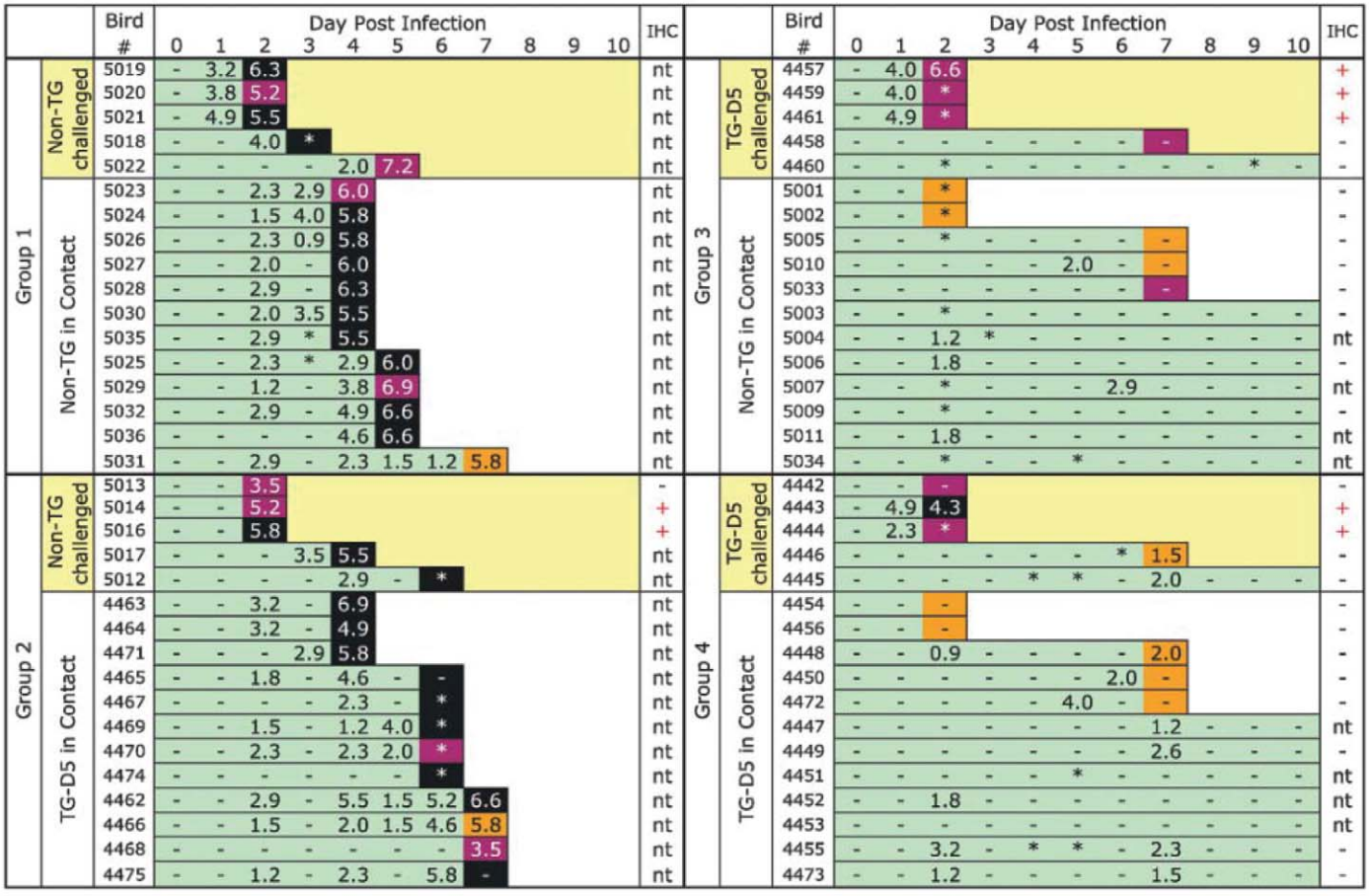

Fig. 2. Mortality and virus shedding data for challenge and in-contact groups in study 2. Groups of five TG-D5 or non-TG "challenged" birds infected with influenza virus A/turkey/Turkey/1/05 (H5N1) on day 0 were housed with groups of 12 TG-D5 or non-TG "in-contact birds." groups 1 and 2: Non-TG challenged birds; groups 3 and 4: TG-D5 challenged birds; Groups 1 and 3: Non-TG in-contact birds; and groups 2 and 4: TG-D5 in-contact birds. Survival is indicated by the length of the green bar. Terminal block color indicates day and cause of death (black, found dead; magenta, moribund; orange, healthy birds killed for immunohistological studies). Numbers for each day are the $\log_{10}$ of the number of viral RNA copies present in buccal swab samples (data for cloacal swabs are shown in fig. S3). Sample negative by RT-PCR (–), sample unavailable (*). The IHC column summarizes the immunohistochemistry data shown in table S1. Virus antigen detected (+); no virus antigen detected (–); not tested (nt).

points, but was not seen at earlier time points or in the two unexposed control birds. This may be indicative of antigen or viral exposure or an abortive infection.

These data show that the TG-D5 chickens did not efficiently transmit infection to birds housed with them, but the specific mechanism underlying this effect is not known. Polymerase decoys may disrupt replication by direct binding to polymerase or indirectly by influencing the level of expression of the recently discovered, putative regulatory small viral RNA molecules (*14*, *15*) (which may also have a role in innate immunity). Although decoy 5 suppressed polymerase activity in cell culture, this did not translate into a quantitative reduction in virus shedding from infected birds (Fig. 2) (nor have we found any effect in ovo or in fibroblast cell culture). Polymerase-RNA interactions may be involved in the virus packaging process, but after passage through TG-D5 chick embryo fibroblasts in cell culture, we have not found any effect on the genome:plaque-forming unit ratio of the virus to support the hypothesis that the decoy induced the formation of defective virus particles. The standard intravenous pathogenicity index of the virus shed from one of the TG-D5 chickens (#4457, dpi = 2) was determined after a single passage in embryonated hens' eggs and found to be unaltered, indicating that passage through TG-D5 chickens does not rapidly select for a stable genetic change that reduces the virulence of the shed virus.

Our goal was a proof-of-principle demonstration that genetic modification can be used to prevent avian influenza infection in chickens. The TG-D5 birds exhibited a marked absence of onward transmission of infection, even to unprotected (nontransgenic) chickens housed in direct contact with them. This property could have a major impact on susceptibility and propagation of infection at the flock level and supports the concept of genetic modification for controlling AIV infection in poultry. Our strategy offers substantial potential benefits over vaccination. Although conventional AIV vaccines can achieve strain-specific clinical resistance to primary challenge, sterile immunity is not achieved (*3*). Such vaccination can allow the cryptic circulation of virus in flocks, facilitating antigenic drift and posing a risk to unvaccinated birds and humans that come into contact with them. In contrast, onward transmission and circulation at the flock level are absent in the TG-D5 chickens. The decoy 5 RNA corresponds to an absolutely conserved sequence that is essential for the regulation of viral transcription, replication, and packaging of all subtypes of influenza A virus, offering pan-subtype A protection, whereas vaccination offers no protection against unmatched viral strains. Unlike proposed microRNA-based strategies (*4*, *5*), the development of resistant virus is intrinsically unlikely, requiring mutations in the polymerase and the promoter of all eight genome segments simultaneously, a statistically highly improbable event.

The control of avian influenza by genetic modification brings obvious health benefits to consumers and producers, as well as welfare and productivity benefits to the birds. Nevertheless, it is important to assess any genetic modification for potential hazards. Here, the transgene encodes an innocuous decoy RNA, expressed at steady-state levels that are barely detectable by conventional methods and unlikely to present a risk to consumers, birds, or the wider environment. There are no apparent ill-effects on uninfected transgenic birds, which are phenotypically normal and show no significant deviation from the expected Mendelian frequency or differences in hatch weights (fig. S4 and table S2). The transgene is not expected to alter susceptibility to other pathogens, although this has yet to be confirmed. Transgenes can be introduced into multiple founder lines as discrete traits without affecting other genetic properties of the lines. This will facilitate the permanent introduction of novel disease-resistance traits into the mass population of production birds via conventional breeding techniques, with little impact on genetic diversity or valuable production traits. Our approach is technically applicable to other domestic species that are hosts of influenza A, such as pigs, ducks, quail, and turkeys. Further development of transgenic disease resistance in poultry and other farm animals will undoubtedly stimulate debate about the application of this technology in food production.

References and Notes

1. R. G. Webster, G. B. Sharp, E. C. Claas, *Am. J. Respir. Crit. Care Med.* **152**, S25 (1995).
2. I. Capua, S. Marangon, *Vaccine* **25**, 5645 (2007).
3. D. E. Swayne, J. R. Beck, M. L. Perdue, C. W. Beard, *Avian Dis.* **45**, 355 (2001).
4. C. V. Hunter, L. S. Tiley, H. M. Sang, *Trends Mol. Med.* **11**, 293 (2005).
5. J. Chen, S. C. Chen, P. Stern, B. B. Scott, C. Lois, *J. Infect. Dis.* **197** (suppl. 1), S25 (2008).
6. G. Luo, S. Danetz, M. Krystal, *J. Gen. Virol.* **78**, 2329 (1997).
7. R. M. Das *et al.*, *Dev. Biol.* **294**, 554 (2006).
8. Materials and methods are available as supporting material on *Science* Online.
9. L. S. Tiley, M. Hagen, J. T. Matthews, M. Krystal, *J. Virol.* **68**, 5108 (1994).
10. E. Fodor, D. C. Pritlove, G. G. Brownlee, *J. Virol.* **68**, 4092 (1994).
11. W. Howard *et al.*, *Avian Dis.* **51** (suppl.), 393 (2007).
12. S. K. Biswas, D. P. Nayak, *J. Virol.* **70**, 6716 (1996).
13. J. A. van der Goot, G. Koch, M. C. de Jong, M. van Boven, *Proc. Natl. Acad. Sci. U.S.A.* **102**, 18141 (2005).
14. J. T. Perez *et al.*, *Proc. Natl. Acad. Sci. U.S.A.* **107**, 11525 (2010).
15. J. L. Umbach, H. L. Yen, L. L. Poon, B. R. Cullen, *MBio* **1**, e00204-10 (2010).

16. We thank S. Lillico, F. Song, and H. Gilhooley for advice on laboratory methods and technical support; R. Mitchell, F. Thomson, and M. Hutchison for assistance in production and breeding of transgenic birds; S. Essen and W. Cox for assistance with the in vivo challenge studies at the Veterinary Laboratories Agency, Weybridge; P. Digard and W. Barclay for providing the component plasmids of the minireplicon assays; and Cobb-Vantress Ltd. for supporting part of this work. This work was supported by the Biotechnology and Biological Sciences Research Council (grants BB/G00479X/1, BBS/B/00239, and BBS/B/00301) and by the Cambridge Infectious Diseases Consortium Department for Environment, Food and Rural Affairs–Higher Education Funding Council for England (grant VT0105). Crown Copyright 2010.

Supporting Online Material

www.sciencemag.org/cgi/content/full/331/6014/223/DC1
Methods
Figs. S1 to S4
Tables S1 and S2
References

21 September 2010; accepted 1 December 2010
10.1126/science.1198020

Human Tears Contain a Chemosignal

Shani Gelstein,[1]* Yaara Yeshurun,[1]* Liron Rozenkrantz,[1] Sagit Shushan,[1,2] Idan Frumin,[1] Yehudah Roth,[2] Noam Sobel[1]†

Emotional tearing is a poorly understood behavior that is considered uniquely human. In mice, tears serve as a chemosignal. We therefore hypothesized that human tears may similarly serve a chemosignaling function. We found that merely sniffing negative-emotion–related odorless tears obtained from women donors induced reductions in sexual appeal attributed by men to pictures of women's faces. Moreover, after sniffing such tears, men experienced reduced self-rated sexual arousal, reduced physiological measures of arousal, and reduced levels of testosterone. Finally, functional magnetic resonance imaging revealed that sniffing women's tears selectively reduced activity in brain substrates of sexual arousal in men.

Charles Darwin suggested that expressive behaviors initially served emotion-relevant functions, before evolving to serve as emotion-signals alone (*1*, *2*). Thus, the behavior of emotional tearing, considered uniquely human (*3*), is a paradox: Whereas tears clearly serve as an emotional signal (*4*), tears were not related to any emotionally relevant function. Despite psychological theories on the meaning of tears (*5*, *6*) and biological theories describing tears as an adaptation related to their eye-protective nature (*3*) or a mechanism for expelling toxic substances (*7*), the functional significance of emotional tears remains unknown (*8*).

Tears are drops of liquid produced by the lacrimal, accessory lacrimal, and Meibomian glands, which contain proteins, enzymes, lipids, metabo-

[1]Department of Neurobiology, Weizmann Institute of Science, Rehovot 76100, Israel. [2]Department of OtoRhinoLaryngology and Head and Neck Surgery, Edith Wolfson Medical Center, Holon 58100, Israel.

*These authors contributed equally to this work.
†To whom correspondence should be addressed. E-mail: noam.sobel@weizmann.ac.il

lites, electrolytes, and traces of drugs (*9*). In mice, tears contain a chemosignal or pheromone (*10*–*12*). Because the chemical makeup of human emotional tears differs from that of reflexive eye-protective tears (*13*), we hypothesized that human tears may similarly convey a chemosignal.

We first asked whether emotional tears have a discernable odor. We obtained negative-emotion tears from two donor women (ages 30 and 31)

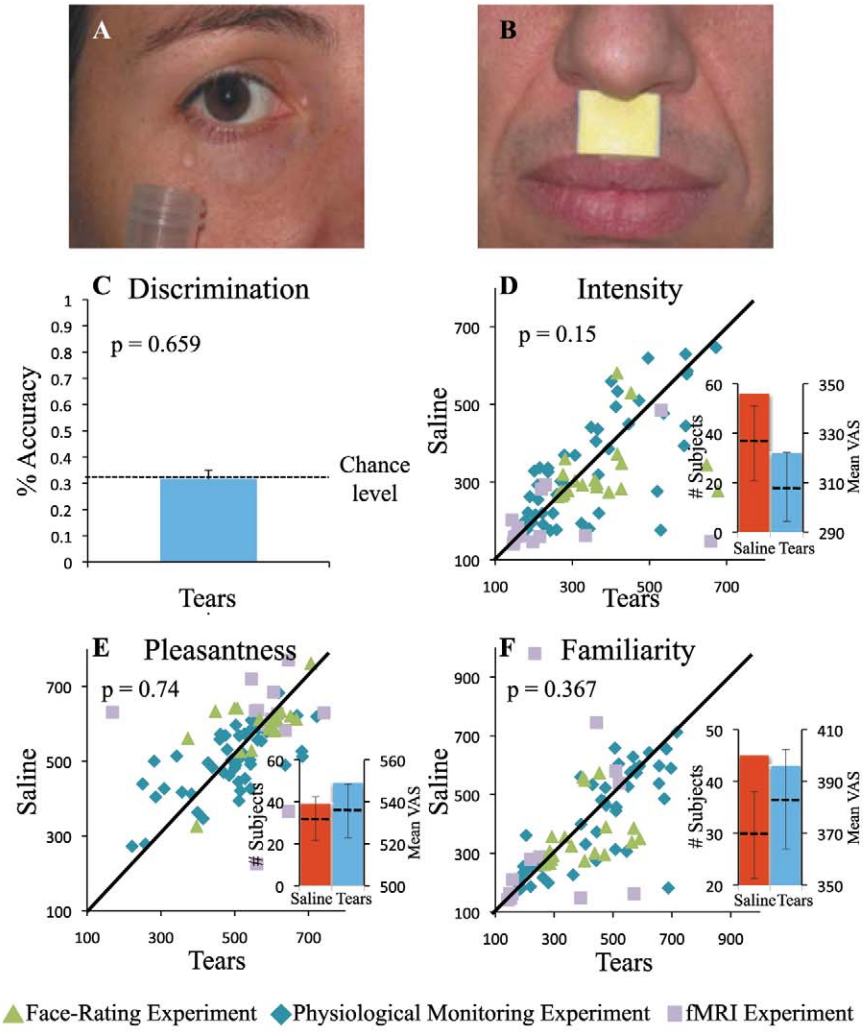

Fig. 1. Emotional tears are odorless. (**A**) To obtain tears, donor women watched sad films in isolation, using a mirror to capture tears into a vial. A typical donation contained ~1 ml. (**B**) For continuous exposure, tears deposited onto a pad allowed ongoing nasal airflow exposure but not transdermal diffusion. (A) and (B) are illustrations. (**C**) Accuracy of discrimination of tears from saline. (**D** to **F**) Scatterplots of (D) intensity, (E) pleasantness, and (F) familiarity estimates of tears and saline in all experiments. Within-participants comparisons [(D) to (F) here and in all other figures] are presented in scatterplots along a unit slope line ($x = y$), where each point reflects a participant. If data accumulate under the line, then values were greater for tears; if data accumulate above the line, then values were greater for saline. If data accumulate on the line, then there was no difference between tears and saline. (Insets) Bars reflect the number of participants on each side of the unit slope line (left ordinate), and the horizontal dashed line reflects the mean values and standard error (right ordinate).

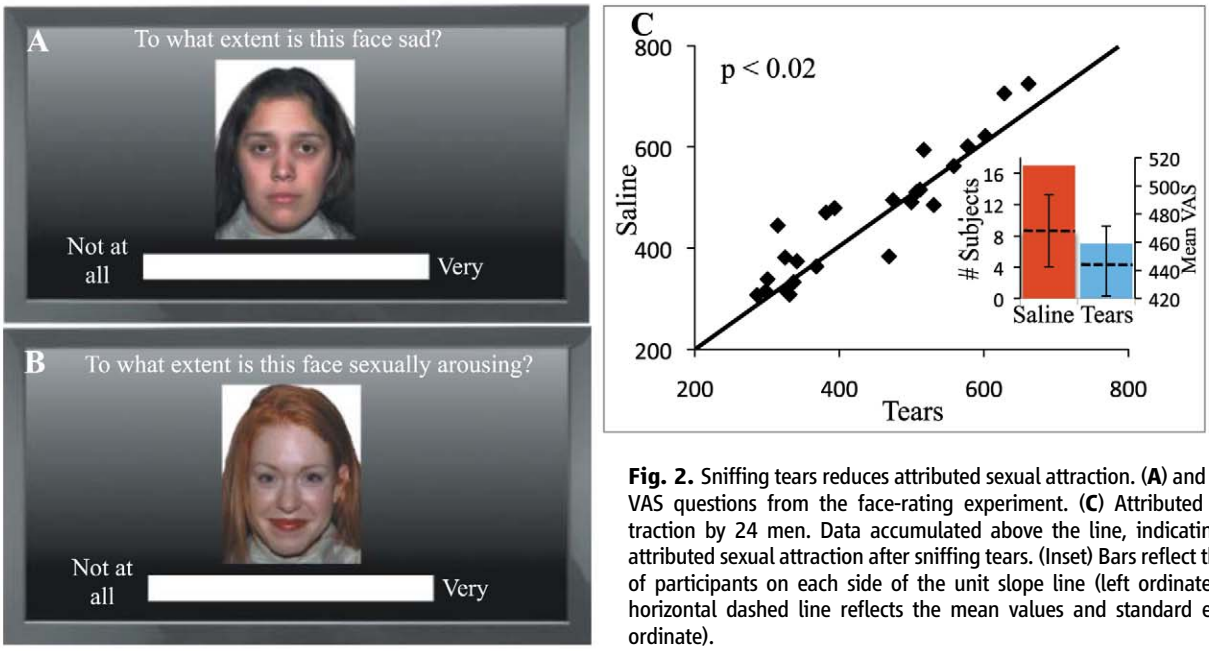

Fig. 2. Sniffing tears reduces attributed sexual attraction. (**A**) and (**B**) Typical VAS questions from the face-rating experiment. (**C**) Attributed sexual attraction by 24 men. Data accumulated above the line, indicating reduced attributed sexual attraction after sniffing tears. (Inset) Bars reflect the number of participants on each side of the unit slope line (left ordinate), and the horizontal dashed line reflects the mean values and standard error (right ordinate).

who watched sad films in isolation [Fig. 1A and suporting online material (SOM)]. We then tested whether 24 men (mean age 28.12 ± 4.05 years) could smell a difference between these fresh tears and saline. The saline was first trickled down the cheek of the donor women to account for any skin-bound odor sources. Participants failed to discriminate the smell of tears from the smell of saline [mean correct = 31 ± 14%, $t(23) = 0.81$, $P < 0.659$; Fig. 1C], indicating that emotional tears did not have a discernable odor.

We next asked whether sniffing such odorless tears influences perception. We compared two alternative hypotheses: (i) Tears may contain a chemosignal related to their typical context of sadness (*14*). Indeed, seeing tears on faces renders the faces sadder in appearance (*4*). (ii) Alternatively, human tears may function like mouse tears, where they signal information related to sociosexual behavior (*10*–*12*).

Twenty-four men (mean age 26.92 ± 3.13 years) first sniffed a jar containing a compound (fresh tears or trickled saline; tears were from three donor women, mean age 30.33 ± 0.5 years) and then rated the compound's intensity, pleasantness, and familiarity. To keep study participants exposed to the compound for the rest of

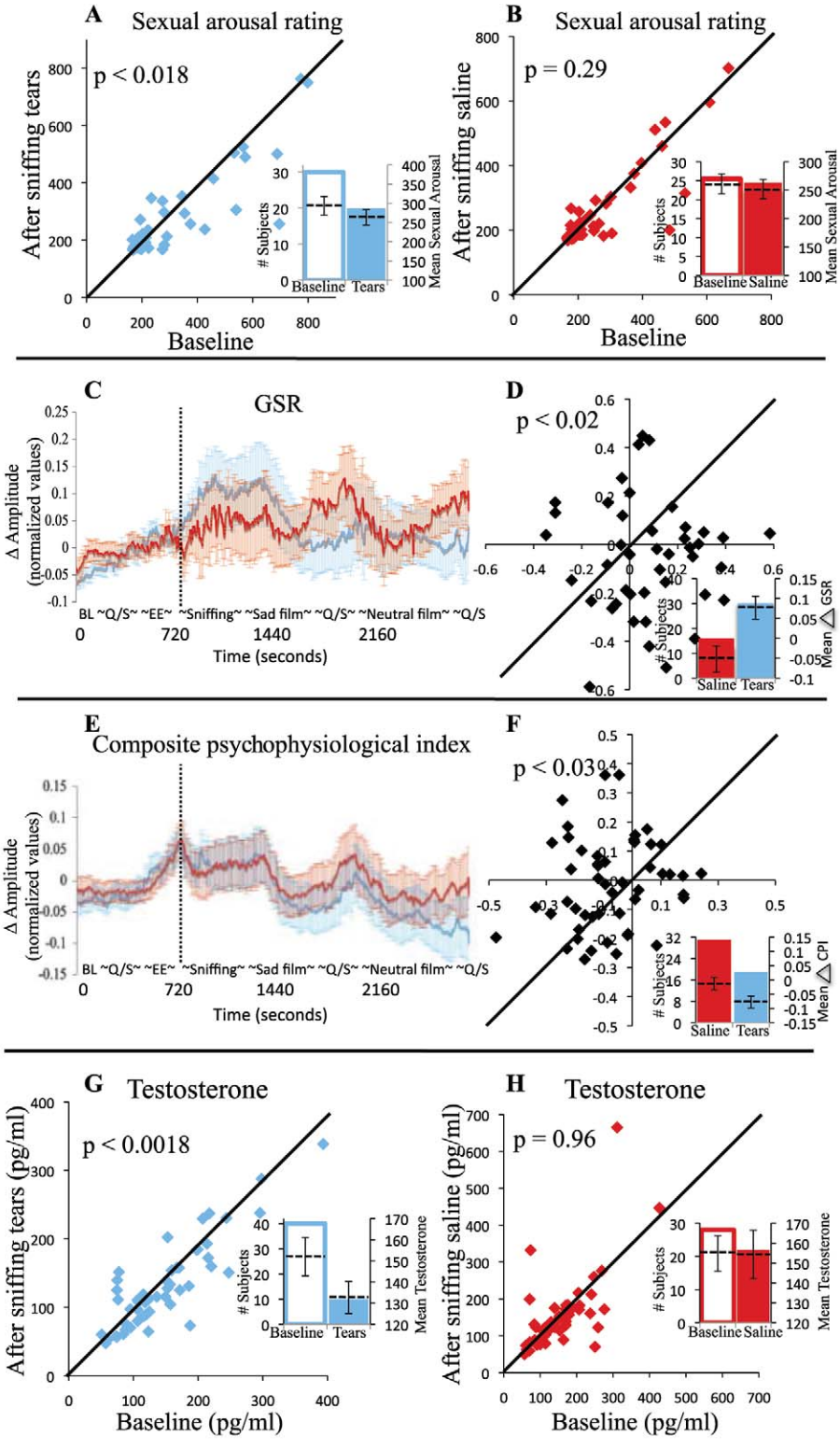

Fig. 3. Sniffing tears reduces arousal. (**A**) Shift in self-rated sexual arousal from baseline to ~5 min after sniffing tears, indicating a drop in arousal. (**B**) Shift in self-rated sexual arousal from baseline to ~5 min after sniffing saline, indicating no change. (**C** and **E**) Timeline of psychophysiological data. Data were aligned in time to the first sniff (dashed vertical line). The abscissa lists the time in seconds and the experimental phases. BL, baseline; Q/S, VAS mood questionnaire, followed by a saliva sample; EE, experimenter enters room. Experimental phases are approximately (~) accurate in time, because participants differed in questionnaire latency, resulting in a shift of a few seconds. Error bars reflect between-participants variance, here displayed only to give a better sense of the data. The statistically relevant variance is the within-participants variance displayed in scatterplots (**D**) and (**F**). (C) Timeline of ongoing GSR amplitude, indicating greater GSR response for tears during sniffing only. (D) GSR change from sniffing to the end of a sad movie, indicating greater change for tears. (E) Timeline of the CPI, indicating reduced arousal after sniffing tears. (F) CPI at the final stage of the study, indicating significantly lower arousal after sniffing tears versus saline. (**G**) Shift in salivary levels of testosterone from baseline to last saliva collection after sniffing tears, indicating a drop from baseline. (**H**) Shift in salivary levels of testosterone from baseline to last saliva collection after sniffing saline, indicating no change. (Insets) Bars reflect the number of participants on each side of the unit slope line (left ordinate), and the horizontal dashed line reflects the mean values and standard error (right ordinate).

the experiment, 100 µl of the compound was deposited onto a pad pasted onto the participant's upper lip, directly under his nostrils (Fig. 1B). The jar was presented by an additional, non-crier female experimenter who was blind to the jar's contents (*15*). Participants next viewed on-screen emotionally ambiguous pictures of women's faces and used a visual-analog scale (VAS) to rate the sadness (24 faces, Fig. 2A) and sexual attraction (18 faces, Fig. 2B) attributed to each face. Interleaved with these ratings were 40 VAS questions from a standardized questionnaire that assesses empathy (*16*). Each man participated twice, on consecutive days, once with tears and once with saline, counterbalanced for order across participants, and double-blind as to compound identity.

Tears did not differ from saline in perceived intensity, pleasantness, or familiarity [$F_{1,23}$ = 1.26, P = 0.27] (Fig. 1, D to F). However, VAS ratings of faces differed after sniffing tears or saline [$F_{1,23}$ = 7.46, P < 0.02]. This difference did not reflect a shift in sadness attributed to the faces [mean VAS tears = 572 ± 118, mean VAS saline = 592 ± 94, t(23) = 1.2, P = 0.23] but rather a shift in sexual attraction attributed to the faces, whereby the faces appeared less sexually attractive after sniffing tears than after sniffing saline for 17 of the 24 participants [mean VAS tears = 439 ± 118, mean VAS saline = 463 ± 125, t (23) = 2.5, P < 0.02] (Fig. 2C). Sniffing tears did not influence empathy [mean VAS tears = 593 ± 56, mean VAS saline = 587 ± 56, t(23) = 1.2, P = 0.24].

Tears may have failed to influence sadness or empathy because the experimental context was not explicitly sad. We therefore studied 50 men (mean age 28.2 ± 3.8 years) using a paradigm that generates negative emotions (*15*, *17*). We measured psychophysiological arousal [galvanic skin response (GSR), heart rate, respiration rate, and skin temperature], VAS self-ratings of mood (*18*), and salivary levels of testosterone, before (baseline), during, and after participants sniffed either tears (from five donor women, mean age 29.2 ± 2.3 years) or saline. After sniffing, participants watched a sad film. Each man participated twice, on consecutive days, once with tears and once with saline, counterbalanced for order across participants, and double-blind (see SOM) as to compound identity.

Tears did not differ from saline in perceived intensity, pleasantness, or familiarity [$F_{1,49}$ = 0.36, P = 0.55] (Fig. 1, D to F). The paradigm successfully reduced positive mood [tears and saline combined, positive mood VAS change from baseline = –69.81 ± 99, t(49) = 4.95, P < 0.0001] and increased negative mood [negative mood VAS change from baseline = 50.57 ± 58.5, t(49) = 4.95, P < 0.0001]. Despite this negative emotional setting, VAS self-ratings of mood did not differ after sniffing tears as compared to saline [$F_{1,49}$ = 0.1, P = 0.74]. However, observation of the response within each session revealed a modest effect whereby tears reduced self-ratings of sexual arousal [baseline mean VAS rating = 293.48 ± 173.3; after sad film, mean VAS rating = 263.44 ± 140, t(49) = 2.46, P < 0.01] (Fig. 3A), yet saline did not [baseline mean VAS rating = 260.96 ± 124; after sad film, mean VAS rating = 251.8 ± 120.4, t(49) = 0.81, P = 0.29] (Fig. 3B).

Whereas the effect on subjective self-rated sexual arousal was modest (*19*), the effects on objective psychophysiology and hormonal expression were pronounced [all measures: $F_{1,49}$ = 4.27, P < 0.05]. During sniffing, there was an increase in GSR, greater for tears than for saline [mean tears = 0.08 ± 0.03, mean saline = –0.05 ± 0.04, t(42) = 2.68, P < 0.02] (Fig. 3, C and D), yet after sniffing there was a progressive reduction in arousal, greater for tears than for saline. This was evident in several independent measures (fig. S1), as well as in a conservative composite index (CPI) (*17*, *20*) that equally weighted all recorded measures [end of experiment: CPI mean tears = –0.08 ± 0.02, mean saline = –0.01 ± 0.02, t(49) = 2.29, P < 0.03] (Fig. 3, E and F). Finally, and critically, levels of salivary testosterone were progressively lower after sniffing tears as compared to the baseline period [baseline testosterone = 151.96 ± 76 pg/ml, last testosterone = 132.66 ± 63.1 pg/ml, t(49) = 3.3, P < 0.001] (Fig. 3G), an

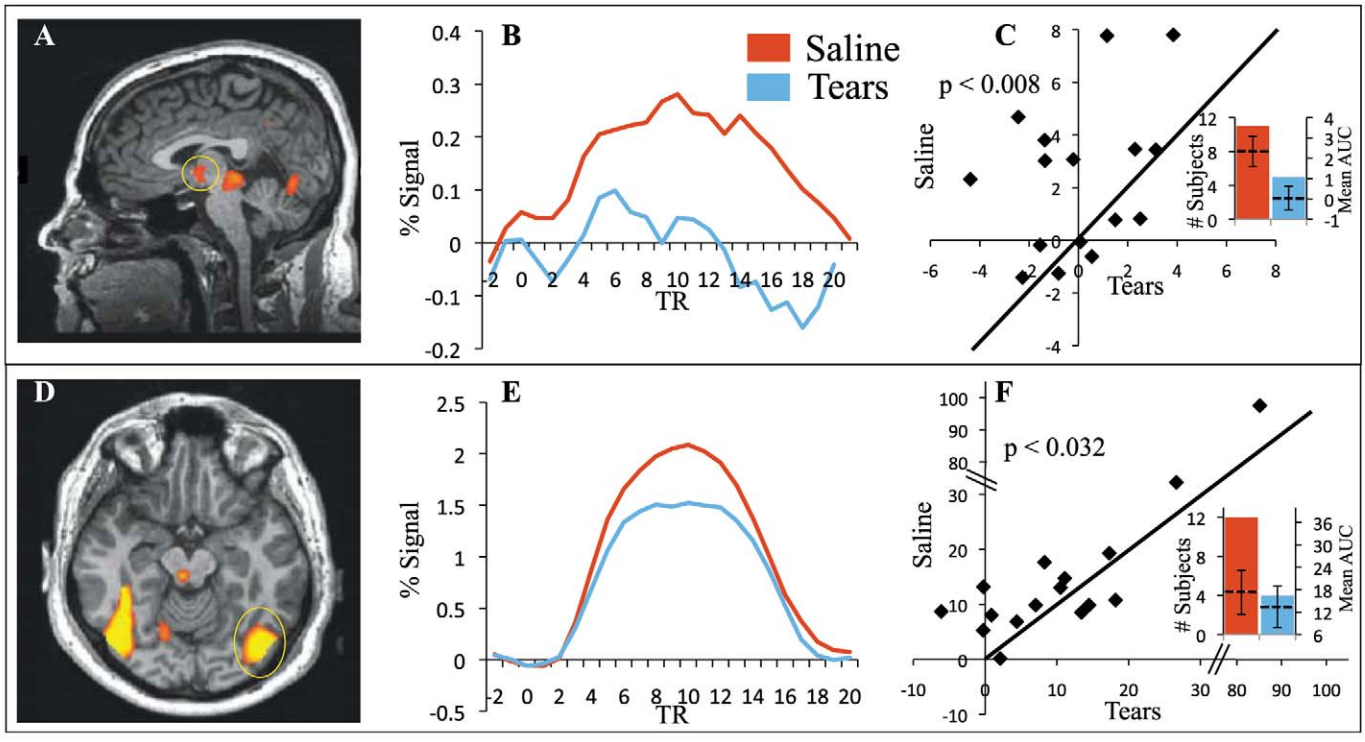

Fig. 4. Sniffing tears reduces brain activity in substrates of sexual arousal. (**A**) Activity induced by an erotic film generated a region of interest (ROI) in the hypothalamus. (**B**) Average activity time-course from 16 men within the previously identified hypothalamic ROI. This activity was induced by a sad film clip after sniffing either tears (blue) or saline (red). (**C**) Area under the curve of activation from (B), providing a measure of variance across participants. (**D**) Activity induced by an erotic film generated an ROI in the left fusiform gyrus. (**E**) Average activity time-course from 16 men within the previously identified fusiform gyrus ROI. This activity was induced by a sad film clip after sniffing either tears (blue) or saline (red). (**F**) Area under the curve of activation from (E), providing a measure of variance across participants. (Insets) Bars reflect the number of participants on each side of the unit slope line (left ordinate), and the horizontal dashed line reflects the mean values and standard error (right ordinate).

effect not evident for saline [baseline testosterone = 154.8 ± 74.4 pg/ml, last testosterone = 154.34 ± 101.8 pg/ml, $t(49) = 0.81$, $P = 0.96$] (Fig. 3H). Reductions in testosterone are a significant indicator of reductions in sexual arousal in men (*21*).

Brain imaging has uncovered brain activity associated with human chemosignals (*22*–*24*). Because sniffing women's odorless tears consistently reduced sexual arousal in men in a nonsexual setting (viewing pictures of faces and sad or neutral films), we next used functional magnetic resonance imaging to ask whether this was reflected in brain activity. We first presented sexually arousing pictures and movies in order to delineate sexual arousal–related brain structures, and then separately measured the response within these regions to sad, happy, and neutral movies after sniffing either tears or saline. Each of 16 male participants (mean age 28 ± 2.67 years) participated twice, on consecutive days, once with tears and once with saline (from five donor women, mean age 33.6 ± 7.5 years), counterbalanced for order across participants, and double-blind as to compound identity. In order to ensure that participants sniffed the compound, they were asked to provide estimates of intensity, pleasantness, and familiarity, which revealed no perceptible odor for tears [$F_{1,15} = 0.02$, $P = 0.88$)] (Fig. 1, D to F).

Sexually arousing stimuli outlined a brain network consistent with that previously implicated in brain imaging studies of sexual arousal (*25*) (table S1; see fig. S2 for activity induced by tears alone), most notably the hypothalamus (Fig. 4A) and left fusiform gyrus (Fig. 4B). Within these regions, activity induced by the sad film was significantly lower after sniffing tears than after sniffing saline [hypothalamus, area under the curve (AUC) % change tears = 0.04 ± 2.26, AUC % change saline = 2.33 ± 2.86, $t(15) = 3.05$, $P < 0.008$ (Fig. 4, B and C); left fusiform gyrus, AUC % change tears = 13.42 ± 21.33, AUC % change saline = 17.27 ± 22.7, $t(15) = 2.38$, $P < 0.031$ (Fig. 4, E and F)].

Subjective ratings of attributed sexual appeal, together with objective measures of psychophysiological arousal, testosterone expression, and brain activity, jointly suggest that women's emotional tears contain a chemosignal that reduces sexual arousal in men. We have thus identified an emotionally relevant function for tears.

These effects materialized despite the fact that participants did not see a woman cry, nor were they aware of the compound source. Moreover, in Western culture, exposure to tears is usually in close proximity. We hug a crying loved one, often placing our nose near teary cheeks, typically generating a pronounced nasal inhalation as we embrace. Such typical behavior entails exposure equal to or greater than that experienced here, hence the effects we observed in the laboratory are relevant to human behavior.

All mammals, including humans, use chemosignals. The most commonly studied carrier of human chemosignals is sweat (*25*–*27*), yet most mammals don't sweat like humans do. Although cursory observation of nonhuman mammalian behavior suggests that most chemosignals are carried by urine or anal/vaginal secretions, careful observation reveals that mammals investigate facial chemosignals as well (*28*). Indeed, specific chemosignals have been identified in the lachrymal secretions of mice (*10*, *12*), that is, in the mouse equivalent of tears. Thus, although it is commonly stated that only humans shed emotional tears, our findings may serve to tie human emotional crying to tear-shedding in other species (*7*, *29*).

The action of mammalian chemosignals can range from "releasers" that generate a response de novo (such as lordosis), to "primers" that modify a long-term process (such as sexual maturation), to "signalers" that provide information (for example, about kinship), and "modulators" that modify an ongoing response (*30*). In our view, "modulator," a term coined primarily to describe the action of human pheromones (*31*), best fits the effects of tears as measured here. Here, women's tears modulated (reduced) sexual arousal, physiological arousal, testosterone levels, and brain activity in men.

These findings pose many questions: What is the identity of the active compound/s in tears? Do chemosignals in women's tears signal anything else but sexual disinterest, and is this signaling restricted to emotional tears alone? Moreover, could the emotional or hormonal state (menstrual phase/oral contraceptives) of the crier/experimenter influence the outcome? In turn, what if any are the signals in men's tears (see SOM) or children's tears, and what are the effects of all these within, rather than across, gender? Despite these open questions, the current results conclusively demonstrate a chemosignal in human tears. In this, we illustrate a previously unknown functional role for crying.

References and Notes

1. C. Darwin, *The Expression of the Emotions in Man and Animals*, with an introduction, afterword, and commentaries by Paul Ekman (Oxford Univ. Press, New York, 1872).
2. H. A. Chapman, D. A. Kim, J. M. Susskind, A. K. Anderson, *Science* **323**, 1222 (2009).
3. A. Montague, *Science* **130**, 1572 (1959).
4. R. R. Provine, K. A. Krosnowski, N. W. Brocato, *Evol. Psychol.* **7**, 78 (2009).
5. A. Vingerhoets, R. R. Cornelius, G. L. Van Heck, M. C. Becht, *Rev. Gen. Psychol.* **4**, 354 (2000).
6. M. C. Hendriks, M. A. Croon, A. J. Vingerhoets, *J. Soc. Psychol.* **148**, 22 (2008).
7. W. H. Frey, M. Langseth, *Crying: The Mystery of Tears* (Winston Press, Minneapolis, MN, 1985).
8. N. H. Frijda, *The Emotions* (Cambridge Univ. Press, 1986).
9. N. J. Van Haeringen, *Surv. Ophthalmol.* **26**, 84 (1981).
10. R. N. Thompson, A. Napier, K. S. Wekesa, *Physiol. Behav.* **90**, 797 (2007).
11. H. Kimoto *et al.*, *Curr. Biol.* **17**, 1879 (2007).
12. H. Kimoto, S. Haga, K. Sato, K. Touhara, *Nature* **437**, 898 (2005).
13. W. H. Frey 2nd, D. DeSota-Johnson, C. Hoffman, J. T. McCall, *Am. J. Ophthalmol.* **92**, 559 (1981).
14. J. J. Gross, B. L. Frederickson, R. W. Levenson, *Psychophysiology* **31**, 460 (1994).
15. This cross-gender method was used because it has been shown to increase the influence of sniffing putative human pheromones (*32*).
16. A. Mehrabian, N. Epstein, *J. Pers.* **40**, 525 (1972).
17. M. Bensafi *et al.*, *Behav. Neurosci.* **117**, 1125 (2003).
18. R. W. Levenson, P. Ekman, W. V. Friesen, *Psychophysiology* **27**, 363 (1990).
19. We refer to this effect on self-rated sexual arousal with caution and describe it as modest because this was the only measure in this manuscript where, by chance, baseline values for saline were lower than for tears, thus generating a potential floor-effect for saline that favored the effect.
20. C. Wyart *et al.*, *J. Neurosci.* **27**, 1261 (2007).
21. S. G. Stoléru, A. Ennaji, A. Cournot, A. Spira, *Psychoneuroendocrinology* **18**, 205 (1993).
22. N. Sobel *et al.*, *Brain* **122**, 209 (1999).
23. J. N. Lundström, J. A. Boyle, R. J. Zatorre, M. Jones-Gotman, *Cereb. Cortex* **18**, 1466 (2008).
24. I. Savic, H. Berglund, B. Gulyas, P. Roland, *Neuron* **31**, 661 (2001).
25. W. Zhou, D. Chen, *J. Neurosci.* **28**, 14416 (2008).
26. K. Stern, M. K. McClintock, *Nature* **392**, 177 (1998).
27. G. Preti, C. J. Wysocki, K. T. Barnhart, S. J. Sondheimer, J. J. Leyden, *Biol. Reprod.* **68**, 2107 (2003).
28. M. Luo, M. S. Fee, L. C. Katz, *Science* **299**, 1196 (2003).
29. J. M. Masson, S. McCarthy, *When Elephants Weep: The Emotional Lives of Animals* (Bantam Doubleday Dell, New York, 1995).
30. C. J. Wysocki, G. Preti, *Anat. Rec. A Discov. Mol. Cell. Evol. Biol.* **281A**, 1201 (2004).
31. S. Jacob, M. K. McClintock, *Horm. Behav.* **37**, 57 (2000).
32. S. Jacob, D. J. Hayreh, M. K. McClintock, *Physiol. Behav.* **74**, 15 (2001).

33. This work was supported by a grant from the Minerva Stiftung Foundation.

Supporting Online Material

www.sciencemag.org/cgi/content/full/science.1198331/DC1
Materials and Methods
Figs. S1 and S2
Table S1
References

27 September 2010; accepted 17 December 2010
Published online 6 January 2011;
10.1126/science.1198331

FLOW CHEMISTRY SYSTEMS

The Asia portfolio consists of high performing, flexible, and easy-to-use systems that are scalable and modular, making it ideal for any flow chemistry requirements. The new systems have a wide temperature (-15 °C to 300 °C) and pressure (0–20 bar) range, as well as an ability to safely provide accurate temperature control. With fast reaction times and microgram to kilogram scalability, its unique design enables manual or automated operation with optional PC control. The Asia flow chemistry range consists of three different series, each with three pre-configured systems providing varying levels of functionality. The Asia 1-series are a manually operated, cost-effective choice. The Asia 2-series systems can automatically perform one experiment at a time, with automated parameters such as reaction temperature, pressure, and collection timings. As a result, they are ideal for users not familiar with flow chemistry techniques. Fully automated for process optimization, the Asia 3-series is ideal for high-end applications.

Syrris

For info: +44-(0)-1763-242555 | www.syrris.com

CRIMPING TOOL

The La-Pha-Pack stainless steel cleanroom crimping tools are designed for a controlled, low-effort method of vial sealing. Available in a range of sizes, from 11 mm to 20 mm, the optimal crimp is provided for a variety of vial sizes. Made entirely from stainless steel, it provides maximum durability and easily withstands dry heat sterilization or autoclaving. The product range is ideal for highly sensitive chromatography cleanroom applications where it is essential that the environment remains free from any potential contaminants. The mechanism of the La-Pha-Pack crimping tools is both corrosion- and heat-resistant, making it extremely durable with a long lifespan. Furthermore, the stainless steel construction removes the need for any protective coating on the handle or crimp head. Pressure and height of the La-Pha-Pack stainless steel crimping tools are easily adjustable, enabling optimal torque to be applied to a wide variety of vial styles.

Thermo Fisher Scientific

For info: 215-943-1141 | www.la-pha-pack.com

CHROMATOGRAPHY COLUMNS

HiScale is a line of pressure-stable empty columns optimized for process development and preparative chromatography. The empty columns are available in inner diameters of 16 mm, 26 mm, and 50 mm and in lengths of 20 cm and 40 cm. The columns offer an easy-to-use design, providing reproducibility, robustness, and process control. HiScale columns are pressure stable up to 20 bar, ensuring compatibility with modern BioProcess media such as MabSelect and Capto. The ability to axially compress the gel bed and a non-rotating plunger mechanism enable a wide range of packing protocols. The measurement scale on the column and user-friendly, ergonomic design enable precise packing, thereby increasing process control and reproducibility. The QuickLock mechanism of the end caps facilitates column handling and cleaning. HiScale columns can be used with nearly all organic solvents commonly used in liquid chromatography of macromolecules. These columns were developed for scale-up during process development, and enable packing with high-flow agarose media which require higher pressure.

GE Healthcare

For info: 800-526-3593 | www.gelifesciences.com

SOLUBLE MAMMALIAN PROTEIN EXPRESSION

SoluBL21 competent *E. coli* is a significantly improved BL21 host strain for soluble mammalian protein expression. Using a directed evolution approach, a mutant strain of BL21(DE3) *E. coli* has been developed that can produce soluble protein in the majority of cases where expression in the parent BL21(DE3) yielded no detectable soluble product. With SoluBL21, a major obstacle to effective protein expression in *E. coli* has been overcome for many mammalian proteins. This significant improvement should enable scientists to make progress in a wide range of applications quicker and far less expensively than in the past. Use of the SoluBL21 Competent *E. coli* follows a simple and straightforward protocol, and the product is compatible with all T7 promoter-based expression vectors.

AMS Biotechnology

For info: +44-1235-828200 | www.amsbio.com

MOTORIZED PIPETTES

Extremely comfortable, easy-to-use, accurate, and durable are the main features of the new Pipetman M range. These pipettes, covering the range of 0.5 µL to 1000 µL, are fully motorized and require virtually zero pipetting force. Designed for both experienced and inexperienced users, Pipetman M pipettes are intuitive and require no learning curve. With four essential pipetting modes, including reverse, mix, repetitive, and pipetting, these pipettes offer the same high reproducibility, accuracy, and precision that users expect from Gilson pipette products. The motorized piston virtually eliminates pipetting variability among users. Because the speed of the piston is adjustable, users can pipette denser samples with accuracy and confidence. Other features include lockable volume, service alert reminders, and color-coded push-button that correspond to matching Gilson tip packaging. Also, Pipetman M are fitted with a universal tip holder that ensures a secure fit for most brands of tip, eliminating the need for a dedicated tip brand.

Gilson

For info: 800-445-7661 | www.gilson.com

Electronically submit your new product description or product literature information! Go to **www.sciencemag.org/products/newproducts.dtl** for more information.

Newly offered instrumentation, apparatus, and laboratory materials of interest to researchers in all disciplines in academic, industrial, and governmental organizations are featured in this space. Emphasis is given to purpose, chief characteristics, and availability of products and materials. Endorsement by *Science* or AAAS of any products or materials mentioned is not implied. Additional information may be obtained from the manufacturer or supplier.

POSITIONS OPEN

CASE WESTERN RESERVE UNIVERSITY EST. 1826

FACULTY
CWRU Department of Nutrition

The Department of Nutrition of the Case Western Reserve University School of Medicine seeks an established investigator who will expand currently ongoing metabolic investigations (see **website: http://www.case.edu/med/nutrition/home.html**). This is an **ASSOCIATE PROFESSOR/PROFESSOR,** tenured/tenure-track position. The faculty's research program should preferably focus on the metabolism of brain, heart, liver, or beta cells, in health and disease, via the association of metabolomics and stable isotope technology. Please send curriculum vitae, summary of research accomplishments, and outline of future research directions to **Dr. Henri Brunengraber** at **e-mail: henri.brunengraber@case.edu** or mail to: **The Department of Nutrition, 10900 Euclid Avenue, Cleveland, OH 44106-4954.**

In employment, as in education, Case Western Reserve University is committed to Equal Opportunity and Diversity.

POSTDOCTORAL POSITION in Antibacterial Drug Discovery

A research position for a postdoctoral associate is available in the Department of Pharmacology at Baylor College of Medicine in the area of antibacterial drug discovery. The laboratory is interested in the structure, function, and inhibition of antibiotic resistance enzymes. The studies will involve protein purification and enzymatic screens of small molecule libraries and combinatorial libraries for inhibitor molecules as well as biochemical characterization of enzyme-inhibitor interactions. This position is suitable for candidates with experience in protein biochemistry, enzymology, or peptide synthesis. Candidates should have a Ph.D. or M.D. degree and a strong record of productivity as evidenced by publications. Written and oral presentation skills as well as the ability to collaborate effectively are essential.

Interested candidates should electronically send their curriculum vitae, along with the names of three references to the address below:

Timothy Palzkill, Ph.D.
(E-mail: pharmacology@bcm.edu)
Professor and Chair
Department of Pharmacology
Baylor College of Medicine
One Baylor Plaza
Houston, TX 77030

The Department of Biology at Wheaton College (in Illinois) seeks to fill the **STROHSCHEIN CHAIR** in Biology (endowed) with a distinguished teacher and scientist in molecular, genetic, or cellular biology with experience in medical applications and a distinguished record in the integration of science and Christian faith. Rank open. Send letter of interest and curriculum vitae to **Fred Van Dyke,** Biology Department Chair, at **e-mail: fred.vandyke@wheaton.edu.** Applications will be mailed to promising candidates. Review of applications from promising candidates will begin February 1, 2011.

Wheaton College is an evangelical Christian liberal arts college with selective undergraduate admission whose faculty and staff affirms a Statement of Faith and adheres to the expectations of the Wheaton College Community Covenant. The college complies with federal and state guidelines for nondiscrimination in employment. Women and minority candidates are encouraged to apply.

POSTDOCTORAL POSITION
Germline Stem Cells

Studies include culture, differentiation, and gene activity of male germline stem cells. See *Science* **316:**404, 2007 and *Development* **136:**1191, 2009. Send curriculum vitae, names of three references, and a letter describing research experience to: **R. L. Brinster, School of Veterinary Medicine, University of Pennsylvania. E-mail: cpope@vet.upenn.edu.**

POSITIONS OPEN

Penn State University
College of Medicine

A tenure-track faculty position (**ASSISTANT PROFESSOR** level) is available in the Department of Anesthesiology to strengthen and complement existing neurophysiology and neuropharmacology research with ample opportunities for extensive in vitro, whole animal, and human subject research. The candidate must have an outstanding record of research accomplishments, as documented by publications in leading peer-reviewed journals. Specific area of emphasis includes, but is not limited, to opioid research employing electrophysiological, biochemical, imaging, and molecular approaches. The successful applicant will be provided with a generous package including competitive salary, startup funds, and ample laboratory space. The candidate will be expected to establish an externally funded research program and actively collaborate with other basic and clinical investigators in the department. To learn more about the Department of Anesthesiology please visit **website: http://www.pennstatehershey.org/web/anesthesia/home.** Please send a cover letter, curriculum vitae, a two to four page research plan, and arrange for submission of three letters of recommendation. Application materials can be sent electronically to **e-mail: vruizvelasco@psu.edu** or by mail to:

Victor Ruiz-Velasco, Ph.D.
Associate Vice Chair for Basic Science Research
Department of Anesthesiology
Penn State Hershey Medical Center
P.O. Box 850, H187
Hershey, PA 17033

Penn State is committed to Affirmative Action, Equal Opportunity, and the diversity of its workforce.

FACULTY POSITION in Cancer Research at The University of California, Irvine

The Department of Population Health and Disease Prevention, Program in Public Health and the Chao Family Comprehensive Cancer Center at the University of California, Irvine announce the availability of a tenure-track position at the **ASSISTANT PROFESSOR** level. Applicants should hold a Ph.D., M.D., or equivalent degree, and will be expected to establish a vigorous and internationally competitive research program in Cancer Epidemiology, Etiology and Treatment, or Cancer Prevention and Control. The successful candidate is expected to attract or possess extramural funding of his/her research and to teach at the undergraduate and graduate level.

Applicants should upload a description of their research accomplishments including future plans, a short statement regarding teaching interests/philosophy, curriculum vitae, and a list of at least four references. Please visit **website: http://publichealth.uci.edu/** for application instructions. To apply, please go to **website: https://recruit.ap.uci.edu/apply/.**

Deadline for receipt of applications: Review of applications will begin February 15, 2011, and the recruitment will remain open until the position is filled.

The University of California, Irvine is an Equal Opportunity Employer committed to excellence through diversity and strongly encourages applications from all qualified applicants including women and minorities.

POSTDOCTORAL FELLOWSHIP POSITIONS
Department of Neurology
Johns Hopkins University School of Medicine

Postdoctoral fellowship positions for recent Ph.D. graduates are available immediately at the Department of Neurology at Johns Hopkins University School of Medicine to study molecular mechanisms of peripheral nerve regeneration and Schwann cell biology. Experience in regeneration studies in the peripheral nervous system is desirable but not required. Experience in imaging and bioinformatics is preferable. Interested applicants should send their resumes electronically to **Dr. Ahmet Hoke** at **e-mail: ahoke@jhmi.edu.**

UNIVERSITÉ DE GENÈVE
FACULTÉ DE MÉDECINE

OPPORTUNITY AT THE UNIVERSITY OF GENEVA

THE FACULTY OF MEDICINE of **GENEVA** is seeking applications for 3 positions of:

ASSISTANT PROFESSOR OR ASSOCIATE PROFESSOR

in the Section of Fundamental Medicine

These full-time positions at the level of assistant or associate professor involve pre- and postgraduate teaching and research in the fields of metabolism or cardiovascular disease or biology of cancer or host pathogen interactions or stem cells.

Candidates should have demonstrated experience in one of these specific fields. They must be able to develop and lead research programs in a particular aspect of the field and to coordinate research projects in collaboration with other medical specialties. They must be willing to participate in interdisciplinary projects as well as assuming all pertinent administrative tasks.

A Doctorate of Science or Medicine (MD) is required and some knowledge of French is expected at term.

The starting date for the position is June 1st 2011 , or according to agreement.

Applications must be sent before March 1st 2011, to:
The Dean of the Faculty of Medicine
Centre médical universitaire,
1 rue Michel-Servet,
1211 Genève 4 - Switzerland

Information concerning applications and job description are available from:
sylvia.deraemy@unige.ch
Tel. +41 22 379 50 26

Women are encouraged to apply

HUG
Hôpitaux Universitaires de Genève

جامعة الملك عبدالله للعلوم والتقنية
King Abdullah University of Science and Technology

International Scientific Community Invited to Apply for Research Initiative Funding

King Abdullah University of Science and Technology (KAUST) invites interested and qualified members of the international scientific community to participate in a new competitive program, the KAUST Strategic Research Initiative (SRI) program.

The SRI program will provide funding for $1.5M per year for three years, to establish up to three small-scale SRI research centers at KAUST. During the term of these awards, the SRI Director and initial team will establish a research program and organization that could constitute the basis of a new KAUST research thrust, or be incorporated within an existing Research Center.

Areas of potential interest:

- Polymers and Composites
- Sustainable Agriculture in Arid Environments
- Microelectronics (MEMS & NEMS)
- Carbon Dioxide Trapping and Sequestration
- Biophysics
- Subsurface Imaging
- Solar Energy (excluding photovoltaics)
- Soil Remediation
- Microbiology from the Red Sea (from extremophiles to natural products)
- Any other research area within KAUST's scientific merit

Concept Papers must be submitted by February 16, 2011. For more information and how to apply, please visit http://gcr.kaust.edu.sa or email sri@kaust.edu.sa.

About KAUST

King Abdullah University of Science and Technology (KAUST) is an international, graduate level research university located in Thuwal, Saudi Arabia. KAUST is dedicated to inspiring a new age of scientific achievement and has developed four primary strategic research thrusts to support and drive KAUST's research agenda:

- Resources, Energy and Environment
- Biosciences and Bioengineering
- Materials Science and Engineering
- Applied Mathematics and Computational Science

TECHNISCHE UNIVERSITÄT DRESDEN

Medizinische Fakultät Carl Gustav Carus - Reformfakultät des Stifterverbandes für die Deutsche Wissenschaft

Research position (PhD / 50 % post doc)

in translational developmental neuroscience (with a focus on multi-channel EEG, source localization and transcranial magnetic stimulation) at the Department of Child and Adolescent Psychiatry, University Hospital Carl Gustav Carus, Dresden University of Technology, Germany.

PLEASE REPOST FOR INTERESTED PARTIES

Job Description: The Department of Child and Adolescent Psychiatry, Dresden University of Technology, Germany invites applications for a research position (PhD) in clinical neurophysiology and multimodal neuroimaging in developmental disorders with a focus on attention deficit/hyperactivity disorder and tic disorders. This is a full time position within the newly funded Developmental Clinical Neurophysiology Group (Prof. Dr. S. Bender). The group is one of the few international groups that are able to examine the brain potentials evoked by transcranial magnetic stimulation (TMS) in children and adolescents. Source analysis and advanced time-frequency analyses of multi-channel electroencephalographic (EEG) data represent the main analysis techniques.

Responsibilities will include the design of combined EEG and TMS experiments and the analysis of behavioral, TMS and EEG-data. EEG data pre-processing is carried out by BrainVision Analyzer (BrainProducts GmbH), source analysis is performed in BESA (Megis GmbH). Matlab-based tools are also applied, especially with respect to time-frequency analyses, such as event-related EEG coherence. You will supervise patient recruitment and data acquisition.

Applicants for the position must have completed (a) a Master or Diploma degree in a relevant field (Psychology, Biology, Biomedicine, Biophysics, Computer Science, Electrical Engineering) and (b) participated in research activities within the past years. Experience in computer programming (MATLAB), in EEG-data analysis, advanced statistical analyses and scientific writing would be a plus. The successful applicant will join a multidisciplinary team of researchers and clinicians and will receive further training in psychometric and neurophysiological techniques and the application of analysis tools for multimodal neuroimaging.

The position is available for a start date as soon as February 1st, 2011. Review of applications will begin immediately and will continue until the position is filled. The position is guaranteed for one year with the possibility of renewal after positive evaluation.

Salary will be consistent with levels in accordance with the German Research Foundation (50 % TV-L: E 13). Compensation includes health insurance, and vacation time.

To apply or request more information, please send a covering letter detailing professional objectives and interests, CV, and the names and email addresses of two references (all together in one pdf file in German or English) with the subject line "DCN doctoral position" to the address below. Applications from many disciplines may be considered, and the position is open to **qualified international applicants.** Applicants with a disability will be given preference in the selection process.

Prof. Dr. med. Veit Rößner, Klinik und Poliklinik für Kinder- und Jugendpsychiatrie und -psychotherapie, Universitätsklinikum Carl Gustav Carus Dresden an der TU Dresden, Goetheallee 12, 01309 Dresden, E-Mail: KJPChefsekretariat@uniklinikum-dresden.de.

Please refer to our homepage: www.kjp-dresden.de for more detailed information.

DSHB

Post-doctoral Associate Position for the Development of Monoclonal Antibody Platforms Identifying the Subgroups of the Major Cancers

The Developmental Studies Hybridoma Bank (DSHB) at the University of Iowa is embarking on an innovative approach for identifying the subgroups of the major human cancers and searching for accurate cancer stem cell markers. Both projects will involve development of complex microarray technology using monoclonal antibodies (antibody chips). The selected candidate will contribute to this pioneering approach in a newly initiated Institute for Monoclonal Antibody Technologies. We seek an individual with varying experience in biochemistry, proteomics, microarray techniques, bioinformatics and cancer biology. Candidates must have a Ph.D. A background in antibody techniques and/or stem cell research would be advantageous. Significant scientific resources are available to attain the projected goals within a well-established, innovative and interactive research group. Salary is commensurate with prior research experience and NIH guidelines.

Please send a cover letter and CV with three reference letters to: **Dr. David R. Soll, University of Iowa, Department of Biology, 300 BBE, Iowa City, IA 52242. E-mail: david-soll@uiowa.edu**.

INSTRUMENTATION DIVISION HEAD AT BROOKHAVEN NATIONAL LABORATORY (BNL)

BNL seeks a distinguished scientist to head a Division charged with developing state-of-the-art instrumentation for the diverse experimental research programs at BNL. The Division's current expertise spans semiconductor, gas and noble liquid detectors, low-noise microelectronics, lasers and optical metrology, and micro/nano-fabrication.

The Division currently comprises 42 FTE, including 14 Ph.D. scientists and 12 engineers, with an annual budget around $8M, including support from BNL overhead funds. The Division Head is expected to: integrate, prioritize and manage the diverse R&D efforts; collaborate with Laboratory scientists to provide and execute a vision matched to BNL's overall research strategies; and attract, retain and foster the development of a team of innovative specialists matched to that vision.

Qualified candidates should have a doctorate or equivalent degree in physics or electronics; at least ten years of research experience beyond that degree; an active internationally recognized research program overlapping some of the Division's core technologies; and demonstrated experience in leading highly successful, integrated R&D teams.

For more information and how to apply, go to **www.bnl.gov/HR**, and select "Job Opportunities," referring to job #15619 listed under Management. BNL is an AA/EOE employer committed to developing a diverse workforce.

BROOKHAVEN NATIONAL LABORATORY
a passion for discovery.

www.bnl.gov

Institute of Immunology and Translation Medicine (IITM)

Institute of Immunology and Translation Medicine (IITM) invites applications for full Professors and Associate Professor positions in the following areas of research:

1) Immune receptor and signaling;
2) Biology of antigen presenting cells and innate immunity;
3) Biology of T lymphocytes;
5) Biology of Inflammation;
6) Interaction between the immune system and HBV/HCV.
7) System biology/Bioinformatics

IITM is a new Institute affiliated with Jilin University and The First Hospital of Jilin University. IITM is established under the leadership of Executive Scientific Board:

Yong-Jun Liu (Chair): Professor and Chairman, Department of Immunology; Director, Center for Cancer Immunology Research. University of Texas, M. D. Anderson Cancer Center.

Xue Tao Cao (Co-Chair): Professor and Director, Institute of Immunology; Director, National Key Laboratory of Medical Immunology; Second Military Medical University.

The mission of IITM is to understand the pathophysiology of human diseases by conducting basic and translational immunology research using cell and molecular biology, system biology, genomic and proteiomic approaches.

The goal of IITM is to develop new methods of diagnosis and more effective treatment for human diseases including infectious diseases, autoimmune and inflammatory diseases and cancers.

IITM is house in a 9,000 SM new building equipped with the state of the art cutting edge core facilities, including flowcytometry, imaging, antibody production, microarry and system biology, Mass Spectrometry and immunohistochemstry.

IITM provides competitive salary, housing and start up funds. Please electronically send your CV, a summary of research plan and name of three references to e-mail: **kjkliubin@126.com**

UNIVERSITY OF WASHINGTON

The Electrical Engineering Department at the University of Washington is seeking to further grow its expertise in **Molecular Engineering** and **Nanotechnology**. Applications for a full-time, junior level position in Molecular Engineering and Nanotechnology are invited from candidates with expertise in molecular/nano devices in one or more of the following areas:

- Low power/dense electronics
- Electrical (RF and other methods) readout and control of biochemical processes
- Sensors for low concentration/single molecule detection/sequencing of biomolecules
- Energy conversion and storage at nanoscale
- Circuits and systems using molecular devices
- Biocompatible electronic materials and devices

The candidate should hold a PhD, have an interdisciplinary background; prior post-doctoral or higher level experience is valued. The successful candidate will be expected to develop an internationally recognized research program and to participate in the teaching and service missions of the department. Scientists and engineers who apply should show evidence of excellence, originality and productivity in research and potential for excellent teaching. The candidate would be expected to interact with the Chemistry department in the College of Arts and Science as well as other departments in the College of Engineering and other colleges in the University. It is anticipated that the appointment will be at the level of Assistant Professor. All offers will be contingent on budgetary approval by the University.

UW HAS THE HIGHEST LEVEL of federal funding of all public universities, and the second highest among all universities in the nation. The Electrical Engineering Department currently has 42 tenure track faculty (34 men/8 women). External research expenditures of the department in 2009–2010 were nearly $18M (see **www.ee.washington.edu**). The University of Washington faculty engage in outstanding teaching, research and service.

PLEASE SUBMIT YOUR CV, three representative publications, plan for future research, teaching statement, and the names and addresses of at least three references to our website: **http://www.ee.washington.edu/facsearch/**. Applications will be accepted until **April 15, 2011**. For any administrative issues related to the search, please contact Sarah Espe (**assist_to_chair@ee.washington.edu**).

THE UNIVERSITY OF WASHINGTON is building a culturally diverse faculty and strongly encourages applications from female and minority candidates. The University of Washington is the recipient of a 2006 Alfred P. Sloan Award for Faculty Career Flexibility and a 2001 National Science Foundation ADVANCE Institutional Transformation Award to increase the advancement of women faculty in science, engineering, and mathematics (see **www.engr.washington.edu/advance**).

The University of Washington is an Equal Opportunity, Affirmative Action Employer and is responsive to the needs of dual-career couples.

University of Haifa

The departments of Human Biology and Biology at the University of Haifa are seeking two candidates for tenure-track positions for the newly established program in medical sciences. Candidates with an MD or preferably MD/PhD are encouraged to apply. We are particularly seeking candidates with a strong research background in systems physiology or microbiology and infectious diseases.

Please send CV, list of publications, short statement of research and teaching interests and three names of people who can provide recommendation letters.

Applications can be sent by e-mail to:
Prof Avi Karni, Chair, Department of Human Biology at

avikarni_hb@yahoo.com

or Prof Edi Barkai,Chair, Department of Biology at

ebarkai@research.haifa.ac.il

JOHNS HOPKINS MEDICINE
SCHOOL OF MEDICINE

Faculty Positions in the Brain Science Institute at The Johns Hopkins University

Applications are invited for tenure-track faculty positions in the Brain Science Institute at the Johns Hopkins University School of Medicine (**http://www.brainscienceinstitute.org/**). Applicants should have interests in synapses and circuits in normal brain function or in cognitive disorders such as autism, schizophrenia and Alzheimer's disease. Applicants should be using molecular, cellular, developmental, systems or behavioral methods, have a Ph.D. or M.D., and a strong record of research accomplishments. Faculty will receive primary appointments in a relevant Department such as Neuroscience, Neurology or Psychiatry. Faculty members are expected to establish creative active independent research programs and participate in teaching graduate and medical students.

Deadline for applications is **February 15, 2011**. The Johns Hopkins University is committed to enhancing the diversity of its faculty and encourages applications from women and minorities. Please submit a PDF file containing curriculum vitae and a brief description of current and future research interests and arrange for three letters of reference to be sent on your behalf.

Richard L. Huganir
Chair Search Committee
Brain Science Institute
The Johns Hopkins University
School of Medicine
725 North Wolfe Street, Hunterian 1009A
Baltimore, Maryland 21205
HopkinsBSiSearch@jhmi.edu

An EEO/AA Employer.

John Innes Centre

INDEPENDENT RESEARCH FELLOWSHIPS

The John Innes Centre (JIC), Norwich, UK is a world leading centre of excellence in plant and microbial sciences based on the Norwich Research Park. We are inviting applications from outstanding researchers who either hold, or wish to apply for Independent Research Fellowships, to attend a Conference at the JIC on 9/10 May 2011. At the meeting you will be able to present a talk about your proposed area of research and to discuss your proposals, the development of your group and your future career plans in depth with senior JIC Scientists.

After the Conference we will select and mentor outstanding candidates in writing Fellowship applications and/or offer the opportunity to move existing Fellowships to the JIC.

Further details and particulars can be found at http://www.jic.ac.uk/corporate/opportunities/vacancies/fellows.htm

Please e-mail a 2-page summary of your research plan, a copy of your CV and arrange for three letters of recommendation to be emailed to dawn.barrett@bbsrc.ac.uk by Friday 18th March 2011

The John Innes Centre is a registered charity (No223852) grant-aided by the Biotechnology and Biological Sciences Research Council and is an Equal Opportunities Employer.

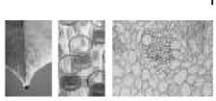

Nontraditional Careers:

Opportunities Away From the Bench

Webinar

Want to learn more about exciting and rewarding careers outside of academic/industrial research? View a roundtable discussion that looks at the various career options open to scientists across different sectors and strategies you can use to pursue a nonresearch career.

Now Available
On Demand
www.sciencecareers.org/webinar

Participating Experts:

Dr. Lori Conlan
Director of Postdoc Services,
Office of Intramural Training and Education
National Institutes of Health

Pearl Freier
President
Cambridge BioPartners

Dr. Marion Müller
Director, DFG Office North America
Deutsche Forschungsgemeinschaft
(German Research Foundation)

Richard Weibl
Director, Center for Careers in Science and Technology
American Association for the Advancement of Science

Produced by the
Science/AAAS Business Office.

Science Careers
From the journal *Science* AAAS

Creighton UNIVERSITY
School of Medicine

FACULTY POSITION
Associate Professor of Biomedical Sciences

The Department of Biomedical Sciences in the Creighton University School of Medicine invites applications for a tenure-track faculty position at the Associate Professor level beginning in the fall of 2011. We seek an outstanding scientist with a Ph.D., M.D., or equivalent terminal degree with teaching experience and a record of academic scholarship and external funding appropriate for the Associate level. Teaching duties include lectures to medical students and graduate students in clinical gross anatomy, anatomy dissection laboratories, and management of the Clinical Anatomy graduate program, as well as some neuroscience. Laboratory space with start-up funding will be available. While the candidate's research interests should complement the research strengths of the department and the school, excellence of the candidate is more important than their research focus. Research strengths within the Department of Biomedical Sciences include mechanisms controlling the development of the inner ear and brain, auditory physiology, developmental and neurosensory biology, bone growth and development, asthma, skin carcinogenesis, regulation of respiratory and cardiovascular functions and diseases, and proteonomics.

The School of Medicine is one of nine schools or colleges, including professional schools of Business, Law, Nursing, Dentistry, Pharmacy and Health Professions, and a Graduate School, within Creighton University. Founded in 1878, Creighton University is a Jesuit institution with an enrollment of approximately 7,000 students. Creighton University is consistently ranked as one of the finest comprehensive universities in the nation by *U. S. News and World Report*. Omaha, the nation's 42nd largest city, offers an outstanding school system, low cost of living and numerous recreational and cultural activities.

Applicants should submit a curriculum vitae, a brief statement of research goals and a list of 3 references to: **Dr. Laura Bruce, Search Committee Chair, Department of Biomedical Sciences, Creighton University School of Medicine, 2500 California Plaza, Omaha, NE 68178. E-mail: lbruce@creighton.edu**. Review of applications will begin on **February 15, 2011**, and will continue until position is filled.

Women and minority candidates are encouraged to apply. Creighton University is an Equal Opportunity, Affirmative Action Employer.

ASSISTANT PROFESSOR
CHILDREN'S HOSPITAL BOSTON AND HARVARD UNIVERSITY

The Department of Stem Cell and Regenerative Biology at Harvard University and the Department of Orthopaedic Surgery at Children's Hospital Boston invite applications for a tenure-track appointment at the Assistant Professor level. The appointee will be given laboratory space in the Orthopaedic Research Laboratories at Children's Hospital Boston (**http://www.childrenshospital.org**) and be an affiliate member and active participant in the Department of Stem Cell and Regenerative Biology at Harvard University (**http://www.scrb.harvard.edu**).

The successful candidate is expected to direct innovative and independent research in the fields of skeletal biology and regenerative medicine, preferably addressing questions related to pediatric skeletal health and disease, and to participate in the teaching activities of the Department of Stem Cell and Regenerative Biology and the Department of Orthopaedic Surgery. Applicants must hold a Ph.D. and/or M.D. degree, have completed post-doctoral training, and have a strong record of research accomplishment.

Applications will be considered on a rolling basis, but should be completed before **May 1, 2011**. Complete applications must include a curriculum vitae, a 3-page description of research accomplishments and future research interests, reprints of 1 or 2 important publications, and letters of recommendation from 3 referees. Applications, letters of recommendation, and enquiries regarding the position should be sent by e-mail to: **orthopaedicresearch@childrens.harvard.edu**.

Children's Hospital Boston and Harvard University are Equal Opportunity/Affirmative Action Employers. Applications from women and minorities are encouraged.

St. Joseph's Hospital and Medical Center
Barrow Neurological Institute®
A member of CHW

NEUROSCIENCE RESEARCH

The **BARROW NEUROLOGICAL INSTITUTE** is seeking accomplished investigators to complement the preclinical neuroscience research enterprise at a unique and dynamic institution. Qualified applicants holding an M.D., Ph.D. or equivalent degree will be considered as appropriate for appointment at the assistant, associate or full professor levels. Successful candidates will be expected to orchestrate a program of extramurally funded, independent research and to assume educational and administrative responsibilities. The specific area of investigation is open, although institutional strategic interests include translational research in neuro-stimulation and in neuro-trauma.

Interested candidates should e-mail a brief statement of research interests, CV and the names and contact information for three references to **Debbie Nagelhout, Academic Assistant to the Director of The Barrow Brain Tumor Research Center, Barrow Neurological Institute and St. Joseph's Hospital and Medical Center, 350 West Thomas Road, Phoenix, AZ 85013; Debbie.Nagelh@bnaneuro.net** or apply online at **http://www.stjosephs-phx.org/index.htm**.

The BARROW NEUROLOGICAL INSTITUTE is seeking a **postdoctoral fellow** to compliment the preclinical neuroscience research in the laboratory of Nader Sanai, M.D. Qualified applicants holding an M.D., Ph.D., or equivalent degree will investigate the neurobiological basis of neural and glial CNS progenitors (see *Nature* **2004** February 19), particularly in the context of brain tumors. Successful candidates will have skill sets in molecular biology, histopathology, biochemistry, tissue culture assays and mouse models to characterize stem and progenitor cells. Preference will be given to those who also have experience in molecular imaging of neural precursors and applying high field-strength magnetic resonance spectroscopy. The Barrow Neurological Institute is a translationally oriented basic science research facility located in Phoenix, Arizona and located adjacent to the state's largest tertiary care hospital. It is in an urban center of academic, biotechnology, and pharmaceutical research, neighboring Arizona State University and the University of Arizona School Of Medicine. Initial appointment is for two years with the possibility of renewal.

Interested candidates should e-mail a brief statement of research interests, CV and the names and contact information for three references to **Debbie Nagelhout, Academic Assistant to the Director of The Barrow Brain Tumor Research Center, Barrow Neurological Institute and St. Joseph's Hospital and Medical Center, 350 West Thomas Road, Phoenix, AZ 85013**; **Debbie.Nagelhout@bnaneuro.net** or apply online at **http://www.stjosephs-phx.org/index.htm**.

Full-time opportunity for **Research Technician** to join a neural stem cell research laboratory at the Barrow Brain Tumor Research Center. Our laboratory utilizes immunohistochemical, genetic, biochemical, molecular, and cellular approaches to understand the neurobiological basis of adult neural and glial progenitors and the role of human CNS progenitor cells in the formation of brain tumors. Responsibilities will include, but are not limited to, general wet laboratory oversight, preparing grant applications/progress reports, renewing research protocols, facilitating entrance of new lab personnel, ensuring general compliance with institutional regulations, updating reference databases, and coordinating all other laboratory activities. Initial appointment is for one year with the possibility of renewal.

Interested candidates should e-mail a brief statement of research interests, CV and the names and contact information for three references to **Debbie Nagelhout, Academic Assistant to the Director of The Barrow Brain Tumor Research Center, Barrow Neurological Institute and St. Joseph's Hospital and Medical Center, 350 West Thomas Road, Phoenix, AZ 85013; Debbie.Nagelh@bnaneuro.net or apply online at http://www.stjosephs-phx.org/index.htm**.

Affirmative action/Equal Opportunity Employer.

Medicines for Malaria Venture

Medicines for Malaria Venture (MMV) 9th CALL FOR LETTERS OF INTEREST

Medicines for Malaria Venture is a not-for-profit Organization committed to the discovery, development and delivery of affordable anti-malarial drugs through public-private partnerships. We are looking towards the next generation of molecules which will power the agenda for the eradication of Malaria.

Three areas are highlighted:
(a) The development of non 8 aminoquinolines to produce a radical cure by targeting the hypnozoite stages of *Plasmodium vivax*,
(b) New chemotypes that block transmission of plasmodium and
(c) New chemotypes with rapid acting, blood stage (including ring stage) activity against resistant strains that have the potential to replace existing endoperoxides

We are particularly interested in lead generation projects targeting liver stage vivax or transmission blocking.

Blood stage projects will be considered assuming they have reached the Early Lead stage. As such compounds should have an EC50<100nM in the infected *Plasmodium falciparum* erythrocyte assay, selectivity to a mammalian cell line and demonstrated *in vivo* oral efficacy in a rodent malaria model. Virtual proposals and those based on established chemotypes (e.g 4 aminoquinolines, endoperoxides etc) will not be considered.

Any molecule in early stage clinical development are also of particular interest. Before submitting a proposal please contact Dr Joerg Moehrle (**moehrlej@mmv.org**) at MMV to discuss.

Applications may be from single institutions or partnerships between academic centres and pharmaceutical companies.
The initial application should be by sending a letter of interest on the **specified template** of no more than **three** pages electronically to

Dr. Jeremy Burrows
E-mail: proposals@mmv.org

Applications should reach MMV by
March 14th 2011.

More details of the call can be found at
www.mmv.org

AAAS is here – connecting government to the scientific community.

As a part of its efforts to introduce fully open government, the White House is reaching out to the scientific community for a conversation around America's national scientific and technological priorities.

To enable the White House's dialogue with scientists, AAAS launched Expert Labs, under the direction of blogger and tech guru Anil Dash. Expert Labs is building online tools that allow government agencies to ask questions of the scientific community and then sort and rank the answers they receive.

On April 12, 2010, AAAS asked scientists everywhere to submit their ideas to the Obama administration and at the same time launched the first of Expert Labs tools, Think Tank, to help policy makers collect the subsequent responses. The result was thousands of responses to the White House's request, many of which are already under consideration by the Office of Science and Technology Policy.

As a AAAS member, your dues support our efforts to help government base policy on direct feedback from the scientific community. If you are not already a member, join us. Together we can make a difference.

To learn more, visit aaas.org/plusyou/expertlabs

AAAS + U = Δ

AAAS is here – helping scientists achieve career success.

Every month, over 400,000 students and scientists visit ScienceCareers.org in search of the information, advice, and opportunities they need to take the next step in their careers.

A complete career resource, free to the public, *Science* Careers offers a suite of tools and services developed specifically for scientists. With hundreds of career development articles, a grants and scholarships database, webinars and downloadable booklets filled with practical advice, a community forum providing real-time answers to career questions, and thousands of job listings in academia, government, and industry, *Science* Careers has helped countless individuals prepare themselves for successful careers.

As a AAAS member, your dues help AAAS make this service freely available to the scientific community. If you're not a member, join us. Together we can make a difference.

To learn more, visit aaas.org/plusyou/sciencecareers

AAAS + U = Δ

AAAS is here – promoting universal science literacy.

In 1985, AAAS founded Project 2061 with the goal of helping all Americans become literate in science, mathematics, and technology. With its landmark publications *Science for All Americans* and *Benchmarks for Science Literacy*, Project 2061 set out recommendations for what all students should know and be able to do in science, mathematics, and technology by the time they graduate from high school. Today, many of the state standards in the United States have drawn their content from Project 2061.

Every day Project 2061 staff use their expertise as teachers, researchers, and scientists to evaluate textbooks and assessments, create conceptual strand maps for educators, produce groundbreaking research and innovative books, CD-ROMs, and professional development workshops for educators, all in the service of achieving our goal of universal science literacy.

As a AAAS member, your dues help support Project 2061 as it works to improve science education. If you are not yet a AAAS member, join us. Together we can make a difference.

To learn more, visit aaas.org/plusyou/project2061

AAAS + U = Δ

Science & Technology Policy Fellows

The science and engineering challenges that society faces today are far more complex than those of 40 to 50 years ago. The best available scientific, technical, and economic information is required to establish priorities, make decisions, and develop best practices. AAAS manages the Science & Technology Policy Fellowships in four areas to provide the opportunity for accomplished scientists and engineers to contribute to the federal policymaking process while learning firsthand about the intersection of science and policy. And this is just one of the ways that AAAS is committed to advancing science to support a healthy and prosperous world. Join us. Together we can make a difference. **aaas.org/plusyou/fellows**

AAAS + U = Δ

POSITIONS OPEN

STAFF SCIENTIST

OPKO Health, Inc. is undergoing a major expansion of its R&D effort at the Jupiter, Florida laboratories. The focus will be on the discovery of diagnostically useful antibodies for a variety of diseases using a novel combinatorial library screening approach (**Moola, et al.** *Cell* **144:**132-142, 2011). OPKO Health, Inc. is a publicly traded healthcare company involved in the discovery, development, and commercialization of proprietary pharmaceutical products, medical devices, vaccines, diagnostic technologies, and imaging systems.

Applications are encouraged from candidates with expertise in synthetic organic chemistry, biochemistry, proteomics, immunology, and diagnostic sciences. Applicants must have a Ph.D. and postdoctoral experience in one of the above areas and have established a record of outstanding accomplishment. Competitive salary and benefits are offered. OPKO's R&D laboratories are located in Jupiter, just north of West Palm Beach on Florida's Atlantic coast and near the Scripps Florida Research Institute and the Max Planck Florida Institute. Please send full curriculum vitae and arrange to have three letters of recommendation delivered electronically to **e-mail: recruitment@opko.com.**

The University of Michigan's Memorial Phoenix Energy Institute (**website: http://www.energy.umich.edu**) is seeking a **RESEARCH PROFESSOR** in the field of sustainable transportation energy and systems. The work would entail technology assessment, policy and economic analysis, and evaluation of the broader societal impacts. This is a part-time, 50 percent appointment. To review the entire position description and to apply, please visit **website: http://umjobs.org/** and refer to job posting **ID # 54551.** *The University of Michigan is an Equal Opportunity/Affirmative Action Employer.*

Seeking a **POSTDOCTORAL TRAINEE** with M.D. or Ph.D. in a health science with three or more years postdoctoral. Experience in diagnostics. Opening for studies and work in diagnostics and R&D in a small-specialized private laboratory with university ties that has grown for 17 years. Chance for life-long career. Mail curriculum vitae with data on training and visa status to: **Laboratory Director, PO Box 26, Buffalo, NY 14215.**

Science Mobile App Now Available for Android Phones

They say you never know when inspiration will strike. Download the *Science* mobile app for Android devices and be ready the next time you're inspired to read the latest news, research, and career advice from *Science* on your mobile phone.

To download the *Science* mobile app for Android visit **content.aaas.org/mobile**, visit the Android Market on your phone, or just scan this barcode.

Features include:

- Summaries and abstracts from *Science*, *Science Translational Medicine*, and *Science Signaling*.
- Ability to e-mail full-text links.
- The latest news from *Science*NOW.
- Career advice articles from *Science* Careers.
- Access to the *Science* weekly podcast and other multimedia.
- Content caching for reading without wi-fi access.

Science
AAAS

Proteins
Antibodies
ELISAs
Assay Services
MultiAnalyte Profiling
Activity Assays
Stem Cells
ELISpot Kits
Flow Cytometry
Cell Selection

R&D Systems Quantikine® ELISAs

The Most Referenced Immunoassays

A direct measure of product quality is the frequency of citations in the scientific literature. R&D Systems has more than 20 years of experience designing, testing, and optimizing the most cited ELISA kits in the world. Find out why scientists trust R&D Systems ELISAs more than any other brand.

R&D Systems is the Most Referenced ELISA Manufacturer

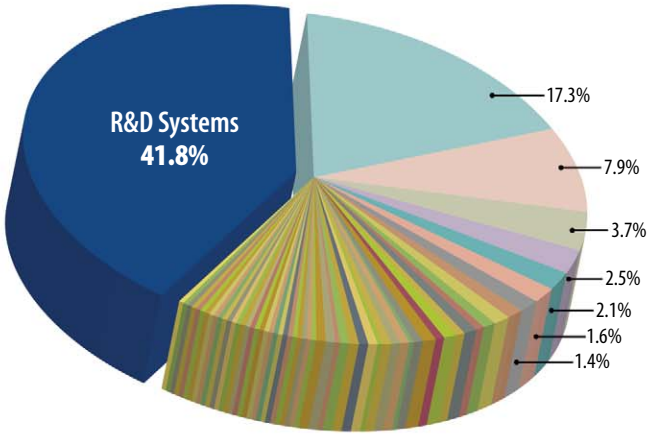

Approximately 42% of Referenced Immunoassays are Developed and Manufactured by R&D Systems. A survey of 860 manuscripts from 44 journals was conducted to compare the number of citations specifying the use of R&D Systems ELISAs to the number citing ELISAs from other commercial sources. A total of 433 ELISA citations referencing immunoassays from 66 different vendors were identified in the survey.

NEW Quantikine ELISA Kits

- α1-Acid Glycoprotein
- Angiopoietin-like 3
- Cathepsin V
- Clusterin
- Dkk-1
- EGF R/ErbB1
- EG-VEGF/PK1
- Fetuin A
- FGF-21
- Galectin-3
- Gas 6
- GDF-15
- IL-17A/F Heterodimer
- IL-19
- Lipocalin-2/NGAL
- MBL
- Proprotein Convertase 9/PCSK9
- Periostin/OSF-2
- Progranulin
- ST2/IL-1 R4
- Thrombomodulin/CD141
- Tie-1
- TIM-1/KIM-1

For more information visit our website at www.RnDSystems.com/go/ELISA

For research use only. Not for use in diagnostic procedures.

R&D Systems, Inc. www.RnDSystems.com

R&D Systems Europe, Ltd. www.RnDSystems.co.uk

R&D Systems China Co., Ltd. www.RnDSystemsChina.com.cn